CONTROLS ON THE DISTRIBUTION OF DENSE NON-AQUEOUS PHASE LIQUIDS IN THE MATRIX OF PERMO-TRIASSIC SANDSTONES

by

Daren Clive Gooddy

A thesis submitted in fulfilment
of the degree of Doctor of
Philosophy, University of
London, June 2003

Department of Earth Sciences
University College London
Gower Street
London, WC1E 6BT

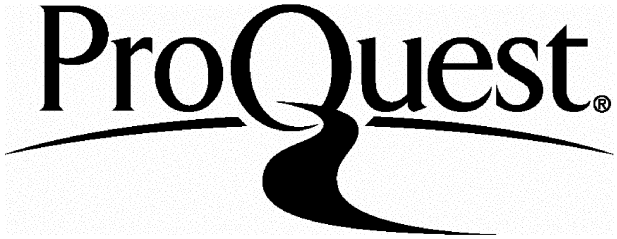

Abstract

The Permo-Triassic sandstones are geographically and lithologically diverse exhibiting large variations in porosity (ϕ), pore-throat size, permeability (k) and mineralogy that influence flow and transport of contaminants in the rock matrix. This thesis investigates how the movement of a dense non-aqueous phase liquid (DNAPL), tetrachloroethene, through the saturated zone of the Permo-Triassic sandstone is affected by the physical and chemical properties of the matrix. Specifically, the thesis aims to establish which parameters need to be determined to improve understanding of DNAPL penetration into the saturated zone of Permo-Triassic sandstones.

A series of standard physical property measurements have been made on a large number of Permo-Triassic sandstones from across the UK. A weak acid extraction has been performed on the samples to determine the bound chemical species in the matrix. In addition, two new laboratory methods have been developed to measure: DNAPL entry pressures using a centrifuge to produce pressure-saturation curves; and liquid relative permeabilities with a DNAPL residual saturation. A percolation based model has been developed to describe data from pore-throat size measurements.

Experimentally determined entry pressures are lower than those predicted by the Washburn equation assuming a pore structure equivalent to a 'bundle of capillaries'. The differences between observed and modelled pore entry pressure can be explained in part by changes in the wettability of the system relating to varying amounts of calcite and dolomite present in the matrix. The results of the percolation model suggests the presence of much larger pores than characterised by standard mercury injection tests. This may also explain in part why observed DNAPL entry pressures are lower than expected on the basis of capillary theory. Experiments show permeabilities decreases by 30-90% when a DNAPL is present. The reduction in permeability positively correlates with the hydraulic diameter. DNAPL present in a core at a given pressure as determined from the pressure-saturation curve also positively correlates with the hydraulic diameter. Knowledge of the sample porosity and permeability should enable good estimates of residual DNAPL and relative permeability in Permo-Triassic sandstones. Key advances are the acquisition of baseline data on representative DNAPL-sandstone systems and the development and application of methodologies from the hydrocarbons sector to contaminant hydrogeology.

Declaration

This thesis is entirely my own work unless otherwise indicated

Daren C Gooddy

Acknowledgments

Many people have contributed in one way or another to the development and completion of this thesis. Firstly I must thank EPSRC/NERC Waste and Pollution Management Programme for funding research programme into 'Transport of halogenated solvents in the matrix of the Permo-Triassic sandstone aquifer' and to BGS Training for paying the university fees. At University College London I am grateful to John Barker for his insight and perceptive and persistent supervision. At BGS Wallingford I am particularly indebted to John Bloomfield for his useful advice, good judgement, support and supervision. Also at BGS Wallingford I would like to thank Adrian Lawrence and George Darling for their help and encouragement and Ann Williams for some simple explanations. Andy Butcher and Jenny Cunningham (BGS Wallingford) were of great help with those little last minute GIS gripes. Janice Trafford (CSIRO Canberra) must also be thanked for going beyond the call of duty in reading far too many drafts. Nic Gedney (Met Office Wallingford) helped greatly by being there when it mattered and for turning push to shove. As part of the 'greater project team' I would like to thank Gavin Harrold and Steve Leharne at the University of Greenwich, David Lerner at the University of Sheffield, and Bernie Kueper from Queen's University, Canada. All good things come to an end...eventually.

Contents

TABLES

FIGURES

1 Introduction

This chapter describes the scope of the work including a note on the topics outside the scope of the thesis. It describes both the general and specific aims of the study and provides a context for the problems being addressed. The roles and responsibilities of the different researchers who have been associated with this work are noted. It is concluded with a description of the thesis structure.

1.1 SCOPE AND AIMS

The aims of this thesis are to obtain new experimental data so as to develop conceptual models specific to the entry, movement and residual saturation of dense non-aqueous phase liquids (DNAPLs) into consolidated, variably cemented, sandstones as a function of both physical and chemical properties of the rock matrix. The findings have significant implications for operational practices associated with management of DNAPL contamination and site investigation. Specifically the thesis aims to establish the parameters that need to be determined in order to better understand DNAPL penetration of the saturated zone of Permo-Triassic sandstones. The likely implications for remediation of the Permo-Triassic sandstones following a DNAPL spill are also discussed. The thesis does not consider fractures in its analysis of solvent movement through the Permo-Triassic, nor does it consider unsaturated zone behaviour, vapour phase movement or specific DNAPL spill scenarios.

Experiments have been carried out at a core-plug scale (i.e. 25 mm cylindrical sub-samples from cored boreholes) but the data is extrapolated, within reasonable constraints, down to the pore scale and up to the aquifer scale. All DNAPL experiments have been carried out using tetrachloroethene and no other DNAPLs have been considered.

1.2 PROBLEM BEING ADDRESSED

Groundwater supplies face a threat from a wide range of synthetic organic chemicals (Lawrence and Foster, 1991). The so-called chlorinated solvents, which are halogenated hydrocarbons and DNAPLs, have been produced for more than a century with the first production taking place in Germany in the late nineteenth century. It was not until

World War II that the widespread use of chlorinated solvents in manufacturing industries began, and this increased markedly during the next three decades. Contamination of groundwater by these compounds went largely unnoticed until the late 1970s since, historically, it was believed that chlorinated solvent released to the unsaturated zone of an aquifer would easily volatilise to the atmosphere. When disposed on dry ground, although a chlorinated solvent may appear to be lost entirely to the atmosphere, some will be transported into the subsurface by gaseous diffusion, by infiltration of contaminated water, and most significantly as a moving non-aqueous phase. Once these contaminants reach the saturated zone, high volatility is of little assistance in removing the solvents.

The denser-than-water nature of liquid chlorinated solvents has led to their becoming known as 'dense non-aqueous phase liquids' or DNAPLs. It is the physical and chemical properties of these compounds and their deleterious environmental effects that have made them a particularly pernicious cause of groundwater contamination (Aurand *et al.*, 1981; Mercer and Cohen, 1990; Jackson and Dwarakanath, 1999). Drinking water limits (or maximum concentration limits, MCLs) for the priority chlorinated solvents have been set at very low concentrations. For example, under the revised EC Drinking Water Directive (Directive 98/83/EC) a maximum concentration of 10 µg/L is set for the sum of tetrachloroethene and trichloroethene. The justification for these standards has been that compounds like trichloroethene, chloroform and carbon tetrachloride are suspected carcinogens. There is also evidence that exposure to carbon tetrachloride and tetrachloroethene may result in kidney and liver damage. The solubilities of the chlorinated solvents are 3-6 orders of magnitude higher than their drinking water limits. They are therefore characterised by high solubility/MCL ratios and so the contamination resulting from a chlorinated solvent DNAPL will typically be greatly in excess of its MCL. One serious spillage, therefore, has the potential to contaminate a very large volume of water to concentrations in excess of the EC limits. Price (1990) estimated that a chlorinated solvent spill of 5000 litres tetrachloroethene could contaminate 4.4×10^{12} litres of porewater in the Chalk aquifer (or the total annual recharge over the entire Chalk outcrop) to concentrations beyond the MCL. In addition to the public health issues related to chlorinated solvent contamination, the combination of high and increasing demand for water in the UK, and the increasing public awareness of water quality related issues, suggests that loss of groundwater resources due to

pollution cannot be sustained. If neglected, the impact of DNAPL contamination on the costs of water supply may significantly impose on UK industry.

There is an extensive historic legacy of solvent contaminated land in the UK (Rivett *et al.*, 1990; Lawrence and Foster 1991; Lawrence *et al.*, 1992). Although improvements in industrial handling practices have reduced the number of recent incidents, land-use changes resulting from urban and industrial redevelopment may lead to mobilisation of contaminants and add to the existing threat to groundwater quality. In a relatively recent strategic study of groundwater issues (Grey *et al.*, 1995) the UK Groundwater Forum identified "groundwater contamination by non-aqueous phase liquids" as a priority issue, and "fundamental processes of dense non-aqueous phase liquid migration" as a specific priority area for research.

The Permo-Triassic sandstones are a typical consolidated sandstone aquifer and in the UK they form the second most important aquifer supplying about a quarter of all licensed groundwater abstractions (Allen *et al.*, 1997). It outcrops extensively in the Midlands and north-west England, and a number of large and formerly industrial towns, including Manchester, Liverpool and Birmingham obtain their water supplies at least in part from the aquifer. The aquifer is therefore susceptible to contamination by a range of pollutants from both contemporary and historic industrial sources. A large body of work exists in the United States pertaining to the movement and fate of DNAPLs in aquifer systems (e.g. Pankow and Cherry, 1996), however much of this work relates to unconsolidated rocks and so is not directly transferable.

Wettability phenomena dominate the behaviour of immiscible liquids at the pore scale. Where two immiscible liquids are in contact with a solid surface, one liquid will preferentially 'wet' the surface. The wetting fluid will tend to coat the surface and occupy the smaller spaces, such as pore-throats, and the non-wetting phase will be confined to the larger openings, generally the open pores. Few wettability studies have been conducted on DNAPLs, although contact angle experiments on chlorinated solvents have shown that the solvents are non-wetting in water (Harrold *et al.*, 2001).

Once the main DNAPL body has passed through the rock matrix, some solvent will remain, as residual saturation (the volume of DNAPL as a fraction of the total pore volume). Residual saturation in granular aquifers is typically in the range 1 to 60% (Hunt *et al.*, 1988). These values are much higher than for a strongly fractured aquifer,

such as the Chalk (Mackay and Cherry, 1989). The implications of this for a spillage are that DNAPL may penetrate less deeply in granular aquifers, such as the Permo-Triassic sandstone aquifer. The residual solvent that remains within the unsaturated zone following the downward migration of a pulse of solvent will act as a secondary subsurface source of contaminant until all the solvent has been mobilised either by dissolution and leaching of water percolating to the water table, or by volatilisation. These processes are likely to be slow, so residual solvent may remain a significant contaminant source within the unsaturated zone for a considerable period of time. Soil gas surveys may be used to detect the presence, but not the quantity or detailed geometry, of this residual solvent. Where a spillage is sufficiently large that the total volume of solvent spilled exceeds the residual saturation capacity of the unsaturated zone then the DNAPL will reach the water table and contaminate the aquifer directly. DNAPL entry may be temporarily abated by the capillary fringe leading to spreading at the water table. Penetration will occur when DNAPL pressure exceeds the interfacial tension. For DNAPL to enter narrow pores in the saturated zone, the pressure exerted by the DNAPL must exceed the capillary pressure across the immiscible liquid interface and matrix aperture size strongly controls DNAPL migration in the saturated zone.

In the saturated zone, residual saturation is found to increase both as the pore size heterogeneity increases and as the ratio of pore volume to pore neck size increases (Chatzis *et al.*, 1983). Where this degree of residual saturation is high there is considerable reduction in the relative permeability for water locally (Mercer and Cohen, 1990). Groundwater would tend to flow around the body of residual solvent saturation and consequently dissolution rates in the centre of the residual saturation would be low (Figure 1.1). Dissolution would therefore result in the gradual contraction of the solvent residual saturation, the rate of contraction depending on the solvent solubility, the surface area to volume ratio of the solvent body, and the groundwater velocity around the solvent body (Geller and Hunt, 1993). Aqueous phase solvents are transported by the bulk motion of flowing groundwater in the direction of the hydraulic gradient.

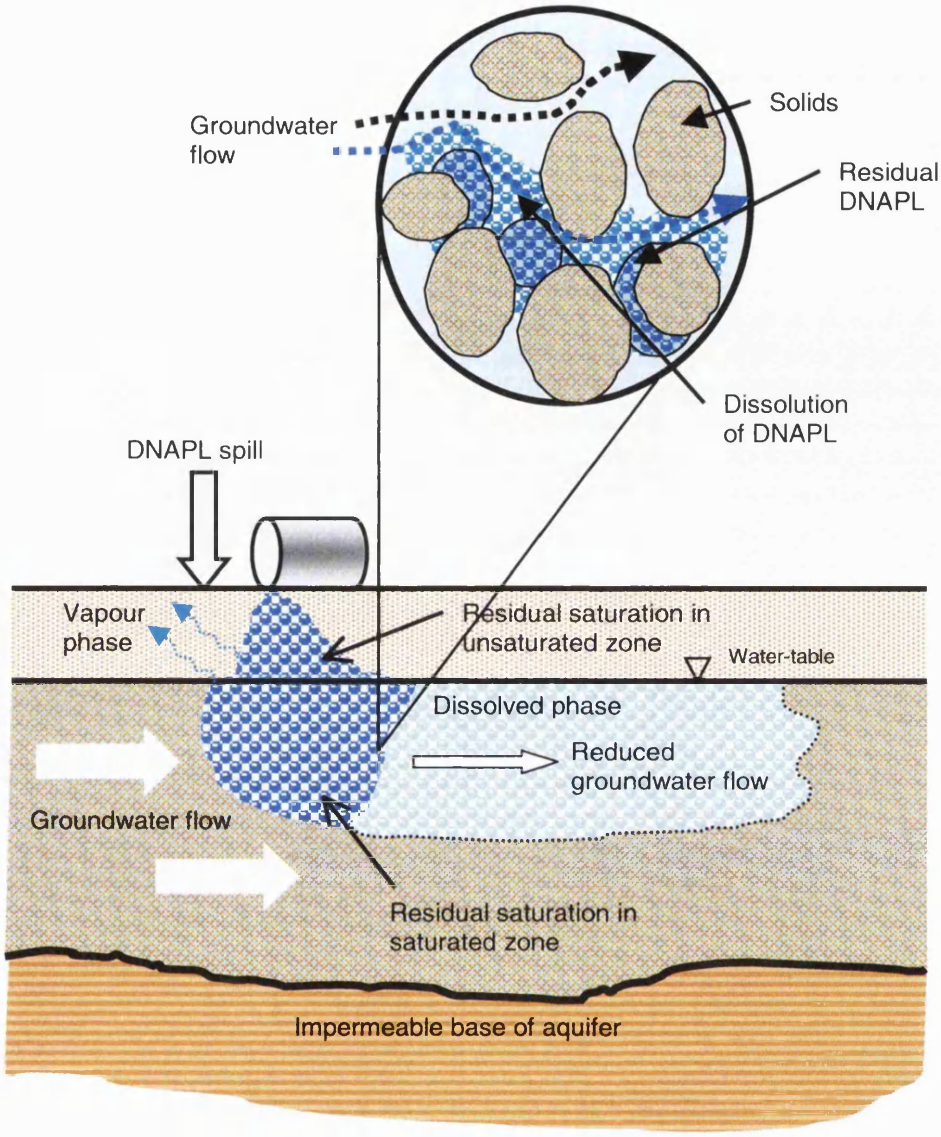

Figure 1-1 Schematic diagram of a DNAPL spill over an aquifer underlain with an aquitard. The presence of a residual saturation in the saturated zone leads to a decrease in groundwater velocity and the dissolution of DNAPL.

Dissolved contaminants spread as they move with groundwater by dispersion. Migration of aqueous phase solvent in the Permo-Triassic Sandstone aquifer may be via bedding plane joints as well as the matrix. During movement along bedding planes, diffusion into the matrix is likely to occur. Diffusion acts so as to initially attenuate solvent plume as aqueous phase solvent moves from a region of high concentration, possibly in the bedding planes, to a region of low concentration, the matrix. With time, however, this concentration gradient can be reversed hence the matrix can become a long term source of DNAPL contaminated water. This can have serious implications for remediation schemes.

If contamination of an aquifer occurs, there are three basic courses of action: to discontinue use of the aquifer and obtain alternative water supplies, to attempt to rehabilitate it, or continue to use the aquifer, but treat the water to remove the contaminants. The course of action taken will very much depend on several factors such as the use of the aquifer, the degree of contamination that has taken place, and the cost of a remediation programme.

Key areas that this thesis will address are:

- Lack of experimental data regarding the pressure required for a DNAPL to enter the saturated zone of consolidated sandstones
- The degree and impact of a DNAPL residual saturation on relative permeability in consolidated sandstones
- The role of solid phase chemistry on the wettability of sandstone-water-DNAPL systems
- The importance of pore structure on DNAPL distribution
- The relationship between physical and chemical properties of the rock and DNAPL saturation

1.3 ROLES AND RESPONSIBILITIES

The work described in this thesis was primarily funded by EPSRC and NERC under the Waste and Pollution Management thematic programme and comprises work carried out by a project team. Therefore, other scientists were involved in collecting and analysing some of the data used in the thesis. Those involved in the project are listed below.

Project Coordinator:	Adrian Lawrence, British Geological Survey
Project Manager:	John Bloomfield, British Geological Survey
Hydrogeochemist:	Daren Gooddy, British Geological Survey
Contaminant Hydrologist:	Mildred Bright, University College London
Isotope Analysis:	George Darling, British Geological Survey
Laboratory Analysis:	Peter Williams, British Geological Survey
Model Development:	John Barker, University College London

The contribution of various project staff to the different activities involved in the project are given below.

1. *Sample Selection.* Carried out jointly by Daren Gooddy and Mildred Bright using core taken from the British Geological Survey core store in Keyworth
2. *Physical Characterisation*
    a. *Porosity.* Peter Williams undertook 50% of porosity measurements, Mildred Bright undertook 30% and Daren Gooddy undertook 20%
    b. *Permeability.* Peter Williams carried out 95% of permeability measurements and Daren Gooddy the remaining 5%
    c. *Mercury Intrusion Capillary Pressure.* Peter Williams carried out 75% of the measurements, John Bloomfield 10%, Mildred Bright 10% and Daren Gooddy 5%
3. *Chemical Characterisation*
    a. *Surface Chemistry.* All surface chemistry extractions were carried out by Daren Gooddy. Analysis of the extracts was carried out by Daren Gooddy
    b. *Carbonate Isotopes.* Samples were prepared for isotopic analysis by Daren Gooddy. Sample analysis by mass spectrometer was carried out by George Darling.
4. *Development of pressure-saturation curve method.* All development work for the pressure-saturation curve method was carried out by Daren Gooddy. Daren Gooddy undertook 75% of the centrifuge experiments with the developed method and Mildred Bright carried out the remaining 25%.
5. *Development of relative permeability method.* All development work was carried out by Daren Gooddy under the supervision of John Bloomfield. Daren Gooddy carried out all experiments with the developed method. Analysis of PCE by GC-ECD was carried out by Daren Gooddy.
6. *Pore-scale modelling* The pore-scale model was developed by John Barker. The model was applied and tested by Daren Gooddy.

1.4 THESIS OUTLINE

This thesis has been divided in to ten chapters. Chapter 2 presents background to the problem including literature reviews on chlorinated solvents and their properties; the geology and hydrogeology of Permo-Triassic sandstones; factors influencing the

transport and fate of DNAPLs in sandstones; pore structure and percolation; and aquifer remediation strategies. Chapter 3 describes the project rational and includes the data and methodological development needs of the thesis. Chapter 4 is a comprehensive chemical and physical characterisation of the samples studied. Chapters 5 and 6 present the development of two methods, identified in Chapter 3 as methodological needs, to a) establish pressure saturation curves for a DNAPL-water-sandstone system and b) determine DNAPL relative permeability in sandstones. Chapter 7 uses a specially developed pore-scale model to describe sandstone matrix structures based on probability density functions and MICP data obtained in Chapter 4. Chapter 8 is a synthesis of the developed methods and considers the implications arising from the data discussion. Chapter 9 summarises the main conclusions of the thesis and Chapter 10 contains the references used. Table 1.1 identifies some of the key parameters used and discussed in the rest of the thesis.

Table 1-1 Key parameters used and discussed in this thesis

Parameter/Symbol	Description
ϕ	Effective porosity
k_g	Gas permeability
k_f	Relative permeability
Δk_f	Change in relative permeability
R_{sat}	Residual saturation
k_{rnw}	Relative permeability to non-wetting phase
k_{rw}	Relative permeability to wetting phase
$2\sqrt{k/\phi}$	Mean pore-throat diameter
PSD	Pore size distribution, also gives median pore diameter
P_0	Percolation pressure (van Genuchten)
P_d	Breakthrough pressure (Brooks-Corey)
m	Pore size distribution index (van Genuchten)
λ	Pore size distribution index (Brooks-Corey)
S_r	Wetting fluid residual (van Genuchten and Brooks-Corey)
S_m	Maximum water saturation
S_w	Wetting phase saturation
S_e	Normalised wetting phase saturation
Z	Coordination number

1.5 CHAPTER ONE SUMMARY

This chapter has introduced the scope and aims of the thesis and has also noted areas that are not covered. The nature of the problem that is being addressed has been presented with the paucity of data for DNAPL entry and behaviour in consolidated sandstone systems identified as key areas. The roles of different researchers associated with this work has been stated and lastly an outline of the other nine chapters in the thesis presented.

2 Hydrogeological Context

The following sections are intended to place the present work in a hydrogeological context. The main observations are summarised in Section 2.7

2.1 PROPERTIES OF CHLORINATED SOLVENTS

Chlorinated solvents were first produced in Germany in the late nineteenth century. Production in the USA started a few years later in 1906. Widespread use of chlorinated solvents in manufacturing industries began during World War II, and increased markedly during the next three decades. Contamination of groundwater by these compounds went largely unnoticed until the late 1970s. The denser-than-water nature of liquid chlorinated solvents has led to their becoming known as 'dense non-aqueous phase liquids' (DNAPLs). Examples of DNAPLs are given below Table 2.1.

Like petroleum products (*e.g.* diesel, fuel oil and unleaded petrol), chlorinated solvents are usually used in an organic liquid form (*i.e.* 'free product' liquids) but are generally found in water supplies in dissolved form at microgram per litre (µg/L) to milligram per litre (mg/L) concentrations. Unlike petroleum products, however, the chlorinated solvents are generally: 1) not noticed by taste or odour at typical groundwater contamination concentrations; and 2) not stopped at the water-table when released in DNAPL form to the subsurface in significant quantities. Once in an aquifer, DNAPL source material is usually very difficult to find. In contrast, when petroleum products are spilled in significant volumes, they float on the water-table where they can be detected easily. Historically, since chlorinated solvents in DNAPL form were found only rarely in wells, recognition of the problem posed by these compounds in groundwater had to await the development and general availability of analytical methods which allowed determination of dissolved organic compounds in water at the 1-100 parts in a thousand million. Of the many industrial organic chemicals identified in groundwater, the common chlorinated organic solvents (see Table 2.2) are the most ubiquitous.

Table 2-1 Organic compounds that are more dense than water.

Compound Class	Compound
Chlorinated Solvents	Tetrachloroethene
	Trichloroethene
	1,1,1-Trichloroethane
	Dichloromethane
	Trichloromethane (Chloroform)
	Tetrachloromethane (Carbon Tetrachloride)
	Chlorobenzene
Other Halogenated Organics	Benzyl Chloride
	Bromobenzene
	Bromodichloromethane
	Bromoform
	Dibromochloromethane
	1-Chloro-1-nitropropane
	1,2-Difluorotetrachloroethane
	1-Iodopropane
	Hexachlorobutadiene
	Pentachloroethane
Substituted aromatics, phthalates	Chloroanilines
and miscellaneous organics	Chlorotoluenes
	Nitrobenzene
	Benzyl butyl phthalate
	Diethyl phthalate
	Phenyl ether
	Tri-*o*-cresol phosphate
PCB mixtures	Aroclor 1221
	Aroclor 1232
Pesticides	Chlordane
	1,2-Dibromo-3-chloropropane
	Malathion
	Parathion

Table 2-2 Most common chlorinated solvents.

Chemical Name	Synonyms
Tetrachloroethene	PCE, perchloroethylene, tetrachloroethylene, ethylene tetrachloride, Nema, Tetracap, Tetropil, Perclene, Ankilstin, Didakene, PerSec
Trichloroethene	TCE, trichloroethylene, ethinyl trichloride, Tri-Clene, Trielene, Trilene, Trichloran, Trichloren, Algylen, Trimar, Trline, Tri, Trethylene, Westrosol, Chlorylen, Gemalgene, Germalgene
1,1,1-Trichloroethane	TCA, methyl chloroform, Chlorothene, Solvent 111, TRI-ETHANE
Tetrachloromethane	CT, carbon tetrachloride, carbon tet, perchloromethane, methylene tetrachloride.
Trichloromethane	CF, chloroform, methylene trichloride
Dichloromethane	DCM, methylene chloride, methylene dichloride, methylene bichloride

2.1.1 Fluid Properties

The high densities of the chlorinated solvents (1.2-1.7 g/cm^3) relative to that of pure water (1.0 g/cm^3) mean that if a sufficient volume of a typical chlorinated solvent is spilled, then the liquid may be able to penetrate the water-table. In the saturated zone, the unstable nature of the solvent movement and flow causes the solvent to form thin 'fingers' which can lead to the collection of large amounts of solvent in one or more 'pools' on top of less permeable layers (Schwille, 1988). Since a pool presents a very low cross section to on-coming groundwater flow, absolute removal rates of dissolved solvent from the pool will usually be very low (Fountain *et al.*, 1995; Geller and Hunt, 1993).

The relatively low viscosities of the chlorinated solvents allow relatively rapid downward movement in the subsurface. The subsurface mobility of chlorinated solvents increases with increasing density/viscosity ratios.

The low interfacial tension between a liquid chlorinated solvent phase and water allows the solvent to easily enter small fractures and pore spaces, enabling deep

penetration into the subsurface. Low interfacial tension also contributes to the low retention capacities of soils for chlorinated solvents (Dawson and Roberts, 1997).

The low absolute solubilities of the chlorinated solvents (typically a few hundred mg/L in water) mean that when a significant quantity of such a compound is spilled on the ground surface, liquid solvent will be able to migrate as a DNAPL phase in the subsurface. Thus DNAPL has the potential to accumulate into pools resting on top of low permeability layers. The low solubility will then allow such pools to persist as a groundwater contaminating source for decades to centuries (Bradford *et al.*, 2000). The high relative solubilities of the chlorinated solvents mean that a solvent spill can cause groundwater contamination at concentrations which are high relative to concentrations which appear harmful to human health. Also, the low partitioning to soil material exhibited by the chlorinated solvents means that soil and rock materials will bind these compounds only relatively weakly (Hayden *et al.*, 1997). This applies to both the saturated and unsaturated zones. So sorption to soils will not significantly retard the movement of a chlorinated solvent, and zones of contamination can grow essentially as quickly as the groundwater can move.

Table 2-3 Physical properties of six priority DNAPLs (adapted from Lawrence *et al.*, 1992).

Chemical Compound	Formula	Density (g/cm^3)	Kinematic Viscosity (mm^2/s)	Solubility at 25°C (mg/L)	WHO Max (µg/L)	Solubility/ Maximum ratio
Tetrachloroethene	C_2Cl_4	1.6	0.5	160	40	4×10^3
Trichloroethene	C_2HCl_3	1.5	0.4	1100	70	2×10^4
1,1,1-trichloroethane	$C_2H_3Cl_3$	1.4	0.6	720	2000	4×10^2
Tetrachloromethane	CCl_4	1.6	0.6	785	2	4×10^5
Trichloromethane	$CHCl_3$	1.5	0.4	8200	200	4×10^4
Dichloromethane	CH_2Cl_2	1.3	0.3	20000	20	1×10^6

The low degradabilities of the chlorinated solvent compounds, either by biological means or by abiotic-chemical reactions, means that subsurface lifetime of these chemicals can be very long (Barbee, 1994). Nearly all of the compounds produced by degradation reactions are relatively stable, and some are more hazardous in drinking water than the initial compounds (Vogel *et al.*, 1987).

Table 2.1 noted that organic chemicals other than the chlorinated solvents are classifiable as DNAPLs. These compounds include the halogenated benzenes, the polychlorinated biphenyls (PCBs), some pesticides, coal tar, and creosote. These chemicals have not been found in groundwater nearly as frequently as have the chlorinated solvents. There are several reasons for this. Firstly, compared to the chlorinated solvents, these other chemicals have not been used in as many industrial applications, or in quantities that are nearly as large. Secondly, they do not possess a combination of physical and chemical properties that impart a high propensity for widespread groundwater contamination. For example, some of these other DNAPL chemicals are much less soluble than the chlorinated solvents, and so they are much less mobile because they sorb strongly to soil materials. In the case of compounds like creosote and coal tar, they contain soluble components which are considerably more degradable in groundwater than most chlorinated solvents.

2.2 SOURCES OF GROUNDWATER CONTAMINATION BY DNAPLS

A major controlling factor over how a pollution plume develops and migrates in groundwater is the mechanism by which the contaminant enters the subsurface. An overnight leakage of 5,000 litres, for example, is likely to produce a very different plume to that caused by regular contaminated drainage infiltrating from a soakaway in a factory yard. The former is likely to result in the immiscible phase penetrating the aquifer deeply, whilst the later will produce shallow contamination in the aqueous phase. An indication of the types of activity that might produce contamination and the probability of the immiscible phase being present is given in Table 2.4.

Table 2-4 Mode of entry for a DNAPL into groundwater.

PROBABILITY OF IMMISCIBLE PHASE				
NATURE OF DISCHARGE		LOW	MEDIUM	HIGH
	CONTINUOUS	Leaking industrial sewers and lagoons	Infiltration from landfill waste disposal	Leaking underground storage tanks
	INTERMITTENT	Courtyard drainage	Effluent soakaways	
	SINGLE PULSE			Major spillages

2.2.1 Primary Sources

Primary sources are defined here as solvents spilled, discharged or leaked into the surface. These could include leakages from storage tanks, soakaway drainage and landfills.

a) DNAPL - Solvents spilled or leaked into the surface will migrate through the sandstone matrix to the water-table. Large spillages may result in DNAPL penetration to the water-table. Rates of downward movement are difficult to predict but, where sandstone pore-throat openings are large, could be relatively rapid.

b) Continuous source leached by precipitation – Organic solvents may be leached, by precipitation, from the contaminated soil zone. Transport of aqueous phase solvent through the unsaturated zone would be similar to that described for inorganic solutes, such as nitrate (Kinniburgh *et al.*, 1999) for which downward rates of flow of about 0.5-1 metres per year for the bulk of the contaminant are considered typical.

c) Intermittent sources under high hydraulic loading – In many instances aqueous phase solvents have been discharged into the ground, soakaways or lagoons under high hydraulic loading such that rapid transport through the unsaturated zone can be anticipated.

In both b) and c), once at the water-table, the solvent will migrate in the direction of groundwater flow and its movement will be controlled by processes already

described. The contaminant plume is likely to remain close to the water-table unless subject to strong vertical groundwater gradients within the aquifer, since the density contrast between the contaminated and uncontaminated water is very small.

2.2.2 Secondary Sources

In many cases groundwater contamination is only discovered after the primary source at the surface has stopped or been exhausted (Lawrence *et al.*, 1991). However, solvent that has already entered the aquifer will act as a secondary source (or subsurface) source and will contribute to the aqueous phase plume. Secondary sources include:

a) Residual DNAPL within the unsaturated zone

b) Residual DNAPL within the saturated zone

c) DNAPL dissolved in LNAPL (light non-aqueous phase liquids such as petroleum hydrocarbons) present in the unsaturated zone or floating on the water-table

d) Aqueous phase solvent in the unsaturated zone matrix

e) Aqueous phase solvent in the saturated zone matrix

In the case of secondary sources a), c) and d) the resulting contaminant plumes are likely to be concentrated close to the water-table. Conversely, in b) and e), contaminant plumes may occur throughout the entire depth of the aquifer. Highest concentrations may occur in less permeable horizons within the aquifer, where DNAPL may have originally been retained.

Groundwater contamination by halogenated solvents is a complex process and is not well understood. Firstly, the source term is rarely well defined. The quantities leaked or spilled and the time period over which release of the contaminant occurred are often extremely uncertain. In the case of disposal through landfill sites, where many hundreds of small liquid sources may have been disposed each year, the source may be regarded as producing a spectrum of overlapping plumes rather than a single continuous plume.

Secondly, transport through the unsaturated zone can be highly variable and is dependent, amongst other factors, upon whether DNAPL is present and the hydraulic loading of any aqueous phase solvent. In addition, the presence of multiple phases (NAPL, aqueous phase and vapour phase) will further complicate the system and hence increase uncertainty with regard to predicting fate and transport.

Thirdly, even within the saturated zone where only two phases are present (NAPL and aqueous phase) the heterogeneity of the aquifer can make prediction of contaminant migration difficult. At any given contaminated site a multitude of processes may occur e.g. spreading of DNAPL along bedding planes; migration of the vapour phase; transfer to the aqueous phase; DNAPL dissolving in LNAPL at the water-table; transfer to the aqueous phase of DNAPL dissolved in LNAPL following lateral migration; sorption onto aquifer solids. This raft of possible processes greatly increases the complexity of any site investigation (Hunt *et al.*, 1988).

2.3 SANDSTONE CHARACTERISTICS

2.3.1 Sands and Sandstones

Sands and clastic sediments, in general, differ from igneous and other crystalline rocks in possessing a framework of grains. Unlike the grains of the igneous and related rocks which are in continuous contact with their neighbours, the grains in a sand are generally in tangential contact only and so form an open, three-dimensional network (Netto, 1993). As a consequence, sands tend to have a high porosity. The unequal distribution of stress along grain boundaries may lead to solution at points of pressure and deposition elsewhere, increasing the surfaces of contact and decreasing the pore space. Such action, coupled in some cases with the introduction of cementing materials, leads to the ultimate end-product, a rock with grains in continuous contact and with minimal porosity. In this manner, a sand with tangential contacts and a porosity of 35-40% is converted to an interlocking crystalline mosaic with very low or zero porosity.

Sandstones are principally composed of silica and contain a mixture of mineral grains and rock fragments coming from naturally disaggregated products of erosion of rocks of all kinds. The total variety of rock types in any given watershed may be represented in the sediment product. A given specific sandstone might be expected to have a large variety of minerals but in fact the abundant minerals of sandstones belong to a few major groups.

The mineral composition of sandstones may be drastically altered by dissolution, precipitation, or alteration during diagenesis (Pettijohn *et al.*, 1972). In this process unstable minerals may be lost completely or partially. New minerals, carbonates in particular, may be added by precipitation from solution.

The carbonate minerals in sandstones are both detrital and chemically precipitated, with the latter process by far predominating. Detrital carbonate is abundant in calcareous sands as skeletal fragments, oolites and faecal pellets, none of which are derived from distant sources. Such debris may also be admixed in varying, but usually minor amounts, in terrigenous sandstones. Detrital carbonate grains are also derived from source regions outside the basin and are present in some sandstones. Such grains have rounded, abraded boundaries. High relief and arid climate both favour terrigenous carbonate. The solubility of carbonate plus its softness and cleavage all decrease the probability of its survival by stream transport.

Calcite and dolomite are abundant in sandstones as pore filling and replacement cements of post-depositional origin. Some pore filling cement may be recrystallised from originally detrital carbonate grains or may be a precipitate from an aqueous solution in an originally empty pore. In contrast to the carbonate of many modern sediments, the sandstone cements are apparently very pure, with no excess Mg in the calcite and no excess Ca in the dolomite.

The iron-rich carbonates are less abundant than calcite and dolomite in most sandstones, but are abundant constituents of some, notably as siderite and ankerites (iron-rich dolomites). Rhodochrosite is known in some concretionary forms in sandstones, but has rarely been recognised as cement.

The precipitation of calcite and dolomite is primarily influenced by the variables of Ca and Mg abundance and the pH of the environment, whereas the iron and manganese carbonates have an additional dependence on the oxidation-reduction balance of the environment. Since iron and manganese can be in carbonate minerals only in their reduced state, a redox potential is immediately established. The most probable reducing agent responsible for the reduction of iron is organic matter.

Organic matter in sandstones is a biochemical precipitate characteristic of the environment. The organic matter always has been profoundly altered by diagenesis. The varieties of organic matter in sandstones range from oil and gas to solid particles of high carbon content material. Sandstones in general are characterised by extremely small amounts of organic matter, less than 0.1 percent as opposed to shales and limestones. Most of the fluid organic matter, oil and gas, has been introduced into the sandstone after deposition by migration from the beds in which the organic matter was indigenous.

The organic matter that is native to sandstones is dominantly detrital. The presence of oxygen and the generally high permeability of sandstones promotes oxidation of much of the organic matter.

2.3.2 The Permo-Triassic Aquifer

The Permo-Triassic sandstones of the UK are typical of many other consolidated sandstone aquifers, such as the Cretaceous aquifers of the Colorado Plateau (Driscoll, 1986) and the Northern Great Planes aquifer (Whitehead, 1996), and they are broadly representative of the Permo-Triassic sandstone aquifers found throughout Europe, for example, The Upper Triassic Keuper Sandstone of Germany. They form the second most important aquifer in the UK, supplying around 25% of licensed groundwater abstractions in England and Wales (Monkhouse and Richards, 1982). The aquifer provides important groundwater resources, especially in northern and central England, where the Sherwood Sandstone Group forms the most important aquifer. A number of large towns obtain their water supplies at least partly from the Permo-Triassic sandstones, among them are Manchester, Liverpool, Birmingham, Leeds, Doncaster and Nottingham. Single well yields from the aquifer can be up to 10,000 m^3/d in the Midlands, although elsewhere they are lower with a 50% probable yield of 200 m^3/d for the country as a whole suggested by Monkhouse and Richards (1982).

The Permo-Triassic sandstones outcrop in the southwest, central, north-east and north-west of England, and in the Vale of Clwyd. In general, they are preserved within the onshore extensions as a number of major offshore sedimentary basins. The sandstones have variable and often substantial, thickness. In Lancashire, the Sherwood Sandstone Group is up to 600 m thick, and around the northern edge of the Cheshire basin the sandstones approach 1000 m in thickness. The Sherwood Sandstones Group is about 90 m thick in south Nottinghamshire, increasing to 180 m further north in Yorkshire. The combined thickness of the Permo-Triassic sandstones in the Vale of Eden and along the Cumbrian coast exceeds 900 m (Day, 1986).

In the south-west and north-east of England, the sandstones dip to the east and become confined down dip by the Mercia Mudstone Group, the aquifers feathering out to the west. In the west Midlands the aquifer occurs in a number of basins and in the north west, dip beneath the Irish Sea. The aquifer properties of the sandstones are greatly affected by their sedimentary structure and by post-depositional diagenesis.

The absence of significant sedimentary compaction and the relatively high porosity of the Permo-Triassic sandstones suggests that, while they were initially cemented, much of the primary cementation has subsequently been dissolved. Strong (1993) has identified a variety of cements now found including calcite, dolomite, various forms of anhydrite, halite, iron oxide and clay minerals. Anhydrite (calcium sulphate) is found deep in the Wessex basin (for example, the Winterbourne Kingston Borehole) and in north eastern England at Cleethorpes. It has been suggested (Strong and Mildowski, 1987; Knox *et al.*, 1984) that dissolution of anhydrite has formed the majority of the secondary porosity. In the north-west and Birmingham area there is less calcite towards the top of the aquifer than at depth. Deeper flowing waters tend to be supersaturated with calcite most likely from mineral dissolution. The low concentrations of calcite may also reflect recent anthropogenic activity and deposition of acid precipitation (Moss and Edmunds, 1992).

A variety of clay minerals may be present within pore spaces (Burley, 1984). For example kaolinite may be present as a late freshwater pore infilling. Illite can form structures across pores, reducing permeability by orders of magnitude without substantially affecting porosity.

2.3.3 Hydrogeology

The Permian sandstones and Triassic Sherwood Sandstones Group, which when combined comprise the Permo-Triassic sandstones, form a major aquifer. Where marls are present in the Permian an aquitard is formed, effectively separating the Permian sandstones from the overlying Triassic sandstones. Another aquitard is formed by the Mercia Mudstone Group, which overlies and confines the Sherwood Sandstone Group. Generally the Mercia Mudstone acts as an aquitard and as such confines the Sherwood Sandstone Group. However at a local scale and especially around the mudstone/sandstone junction, there is considerable interlayering of sandstones and mudstones in fining up cycles.

Fracture flow can locally play a significant role in saturated groundwater flow throughout the Permo-Triassic sandstones. The discontinuities include bedding plane fractures, including joints of either tectonic or diagenetic origin, and solution enlarged fractures (Lovelock, 1977). They can provide preferential flow paths and have a significant effect on the physical properties of the aquifer. Adjacent to pumping

stations, fractures may be developed or enhanced as sand is removed from the fractures into the borehole (Price *et al.*, 1982). Other authors have noted the presence of infilling in fractures so reducing permeability (Wealthall *et al.*, 2001). The hydraulic effects of faults in the Permo-Triassic sandstones vary widely, ranging from impermeable features which form barriers to groundwater flow, to high transmissivity features which may act as recharge boundaries.

Matrix hydraulic conductivity varies according to lithology. Grain size and geometry, particle size distribution and the degree and extent of cementation are of primary importance, greatly influencing the intergranular hydraulic conductivity and hence the general transmissivity distribution of the aquifer, due to the variable nature of the sediments.

A number of general aquifer properties are common to all of the Permo-Triassic sandstones of England and Wales. Both matrix hydraulic conductivity and porosity are functions of cementation, compaction, and the size and extent of sorting of the grains. The nature and degree of cementation affects both porosity and hydraulic conductivity, but by different mechanisms. Hydraulic conductivity is controlled by the size of the pore-throats and the degree to which these are interconnected (Bloomfield *et al.*, 2001). Therefore, highly porous sands only have high intergranular hydraulic conductivities if the pore-throats are also large.

Spatially, the Permo-Triassic sandstone aquifer is both heterogeneous and anisotropic. Lateral and vertical lithological and structural variations affect both horizontal and vertical flows. The anisotropy and heterogeneity resulting from the fine grained layers causes deviations from ideal aquifer flow behaviour making prediction problematic. Temporally, the presence of interlayered sediments of variable permeability has a major influence on the short term response of the aquifer. The permeabilities characterising the Permo-Triassic sandstone aquifer are highly scale dependent. Core-scale measurements can show the matrix properties but do not indicate the influence of fractures.

2.4 TRANSPORT AND FATE OF DNAPLS IN SANDSTONES

Solvent transport mechanisms are complex in homogeneous media (Schwille, 1988) but these complexities are compounded in heterogeneous media such as the Permo Triassic sandstones (Eastwood *et al.*, 1991). A spillage of a significant volume of DNAPL could

result in the solvent reaching the water-table within weeks or months of the spillage. Conversely, slow release of solvent from contaminated soil as a result of leaching by precipitation, could result in the solvent not reaching the water-table for many years.

Many of the contamination problems occurring in Permo-Triassic sandstone aquifers within the UK result from the use of solvents several decades previously (Burston *et al.*, 1993; Rivett *et al.*, 1990). This delay between spillage or release of solvents at the surface and their detection in a public-supply borehole reflects both the extended transport times that can be anticipated and the fact that routine groundwater monitoring for these compounds only commenced in the UK during the early-mid 1980s. Resistance of these compounds to chemical or biochemical breakdown in the subsurface environment (Aurand, 1981; Semprini *et al.*, 1990; Jackson 1998) has ensured that the chlorinated solvents persist in groundwater following their disposal and handling many years or even decades previously (Lawrence and Foster, 1991; Lerner *et al.*, 1993).

In the unsaturated zone, larger pores and fractures are generally drained and only the smaller pores retain water. DNAPL will enter the larger pores as it will tend to be repelled by water occupying smaller pores. The solvent content of the unsaturated zone will accordingly be dependent upon the antecedent moisture content of this zone. Once the main DNAPL body has passed through, some solvent will remain, infilling some of the pore spaces. The fraction of the DNAPL that is retained is referred to as the residual saturation, which is the volume of NAPL trapped in the pores relative to the total pore volume. Residual saturation for granular aquifers is typically in the range 1 to 60% (Hunt *et al.*, 1988) which contrast strongly with the much smaller values found in fractured aquifers (Mackay and Cherry, 1989). The implication of this observation is that for a similar spillage, the DNAPL may penetrate less deeply in granular aquifers such as a sandstone than in a heavily fractured aquifer.

The residual solvent within the unsaturated zone following the downward migration of DNAPL will act as a secondary or subsurface source of the contaminant and will remain so until all the solvent has been mobilised by:

1) dissolution and leaching by waters percolating through the unsaturated zone to the water-table

2) volatilisation – transfer of solvent molecules from the liquid to vapour phase

3) dissolution and leaching by groundwater within the zone of water-table fluctuation – although in fact water-table fluctuations in the Permo-Triassic sandstones are usually small and range between 1-2 metres.

These processes are likely to be slow so residual solvent may remain a significant contaminant source within the unsaturated zone for a considerable period of time.

Modelling DNAPL migration in the unsaturated zone is very difficult given the uncertainty as to the volume and shape of bodies of residual solvent and the complexity of a three-phase system (Busby *et al.*, 1995; Kosugi, 1996; Lenhard, 1992). The models developed are commonly suitable for homogenous systems and difficult to apply to a heterogeneous aquifer (Ataie-Ashtiani *et al.*, 2002; Bradford and Leij, 1995; Lenhard and Oostrom, 1998).

Where a spillage is sufficiently large that the total volume of DNAPL spilled exceeds the saturation capacity of the unsaturated zone then the DNAPL will reach the water-table and contaminate the aquifer directly. The capillary fringe may initially obstruct the entry of DNAPL into the saturated zone. This may lead to temporary spreading of DNAPL at the water-table. However, when a sufficient volume of DNAPL has been released the water-table will be penetrated.

For a DNAPL to enter a water-table the pressure exerted by the DNAPL must exceed the capillary or excess pressure across the interface between itself and the water.

2.4.1 Capillary Pressure

In the interior of a homogeneous fluid, a molecule is surrounded by other molecules exerting cohesive forces between one another. At the interface between two immiscible fluids however, there are few if any like molecules across the interface. A molecule at the interface is attracted to molecules of its own phase by a force greater than the force attracting it to molecules of the immiscible phase across the interface. This unbalanced force draws molecules along the interface inward and results in the tendency for the fluid-fluid interface to contract. If the interface is stretched, it acts like an elastic membrane. The restoring force seeking to minimize the interfacial area between the two immiscible fluids, is called the interfacial tension, σ. When encountered between a liquid and a gas, this same force (per unit length) is called the surface tension, λ.

For a system of two immiscible fluids (e.g. water and organic liquid) in contact with a solid phase both the cohesive forces within the fluids and the adhesive forces between the solid and each of the fluids are at work at the line of contact. If the adhesive forces between the solid and the water phase are greater than the cohesive forces inside the water itself and greater than the forces of attraction between the organic phase and the solid, then the solid-water contact angle, α, will be acute and the water will preferentially wet the solid.

By convention, the wettability of a system is measured through the aqueous phase (Figure 2.1). A system is considered to be water wet if the contact angle is <70°, and oil or solvent wetting if the contact angle is >110°. If the contact angle is in the range 70-110° then the system is described as neutral wetting (Anderson, 1987a). It has been observed in water-hydrocarbon systems that sandstones tend to be water-intermediate wetting, whereas carbonate rocks tend to be intermediate or oil wetting (Lake, 1989; Taylor *et al.*, 2000). Most saturated media are preferentially wet by water. The contact angle provides the only direct measurement of wettability but is a difficult measurement to make under laboratory conditions without compromising the integrity of true environmental conditions.

As a result of the contact angle, a meniscus is formed between the fluid phases. As tubes (or capillaries) get narrower so too does the radius of curvature between the two immiscible phases. Similar to the curvature produced by a pressure difference across a membrane, the presence of curvature implies a pressure difference across the fluid-fluid interface, called the capillary pressure.

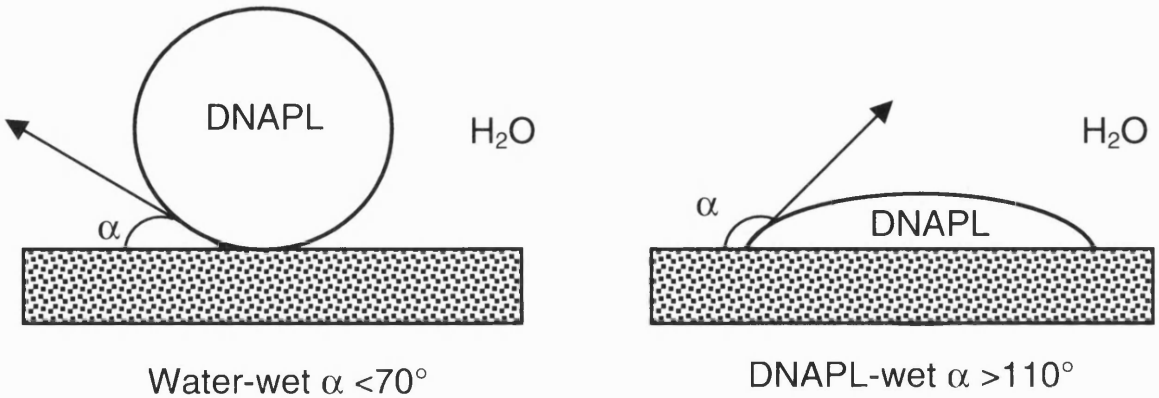

Figure 2-1 Schematic diagram showing a DNAPL-water-solid system under water wetting and DNAPL wetting conditions.

Capillary pressure causes porous media to draw in the wetting fluid and repel the nonwetting fluid due to the dominant adhesive force between the wetting fluid and the media solid surfaces. For a water-NAPL system with water being the wetting phase as in an aquifer, capillary pressure equals the NAPL pressure minus the water pressure. The geometry of an interstitial pore space is obviously highly complex. Nevertheless, it is possible to conceive of a network of interstitial spaces connected by pore-throats of a smaller characteristic dimension. A version of the Washburn equation (below) predicts the threshold value of the capillary pressure that must be exceeded for DNAPL to pass through a pore-throat of radius *r*.

$$\Delta P = \frac{2\sigma \cos\alpha}{r} \tag{2.1}$$

Where ΔP is the change in entry pressure, σ is the interfacial tension and α is the contact angle. Thus, DNAPL is denied access to an interstitial pore until the capillary pressure exceeds the threshold value associated with the largest throat already in contact with the DNAPL. Once entry has been achieved, the DNAPL moves into the pore. The water-DNAPL interfaces then position themselves across regions of the pore space that support radii of curvature consistent with the prevailing capillary pressure.

The pressure exerted by the DNAPL is:

$$H\Delta\rho g \tag{2.2}$$

Where H is the height of the DNAPL column, $\Delta\rho$ is the density difference between DNAPL and water, and g is acceleration due to gravity.

Equating these pressures for a circular capillary tube gives:

$$H = \frac{2\sigma \cos\alpha}{r\Delta\rho g} \tag{2.3}$$

In the case of tetrachloroethene the interfacial tension is reported by Dean (1979) as 0.044 N/m although Harrold *et al.* (2002) measured a lower value of 0.038 N/m. Tetrachloroethene has a density of 1.6 g/mL, therefore the density difference with water is 0.6. Dean (1979) also determined a contact angle of 33-45° for a water -(fine-coarse) sand system. A contact angle of 40° and a density difference of 0.6 g/mL have been used in equation (2.3) to produce a plot showing the height of

column of solvent required to enter various pore-diameters for four different interfacial tensions (0.044 N/m, 0.038 N/m, 0.022 N/m and 0.005 N/m) as shown in Figure 2.2.

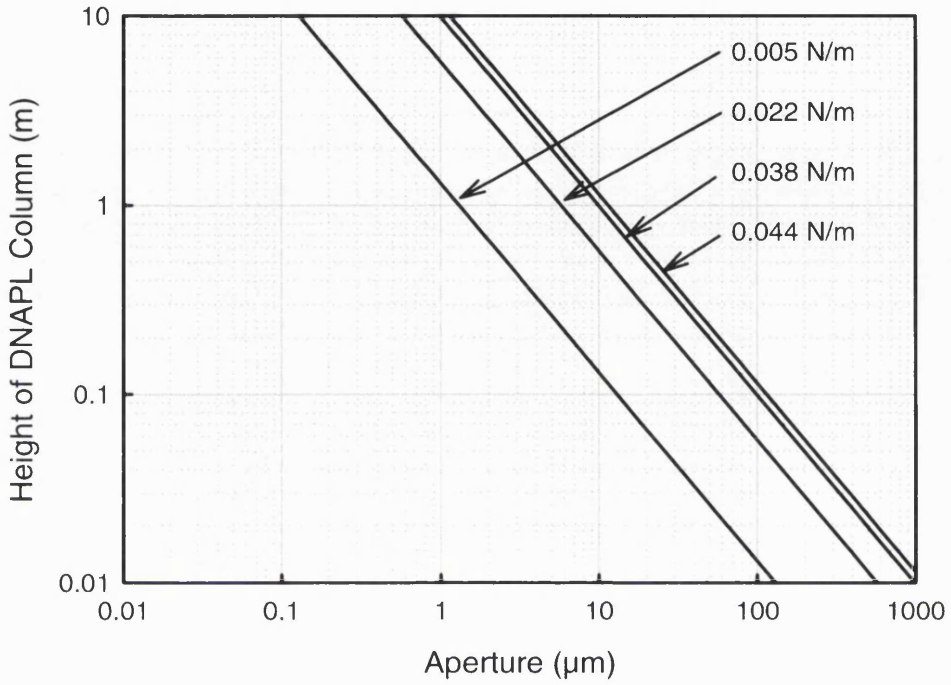

Figure 2-2 Relationship between aperture size and head of DNAPL required to invade a capillary for a contact angle of 40° and ΔP= 0.6 g/mL based on Equation 2.3, for four σ values.

2.4.2 Measuring Capillary Pressures

Capillary pressure measurements are essential for the complete characterisation of the movement of immiscible phases through an oil reservoir or aquifer and for determining the degree of penetration likely to occur in an aquifer system after the spillage of a DNAPL. A plot of capillary pressure against saturation for a rock core, called the capillary pressure curve, may be a useful way of estimating the potential risk to groundwater from any given DNAPL spill incident. These curves also provide data on the irreducible water saturation and the entry pressure of LNAPL or DNAPL into a water-saturated reservoir.

Two main types of methods are available to determine capillary pressure-saturation $P_c(S_w)$ relations in porous media: i) displacement methods based on establishing successive states of hydraulic equilibrium, and ii) dynamic methods based on establishing successive rates of steady flow of wetting and non-wetting fluids. Displacement methods are used more commonly than dynamic methods.

Three static (non-flow) methods of obtaining capillary pressure curves are the porous plate, mercury injection, and centrifuge methods. The centrifuge method compares favourably with the other methods of preparing capillary pressure curves. The porous plate method may require weeks whereas the centrifuge can take only days. Any fluid combination (gas-oil, gas-water, water-LNAPL, water-DNAPL, gas-water-LNAPL, gas-water-DNAPL) can be used in the centrifuge. The centrifuge method is non-destructive and the results are reproducible. Both drainage and imbibition curves can be produced. Interphase differences up to 7 MPa can be developed in an air-liquid system, extending the range of permeability down to one millidarcy (mD) or less. Unconsolidated samples can be evaluated on the centrifuge.

The seminal work on the centrifuge method was by Hassler and Brunner (1945). Slobod *et al.* (1951) demonstrated the simplicity, reproducibility and speed in the centrifuge method, and its good correlation with the porous plate method. They also indicated the very high pressure differences between the phases. Marx (1956) discussed the use of the centrifuge in a gravity drainage investigation. Hoffman (1963) performed dynamic (time-dependant) measurements of saturation in core samples using a constantly accelerating centrifuge, with considerable time savings. Donaldson (1969) used the centrifuge for capillary pressure measurements in a study of wettability. Szabo (1970) extended the method to include imbibition capillary pressure curves. He also used the centrifuge to measure electrical resistivity as a function of saturation. Samaroo and Guerrero (1981) used a centrifuge to measure the effects of temperature on drainage capillary curves. Hagoort (1980) and van Spronsen (1982) have both used the centrifuge to make two- and three-phase relative permeability measurements. More recently researchers have been focusing on using ultracentrifuges to obtain higher quality continuous data and to improve iterative methods for calculating capillary pressure curves (Ruth and Wong, 1990; Kantzas *et al.*, 1995; Nikakhtar *et al.*, 1996). Kinniburgh and Miles (1983) used immiscible fluid displacement of water from consolidated and unconsolidated media by using the centrifuge but were not interested in investigating pore-entry pressure relationships. It is only very recently that the centrifuge has been used to measure pore-entry pressure for solvents in consolidated media (Gooddy *et al.*, 1999; Harrold *et al.*, 2001; Pantazidou *et al.*, 2000).

The simple model developed by Hassler and Brunner (1945) assumes that, at equilibrium, there is a network of DNAPL filled pore-throats that are connected to the

surface layer of DNAPL. The aqueous phase is also assumed to form a similar nexus. The aqueous phase is only displaced from pore-throats in which the driving pressure, due to the density difference between the two phases, exceeds the capillary pressure retaining the water in the pore-throats.

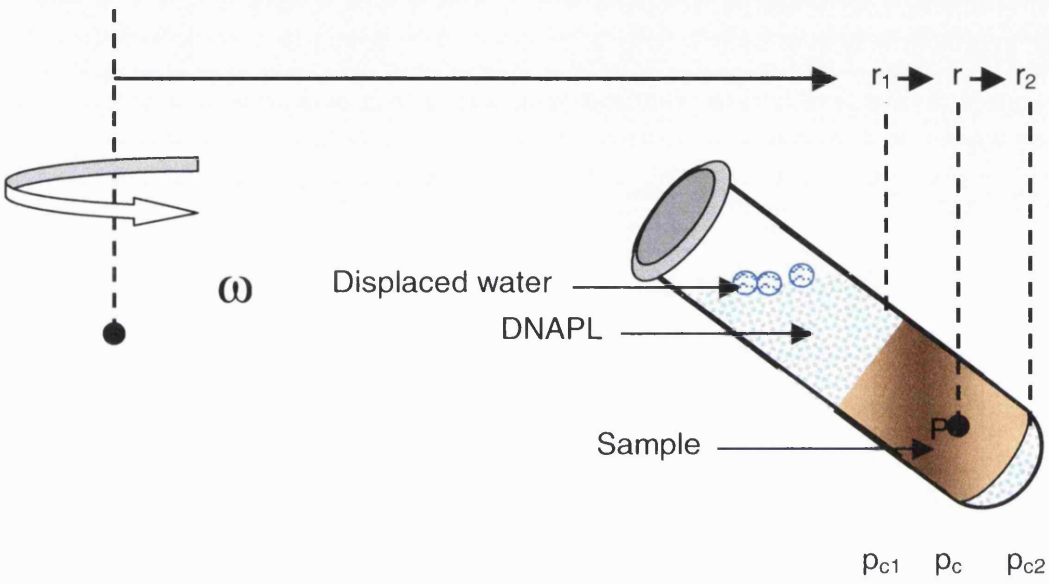

Figure 2-3 DNAPL displacement of water using a fixed-angle rotor.

The driving pressure at any point in the sample depends on the distance to the centre of rotation and varies continuously through the sample (Figure 2.3). The average residual water saturation is a weighted average of the residual water saturation at each point in the sample.

At equilibrium, the driving pressure will be balanced by a capillary pressure, p_c. Consequently, the capillary pressure gradient at a point P distance r from the centre of rotation (Figure 2.3) is related to the angular velocity, ω, and density difference between the fluid phases by

$$\frac{dp_c}{dr} = \Delta\rho\omega^2 r \qquad (2.4)$$

where

$$\Delta\rho = \rho_{dnapl} - \rho_{water} \tag{2.5}$$

and

$$\omega = \frac{2\pi v}{60} \tag{2.6}$$

where ρ_{dnapl} and ρ_{water} are the densities of the DNAPL and water respectively, and v is the centrifuge speed in rpm (ω is in s^{-1}). Integrating equation 2.4 between the inner surface of the sample, distance r_1 from the centre of rotation, to point P and assuming that the capillary pressure at the inner surface, p_{c1}, is zero gives the driving pressure at P

$$p_c(r,\omega) = \int_{r_1}^{r} \Delta\rho\omega^2 r\delta r = \frac{\Delta\rho\omega^2}{2}\left(r^2 - r_1^2\right), \tag{2.7}$$

In particular

$$p_{c2}(\omega) = \frac{\Delta\rho\omega^2}{2}\left(r_2^2 - r_1^2\right) \tag{2.8}$$

where p_{c2} is the capillary pressure at the base of the sample distance r_2 from the centre of rotation.

The average saturation of the sample, $\bar{S}(\omega)$ can be related to the saturation vs. capillary pressure curve by integrating the saturation, $S(P_c)$ vs. distance curve for a sample of uniform cross section

$$\bar{S}(\omega) = \frac{1}{r_2 - r_1}\int_{r_1}^{r_2} S(p_c)dr \tag{2.9}$$

By using equations 2.7 and 2.8, assuming p_{c1}=0 and changing variables, Kinniburgh and Miles (1983) show

$$\bar{S}(\omega) = \frac{r_2 + r_1}{2p_{c2}r_1}\int_{0}^{p_{c2}} \frac{S(p_c)dp_c}{\left[1 + (p_c/p_{c2})(r_2^2/r_1^2 - 1)\right]^{0.5}} \tag{2.10}$$

The Hassler-Brunner theory rests on several assumptions that should be kept in mind whenever interpreting data. The model is one-dimensional. Centrifugal acceleration and fluid flow are assumed to be parallel to the axis of the core and the theory is based on the "bundle of capillary tubes" model of the porous medium.

The bundle of capillary tubes model is the simplest possible model of pore structure for capillary pressure purposes. It assumes a bundle of cylindrical capillary tubes of different diameters and equal lengths, where every capillary has a uniform diameter along its entire length. The drainage capillary pressure curve can be interpreted in terms of this simple model by postulating that at the threshold capillary pressure of penetration of the nonwetting fluid, the largest capillary gets penetrated and filled, and at increasing capillary pressures, increasingly smaller tubes become filled. It is evident that this simple model is incapable of accounting for capillary hysteresis caused by entrapment of DNAPL and for the existence of irreducible wetting and residual nonwetting phase saturation (Dullien, 1992).

2.4.3 Empirical Capillary Pressure-Saturation Relationships

In materials where there is a range of pore sizes, the capillary behaviour of a material is a function of the material saturation and it can be described graphically using capillary pressure-saturation curves, $P_c(S_w)$. A number of empirical functions have been proposed to describe the relationship between capillary pressure and saturation (Brooks and Corey, 1966; van Genuchten, 1980; Kool and Parker, 1987; Lenhard and Oostrom, 1998). Among the most popular is the van Genuchten (1980) equation. This was developed to describe capillary pressure-saturation phenomena in structured soils, but has been applied extensively to a range of materials.

$$P_c = P_0\left(S_e^{-\frac{1}{m}} - 1\right)^{1-m} \tag{2.11}$$

where P_0 is the characteristic capillary pressure and m is a fitting parameter determined by the pore-size distribution. Another popular expression is the Brooks-Corey (1966) equation:

$$P_c = P_d S_e^{-\frac{1}{\lambda}} \tag{2.12}$$

where P_d is the displacement pressure for the medium, and λ is a pore-size distribution index.

In both these expressions, S_e is the normalised wetting fluid saturation defined as:

$$S_e = \frac{S_w - S_r}{S_m - S_r} \tag{2.13}$$

where S_r is the residual saturation, S_m is maximum water saturation and S_w is the wetting phase saturation. The parameters m, P_0, and S_r in the van Genuchten equation are evaluated by fitting the equation to experimental data. The values of P_d, λ, and S_r in the Brooks-Corey equation are similarly determined. Values of λ, the Brooks-Corey pore size distribution index, must be greater than zero: values typically range from about 0.5 for materials with a large range of pore sizes to 4 for very uniform materials. In the van Genuchten equation values for m must fall between zero and one and they usually range from 0.35 to 0.8 (Morel-Seytoux *et al.*, 1996).

Figures 2.4 and 2.5 show how the shape of curves change for different values of P_0 and m for the van Genuchten equation and P_d and λ for the Brooks-Corey equation respectively.

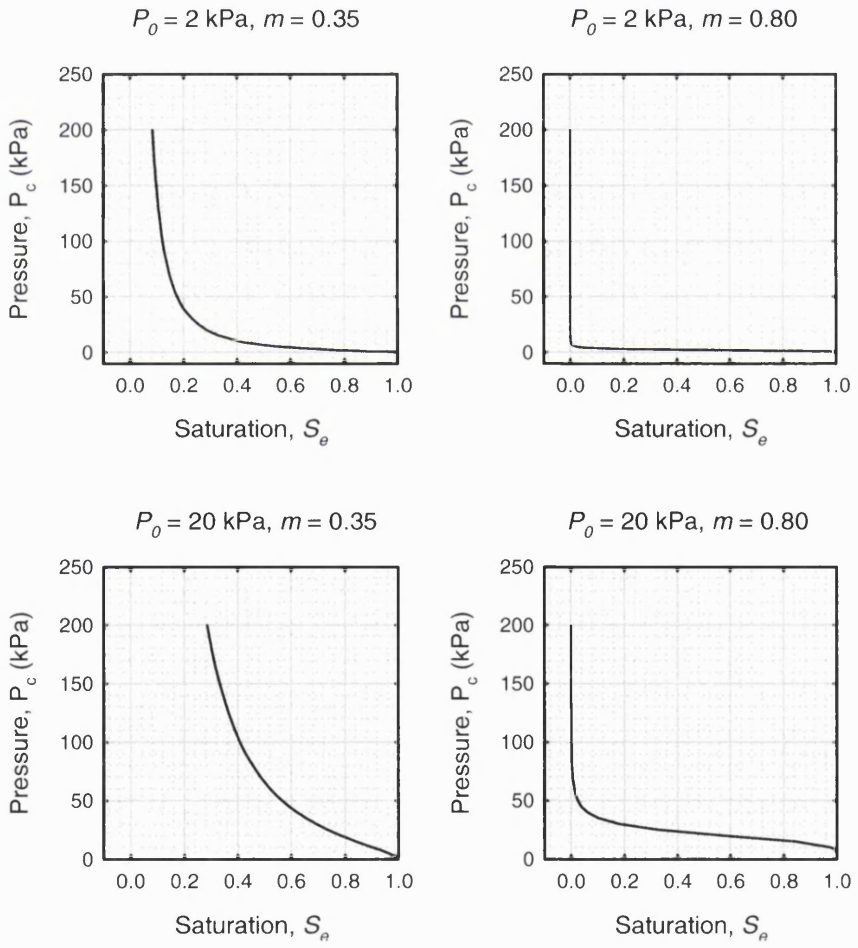

Figure 2-4 Typical curves for the van Genuchten equation based on different values of P_0 and m.

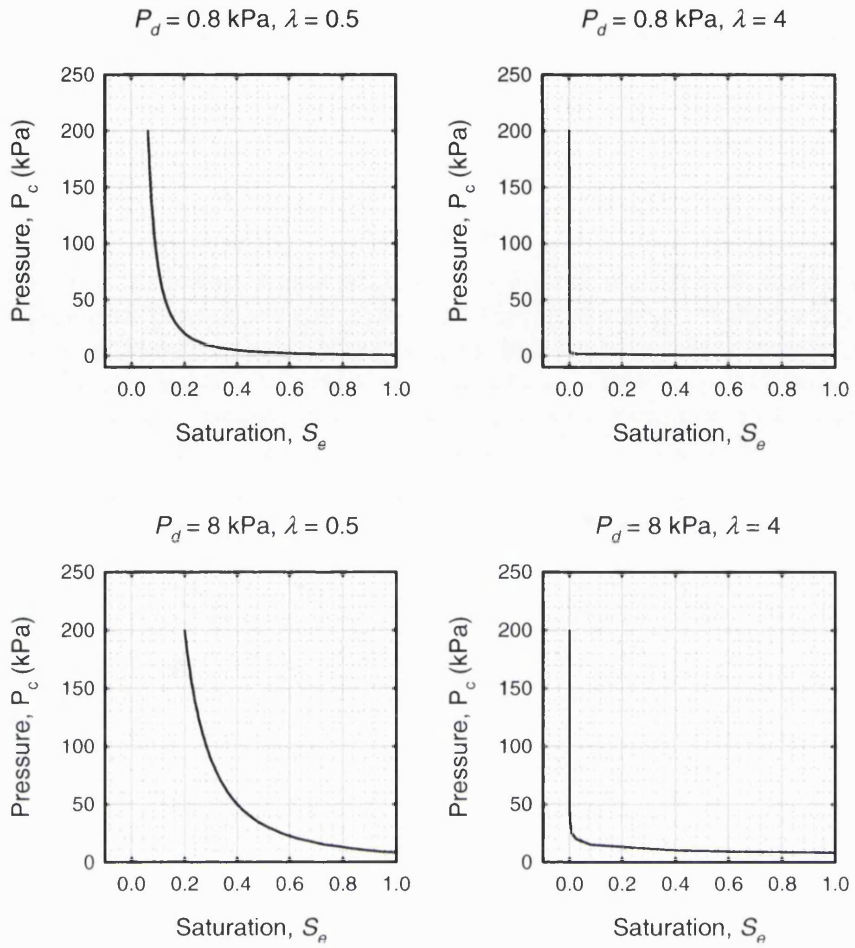

Figure 2-5 Typical curves for the Brooks-Corey equation based on different values of P_d and λ.

Lenhard *et al.* (1989) suggest there is some correspondence between the Brooks-Corey and van Genuchten models. To estimate the Brooks-Corey parameter λ, Lenhard *et al.* (1989) equate the differential fluid capacities of the two models at S_e=0.5. Thus

$$\lambda = \frac{m}{(1-m)}\left[1-0.5^{\frac{1}{m}}\right] \tag{2.14}$$

2.4.4 Residual Saturation and Relative Permeability

Once a DNAPL has penetrated the water-table a two-phase system exists. The coexistence of another fluid in the pores reduces the area available for flow of either fluid and increases the tortuosity of the flow path which fluid elements must traverse. The simultaneous flow causes each fluid to interfere with the flow of the other. It is customary to express the effective permeabilities as fractions of the permeability k of the medium. These are the so-called 'relative permeabilities', k_{r1} and k_{r2} defined as follows:

$$v_1 = -(kk_{r1}/\mu_1)(\nabla P_1 - \rho_1 g) \tag{2.15}$$

$$v_2 = -(kk_{r2}/\mu_2)(\nabla P_2 - \rho_2 g) \tag{2.16}$$

where v is the flow rate per unit area, μ is the dynamic fluid viscosity, ∇P is the pressure gradient, ρ is the fluid density and g is the gravitational acceleration vector.

The permeability, k, is considered to be a function only of the rock pore size. The relative permeability, k_r, is a function of the amount of fluid present in the rock pores; it is a dimensionless property. The relative permeability is not determined by the pore structure of the porous medium but also depends on the parameters characterising the system: DNAPL/water/ solid matrix.

During migration, a significant portion of DNAPL is retained in porous media (Illangasekare *et al.*, 1995). Below the water-table, residual saturation of DNAPL is the saturation at which DNAPL is immobilised (trapped) by capillary forces as discontinuous ganglia under ambient groundwater flow conditions (Dawson and Roberts, 1997). Dullien (1992) defines residual nonwetting phase saturation as "the reduced volume of the nonwetting phase that is entrapped when the externally measured capillary pressure is decreased from a high value to zero". In the unsaturated zone residual DNAPL may be more or less continuous depending on the extent to which DNAPL films develop between the water and gas phases thereby interconnecting isolated DNAPL blobs (Wilson *et al.*, 1990). The physics of entrapment and development of methods to minimize residual saturation by enhanced oil recovery (EOR) are of great economic importance to the oil industry (Akselrod and Putkaradze, 1994; Morrow *et al.*, 1985). Similarly, residual saturation has important consequences in the migration and remediation of subsurface DNAPL (Van Geel and Sykes, 1997). Residual saturation for the wetting fluid is conceptually different from that for the nonwetting fluid. The nonwetting fluid is discontinuous at residual saturation, whereas the wetting fluid is continuous.

In the unsaturated zone, NAPL is retained as films, wetting pendular rings, wedges surrounding aqueous pendular rings, and as nonwetting blobs in pore-throats and bodies in the presence of water (Kia, 1988). NAPL will spread as a film between the water and gas phases given a positive spreading coefficient. DNAPLs such as halogenated solvents typically have negative spreading coefficients and will not spread as films in the unsaturated zone due to their internal cohesion.

Based on laboratory determinations using various NAPLs and saturated soils, Wilson *et al.* (1990) found that residual saturation could not be reliably predicted from soil texture because very minor textural differences, such as the inclusion of trace silt or clay in sand, and the presence of heterogeneities significantly affect residual saturation values. For a given DNAPL release volume, residual saturation in fractures and macropores tend to be less than in homogeneous porous media but can be expected to extend over a larger portion of the aquifer (Reitsma and Kueper, 1994). In addition residual saturation in heterogeneous media containing discontinuous coarse lenses tends to be greater than in homogeneous media. Recent work has shown the presence of subsurface chemical heterogeneities such as variations in aqueous phase chemistry (Demond *et al.*, 1994), mineralogy (Anderson, 1987a,b,c; Bradford *et al.*, 1998), organic matter distributions (Dekker and Ritsema, 1994), and contaminant ageing (Harrold *et al.*, 2001) can substantially alter the wettability and both water- and organic-wet solid surfaces occur within the same porous medium.

Laboratory experiments (Huling and Weaver, 1991; Bloomfield *et al.*, 1997) have indicated that residual saturation within the unsaturated zone is approximately one third of the residual saturation in the saturated zone. The increase in residual saturation in the saturated zone is due mainly to the greater fluid density ratio of DNAPL/air compared to DNAPL/water which favoured greater drainage of the unsaturated zone.

Residual saturation increases both as the pore size heterogeneity increases and as the ratio of pore volume to pore neck size increases (Chatzis *et al.*, 1983). In some granular aquifers, residual saturation can be as high as 60% of the total porosity (Hunt *et al.*, 1988). These high residual saturations will considerably reduce the relative permeability for water locally (Mercer and Cohen, 1990). Groundwater would therefore tend to flow around the body of residual saturation rather than through it and as a consequence, rates of dissolution in the centre of the residual saturation would be very low. Dissolution would result in the body of residual saturation contracting towards the centre.

A DNAPL will continue to migrate downwards until either the residual saturation within the aquifer approaches the volume of the solvent spilled or an impermeable layer is reached. In the latter case a significant 'pool' of DNAPL may form infilling depressions on an aquifer-aquiclude interface (Pankow and Cherry, 1996). Permo-Triassic sandstones frequently exhibit cross-bedding which may result in

the direction of maximum permeability being at a steep angle to the horizontal. This feature can specifically enhance downward migration of DNAPLs in Permo-Triassic sandstones.

2.4.5 Determining Relative Permeability using the Brooks-Corey-Burdine Equations and the van Genuchten-Maulem Equations

While it is possible to measure relative permeability functions in the laboratory, it is often found convenient to calculate them from $P_c(S_w)$ data. Burdine (1953) and Mualem (1976) developed models that connect relative permeability to the capillary pressure-saturation function. These models can be used to derive closed-form expressions for the relative permeability to the wetting phase saturation - $k_{rw}(S_w)$ - and the relative permeability to the non-wetting phase saturation - $k_{rnw}(S_w)$. Brooks and Corey (1966) used their equation in the model of Burdine (1953) to derive for the wetting phase

$$k_{rw} = S_e^{(2+3\lambda)/\lambda} \tag{2.17}$$

and for the non-wetting phase

$$k_{rnw} = (1-S_e)^2\left(1-S_e^{2+\lambda/\lambda}\right) \tag{2.18}$$

By evaluating the Mualem (1976) model with the van Genuchten function, van Genuchten (1980) for the wetting phase derived

$$k_{rw} = S_e^{0.5}\left[1-\left(1-S_e^{1/m}\right)^m\right]^2 \tag{2.19}$$

for the relative permeability of the nonwetting phase, Parker *et al.* (1987) used the same procedure to write

$$k_{rnw} = (1-S_e)^{0.5}\left(1-S_e^{1/m}\right)^{2m} \tag{2.20}$$

Typical relative permeability functions are shown in Figure 2.6 By definition, these functions range from zero to unity. The relative permeability to the wetting phase (water) is usually considered to be free of hysteresis. On the other hand, the saturations at which k_{rnw} is zero in a wetting or draining process are not usually the same because of entrapment of the non-wetting fluid (DNAPL) during the wetting process. It is usual to assume that k_{rnw} is greater than zero in a draining process for all $S_w < 1$. In reality there

is a threshold saturation of nonwetting phase required to bring about an initial network of connected pore-throats across the sample volume of interest. During wetting, the relative permeability of DNAPL becomes zero at $S_w = 1 - S_m$. It is worth noting that the relative permeability during wetting does not become unity because of the presence of residual DNAPL.

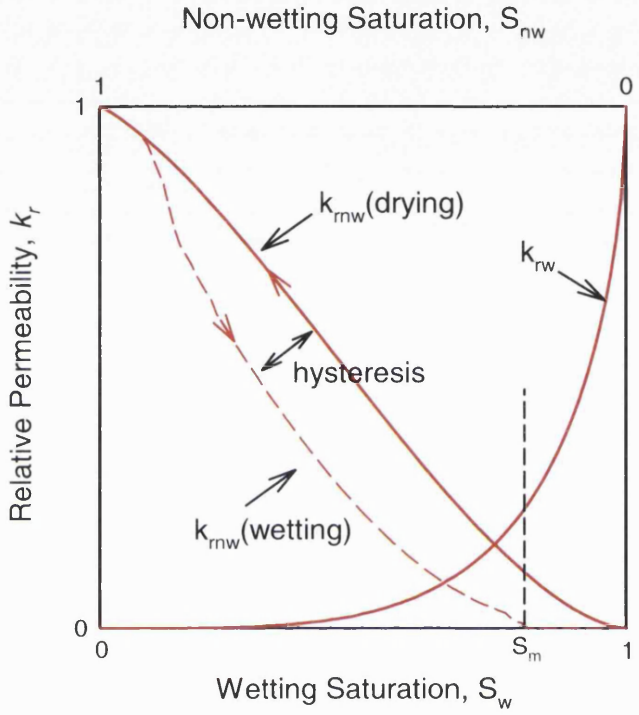

Figure 2-6 Typical relative permeability curves

2.5 PORE STRUCTURE AND PERCOLATION

To understand DNAPL distribution it is important to understand pore structure and how the DNAPL moves at the pore scale. Historically, porous media systems have been modelled by analogy to fluid behaviour in capillary tubes, where the pore space of a porous solid is idealized as a collection of capillaries. For example Washburn (1921) studied dynamic invasion of a fluid into a capillary, Carmen (1941) used the concept of hydraulic radius to define equilibrium positions of fluid-fluid interfaces in tubes of different cross sections, Haines (1930) examined the motion of unstable interfaces and Fatt (1956 a,b,c) introduced the idea of network models.

Many models of the pore space of a porous solid are based on some form of bundles of capillary tubes. These include the models of Childs and Collis-George (1950), Burdine (1953), and Mualem (1976). The use of the bundle-of-tubes concept

allows simple analytical formulas to be derived for properties such as relative permeability, however such models miss a fundamentally important topological characteristic of porous solids, namely interconnectedness of the pore space. This failing has led to the development of models of the pore space that arrange capillary tubes in two- or three-dimensional networks (Larson *et al.*, 1981a,b; Spearing and Matthews, 1991). The movement of fluids, and the interfaces that separate different fluid phases, through such a network of capillary tubes, forms the basis of pore-scale network models. The pioneering work in these types of network models was that of Fatt (1956 a,b,c), who used two-dimensional networks of capillary tubes with randomly distributed radii to model the pore space. Since then, there have been many extensions of the network modelling approach.

While Fatt (1956) used volumeless junctions in the networks, most models now use pore-space descriptions that include junctions characterized by an effective radius, where the junction is referred to as a pore body or a "site" of the lattice. The pore bodies are meant to correspond to the larger void spaces found in natural porous media. The narrow openings that connect adjacent pore bodies are modelled by the capillary tubes of the network model, which are called pore-throats or "bonds" of the lattice. Pore bodies are usually represented by spheres whose size distribution is representative of pore bodies found in the particular porous medium of interest, while the pore-throats are usually represented as cylinders or conical shapes with an analogous size distribution that is characteristic of the narrow openings that connect the pore bodies. Connectedness is usually characterized by the coordination number (typically assigned the symbol z), which corresponds to the number of bonds that meet at a site (Larson and Davis, 1982).

There are a number of publications related to network modelling and pore-scale displacement processes many of which are described by Dullien (1992) and Sahimi (1995). Most of these have appeared in the chemical engineering (Larson *et al.*, 1981a,b; Larson and Morrow, 1981), petroleum engineering (Chatzis and Dullien, 1977; Morrow, 1976), and physics literature (Hirsch and Thompson, 1994; Wilkinson, 1984). These include fundamental work in computational methods; experimental studies, often involving etched-plate micromodels; and theoretical developments, usually involving aspects of percolation theory.

Closely allied with computational network models is the concept of percolation theory. Generally credited as being introduced by Broadbent and Hammersley (1957), percolation theory provides a mathematical framework to analyse deterministic motions in a random medium. The general topic of percolation theory, with specific application to hydrology, has been reviewed by Berkowitz and Balberg (1993).

Wilkinson and Willemsen (1983) developed invasion percolation, a new form of percolation theory taking into account the fluid transport process. The theory is based on mapping the threshold pressure of each pore to an occupation probability. In an idealized medium the network of pores and throats may be viewed as a regular lattice in which the sites and the bonds represent the pores and the throats. A random number (p) in the unit interval is assigned to each site and bond to correspond to the threshold pressure. Thus, p is the occupation probability indicating that the actual site or bond is filled with the invading fluid at the capillary pressure corresponding to p. The invasion percolation process proceeds by letting the displacing fluid expand each time step to occupy the accessible site along the front having the smallest random number. Regions of defending fluid which become disconnected from the outlet are trapped, and the site of the trapped cluster cannot be invaded. The process is stopped when the invading fluid first percolates, i.e. forms a connected path between the inlet and the outlet. The invasion percolation process is only valid in the limit of extremely slow displacement. In that limit the capillary pressures due to the pore-interfaces are assumed to be in capillary equilibrium and a pore or throat is only invaded by displacing fluid if the capillary pressure is equal to or larger than the corresponding threshold pressure.

It is possible to distinguish one-, two- and three-dimensional networks. A one-dimensional network is a chain and as such not a network in the true sense. The only difference between the bundle of uniform capillary tubes model and a 1-D network is that in the former model each tube has a uniform diameter, whereas in the latter the diameter of the tube can change along the axis of the tube in either a regular or irregular manner. A two-dimensional network is a lattice and does not necessarily need to be a regular structured network. In two-dimensional networks only one phase can be continuous – the second phase must be discontinuous. It is only in three-dimensional networks that it is possible to have two continuous phases present simultaneously (Dullien, 1975).

Jerauld and Salter (1990) investigated the effects of spatial correlation within a network. Size correlations between neighbouring pore-throats and pore bodies (site-bond correlation), and between adjacent throats (bond-bond correlation) and adjacent sites (site-site correlation), were considered. Bond-bond or site-site correlation was found to be more significant than site-bond correlation. A regular cubic lattice was used by Jerauld and Salter because they concluded from tests on other network structures that the influence of coordination number and the effects of random versus regular lattice structure were secondary to those due to aspect ratio and to pore-to-pore size correlation. Tsakiroglou and Payatakes (1991) examined the effect of spatial structure on simulations of mercury porosimetry curves and concluded that the combination of site-site and site-bond correlation has a much greater influence on the resulting curves than site-bond correlation alone. Both Tsakiroglou and Payatakes (1991) and Ioannidis and Chatzis (1993) observed that in the correlated networks, each correlated sub network is invaded almost completely over a very small capillary pressure range. This is likely a result of both the correlation itself, and of the larger-scale accessibility limitations caused by the block-like structures.

Renault (1991) performed a study that focused on percolation thresholds on networks that included spatial correlation. On three-dimensional lattices, Renault (1991) observed that the percolation threshold decreased as the correlation length increased, reaching an asymptotic value with little change beyond correlations of approximately five bond lengths. This may be interpreted to mean that statistically reproducible results occur within each correlated sub region for sizes beyond those implied by a correlation length of five. These results are similar to those of Ferrand and Celia (1992), who looked at the analogous network modelling problem using heterogeneities based on statistically homogeneous sub-blocks.

2.6 AQUIFER REMEDIATION

If quantities of DNAPL do enter an aquifer there are three basic courses of action: to discontinue use of the aquifer and obtain alternative water supplies, to attempt to rehabilitate it, or continue to use the aquifer, but treat the water to remove the contaminants (Lawrence and Foster, 1991). The course of action taken will very much depend on three factors: i) the use of the aquifer, which is generally a function of groundwater quality; ii) the degree of contamination that has taken place, i.e. is the contamination widespread or local; and iii) the cost of a remediation programme. A

review detailing many of the remediation techniques currently available, their applicability, and their potential shortfalls in UK aquifer systems has previously been carried out by Gooddy and Lawrence (1994).

Before any remedial action can be undertaken, a number of criteria must be met. Firstly, there must be a thorough understanding of the hydrogeology. Ignoring this first crucial stage could lead to massive over expenditure and even a compounding of the pollution problem. Secondly, the contaminant distribution between soil, unsaturated and saturated zones must be ascertained. It is necessary to know whether the contaminants are in the non-aqueous, dissolved, gaseous or sorbed phase, or indeed any combination of these phases. Determination of the solvent state substantially affects the choice of remedial strategy. Thirdly, a realistic remediation goal needs to be set. This is the level to which contamination should be reduced within a certain time span (Fountain *et al.*, 1995). Lastly, an appropriate monitoring strategy needs to be developed that realistically reflects the degree of groundwater contamination.

2.6.1 Application of remediation techniques

Where gross contamination of the aquifer has occurred, particularly where DNAPL is suspected, then removal of the contaminant source and prevention of the spread of the polluted groundwater away from the site are priorities (Hunt *et al.*, 1988). Excavation and installation of physical barriers are unlikely to be of use in the UK for anything but superficial cover, i.e. the soil zone and recent deposits including boulder clay and sands. Rapid action following a single pulse spillage will minimise aquifer contamination.

In many cases DNAPLs will migrate through any superficial cover and contaminate the unsaturated and saturated zone directly. Vapour extraction methods are a possible approach for the unsaturated zone (Woodwell, 1989).

Where the saturated zone of the aquifer has been contaminated the most effective methods of remediation at current technological levels are likely to be containment by active hydrodynamic control, combined with removal and treatment of contaminated water. Traditional pump-and-treat systems are designed to effectively capture and remediate contaminated groundwater plumes (Meiri *et al.*, 1990; O'Brian and Stenzol, 1984). Contaminant mass removal in pump-and-treat systems is usually significant, however the rate of contaminant removal often declines rapidly, and tends towards an asymptotic value above drinking water guidelines. The use of surfactants

(West and Harwell, 1992; White and Oostrom, 1998) may overcome some of the current problems of pump-and-treat technology by mobilising the residual, although this is not a routine operation (Pennell *et al.*, 1996; Field *et al.*, 2000) and the introduction of surfactants can cause contamination issues of their own.

Bioremediation is an appealing technology since there should be no hazardous end product. A raft of literature has been dedicated to bioremediation at both the laboratory (Aziz *et al.*, 1995; 1995Bouwer *et al.*, 1981; Halden and Chase, 1991; Lanzarone and McCarty, 1990; Milde *et al.*, 1988; Nelson *et al.*, 1988 Thomas and Ward, 1989) and field scale (Brown *et al.*, 1985; Jackson 1998; Roberts *et al.*, 1990; Semprini *et al.*, 1990; Speitel and Closmann, 1991; Standberg *et al.*, 1989; Wilson *et al.*, 1986). Pore neck sizes in sandstones are large enough to allow many bacteria through a significant proportion of sandstone facies (Bloomfield *et al.*, 2001). The problems of injecting bacteria and/or nutrients into a highly heterogeneous aquifer such as the Permo-Triassic sandstone aquifers, so that the microbial cocktail is well distributed, is a major challenge (Huling and Weaver, 1990; Hutchins *et al.*, 1991). Above-ground bioreactors do circumvent this problem and there is much literature claiming to show degradation (Berger *et al.*, 1987; Flathman *et al.*, 1989; Vogel and McCarty 1985). However, many solvents are not easily degraded and the rate of degradation in many cases could make the remediation time of the same order of magnitude as pump and treat (Travis and Doty, 1990).

An emerging in-situ remediation approach is that of permeable reactive barriers. A permeable reactive barrier (PRB) is a zone of reactive material placed in the subsurface so that contaminated groundwater flows through and contamination is either contained or destroyed in the process. Iron filings can be a suitable treatment material for TCE contaminated groundwater. Laboratory batch and column studies conducted with simulated TCE contaminated groundwater and iron filings indicated successful removal of the contaminant within a short time period (Orth and Gillham, 1996). Scaling up these findings is the subject of current research (O'Hannesin and Gillham, 1998). For this technology, an understanding of the flow mechanisms and matrix structure is crucial to establishing contact between the iron and the contaminated groundwater.

In the USA where pump-and-treat technologies have been extensively used on less complicated aquifer systems than those in the UK, no single site has yet been

'cleaned-up'. Researchers in this field have even argued that contaminated aquifers can never be restored to a pristine state (Travis and Doty, 1990), but that there is a need to reassess the level to which remediation is required for each site. It may be possible to treat the groundwater but never remediate the aquifer. A US EPA study (SITE, 1989) involving 19 sites where pumping and treating had been ongoing for up to 10 years concluded that although significant mass removal of contaminants had been achieved, there had been little success in reducing concentrations to the target levels. Unless reasonable remediation goals are established, it is possible that there will be more well-head treatment of contaminants and less actual attempted remediation of the aquifer.

2.7 CHAPTER TWO SUMMARY

Dense non-aqueous phase liquids have been identified as posing a considerable threat to groundwater quality because of their physical and chemical properties. The mode of entry of a DNAPL into the subsurface can significantly affect subsequent behaviour. The Permo-Triassic sandstones form the second most important aquifer group in the UK. Spatially these sandstones are both heterogeneous and anisotropic which makes assessing DNAPL transport mechanisms complex. An understanding of capillary pressure and its controlling variables is required to understand the likely depth of penetration and the degree of saturation of a DNAPL. Pressure-saturation relationships for DNAPL-water-sandstone systems can be established by using a centrifuge method and the resultant curve can be parameterised empirical functions such as those developed by van Genuchten (1980) and by Brooks and Corey (1966). The presence of DNAPL in an otherwise water saturated sandstone will reduce the permeability. This reduction can be measured experimentally or determined from parameters in the van Genuchten or Brooks-Corey pressure-saturation functions. An understanding of pore structure is important for interpreting DNAPL movement at the pore-scale. Many of the pore-scale models are based on percolating networks. Several techniques exist for the remediation of contaminated aquifers although it may not be possible to return groundwater to a pristine state.

3 Project Rationale

This chapter describes the logical basis for undertaking the work. The matrix of the Permo-Triassic sandstone is considered to be particularly vulnerable to DNAPL contamination although the only estimates of DNAPL entry pressures into the saturated matrix are based on theoretical considerations. Existing methods for determining entry pressure, relative permeability and residual saturation are introduced and shown to be inappropriate for use in consolidated DNAPL-water-sandstone systems prompting the development of new methods (described in subsequent chapters). A description of the core sampling procedure is given along with a summary of the samples taken and their geographical location.

3.1 DATA NEEDS

It is commonly assumed that in consolidated fractured-porous aquifers, like the Permo-Triassic sandstones, a DNAPL migrates rapidly and to depth via fractures (Wealthall *et al.*, 2001). Further, because DNAPL migration is density-driven there will be little lateral displacement (from the initial spill) where near vertical fractures exist. However, these assumptions are challenged for the Permo-Triassic sandstone for the following reasons. Firstly, because DNAPL will be in contact with a much larger area of matrix compared to fractures, many localized spills (e.g. resulting from a leaking tank) may not encounter a fracture. Secondly, in the unsaturated zone, many of the sandstone's pores are air-filled (often in excess of 50% of total porosity) so that DNAPL entry into the matrix is comparatively easy. Thirdly, the unsaturated zone can be deep: 10-30 m is quite common. Thus DNAPL migration through the consolidated or cemented matrix of the sandstones is likely to be important. Some data are currently available on DNAPL transport in aquifers, principally from North American studies based on shallow unconsolidated aquifers and fractured till. However, these lithologies are unlikely to be representative of DNAPL behaviour in the consolidated Permo-Triassic sandstones.

The Permo-Triassic sandstones exhibit a wide range of lithologies with a corresponding wide range in their transport characteristics relevant to DNAPL migration. Consequently, a primary aim of this study has been to determine rock-matrix parameters of the Permo-Triassic sandstones and characterize processes that control the distribution of solvent contamination in the sandstone aquifer. The objective has been to

provide information to improve predictions, and hence reduce uncertainty, of the depth of penetration and distribution of both liquid or free-phase halogenated solvents following a spill to enable more effective assessment and management of DNAPL contamination. By understanding these factors it is hoped that questions such as: 'How long will the contamination last?', 'Where and when will it go?', and 'How toxic is the sub-surface now and in the future?', will be answerable and therefore assist in formulating target and action levels for contaminated land.

The only estimate of DNAPL entry pressures into the saturated matrix of consolidated sandstones, prior to this research, was based on theoretical considerations (Lawrence *et al.*, 1991). There is a very real need to test the validity of the underlying assumptions behind these considerations. The pressure required for DNAPL to displace water varies for the different lithologies and ranges from centimetres of DNAPL for the coarser sandstones to several metres for the finer-grained siltstones. The controlling factor on this pressure is assumed to be the pore diameter of the rock matrix. In addition, no pressure-saturation functions had been determined for DNAPL-water-sandstone systems.

Similarly, no data was available for either DNAPL residual saturations in Permo-Triassic sandstones or for the likely reduction in relative permeability resulting from a DNAPL spill. Where DNAPL residual is present below the water-table it will reduce groundwater velocities and acts as a source for aqueous plume migration. Aqueous phase concentrations will only start to decrease when the residual DNAPL length becomes very short. Therefore an understanding of likely residual volumes and the concomitant reduction in relative permeability is a crucial step in determining the duration and likely extent of a contaminant plume and essential for any remedial programme.

3.2 METHODOLOGY NEEDS

3.2.1 Determining Entry Pressure and Capillary Pressure-Saturation Functions

Entry pressures and capillary pressure has traditionally been determined in the oil industry using the porous diaphragm method (Figure 3.1). Usually the experiment is started with the sample saturated with the wetting fluid, which is commonly a brine. The sample chamber is filled with the nonwetting fluid (oil). In order to prevent breakthrough of the oil across the frit, the latter must have much smaller pores than the

core. As the pressure on the oil is raised, the brine is displaced from increasingly smaller pores of the sample. The wetting fluid is forced out of the pores of the sample by the non-wetting fluid across the fritted glass disk, into the U-tube where its volume is determined in the graduated portion of the tube. The gas pressure applied is read simultaneously. The capillary pressure versus saturation curve is determined point by point by displacing the wetting fluid in small pressure increments, at every point waiting until equilibrium is established. The sample saturation is calculated from the initial amount of wetting fluid contained in the pore space and the amount of wetting fluid displaced in each step. Equilibrium is commonly attained at a very slow rate which means it can take weeks or months to determine a single capillary pressure curve.

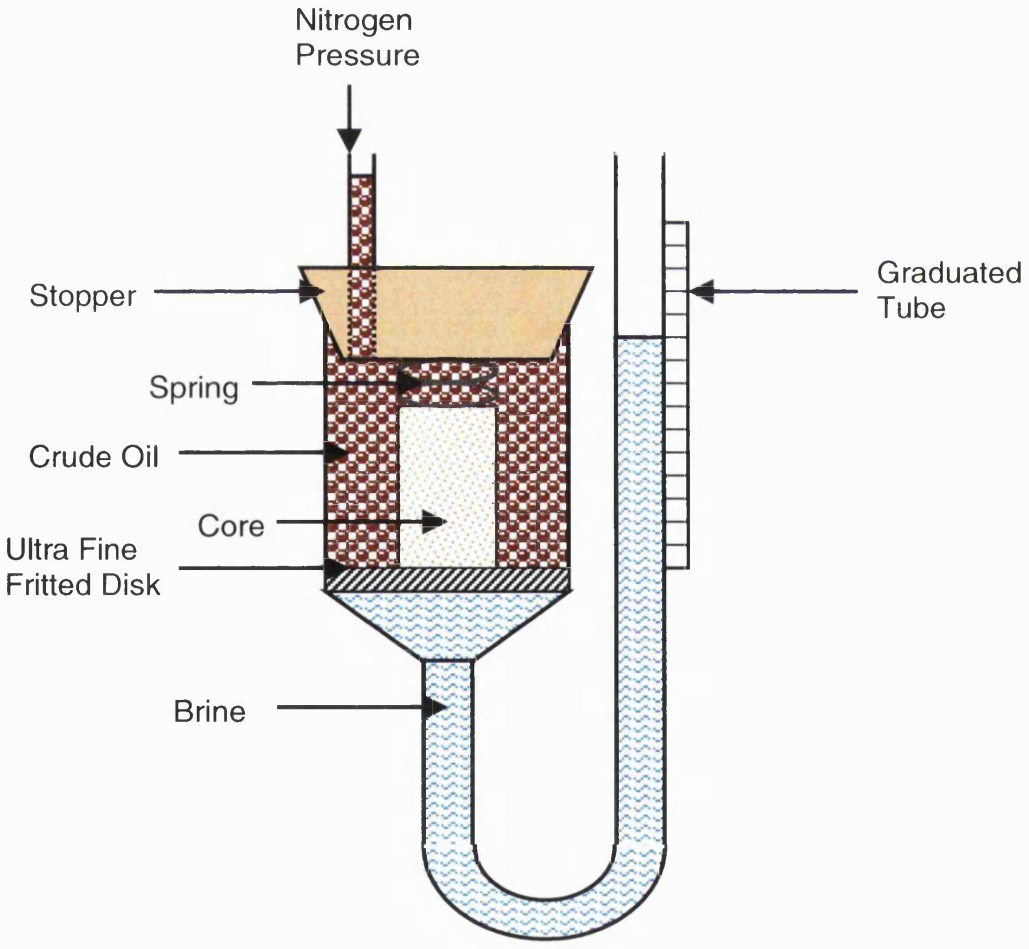

Figure 3-1 Schematic diagram of a porous diaphragm device for capillary pressure determination (after Welge and Bruce, 1947).

A major problem with this approach to characterise entry pressure for DNAPL-water-sandstone systems is the highly aggressive nature of chlorinated solvents towards organic based materials. The standard design of these cells means they are produced in plastic which is susceptible to attack from the chlorinated solvent and consequently deformation. A more serious problem comes with the fritted disks which are fixed in place with an epoxide glue. The glue is dissolved by the solvent so allowing direct passage of the DNAPL into the graduated tube, by-passing the core, hence giving erroneous values as to the amount of water displaced. An additional problem is the rubber seals that are used to connect the glass graduated tube to the core holder. These are also susceptible to attack by the solvents and allow solvent from the core holder and water from the glass tube to escape, again leading to erroneous data.

Kueper *et al.* (1989) developed a capillary pressure cell especially for DNAPLs. This cell was similar to that depicted in Figure 3.1 but was comprised of more metal parts not sensitive to solvent attack. In addition the cell did not use nitrogen gas to induce a pressure on the DNAPL (presumably for health and safety reasons) but relied on moveable reservoirs of wetting and non-wetting fluid. As the height of one of the reservoirs was increased relative to the sample then the pressure on the sample was increased. The apparatus developed by Kueper *et al.* (1989) was specifically designed to be used on unconsolidated samples which generally have considerably lower entry pressures than consolidated samples. Indeed it would not be practical to use this apparatus to obtain capillary pressure-saturation functions on consolidated Permo-Triassic sandstones as significantly higher pressures would be needed.

Therefore there is a need for a reliable and preferably relative rapid method for determining solvent entry pressures and capillary pressure-saturation functions for Permo-Triassic sandstones. The development of such a method is detailed in Chapter 5.

3.2.2 Determining Relative Permeability and Residual Saturation

It is necessary that the relative permeability data measured in the laboratory yield the same relative permeability saturation relationships that would govern the flow of fluids through the sample if it were to occupy its original position in the aquifer. As core samples on which laboratory measurements are made are not surrounded by similar core material, an error in measuring the relative permeabilities may arise from the "boundary effect" which results from a discontinuity in capillary properties of the system at the

effluent end of the core. Osaba *et al.* (1951) conclude that at high rates of flow the error introduced by the boundary effect may be made so small that it will not appreciably affect the measurements of relative permeability.

Bloomfield and Williams (1995) presented a method for measuring the liquid permeability of aquifer materials from Permo-Triassic sandstones from northern England. The method was carried out under steady-state constant flow rate conditions whereby samples were placed in a coreholder and a constant flow rate was established through the samples using a pair of syringe pumps. The pressure and flow-rate above and below the sample were monitored and steady state conditions were assumed to have been achieved when both pressure and flow-rate were constant. Unfortunately this method had no provision for the introduction of an immiscible phase nor of continuously monitoring the pressure response across the core.

Sigmund and McCaffery (1979) devised an improved method for measuring relative permeability in the oil industry. The method used a Hassler core holder to constrain the sample and either oil or water could be directed through. The method used a separator/fraction collector which relied strongly on the lighter-than-water properties of oil. Without considerable redesign the method would not be appropriate for DNAPLs and the issue of the aggressive nature of chlorinated solvents on the construction material would still need to be addressed.

Residual saturation and relative permeability measurements have recently been made using DNAPLs. Thakur *et al.* (1995) used sand packed columns to investigate the flow characteristics of DNAPLs during water-influx displacement, whereas TeKrony and Ahlert (1998) investigated residual saturation of bead packed columns with chlorinated solvents. In both cases, the unconsolidated nature of the materials used means their adaptation of the method for consolidated media is not possible.

Clearly, to measure relative permeability and residual saturation on the same sample a new method is required. The method needs to be reliable and the apparatus construction materials need to be able to withstand attack, leading to significant failure in performance, from the solvents used. The development of such a method is detailed in Chapter 6.

3.3 SAMPLING

The Permo-Triassic sandstones are geographically and lithologically diverse. Unfortunately due to the diverse nature of the sandstones, it was not possible, within the scope of the present study, to sample systematically each of the main lithotypes from all the major sandstone formations. Instead representative samples of consolidated sandstones were collected with a geographical spread and from a range of depths (Figure 3.2). (Unconsolidated sandstones, mudstones and marls were not investigated). Samples were all obtained from the 'Core Store' at the British Geological Survey in Keyworth. Selected samples were taken on five separate occasions. On each occasion the entire core run was laid out and inspected. Short sections of the slabbed core (10-20 cm) were taken on the basis of how representative they were of the entire core run in terms of lithology and colour. Samples were not take across clear lithological boundaries.

A total of one hundred and fifty three samples were taken from thirteen different localities. Of these 153 samples, 45 samples were duplicates which gives a total of 108 separate depth samples. All the samples (including duplicates) were tested for porosity and gas permeability, but only a subset of these (66 samples) were tested by MICP to obtain pore-throat size distributions. Similarly subsets were used in the two methods specially developed. Capillary pressure-saturation curves were measured for 51 samples although on 4 of these samples no DNAPL entry was achieved. Relative permeability and residual saturation was measured on 15 samples.

To ensure that a representative range of measurements was obtained on the subsets, samples were chosen on the basis of the porosity and permeability data in conjunction with visual inspection of the core. Samples used in the MICP tests, for the capillary pressure-saturation curves and for relative permeability were taken from core immediately adjacent to the permeability/porosity samples. Chemical extraction using 0.43 M nitric acid was carried out on all 108 separate depth samples. These samples were also classified on the basis of their Munsell colour as shown in Table 3.1. Isotopic measurement of the carbonate cements was carried out on 20 samples that had sufficiently high carbonate contents.

Core plugs were mostly cut in a vertical plane although to investigate the impact on physical properties of bedding, some cores plugs were also taken in a horizontal plane. In the subsequent DNAPL studies, only samples cut in a vertical plane were

analysed as entry into the saturated zone was considered of primary importance in this study.

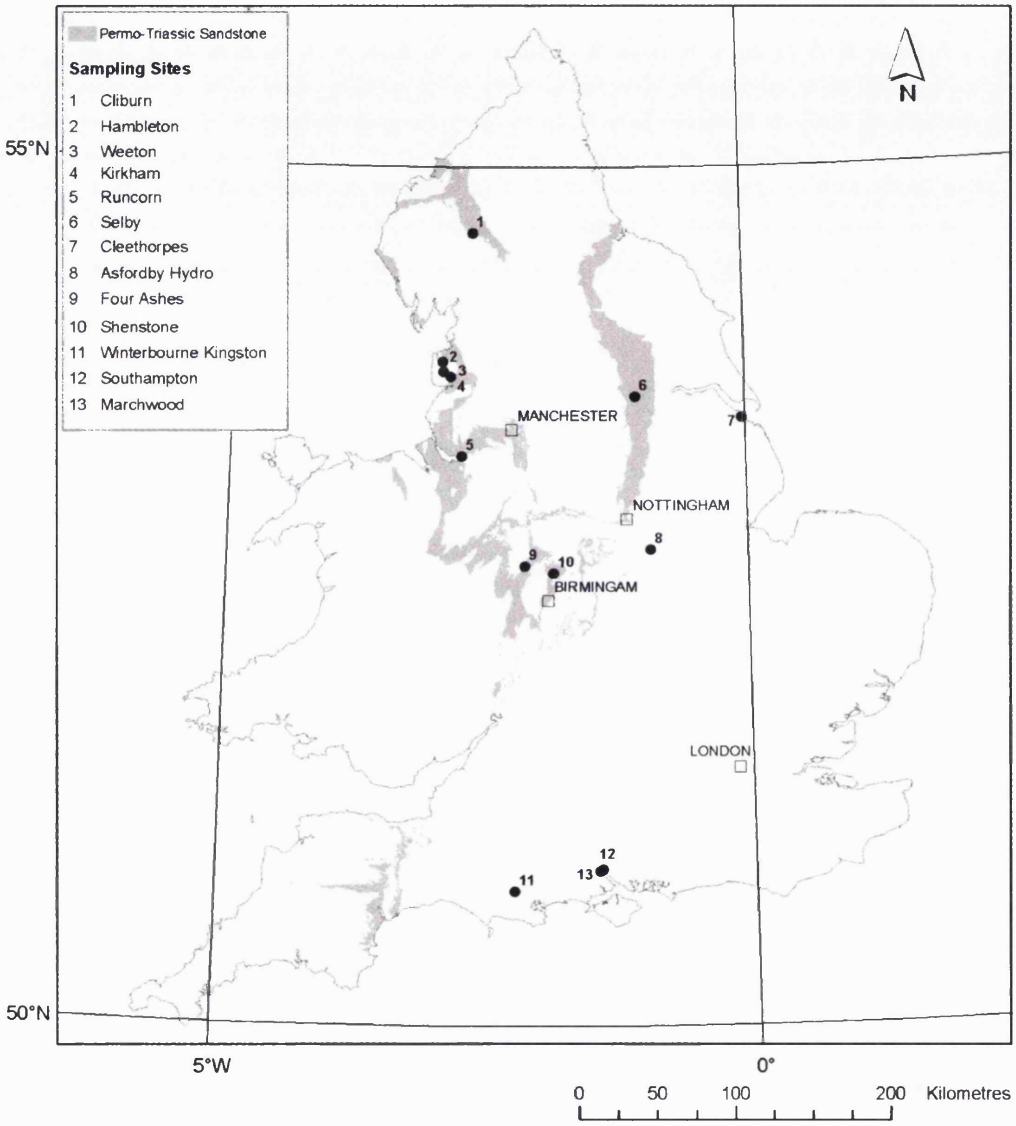

Figure 3-2 Map of surface outcrops of the Permo-Triassic sandstones and location of sampling sites.

Table 3-1 Sample depths, locality and Munsell Colour description.

Sample	Locality	Depth (m)	Stratigraphy	Munsell Colour	Description
1524/1	Selby	11	Sherwood Sandstone	7.5YR5/6	strong brown
1524/2	Selby	12	Sherwood Sandstone	7.5YR5/4	brown
1524/3	Selby	13	Sherwood Sandstone	7.5YR4/6	strong brown
1524/4	Selby	15	Sherwood Sandstone	5YR4/4	reddish brown
1525/1	Selby	7	Sherwood Sandstone	5YR5/6	yellowish red
1525/2	Selby	9	Sherwood Sandstone	5YR5/6	yellowish red
1525/3	Selby	10	Sherwood Sandstone	5YR5/6	yellowish red
1525/4	Selby	11	Sherwood Sandstone	2.5YR4/4	reddish brown
1525/5	Selby	12	Sherwood Sandstone	5YR5/6	yellowish red
1526/1	Selby	7	Sherwood Sandstone	5YR4/6	yellowish red
1526/2	Selby	9	Sherwood Sandstone	5YR5/6	yellowish red
1526/4	Selby	20	Sherwood Sandstone	5YR5/6	yellowish red
1526/6	Selby	28	Sherwood Sandstone	5YR5/6	yellowish red
1526/8	Selby	36	Sherwood Sandstone	5YR4/4	reddish brown
1526/10	Selby	38	Sherwood Sandstone	5YR5/6	yellowish red
1527/1	Marchwood #1	1680	Sherwood Sandstone	5YR4/4	reddish brown
1527/3	Marchwood #1	1688	Sherwood Sandstone	10YR5/2	greyish brown
1527/4	Marchwood #1	1692	Sherwood Sandstone	5YR5/3	reddish brown
1527/5	Marchwood #1	1697	Sherwood Sandstone	2.5YR5/2	weak red
1528/2	Cleethorpes 1	1868	Basel Permian Sands	10YR6/1	grey
1528/4	Cleethorpes 1	1876	Basel Permian Sands	5YR5/2	reddish grey
1529/1	Shenstone 1	49	Sherwood Sandstone	5YR4/3	reddish brown
1529/3	Shenstone 1	52	Sherwood Sandstone	5YR4/3	reddish brown
1529/5	Shenstone 1	54	Sherwood Sandstone	5YR4/3	reddish brown
1529/6	Shenstone 1	56	Sherwood Sandstone	5YR4/3	reddish brown
1529/8	Shenstone 1	59	Sherwood Sandstone	5YR5/3	reddish brown
1529/10	Shenstone 1	63	Sherwood Sandstone	5YR4/3	reddish brown
1529/12	Shenstone 1	65	Sherwood Sandstone	5YR4/3	reddish brown
1530/1	Shenstone 2	18	Sherwood Sandstone	2.5YR4/4	reddish brown
1530/2	Shenstone 2	19	Sherwood Sandstone	2.5YR4/4	reddish brown

Sample	Locality	Depth (m)	Stratigraphy	Munsell Colour	Description
1530/3	Shenstone 2	20	Sherwood Sandstone	2.5YR4/4	reddish brown
1530/6	Shenstone 2	30	Sherwood Sandstone	2.5YR4/4	reddish brown
1530/8	Shenstone 2	34	Sherwood Sandstone	2.5YR4/4	reddish brown
1530/9	Shenstone 2	35	Sherwood Sandstone	2.5YR4/4	reddish brown
1530/10	Shenstone 2	36	Sherwood Sandstone	5YR5/3	reddish brown
1534/3	Cliburn	9	Penrith Sandstone	5YR5/4	reddish brown
1534/4	Cliburn	18	Penrith Sandstone	2.5YR3/6	dark red
1534/5	Cliburn	30	Penrith Sandstone	2.5YR3/6	dark red
1534/6	Cliburn	36	Penrith Sandstone	2.5YR3/6	dark red
1534/7	Cliburn	42	Penrith Sandstone	2.5YR3/6	dark red
1534/10	Cliburn	59	Penrith Sandstone	2.5YR3/6	dark red
1534/11	Cliburn	68	Penrith Sandstone	2.5YR3/6	dark red
1534/12	Cliburn	74	Penrith Sandstone	5YR8/2	pinkish white
1534/13	Cliburn	111	Penrith Sandstone	2.5YR3/6	dark red
1535/1	Weeton	31	Mercia Mudstone	2.5YR6/2	pale red
1535/4	Weeton	43	Mercia Mudstone	2.5YR6/4	light reddish brown
1535/5	Weeton	51	Mercia Mudstone	2.5YR6/4	light reddish brown
1535/9	Weeton	70	Mercia Mudstone	2.5YR6/4	light reddish brown
1535/10	Weeton	81	Mercia Mudstone	2.5YR6/4	light reddish brown
1535/11	Weeton	90	Mercia Mudstone	2.5YR6/2	pale red
1536/1	W'bourne Kingston	2316	Bunter Sandstone	2.5YR3/2	dusky red
1536/3	W'bourne Kingston	2320	Bunter Sandstone	5YR7/2	pinkish grey
1536/4	W'bourne Kingston	2324	Bunter Sandstone	2.5YR3/2	dusky red
1536/5	W'bourne Kingston	2325	Bunter Sandstone	2.5YR6/4	light reddish brown
1536/7	W'bourne Kingston	2330	Bunter Sandstone	2.5YR6/2	pale red
1536/8	W'bourne Kingston	2332	Bunter Sandstone	5YR5/2	reddish grey
1536/9	W'bourne Kingston	2425	Bunter Sandstone	5YR4/2	dark reddish grey
1536/10	W'bourne Kingston	2428	Bunter Sandstone	5YR4/2	dark reddish grey
1537/1	Southampton 1	1732	Bunter Sandstone	5YR7/2	pinkish grey
1537/2	Southampton 1	1737	Bunter Sandstone	5YR7/2	pinkish grey
1537/3	Southampton 1	1742	Bunter Sandstone	10R5/3	brown
1537/4	Southampton 1	1745	Bunter Sandstone	5YR6/2	pinkish grey

Sample	Locality	Depth (m)	Stratigraphy	Munsell Colour	Description
1537/5	Southampton 1	1749	Bunter Sandstone	5YR7/2	pinkish grey
1537/6	Southampton 1	1753	Bunter Sandstone	5YR7/2	pinkish grey
1537/7	Southampton 1	1755	Bunter Sandstone	2.5YR6/2	pale red
1537/9	Southampton 1	1761	Bunter Sandstone	2.5YR5/2	weak red
1538/1	Asfordby Hydro	368	Sherwood Sandstone	2.5YR3/4	dark reddish brown
1538/2	Asfordby Hydro	369	Sherwood Sandstone	10YR7/1	light grey
1538/4	Asfordby Hydro	377	Sherwood Sandstone	2.5YR6/4	light reddish brown
1538/5	Asfordby Hydro	382	Sherwood Sandstone	5YR6/2	pinkish grey
1538/6	Asfordby Hydro	383	Sherwood Sandstone	5YR5/3	reddish brown
1538/7	Asfordby Hydro	385	Sherwood Sandstone	5YR4/3	reddish brown
1538/8	Asfordby Hydro	388	Sherwood Sandstone	5YR6/2	pinkish grey
1538/9	Asfordby Hydro	390	Sherwood Sandstone	5YR5/3	reddish brown
1538/10	Asfordby Hydro	391	Sherwood Sandstone	5YR5/3	reddish brown
1539/1	Kirkham	367	Bunter Sandstone	5YR8/1	white
1539/2	Kirkham	376	Bunter Sandstone	2.5YR3/4	dark reddish brown
1539/3	Kirkham	389	Bunter Sandstone	2.5YR6/4	light reddish brown
1539/4	Kirkham	393	Bunter Sandstone	2.5YR6/2	pale red
1539/5	Kirkham	397	Bunter Sandstone	10R5/3	brown
1539/6	Kirkham	401	Bunter Sandstone	2.5YR3/4	dark reddish brown
1539/8	Kirkham	409	Bunter Sandstone	10R5/3	brown
1539/9	Kirkham	415	Bunter Sandstone	10R5/3	brown
1539/10	Kirkham	424	Bunter Sandstone	10R5/3	brown
1539/11	Kirkham	430	Bunter Sandstone	10R5/3	brown
1539/13	Kirkham	441	Bunter Sandstone	2.5YR3/4	dark reddish brown
1540/1	Hambleton	137	Bunter Sandstone	10YR7/1	light grey
1540/2	Hambleton	138	Bunter Sandstone	10YR7/1	light grey
1540/3	Hambleton	139	Bunter Sandstone	10YR7/2	light grey
1540/5	Hambleton	140	Bunter Sandstone	10YR6/1	grey
1540/6	Hambleton	141	Bunter Sandstone	10YR6/1	grey
1541/1	Four Ashes	10	Bromsgrove Sandstone	2.5YR3/4	dark reddish brown
1541/2	Four Ashes	20	Bromsgrove Sandstone	2.5YR3/4	dark reddish brown
1542/1	Runcorn	1	Helsby Sandstone	5YR3/2	dark reddish brown

Sample	Locality	Depth (m)	Stratigraphy	Munsell Colour	Description
1542/2	Runcorn	5	Helsby Sandstone	10YR7/3	very pale brown
1542/3	Runcorn	8	Helsby Sandstone	10R5/3	brown
1542/4	Runcorn	15	Helsby Sandstone	2.5YR5/4	reddish brown
1542/5	Runcorn	17	Helsby Sandstone	2.5YR5/4	reddish brown
1542/6	Runcorn	22	Helsby Sandstone	2.5YR5/4	reddish brown
1542/7	Runcorn	23	Helsby Sandstone	2.5YR5/4	reddish brown
1542/8	Runcorn	26	Helsby Sandstone	2.5YR3/6	dark red
1542/9	Runcorn	28	Helsby Sandstone	2.5YR3/6	dark red
1542/10	Runcorn	32	Helsby Sandstone	2.5YR3/6	dark red
1542/11	Runcorn	34	Helsby Sandstone	10R3/6	dark red
1542/12	Runcorn	35	Helsby Sandstone	7.5YR6/4	light brown
1542/13	Runcorn	38	Helsby Sandstone	2.5YR5/4	reddish brown
1542/14	Runcorn	39	Helsby Sandstone	7.5YR6/4	light brown
1542/15	Runcorn	40	Helsby Sandstone	2.5YR5/4	reddish brown

3.4 CHAPTER THREE SUMMARY

This chapter has shown that the matrix of the Permo-Triassic sandstones is vulnerable to contamination by DNAPLs but only theoretical estimates as to the depth and degree of penetration are available. Existing methods for determining entry pressures, relative permeability, commonly used by the oil industry, are inappropriate for use with DNAPLs requiring new methods to be developed. The procedures for sample selection are described along with the sample location.

4 Physical and Chemical Characterisation of Sandstones

This chapter describes the techniques employed for physical and chemical characterisation of the Permo-Triassic sandstones investigated. The samples are tested for gas permeability, porosity, pore size distribution and surface chemistry using standard methods. In addition some isotopic measurements are made on samples that have relatively high concentrations of calcite or dolomite. Results are presented showing the broad range of properties that the Permo-Triassic sandstone matrix has.

4.1 DETERMINING GAS PERMEABILITY

The gas permeability tests were performed on clean, oven-dried samples under steady-state conditions. Samples were constrained in a coreholder and a pressure regulated supply of nitrogen applied to one end of the sample. The downstream end of the sample was at atmospheric pressure. Differential gas pressures were in the range 4.7×10^3 Pa to 1.0×10^5 Pa. A soap-film flow meter was used to measure the outflow of nitrogen from the downstream end of the sample. Once the flow rate was stable, a minimum of five flow rate readings were obtained for each sample and an average flow rate calculated. Gas flow rates at the downstream end of the sample were measured in the range 9.0×10^{-3} L/s to 8.3×10^{-7} L/s (Bloomfield and Williams, 1995).

Due to the compressibility of gas during a gas permeability test, the flow velocity varies from one face of a sample to the other. However, by assuming (i) constant temperature, (ii) steady-state conditions and (iii) that the product of pressure and gas velocity is constant throughout a sample (i.e. conservation of mass in a perfect gas) it has been shown that permeability can be calculated by accounting for gas expansion effects by:

$$k_g = \frac{2\mu_g Q_g L p_0}{A\left(p_i^2 - p_0^2\right)} \tag{4.1}$$

where k_g is gas permeability, μ_g is gas viscosity, Q_g is volumetric gas flow rate measured at atmospheric pressure (downstream end of the sample), L is sample length, A is sample cross sectional area, p_0 is the downstream pressure (atmospheric) and p_i is

given by $p_i=p_0+p_g$ (where p_g is the gauge pressure at the upstream end of the sample) i.e. p_i is equivalent to the absolute pressure at the upstream end of the sample.

Results are reported in units of both mD and as μm^2.

4.2 DETERMINING POROSITY

Right-cylindrical plugs of ca. 24.5 mm in diameter and ca. 27.5 mm in length were prepared and oven dried at 60°C for 24 hours prior to testing. Samples were dried to enable a vacuum to be established prior to sample saturation. A sample to be tested was weighed and then placed in a resaturation desiccator. The desiccator was evacuated for at least 24 hours before being flooded with water. The sample was then allowed to saturate for at least a further 24 hours. The saturated sample was then weighed, firstly below the water and then, still saturated with water, in air. For each sample its dry weight, saturated weight under water and its saturated weight in air were recorded, in addition the density of the water was noted. From these values interconnected porosity can be calculated as follows:

$$\phi = \frac{(S_1 - w)}{(S_1 - S_2)} \times 100 \tag{4.2}$$

where w is the dry sample weight (g), S_1 is the saturated sample weight in air (g), S_2 is the saturated sample weight under water (g), and ϕ is the effective porosity expressed as a fraction.

4.3 CALCULATING MEAN PORE RADIUS

The term $\sqrt{k/\phi}$, according to equalisation of the Poiseuille and Darcy equations, can be proven to represent the 'mean pore radius' (r), of the porous rock (Leverett, 1938; Elgaghah *et al.*, 2001). The mean pore radius has been calculated based on 1 mD = 0.000987 μm^2.

$$r = \left(\frac{k_{mD} \times 0.000987}{\phi} \right)^{0.5} \tag{4.3}$$

Mean pore radius is expressed in terms of μm. The mean pore diameter is obviously twice the average pore radius.

4.4 DETERMINING PORE SIZE DISTRIBUTION AND MEDIAN PORE-THROAT SIZE USING MERCURY INTRUSION CAPILLARY PRESSURE

Pore-throat size distributions were measured by MICP tests. These tests rely on the phenomena that a non-wetting fluid will not invade a pore-throat unless the fluid is pressurised, and that the size of the pore-throat or capillary that is invaded is inversely proportional to the capillary pressure, P_c. As pressure is increased, successively smaller pore-throats will be invaded by the non-wetting phase. In an MICP test a sample is placed in a glass vial, placed under a vacuum, and the annulus between the wall of the vial and the sample is filled with mercury. At this stage no mercury has entered the sample, as the mercury is non-wetting with respect to the sample. The mercury is then pressurised hydrostatically in a series of steps, and the amount of mercury intruded into the sample at each pressure step is recorded. Once intrusion is complete the fractional pore volume intruded at each pressure step can be calculated using the total intruded volume. The equivalent pore-throat diameter, D, at each pressure step can be calculated assuming a simple capillary model and is given by the Washburn equation as follows

$$D = \frac{-4W\sigma\cos\alpha}{P_c} \tag{4.4}$$

where W is the Washburn constant (taken to be 0.145), the contact angle α is taken to be 140° and the interfacial tension, σ, is taken to be 485 mN m^{-1}. A Micromeritics AutoPore III was used in the MICP tests. Although it has a maximum working pressure of 414 MPa (equivalent to a pore-throat size of about 0.003 μm), samples were only tested up to 104 MPa (equivalent to a pore-throat size of about 0.01 μm) due to the time constraints imposed by running to this higher pressure. Tests were performed in equilibrated intrusion mode, with intrusion being deemed to have been complete at a given pressure step when the instantaneous mercury intrusion rate fell below 0.005 μL/g-sec.

A previous study (Al-Fossail *et al.*, 1995) has shown that MICP curves are insensitive to the sample size of sandstone samples. In addition, injection capillary curves obtained by rapid and slow injection methods were almost identical. Boukadi *et al.* (1994) used MICP to characterise Berea sandstone and found that steep-convex unimodal capillary pressure curves were typical for this type of formation. Generally

other studies comply with this unimodal distribution of poresizes for sandstones (Hammecker and Jeannette, 1994; Meng, 1994; James, 1995).

Mercury intrusion assesses not only the size but also the connectivity or percolation of the pore-throats present in a material. While a true pore-throat size distribution is not obtained by a mercury intrusion experiment, it does indicate the accessibility of the overall porosity as a function of pore size (Winslow *et al.*, 1994). In actuality, a mercury intrusion experiment is a form of invasion percolation (see Chapter 2, section 2.5) (Larson *et al.*, 1981a). Thus, to be intruded by the mercury at lower pressures, the larger pores must link up and form a continuous or percolated pathway throughout the medium. Results are expressed as median pore-throat size (μm) and as a pore-size distribution. The median pressure ($P_{cmedian}$) is calculated from

$$P_{cmedian} = \frac{I_{tot}}{2} \tag{4.5}$$

where I_{tot} is the total volume of mercury intruded during the MICP experiment. The median pore-throat size is therefore calculated by substituting the median pressure into Equation 4.4.

Tabulated results of porosity, permeability and poresize for all the samples is given in Appendix 1.

4.5 DETERMINING SURFACE CHEMISTRY

Roughly 3 g of dry, disaggregated, sand was accurately weighed into a pre-weighed 50 cm^3 Oak Ridge polypropylene centrifuge tube to which was added 30 ml of 0.43 M HNO_3 (Analytical Reagent grade) (Boekhold *et al.*, 1993). The tubes were shaken on a box shaker for 2 hours before centrifuging for 10 min at 1700 rpm. The supernatant solutions were then decanted and the samples filtered through a 0.45 μm filter. The extracted solutions were all analysed using a Perkin Elmer Optima 3300DV ICP-AES following the procedures of Gooddy *et al.* (1995). A range of elements were determined but the focus in this study was on material supporting the sandstone matrix, for this reason the following cations were focused on: calcium, magnesium, iron, and manganese. In addition concentrations of aluminium, silicon, sulphate and phosphorus were also determined during the same ICP-AES analysis since they can all play an important role in understanding the composition of a sandstone cement. In addition, trace element analysis was carried out using a VG PlasmaQuad ICP-MS. The

instrument configuration, internal standard correction procedures and the use of standard reference materials to check the accuracy of calibrations are given in Gooddy *et al.* (1995). Tabulated results of the full elemental array are given in Appendix 2 and reported as mmol/kg or μmol/kg as appropriate.

4.6 DETERMINING ISOTOPIC CONTENT OF CARBONATE MINERALS

Where samples were found to contain relatively high concentrations of calcium and magnesium, it was decided to undertake analysis for the isotopic composition of the carbonate material to see if this in any way related to physical and chemical composition and how, in turn, this may influence reaction with DNAPLs. Carbon and oxygen isotopic compositions of carbonate sediments and rocks are generally measured on the CO_2 gas released by reacting calcite and dolomite with 100% phosphoric acid. Accurate determination of the oxygen and carbon isotope composition of coexisting carbonate minerals such as calcite and dolomite is often hindered when the carbonate minerals cannot be physically separated (Walters *et al.*, 1972). Epstein *et al.* (1964) developed a technique based on different reaction rates of various carbonate minerals with phosphoric acid under variable reactions temperatures and this has subsequently been refined by Al-Aasm *et al.* (1990). Roughly 20 mg of carbonate as calcite or dolomite is required for the analysis. For the sandstone samples analysed this was equivalent to roughly 200 mg which was ground up using a pestle and mortar to a fine crystalline form, weighed into a durham tube and acidified in a pear shaped reaction vessel with 5 mL of anhydrous phosphoric acid. As the volumes of carbonate in the sample are relatively small, the samples needed to be loaded into 2 durham tubes. Samples for calcite were then heated at 25°C for 2 hours prior to analysis of $\delta^{18}O$ and $\delta^{13}C$ on the evolved CO_2 with a VG-Optima mass spectrometer by the methods detailed in Darling (1999) and Brownless *et al.* (1994). The same samples were then reacted for a further 4 hours at 50°C for the dolomite composition. The evolved CO_2 was then analysed as above. Results are reported in standard delta (δ) notation as parts per thousand deviations relative to the international standards PeeDee Belemnite (PDB).

4.7 RESULTS

4.7.1 Porosity and Permeability

A number of samples were taken in duplicate (adjacent core plugs from the same larger rock core) for both porosity (34 samples) and permeability (36 samples). Figure 4.1

shows how duplicates compare for permeability. Generally agreement between adjacent samples is good as demonstrated by a 1:1 relationship on the graph (R^2 = 0.93). The percentage difference between 2 samples has been calculated from:

$$\%difference = \frac{(SampleA - SampleB)}{(SampleA)} \times 100 \qquad (4.5)$$

where Sample A is the maximum value and Sample B is the minimum value. The smallest difference between adjacent samples is 0.6%. Some large differences do occur however with a maximum difference between two measurements of 73%. The mean difference between duplicate samples is 21%.

Figure 4.2 shows a comparison of duplicates for porosity measurements. Adjacent samples generally agree better than for permeability most likely reflecting the smaller range of porosity values. The smallest difference is 0.1% but two samples do differ by over 50%. The mean difference between duplicates is 6%. It is important to note that the differences in Figures 4.1 and 4.2 are mostly due to local scale variation in the matrix characteristics of sandstones and not experimental errors.

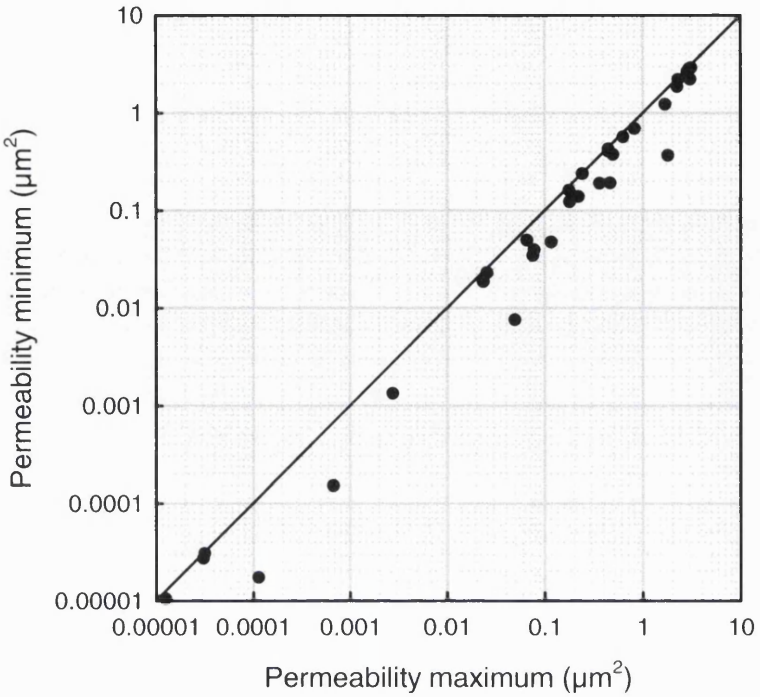

Figure 4-1 Comparison of permeabilities for duplicate samples.

Several samples were taken from the same core in both the vertical plane and in the horizontal plane. Ten comparison samples were made for gas permeability and these are shown in Figure 4.3. The graph clearly demonstrates that in the majority of cases samples taken perpendicular (or horizontal) to the rock core have higher permeabilities than those taken parallel (or vertical) to the rock core. This reflects the laminar nature of sandstones and the way that sand grains have been sorted. The inset figure has been created from finding the percentage difference (as calculated in equation 4.5 and where sample A is the vertical measurement) between vertically and horizontally sampled plugs. The mean difference between samples taken vertically and horizontally is 585% (median 270%).

Figure 4.4 shows a comparison of 11 samples for porosity measured on vertical and horizontal samples taken from the same core. These samples show much less variation than the permeability measurements with the majority of samples falling close to the 1:1 ratio ($R^2 = 0.90$). This is to be expected as the pore volume would be expected to be the same whether measured on the horizontal or vertical plane. The two samples where large differences occur most likely reflect the heterogeneity of the sandstones and the importance of sampling intervals.

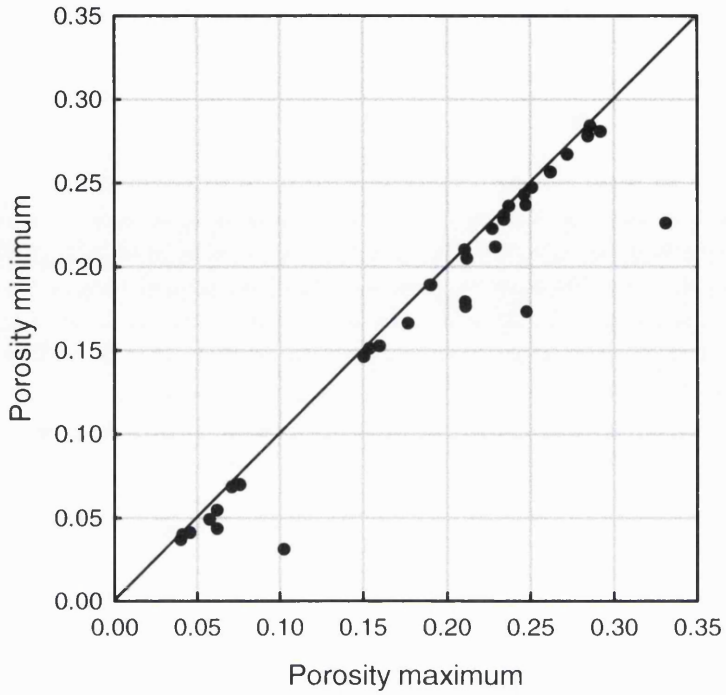

Figure 4-2 Comparison of porosity for duplicate samples.

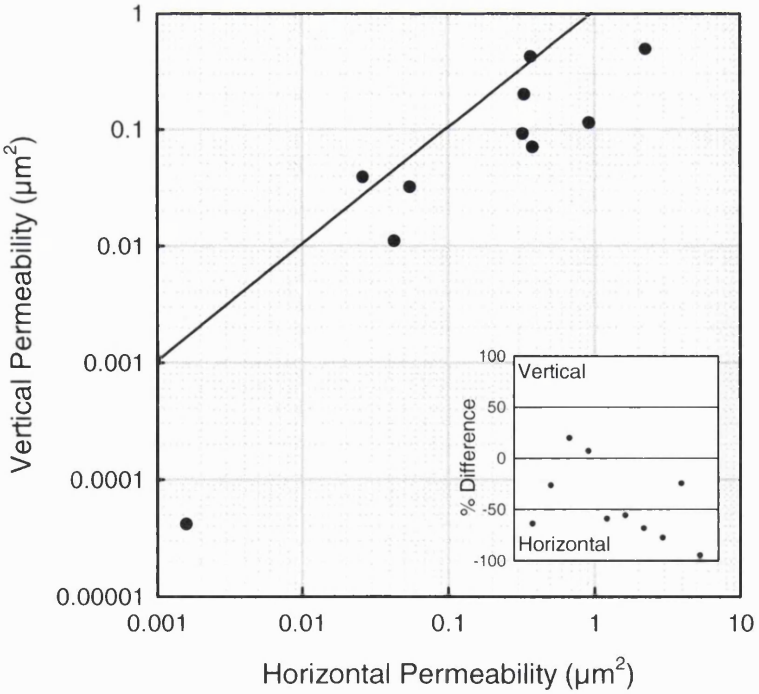

Figure 4-3 Comparison of permeabilities for samples taken vertically and horizontally. Inset is the percentage difference between horizontal and vertical sample pairs.

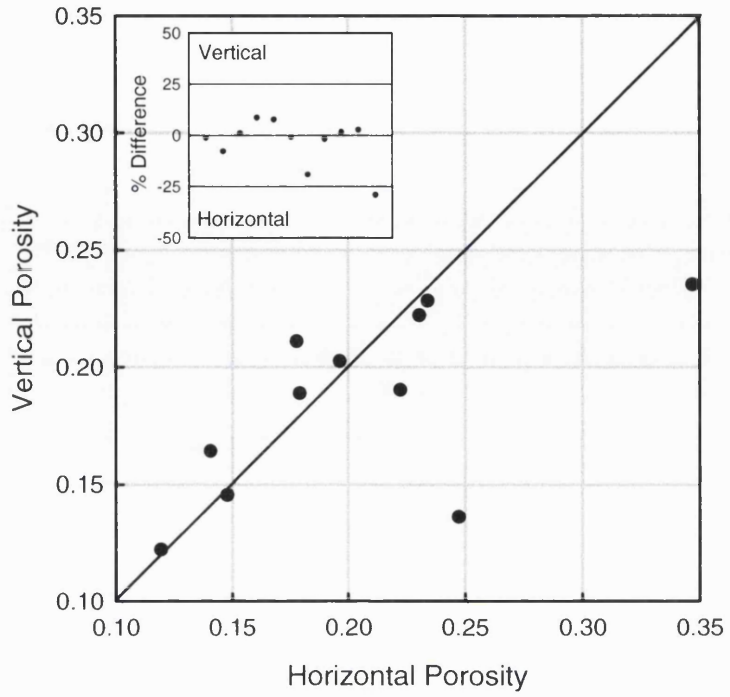

Figure 4-4 Comparison of porosities for samples taken vertically and horizontally. Inset is the percentage difference between horizontal and vertical sample pairs.

The measured physical parameters that strongly dominate fluid flow in porous media have been summarised and displayed in simple statistical form in Table 4.1. The table clearly demonstrates the very large variation in physical properties that Permo-Triassic sandstones can possess with permeability, for example, having a range of 6 orders of magnitude. The range is consistent of a much larger sample set (approximately 10,000 samples) for porosity and permeability determined by Allen *et al.* (1997).

Table 4-1 Statistical summary of gas permeability (k), porosity (ϕ), median pore size from MICP measurement, and the mean pore radius $\sqrt{k/\phi}$. [a]This study, [b]Allen et al. (1997).

	k^a (mD)	k^a (μm^2)	ϕ^a	Pore size[a] (μm)	$\sqrt{k/\phi}^a$ (μm)	k^b (mD)	ϕ^b
Mean	693	0.684	0.192	17.6	1.15	2624	0.238
s.d.	1260	1.244	0.073	15.5	1.19	4089	0.063
Median	132	0.130	0.210	14.3	0.76		
Max	7770	7.669	0.347	81.3	5.32	40908	0.454
Min	0.005	4.8E-06	0.031	0.03	0.008	0.011	0.012
n	152	152	153	66	143	9144	10417

Figure 4.5 shows a histogram of the porosity data. A one sample Kolmogorov-Smirnov test show there is only a 4% probability that the porosity data are normally distributed. Figure 4.6 shows a histogram for the log transformed permeability data. The histogram shows a bimodal distribution, one with relative high permeability which are probably relatively clean sands, and the other with a low permeability which may reflect a higher clay content.

Figure 4.7 shows a cross plot of porosity against permeability. The relationship between the two approximates to a power law of the form:

$$k = 1004\phi^{5.83} \tag{4.6}$$

with an R^2 value of 0.60. On closer inspection two populations may be identified i) with permeabilities less than roughly 0.0001 μm^2 and porosities between roughly 0.05 and 0.2 and ii) with permeabilities between 0.0001 and 10 μm^2 and porosities between 0.05 and 0.35. These have been identified on the graph by the red arrows. The first population identified is relatively insensitive to changes in porosity so even with comparatively high porosity, the permeability can still be low which might suggest small pore-throat sizes and larger pores or finely disseminated porosity.

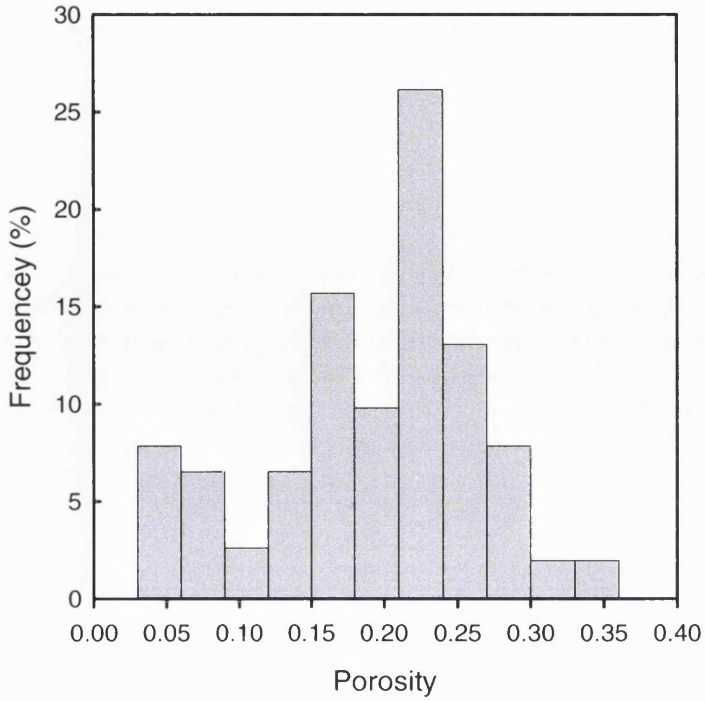

Figure 4-5 Histogram of porosity data. Samples have been binned in units of 0.03.

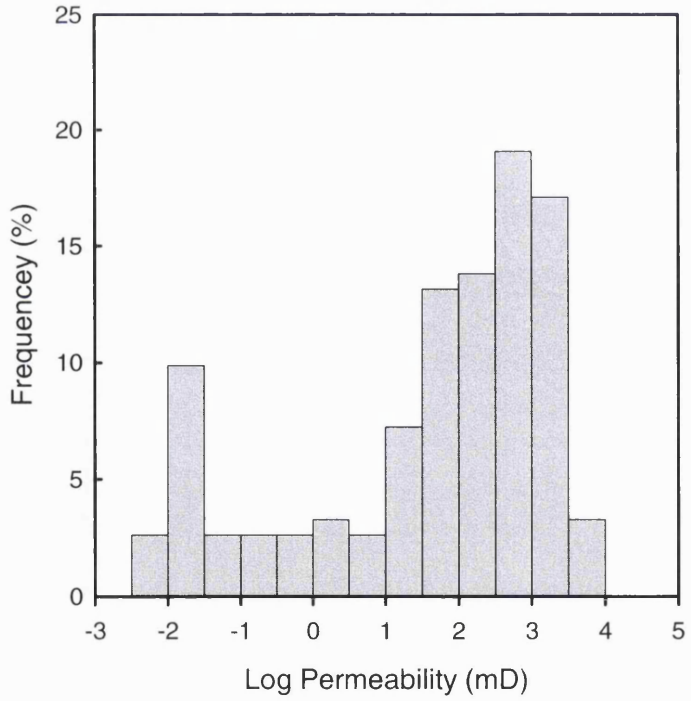

Figure 4-6 Histogram of permeability data. Samples binned in log units of 0.5.

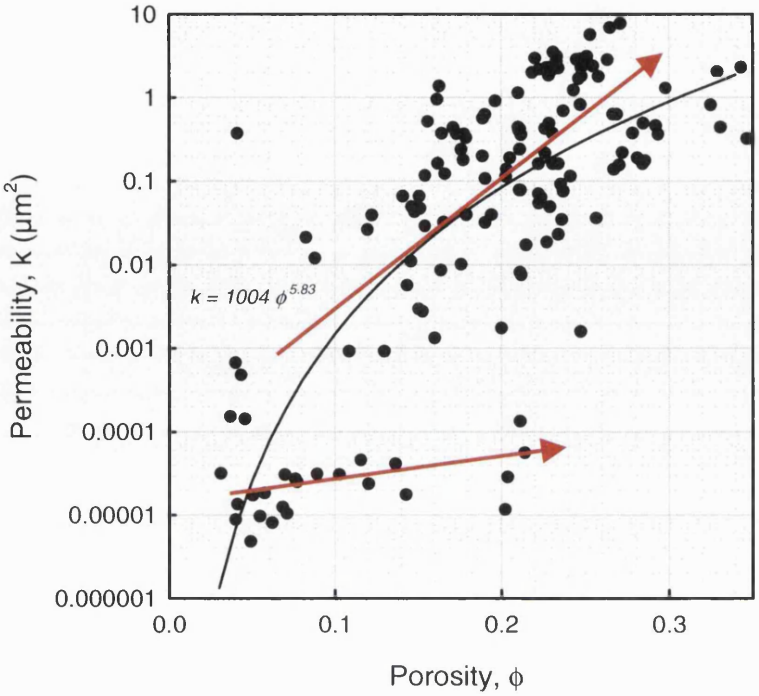

Figure 4-7 Cross plot of porosity against permeability. Red arrows show two possible populations. Continuous black line is best fit exponential.

4.7.2 Median Pore Size and Mean Pore Radius

A typical MICP curve is given in Figure 4.8. A common feature of MICP curves is the apparent intrusion of small volumes of mercury at very low pressures, i.e. an apparent intrusion into relatively large pores or pore-throats. This apparent intrusion is thought to be due to non-conformance of mercury with the rough surface of the sample when the sample vial is initially flooded with mercury prior to pressurisation (Vavra *et al.*, 1992).

It can be seen from Table 4.1 that pore size, both from the MICP determination and from the mean pore size calculation, varies over nearly four orders of magnitude. The calculated mean pore size is approximately $1/7^{th}$ of the measured median pore size.

The mean pore radius has been doubled to create a hydraulic diameter and compared with the pore diameter obtained by MICP measurements in Figure 4.9. The relationship can be described by

$$D_H = 2 \times \sqrt{\frac{k}{\phi}} = 0.141 \times Poresize_{Median} \qquad (4.7)$$

which has an R^2 of 0.65. Figure 4.9b shows that once again the data appears to fall into two approximate populations: i) where the mean pore diameter is roughly 0.05 μm but

the median pore size ranges over roughly 2 orders of magnitude between 0.1 and 10 μm and, ii) where mean pore diameter and pore size follow a fairly constant linear relationship. However, the relatively low values of calculated mean diameter may be associated with underestimation of gas permeability at low permeabilities.

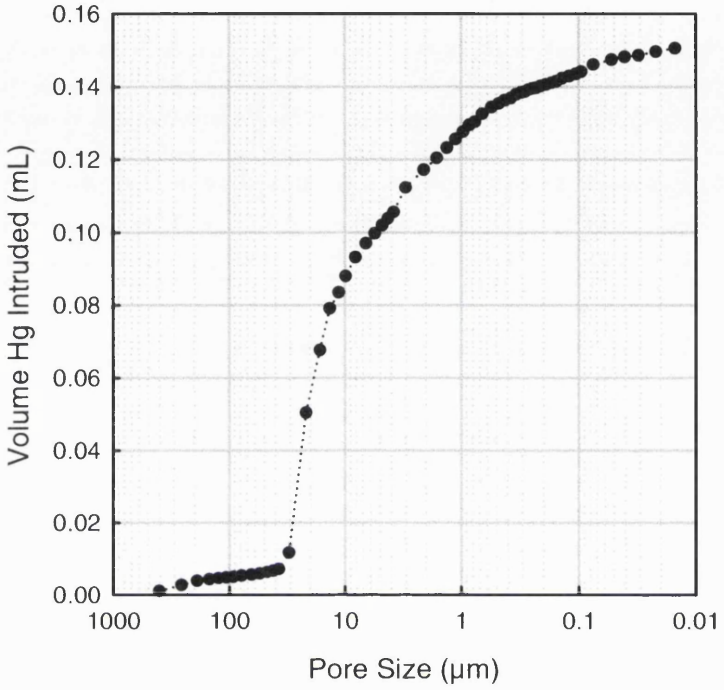

Figure 4-8 Typical pore size distribution curve generated by an MICP run.

An interesting observation is that many of the MICP curves obtained exhibit a power-law distribution over much of the pressure range. An example of this is given in Figure 4.10. The derivative of the MICP curve has been calculated by differencing the values at neighbouring points as in equation 4.8:

$$\frac{dCv}{dPs} = \frac{Cv_{(n+1)} - Cv_{(n)}}{Ps_{(n+1)} - Ps_{(n)}} \tag{4.8}$$

where Cv is the cumulative volume of mercury and Ps is the pore size.

Where a power-law relationship is observed it often extrapolates well over several orders of magnitude and can also be indicative of a fractal structure (Wong, 1988). The power-law is of the form:

$$\frac{dCv}{dPs} = A \times Poresize^{B} \tag{4.9}$$

For 54 of the measured MICP curves it was possible to fit equation 4.9 to the data using Microsoft® Excel Solver. Each data set was fitted over the entire range of pore sizes although some samples showed a different power law trend between 500 - 50 µm (see dotted line on Figure 4.10) compared with the trend from 10 - 0.01 µm. For completeness and ease of comparison all the data was fitted in the same way. A summary of this fitting exercise is shown in Table 4.2. The table shows that both the mean and median of the exponent B are close to –0.9. This power-law behaviour is applicable to sandstones but further work has shown that is not applicable to chalk samples.

Table 4-2 Summary of fitted values for power-law behaviour during MICP measurements on sandstones.

	A	B
Mean	0.0053	-0.8821
s.d.	0.0040	0.1705
Median	0.0044	-0.8830
Max	0.0255	-0.6122
Min	0.0011	-1.2302
n	54	54

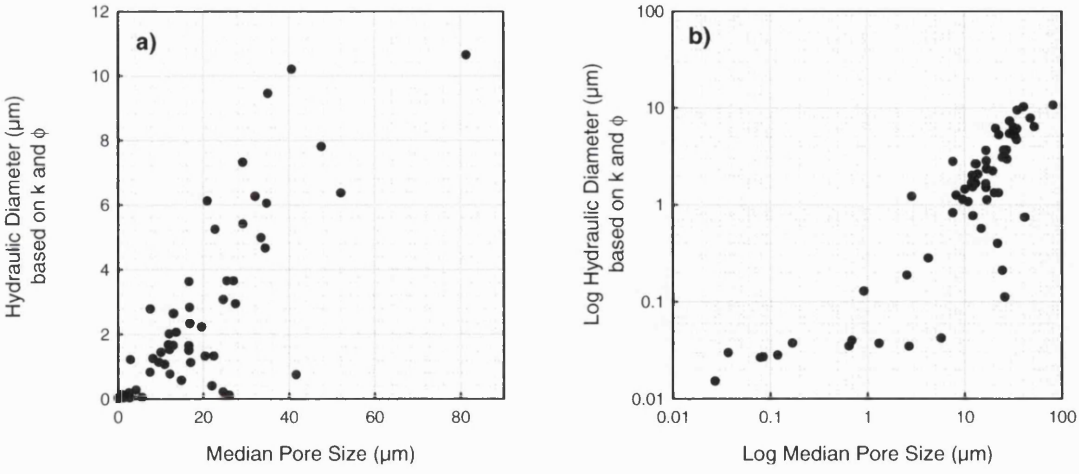

Figure 4-9 Cross plots of median pore size as determined by MICP measurement and hydraulic diameter determined from porosity and gas permeability measurements. Plots are in a) linear space and b) log space.

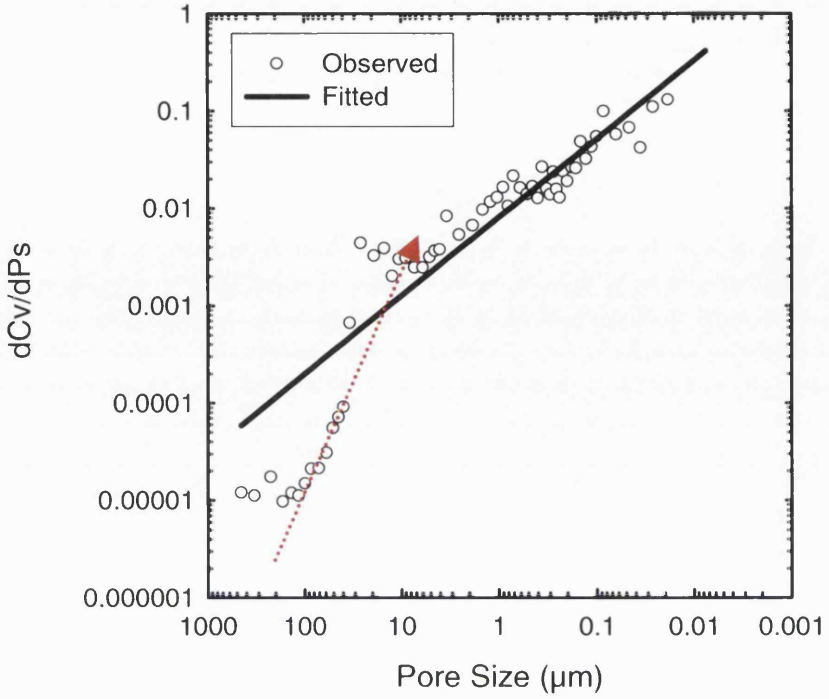

Figure 4-10 Typical differential of invading mercury volume against change in pore size. Solid black line is best fit for all pore sizes, dotted red line indicates possible different power law relationship for larger pores observed for some samples.

4.7.3 Surface Chemistry and Isotopic Content of Carbonates

The 0.43M HNO_3 extractions for surface chemistry is summarized in Table 4.3 (the full dataset is given in Appendix 2). Concentrations for all of these elements can be seen to vary over 3-4 orders of magnitude. Mean values are higher than the median suggesting the presence of a few high concentrations. Figure 4.11 shows histograms for four of the major components. Both calcium (Figure 4.11a) and magnesium (Figure 4.11b) appear to show bimodal distributions which may be related to the permeability (high permeabilities correspond with low total concentrations of calcium and magnesium and relatively low permeabilities correspond with high total concentrations of calcium and magnesium) whereas a one sample Kolmogorov-Smirnov test shows that there is a 90% probability that the iron data (Figure 4.11c) are lognormally distributed. Manganese seems to be skewed towards the higher concentration range although the reasons for this are unclear.

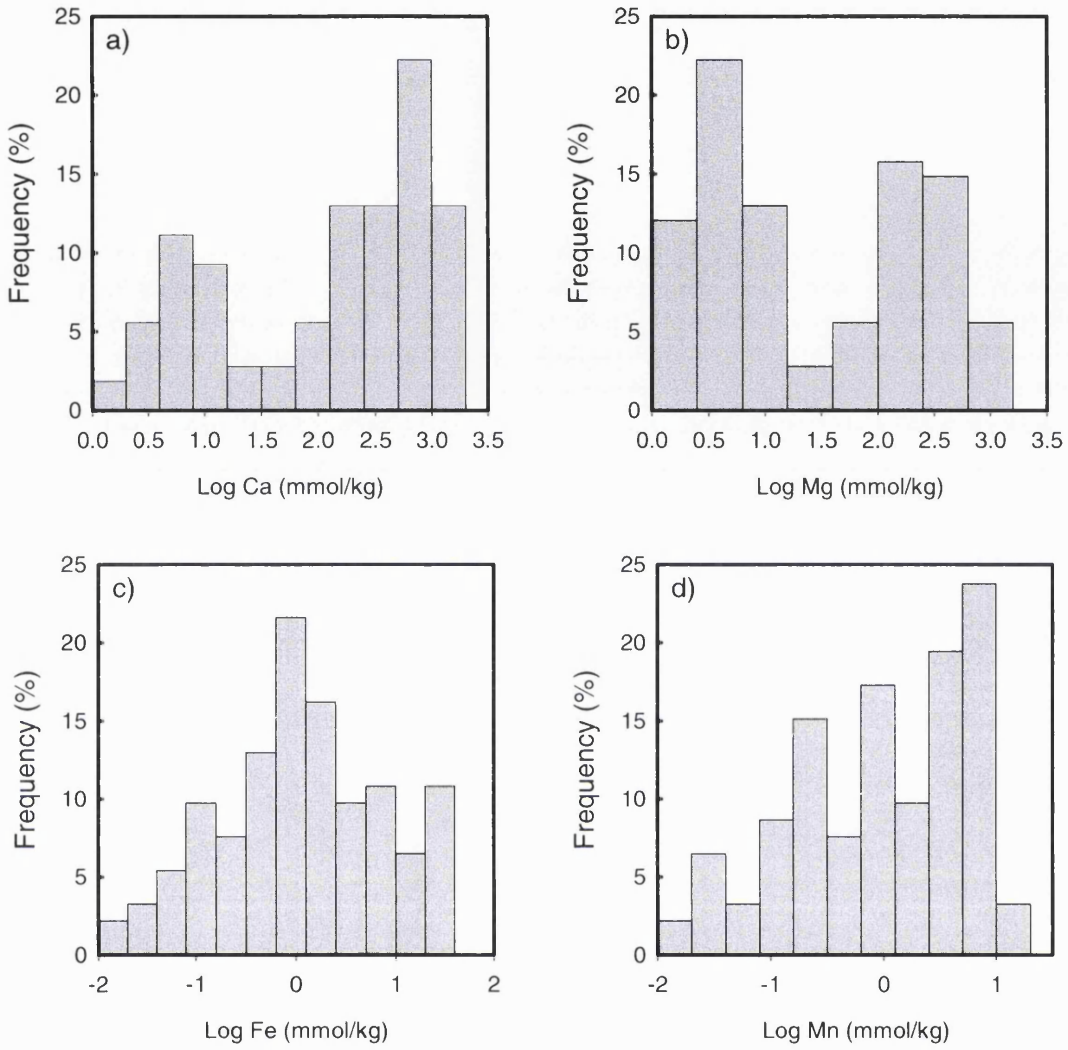

Figure 4-11 Histograms for Log Ca, Log Mg, Log Fe and Log Mn concentrations. Samples have been binned on log unit intervals of 0.3 for a), c) and d) and log unit intervals of 0.4 for b).

Table 4-3 Statistical summary of major chemical components determined by 0.43 M HNO_3 extraction.

	TOC	Ca	Mg	Fe	Mn	Si	Al	S	P
	%	mmol/kg							
Mean	0.11	423	128	4.59	2.73	2.46	3.26	11.2	5.51
s.d.	0.17	465	202	7.49	3.36	1.96	3.77	37.7	4.78
Median	0.04	213	8.33	1.03	1.20	1.73	2.26	1.20	4.97
Max	0.46	1560	749	33.6	18.5	9.32	33.1	204	20.9
Min	0.03	1.34	0.21	0.02	0.01	0.1	0.02	<0.01	<0.01
n	6	108	108	108	108	108	108	108	108

The sum of calcium and magnesium accounts, on average, for more than 80% (median > 90%) of the total extractable cations (Table 4.4). The iron and magnesium rich carbonates are less common than calcite and dolomite in most sandstones, but are abundant constituents of some. In this data set Fe accounts for 0.002 – 14% of the total extractable cations with a mean of 2% and Mn accounts for 0.001 – 0.1% with a mean of 0.01%. Gypsum, anhydrite, and barite are the three common sulphates found as cementing agents in sandstones. The sulphate of these cements is ultimately derived from that dissolved in sea water or in subsurface brines, but the cements, in contrast to bedded deposits of gypsum and anhydrite, are not taken as certain indicators of evaporite formation. A variety of other minerals are of chemical origin, the most important being phosphates. The precipitation of phosphate in most sandstones appears to be related to biota, as reworked products of bone or shell formation. The mineralogy of phosphates can be complex, with most minerals being some mixture of hydroxy-fluor-carbonate apatite [$Ca_5(PO_4,CO_3,OH)_3(F,OH)$]. Phosphate abundance is generally related to organic productivity.

Table 4-4 Statistical summary showing percent composition in terms of total extractable cations.

	Ca	Mg	Fe	Mn	Al
		%			
Mean	61	21	2.1	0.01	8.0
s.d.	23	17	2.3	0.01	14
Median	54	22	1.5	0.01	1.2
Max	99	45	14	0.08	85
Min	7.6	0.28	<0.01	<0.01	<0.01

Cross plots for Ca, Mg, Fe, Mn, Si, Al, P and SO_4 are shown in Figures 4.12a-f. A clear relationship can be seen between Mg and Ca (Figure 4.12a), with two populations evident: one where Mg is absent and the other with a 1:1 molar ratio between Ca and Mg. This is consistent with the samples containing a calcite matrix (all Ca) or a dolomitic matrix (mixture of Ca and Mg). The calcite and dolomite of sandstone cements are relatively pure, with no excess Mg in calcite and no excess Ca in dolomite. Some of the pore filling cement may be recrystallised from originally detrital carbonate grains or may be a precipitate from an aqueous solution in an originally empty pore.

Calcite and dolomite precipitation is generally controlled by the relative amounts of Ca and Mg and also the pH of the environment. The same is true for iron and manganese carbonates but they also have an additional dependence on the oxidation-reduction balance of the environment. Organic matter is the most probable reducing agent responsible for iron and manganese reduction, therefore their presence as metal carbonates is commonly linked to environments where organic matter is abundant. Limited data on the organic carbon content of UK Permo-Triassic sandstones (Table 4.3) shows concentrations to be very low, typically less than 0.1%.

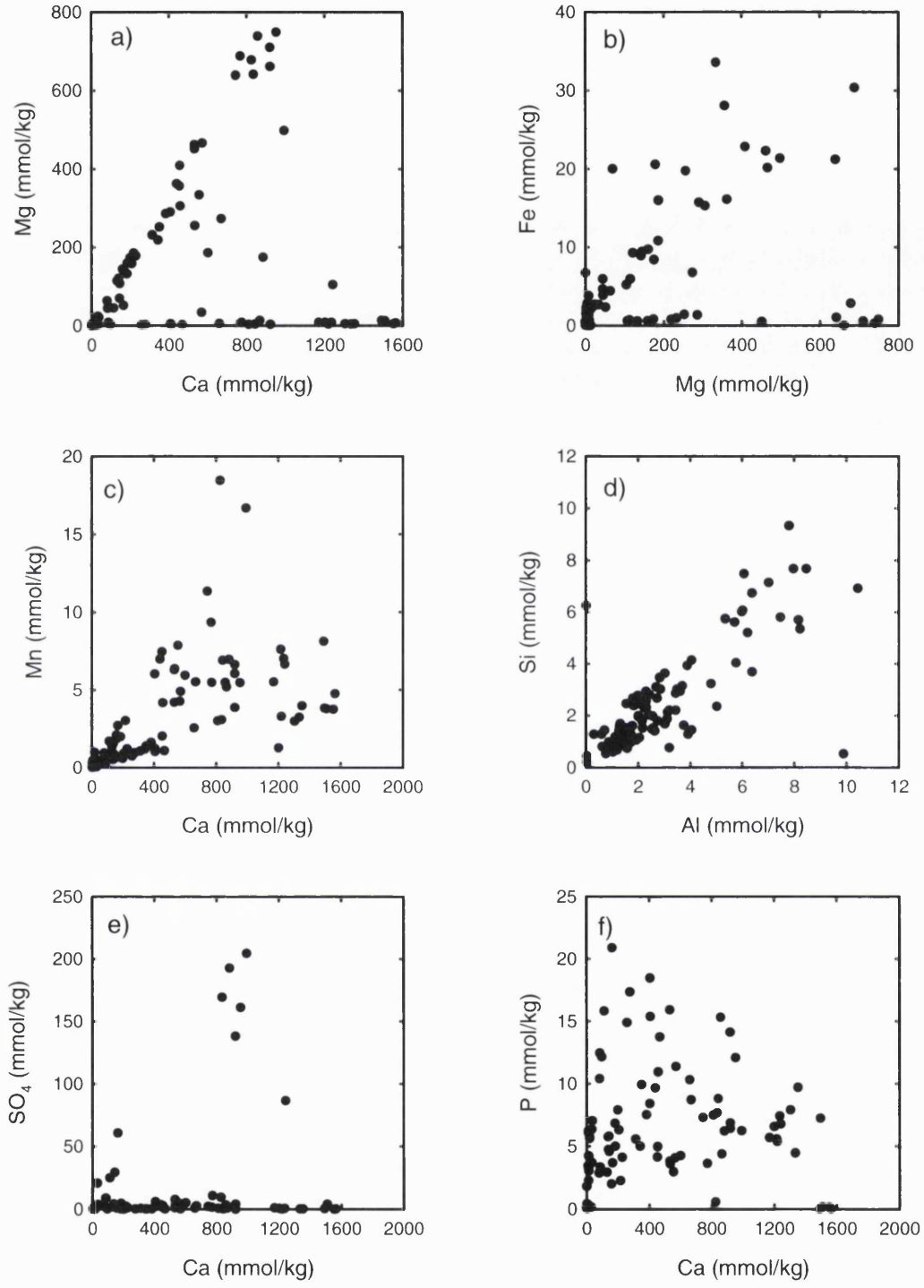

Figure 4-12 Selected cross plots of extracted chemical components.

There does however appear to be a relationship between Mg and Fe (Figure 4.12b) with a ratio of roughly 20:1. Iron-rich magnesium carbonates are frequently found as concretionary accumulations in sandstones; calcite and dolomite concretions are also well known. These concretions could be related to bedding planes, which may be either the result of special permeability along certain bedding planes, or reflect a

particular composition of the water in the environment. However, with this data set, no such relationship is observed between Fe concentration and permeability.

Figure 4.12c shows the relationship between Mn and Ca. From the cross plot, two populations may just be observable. However, this may not be a genuine relationship with Ca, rather it reflects the total sum of cations desorbed and some dissolution of the matrix by the nitric acid. Figure 4.12d supports this with the 1:1 linear molar ratio between Si and Al, indicating some dissolution of the clays rather than purely extracting surface species.

Figure 4.12e indicates that little gypsum is present in any of the samples with just a few samples showing high concentrations of both calcium and sulphate. As the maximum molar ratio of Ca to SO_4 is 4:1, the gypsum is not the major component of the matrix cement. Phosphorus concentrations are generally quite significant although show no relationship with Ca (Figure 4.12f). This may suggest the presence of apatite but at varying abundances in different samples.

A summary of isotopic composition of the samples analysed for calcite and dolomite are shown in Table 4.5. The range of values obtained is quite large although the mean values for calcite are in agreement with those obtained by Bath *et al.* (1979) and are characteristic of late carbonate cements. It is generally considered that variations in $\delta^{13}C$ reflect the composition of the original source of carbon while changes in $\delta^{18}O$ show the influence of environment of deposition more strongly. Figure 4.13 shows that there is a general trend with depth for both calcite and dolomite with both becoming isotopically lighter with depth which may be related to different depositional phases. In this small sub-set of samples it is also interesting to note that the majority of calcite samples are from depths in excess of 1500 m and that the majority of dolomitic samples come from less than 100 m.

Table 4-5 Statistical summary of $\delta^{13}C$ and $\delta^{18}O$ components of calcite and dolomite in selected samples.

	Calcite		Dolomite	
	$\delta^{13}C$ ‰	$\delta^{18}O$ ‰	$\delta^{13}C$ ‰	$\delta^{18}O$ ‰
Mean	-5.21	-5.96	-3.07	-3.44
s.d.	2.55	2.38	3.06	3.73
Median	-5.51	-6.38	-2.86	-1.93
Max	-1.79	-2.40	0.38	0.89
Min	-9.09	-10.13	-7.05	-11.64
n	12	11	8	8

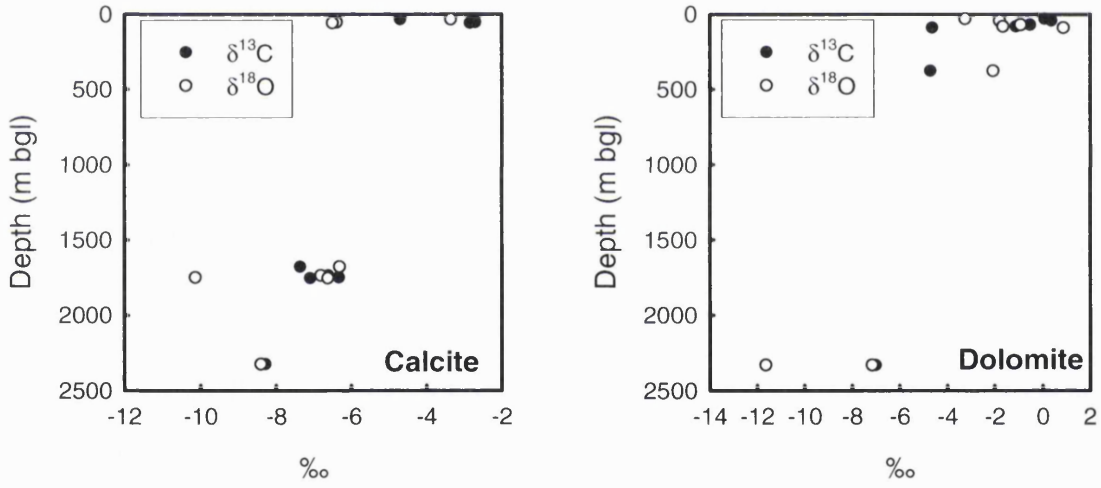

Figure 4-13 Relationship between carbon and oxygen isotopes in calcite and dolomite with depth.

4.8 CHAPTER FOUR SUMMARY

This chapter has shown the standard techniques used to characterise the samples and that the data produced is consistent with a larger data set for the Permo-Triassic sandstones (Allen *et al.*, 1997). Duplicate samples for porosity and permeability measurement show good replication. Duplicate samples taken in a horizontal and vertical plane show much better agreement for porosity measurements than permeability. The mean pore-throat diameter $\left(2\sqrt{k/\phi}\right)$ can be correlated with median pore size as determined from MICP measurements although the mean pore diameter is

found to be roughly 7 times smaller than the median pore diameter. When the derivative of the MICP curve is plotted against pore size a power law relationship is observed for the majority of the samples. The solid phase chemistry shows the samples to be dominated by either calcite or dolomite cements and a 1:1 relationship between aluminium and silicon. Samples from depths in excess of 1500 m have relatively isotopically lighter calcite and dolomite composition than the shallower samples.

5 Development and Application of a Laboratory Method for Determining DNAPL Saturation Curves

This chapter describes the development and testing of a method to produce pressure saturation curves on small consolidated cores by using a centrifuge to provide the driving force. Pressure saturation curves were generated for 51 of the Permo-Triassic sandstone cores and the majority could be parameterised by using both the Brooks-Corey (1966) and van Genuchten (1980) functions. The concurrence between the two algebraic functions is discussed and the relationship between wetting phase saturation and non-wetting phase saturation explored.

5.1 APPARATUS USED

A fully water-saturated cylindrical core sample of about 24.5 mm in diameter and about 27.5 mm in length was placed in a Nalgene test tube. The tube was then filled with PCE so as to immerse completely the sample when the sample is in a horizontal plane. Approximately 30 ml of tetrachloroethene was required. The core was supported by the lower rim of the test tube which is slightly narrower than the top, so allowing solvent to cover the whole core (Figure 5.1). The tube was then loaded into a bench-top Centaur 2 Centrifuge (Sanyo Gallenkamp, UK) fitted with a 4-place swing-out rotor. This arrangement permitted the measurements of volumes of water expelled from the sample during centrifugation as the water floats to the top of the PCE in the centrifuge tube. Four samples could be centrifuged simultaneously by this technique although in practise only two were run at a time so that the centrifuge rotor head was not excessively stressed.

The run began at the lowest speed that could be set on the Centaur 2 centrifuge, 100 rpm which is a force at the base of the core of roughly 0.1 kPa depending upon the size of the core plug (Table 5.1) (see Section 2.4.2, equation 2.8). The rotation rate was held constant for 90 minutes. The centrifuge was then stopped and the displaced water removed with a glass pipette and placed in a 1mL burette with 0.01 mL divisions for accurate measurement. The centrifuge was then restarted and run for a further 30 minutes. This process was repeated until no further water was eluted from any of the cores. For a given driving force, most water was completely eluted within 180 minutes.

The rotation rate was increased incrementally as in Table 5.1, to a maximum of 2800 rpm. This table also shows the force on the sample base for a 35, 30 and 25 mm long core. This final velocity was chosen as it is equivalent of a head of DNAPL (PCE) of around 5-6.5 m which would represent a significant solvent spill. Some low permeability samples were tested up to 20,000 rpm on a Beckman J-2 20 high speed centrifuge, an equivalent head of 180 m of PCE. Many samples began to degrade and ultimately disintegrate when taken beyond 3500 rpm (roughly 10 m of PCE).

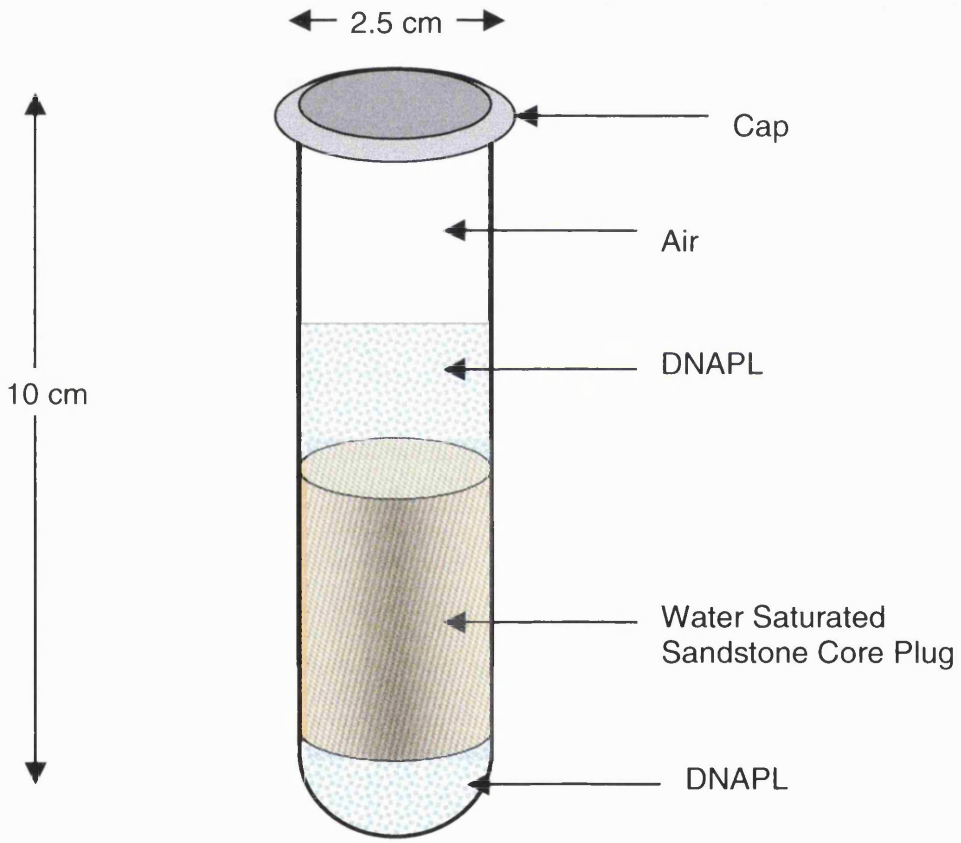

Figure 5-1 Schematic of centrifuge tube used in immiscible displacement centrifuge technique.

Table 5-1 Force per rotation for given core sizes. The pressure given is the pressure calculated for the base of the core.

Rotation (rpm)	Force (kPa)		
	35mm	30mm	25mm
100	0.13	0.12	0.10
200	0.54	0.48	0.41
300	1.21	1.07	0.92
400	2.15	1.90	1.64
500	3.36	2.97	2.55
600	4.84	4.28	3.68
800	8.60	7.61	6.54
1000	13.4	11.9	10.2
1200	19.4	17.1	14.7
1500	30.2	26.8	23.0
2000	53.8	47.6	40.9
2500	84.0	74.3	63.9
2800	105	93.2	80.1

5.2 METHOD VERIFICATION

Each centrifuge run generates an evolved volume of water for each angular velocity. In Figure 5.2a-c, the water displaced by DNAPL has been summed and plotted against rotation speed. It can be seen that the curve shape is very similar to that generated during the MICP experiments and this is of little surprise as the overall processes are the same. In all cases the water started to be displaced at 200-500 rpm, equivalent to pressures between 0.4 and 3.4 kPa.

In Figures 5.2d-f, the rotational speed has been converted to a pressure using equation 2.8. These graphs neatly demonstrate the pressure where most water is displaced. This varies from about 2 kPa for sample 1530/8v, to roughly 5 kPa for sample 1526/4v, to about 10 kPa for sample 1524/4v.

In Figures 5.2g-i the normalised wetting saturation (water) has been plotted against pressure. This is calculated as follows:

$$P_{vol} = \pi r^2 h \phi \tag{5.1}$$

where P_{vol} is the total pore volume, r is the core diameter, h the core height and ϕ the measured porosity.

The normalised wetting phase saturation, S_w, therefore is

$$\frac{\pi r^2 h\phi - W_{disp}}{\pi r^2 h\phi} \tag{5.2}$$

Where W_{disp} is the measured displaced volume of water.

Each plot in Figure 5.2 shows two sets of data which represent adjacent sub-samples (side-by-side) taken from the same core. Generally the duplicates show good agreement. It is interesting to note that although the cumulative volume vs. rotation plot for sample 1524/4v looks to be in close agreement (Figure 5.2a), after a correction has been made for the different pressure exerted on two cores of different length (Figure 5.2d) the agreement does not look as good, and a final correction for the volume difference (Figure 5.2g) shows the final wetting saturations to vary quite considerably (a final saturation of 0.52 compared with 0.46). By comparison the volume vs. rotation graph for sample 1526/4v looks quite different between duplicates, but the final difference in measured wetting phase saturation is smaller (0.51 compared with 0.47). The final wetting phase saturations for sample 1530/8v vary by 0.05 (0.40 compared with 0.35).

Figure 5.3 shows a simple cross plot for all three sets of duplicates, comparing the degree of saturation at each pressure step. The greatest deviation from a 1:1 relationship is for sample 1524/4v (y=1.17x), and the smallest deviation from unity is sample 1530/8v. It is therefore considered that the method is reproducible and can be used to determine $P_c(S_w)$ curves for a number of varying sandstones.

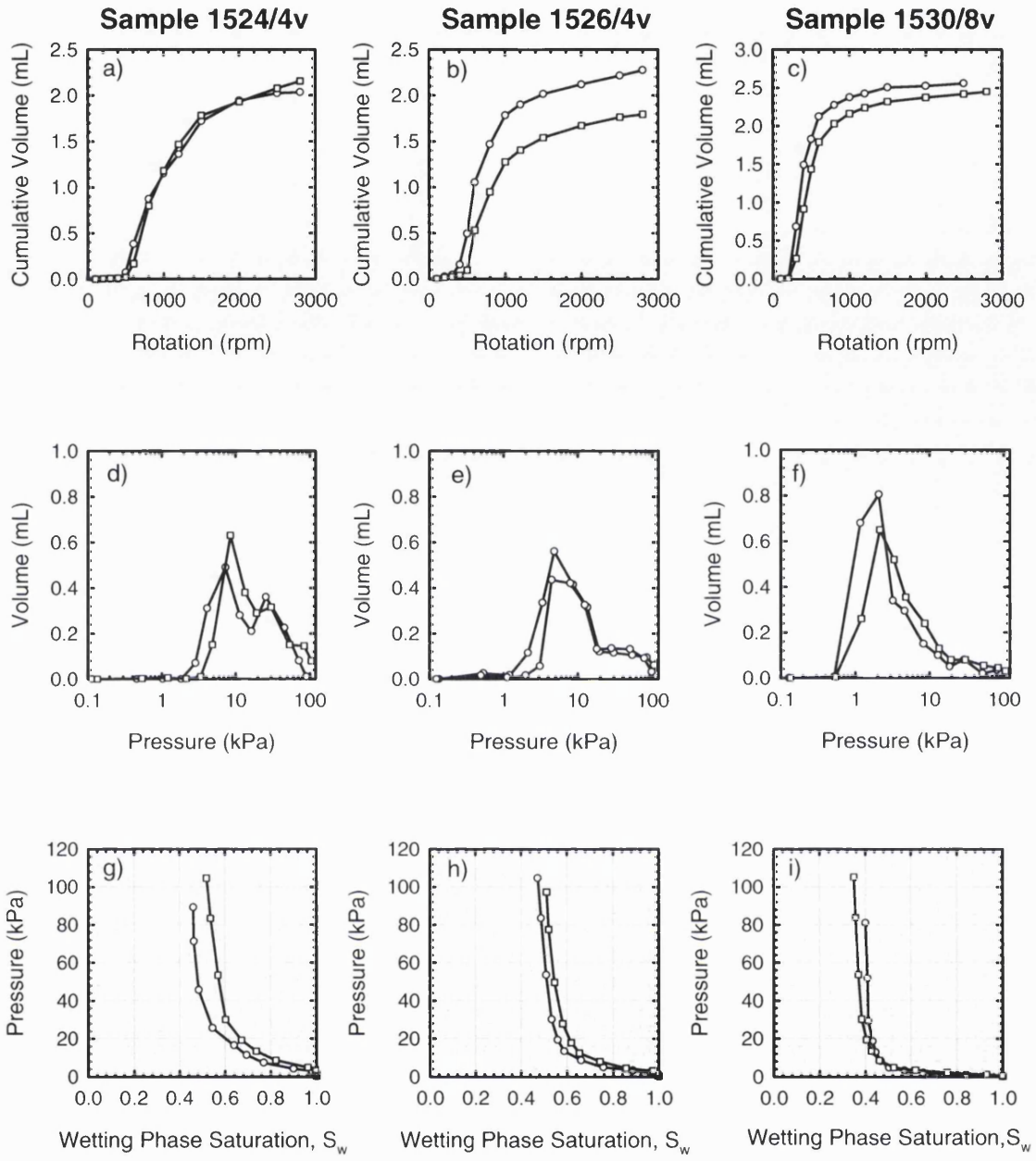

Figure 5-2a-i Sample duplicates for centrifuge immiscible displacement method.

5.3 VALIDITY OF DATA SUBSET USED IN $P_C(S_W)$ EXPERIMENTS

In order to carry out a realistic number of $P_c(S_w)$ experiments it was necessary to take a subset of samples from the larger dataset characterised in Chapter 4. The physical properties of the 51 sample subset used in the DNAPL entry pressure experiments are summarised in Table 5.2. The mean and median permeability is slightly higher in this sub-set than in the full data set (see Table 4.1) although the range is almost identical.

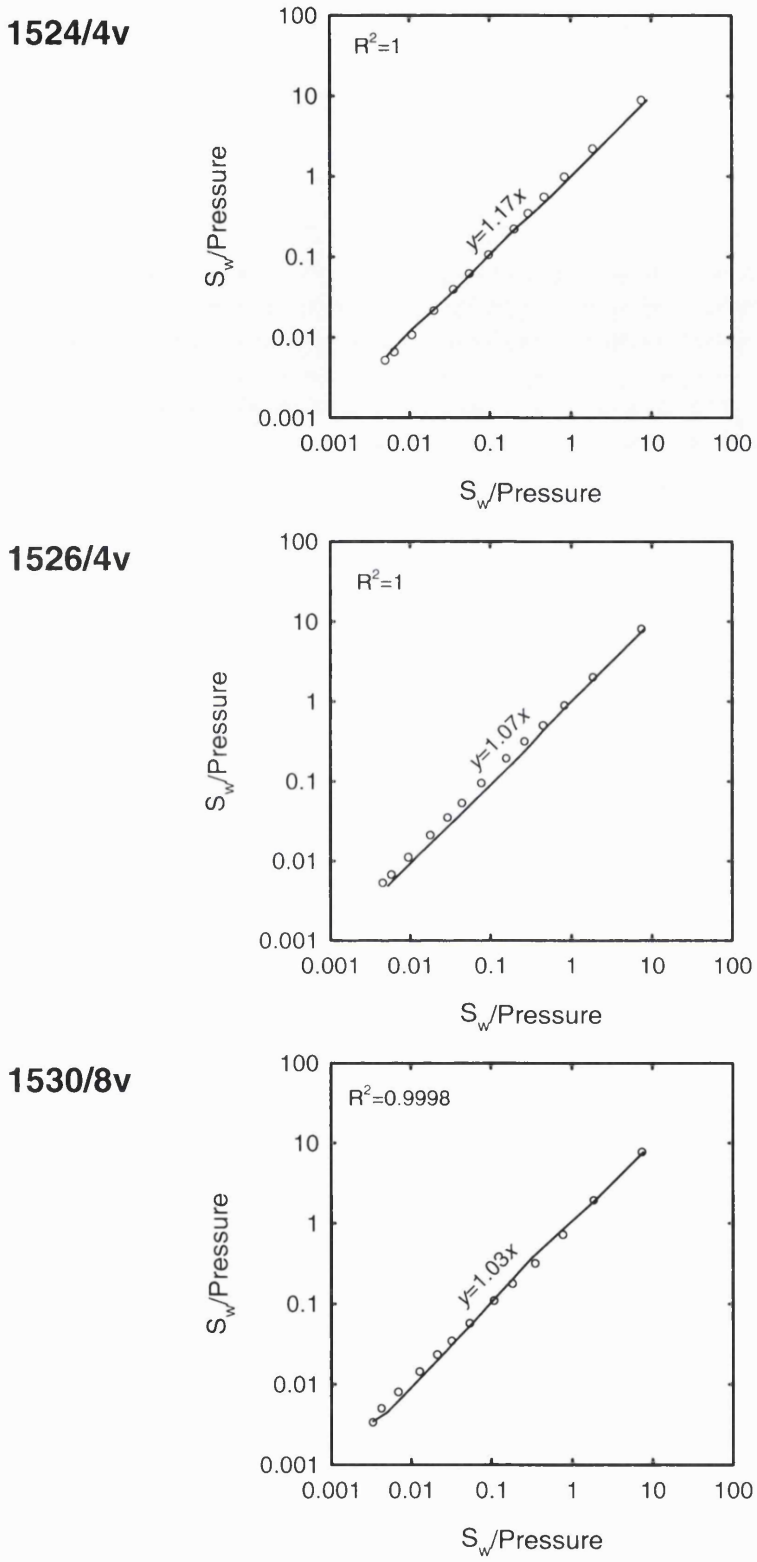

Figure 5-3 Cross plots of residual water saturation per pressure step for duplicate samples.

The porosity values, both mean and median, are nearly identical to the full data set as are the pore sizes of the samples used.

Table 5-2 Statistical summary of physical properties for sub-samples used in DNAPL entry pressure experiments.

	k (mD)	k (μm^2)	ϕ	Median Pore size (μm)	$\sqrt{k/\phi}$ (μm)
Mean	959	0.947	0.196	18.3	1.24
s.d.	1777	1.754	0.087	17.0	5.65
Median	163	0.161	0.218	14.9	0.75
Max	7770	7.669	0.343	81.3	5.32
Min	0.009	8.2E-06	0.037	0.03	0.008
n	51	51	47	42	47

The weak acid extraction data for the 51 sample subset is given in Table 5.3. There are only 41 analyses as a number of samples are duplicates. Mean and median calcium concentrations are slightly higher than the larger data-set (Table 4.3) although the same range is encompassed. Mean and median concentrations for Mg are slightly lower than the larger data set as is the case for Fe, Mn and Si. However, these differences are small and in most cases the range of chemical concentrations covered is similar between the two datasets. It is therefore considered that this sub-set is representative of the larger set of data.

Table 5-3 Statistical summary of 0.43M HNO_3 extraction data for sub-samples used in DNAPL entry pressure experiments.

	Ca	Mg	Fe	Mn	Si	Al	P
	mmol/kg						
Mean	500	79.7	2.80	2.20	2.27	3.01	5.78
s.d.	548	145	6.01	2.50	1.83	2.72	5.20
Median	259	6.39	0.708	1.02	1.62	2.32	5.80
Max	1560	688	30.3	9.34	7.66	12.1	18.5
Min	1.34	0.21	0.02	0.02	0.18	0.04	<0.01
n	41	41	41	41	41	41	41

5.4 FITTING PRESSURE SATURATION CURVES USING BROOKS-COREY AND VAN GENUCHTEN EQUATIONS

In order to describe the $P_c(S_w)$ curves produced by the centrifuge method and to compare them in a rigorous manner it was necessary to fit the data using empirical functions. For comparison the curves were fitted using two different and well established pressure-saturation functions, the van Genuchten function (equation 2.11) and the Brooks-Corey function (equation 2.12) both of which use a normalised wetting fluid saturation as defined in equation 2.13.

Curve fitting was performed using a least squares minimisation routine using Microsoft® Excel Solver, with a precision of 10^{-6}, a tolerance of 5% from true optimal value, and convergence to 0.001. Linear extrapolation was taken from a tangent vector and a quasi-Newtonian method used for the direction of search at each iteration which are default settings for the software. For each function 3 variables are adjusted: P_0, S_r and n (see equations 5.3 and 5.4) for the van Genuchten function and analogously P_d, S_r and λ (see equation 5.5) for the Brooks-Corey function.

There is a range of characteristic pressures associated with $P_c(S_w)$ curves, and a variety of, often conflicting, names have been used to describe these features of intrusion curves (Dullien 1979). 'Entry' pressure may be defined by extrapolating P_c to $S_w = 1$, where S_w is the wetting fluid saturation. This corresponds to the pressure required to invade the largest pores on the exterior of a sample. The value P_d in the Brooks-Corey function is close to this value. 'Breakthrough', 'displacement' or 'threshold' pressure is the pressure that corresponds to the formation of a continuum of non-wetting phase through the pore network. Katz and Thompson (1986, 1987) suggested that threshold pressure is associated with the inflection point on a capillary pressure curve and equated this with the percolation threshold for the system. In the van Genuchten function P_0 is often associated with this inflection point but is not quite equivalent (see section 5.5.3). In some porous media the 'entry' and 'breakthrough' pressures may be close, but in many consolidated media, including some sandstones, the 'breakthrough' pressure may be significantly greater than the 'entry' pressure as has been shown by Bloomfield *et al.* (2001) and illustrated in Figure 5.4.

P_0 and P_d are constrained in the fitting parameters to be greater than zero. In the van Genuchten function, n is constrained to be greater than unity. In the Brooks-Corey function λ is constrained to be greater than zero. S_r in both cases is constrained so that it

is between zero and unity. The wetting-fluid saturation, S_r, is often called the residual saturation. It is approximately the wetting-fluid saturation at which the $P_c(S_w)$ curve appears to approach a vertical asymptotic value (Figure 5.4).

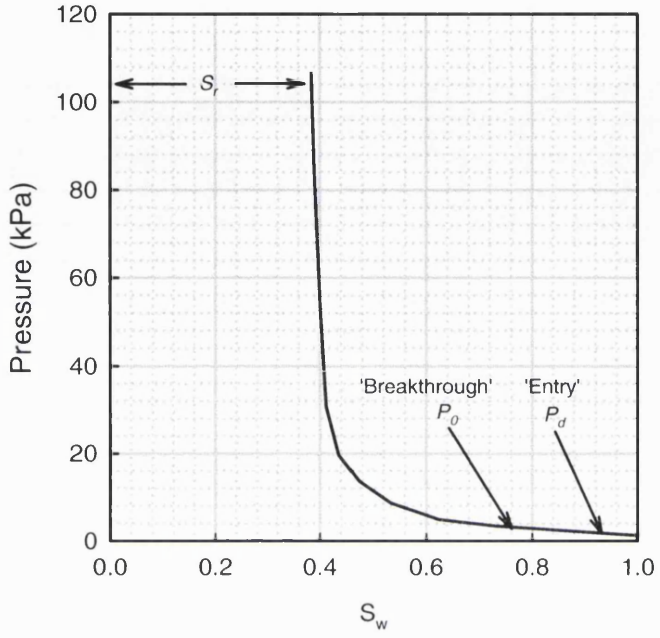

Figure 5-4 Illustration of residual wetting fluid saturation (S_r), 'Breakthrough pressure' (P_0 as determined from the van Genuchten function) and 'Entry pressure' (P_d as determined from the Brooks-Corey function).

The variable S_m is kept constant at unity as this is convention for when DNAPL is invading into a water saturated medium; it is less than unity when water displaces DNAPL because of entrapment of DNAPL although such hysteresis effects are not considered in this thesis.

5.4.1 Rearranging the van Genuchten Function

To fit the van Genuchten function to the $P_c(S_w)$ curve it is necessary to rearrange equation 2.11 to express it in terms of the wetting phase saturation, S_w, as this is the measured parameter in the centrifuge experiments. This gives equation 5.3:

$$S_w = \left(1+\left(\frac{P_c}{P_0}\right)^n\right)^{-m}(S_m - S_r)+S_r \qquad (5.3)$$

where

$$n = \frac{1}{1-m} \tag{5.4}$$

and (from 2.13)

$$S_e = \frac{S_w - S_r}{S_m - S_r}$$

5.4.2 Rearranging the Brooks-Corey Function

Similarly, to fit the Brooks-Corey function to the $P_c(S_w)$ curve it is also necessary to rearrange the function to express it in terms of the wetting phase saturation, S_w. This gives equation 5.5:

$$S_w = (S_m - S_r)\left(\frac{P_d}{P_c}\right)^{\lambda} + S_r \tag{5.5}$$

The raw data from the centrifuge experiment needs to be amended before fitting the Brooks-Corey function. The data is truncated to the pressure when penetration of the DNAPL begins. This is due to the shape of the curve generated by the Brooks-Corey function. Bloomfield *et al.* (2001) also used this approach when fitting the Brooks-Corey function to MICP curves.

5.5 RESULTS

5.5.1 Curve Fitting

A typical result from the pressure-saturation method developed is shown in Figure 5.5 along with best fit curves as calculated by the van Genuchten and Brooks-Corey functions. Both functions provide excellent fits to the curve with R^2 of 0.996 for the van Genuchten function and R^2 of 0.999 for the Brooks-Corey function. Both functions were generally very successful in fitting the $P_c(S_w)$ curves with the van Genuchten function fitting 94% of the samples tested and the Brooks-Corey function able to fit 88% of samples.

All the van Genuchten and Brooks-Corey parameters determined are presented in Table 5.4. Three samples could not be fitted by either the van Genuchten function or the Brooks-Corey function. No penetration of DNAPL was observed in any of these samples up to a pressure of 100 kPa. Sample 27/8v/2 was centrifuged at high speed

generating a final pressure of 2800 kPa. At this pressure just 2.5% of water in the pore space was displaced and no regular shaped $P_c(S_w)$ curve was observed.

Sample 27/1v/1 was also centrifuged at high speed but it was not possible to fit by using the Brooks-Corey function. The van Genuchten function on the other hand was able to provide a reasonable fit to the data (R^2=0.87) as a small inflection point occurred. Samples 1535/5v/1 and 1537/5v/1 were also successfully fitted by the van Genuchten function but not the Brooks-Corey function. In both cases a small volume (<2% of water in pore space) was displaced at a low pressure so generating an L-shaped curve which the van Genuchten function could interpolate. The full data set of pressure saturation is given in Appendix 4 together with the pore volume for each sample.

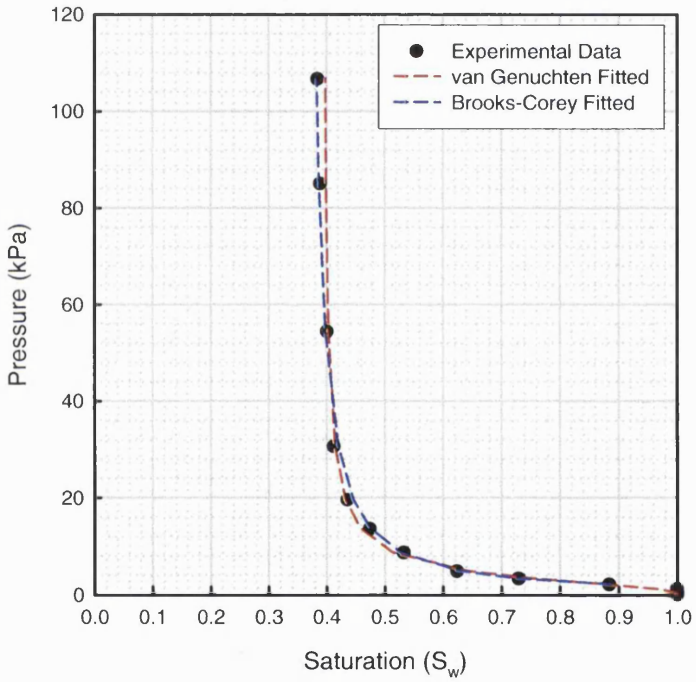

Figure 5-5 Typical pressure saturation relationship for a Permo-Triassic sandstone sample. The curve has been fitted by using both the van Genuchten function and the Brooks-Corey function.

The summary table (Table 5.5) shows good agreement between the mean and median of all the calibrated variables. In an MICP study on sandstones, Bloomfield et al (2001) found a mean for λ of 0.75 and a mean value for m of 0.55. Those values are clearly consistent with this study and previously published values by Morel-Seytoux and co-workers (1996). The range of residual saturations show a larger range for the van Genuchten function and probably reflects it ability to better deal with very high values (>0.98) of S_r .

Table 5-4 van Genuchten and Brooks-Corey parameters obtained during curve fitting of $P_c(S_w)$ curves. The values for P_0 and P_d are both in kPa

	van Genuchten			Brooks-Corey		
Sample	P_0	m	S_r	P_d	λ	S_r
1524/3v/1	2.92	0.59	0.39	1.72	0.84	0.36
1524/4v/1	8.78	0.59	0.52	4.30	0.55	0.42
1524/4v/2	6.41	0.53	0.43	2.74	0.37	0.23
1525/5v/1	5.48	0.60	0.46	2.88	0.68	0.39
1525/6v/1	2.43	0.59	0.42	1.19	0.65	0.37
1526/4v/1	4.02	0.57	0.49	2.03	0.61	0.42
1526/4v/2	5.42	0.58	0.52	2.87	0.68	0.47
1526/6v/2	3.44	0.59	0.44	1.80	0.70	0.38
1526/10v/1	8.12	0.39	0.53	6.33	0.68	0.57
1527/1v/1	28.5	0.07	0.75	*Could not fit*		
1527/2v/1	1.22	0.48	0.29	1.45	1.19	0.31
1527/3v/1	2.66	0.43	0.26	1.11	0.31	0.06
1527/4v/1	7.88	0.56	0.43	3.43	0.38	0.20
1527/5v/1	*Could not fit*			*Could not fit*		
1527/5v/2	*Could not fit*			*Could not fit*		
1527/8v/2	*Could not fit*			*Could not fit*		
1528/2v/1	8.06	0.58	0.46	4.15	0.61	0.37
1528/3v/1	0.28	0.25	0.93	1.30	0.46	0.92
1529/1v/2	2.14	0.61	0.43	1.12	0.75	0.39
1529/6v/1	6.29	0.56	0.50	3.07	0.56	0.42
1529/6v/2	5.11	0.55	0.41	2.87	0.67	0.36
1529/8v/1	4.83	0.56	0.33	2.19	0.44	0.15
1530/1v/1	12.1	0.46	0.41	5.73	0.28	0.09
1530/3v/1	4.27	0.51	0.37	2.13	0.51	0.28
1530/8v/1	1.33	0.59	0.41	0.84	0.93	0.39
1530/8v/2	1.98	0.58	0.37	1.07	0.75	0.33
1530/10v/1	1.55	0.55	0.20	0.61	0.56	0.13
1534/5v/1	1.95	0.60	0.01	1.29	1.05	0.00
1534/6v/1	2.52	0.64	0.09	1.42	0.89	0.04
1534/11v/1	3.67	0.65	0.06	2.27	1.04	0.02

	van Genuchten			Brooks-Corey		
Sample	P_0	m	S_r	P_d	λ	S_r
1534/12v/1	11.8	0.54	0.50	5.28	0.23	0.00
1534/13v/1	1.26	0.60	0.03	0.80	0.98	0.01
1535/5v/1	0.32	0.67	0.99	*Could not fit*		
1536/3v/1	4.03	0.50	0.32	2.01	0.48	0.20
1536/4v/1	8.63	0.52	0.29	4.19	0.37	0.00
1536/9v/1	3.96	0.66	0.28	2.20	0.88	0.22
1536/10v/1	4.29	0.36	0.31	2.21	0.29	0.13
1536/10v/2	7.13	0.37	0.25	4.09	0.34	0.10
1537/2v/1	1.93	0.37	0.60	1.60	0.40	0.53
1537/3v/1	0.09	0.04	0.77	0.09	0.02	0.64
1537/5v/1	0.16	0.50	0.99	*Could not fit*		
1537/6v/1	1.75	0.45	0.41	0.76	0.35	0.28
1537/7v/1	0.29	0.88	0.49	0.12	2.84	0.49
1538/2v/1	3.59	0.56	0.35	1.99	0.68	0.30
1538/4v/1	10.3	0.42	0.30	3.09	0.53	0.45
1538/5v/1	4.25	0.43	0.23	2.24	0.66	0.31
1538/7v/1	5.18	0.40	0.35	2.13	0.22	0.00
1542/2v/1	1.63	0.55	0.16	0.89	0.70	0.11
1542/3v/1	29.2	0.43	0.43	11.90	0.88	0.65
1542/11v/1	2.09	0.56	0.31	1.10	0.68	0.26
1542/14v/1	3.17	0.58	0.33	1.81	0.75	0.28

Table 5-5 Simple statistical summary of van Genuchten and Brooks-Corey parameters obtained during curve-fitting of $P_c(S_w)$ curves. The values for P_0 and P_d are both in kPa.

	van Genuchten			Brooks-Corey		
	P_0	m	S_r	P_d	λ	S_r
Mean	4.87	0.51	0.41	2.16	0.65	0.29
sd	5.83	0.14	0.21	2.02	0.42	0.20
Median	3.81	0.55	0.41	2.03	0.65	0.30
Max	29.2	0.88	0.99	11.9	2.84	0.92
Min	0.09	0.04	0.01	0.09	0.02	0.00
n	48	48	48	45	45	45

5.5.2 Correspondence Between van Genuchten and Brooks-Corey Models

Several authors have dealt with the correspondence and similarities between the van Genuchten and Brooks-Corey models (Lenhard *et al.*, 1989; Stankovich and Lockington, 1995). Figure 5.6 shows a cross plot comparing the λ value with an estimate (λ_{est}) value from m by equating the differential fluid capacities of the Brooks-Corey and van Genuchten models at S_e=0.5 (see equation 2.14). A 1:1 ratio line has been added to aid interpretation. A data point which has an unusually high λ of 2.8 (sample 1537/7v/1) and λ_{est}=4.1 has been omitted as this tends to distract from the majority of the data, although this point follows the same trend as the rest of the data. This sample exhibited a very sharp 'L' shaped curve as considerable imbibition occurred at a low pressure.

The graph shows a fairly linear increasing trend between the calculated value and the value estimated from the value of m as suggested by Lenhard *et al.* (1989). The figure shows that estimated values of λ based on m over-estimates λ obtained by fitting the Brooks-Corey function to the data.

In Figure 5.7 the agreement between the measurement of 'entry' pressure (P_d) by Brooks-Corey and 'breakthrough' pressure (P_0) by van Genuchten is clearly demonstrated with a good correlation. The value for P_d is approximately 55% lower than the value for P_0.

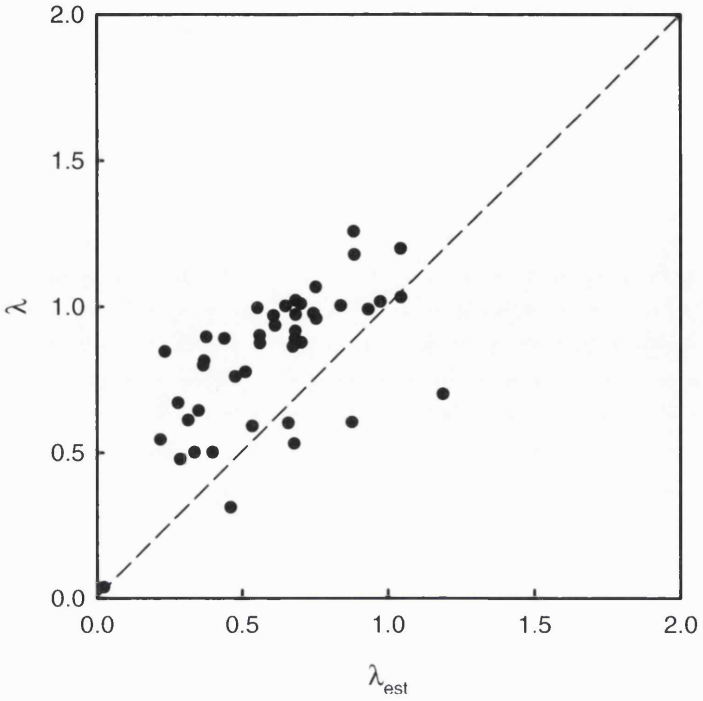

Figure 5-6 Cross plot of calculated values of λ from the Brooks-Corey function and its relationship with m (λ_{est}) from the van Genuchten function as suggested by Lenhard (1989).

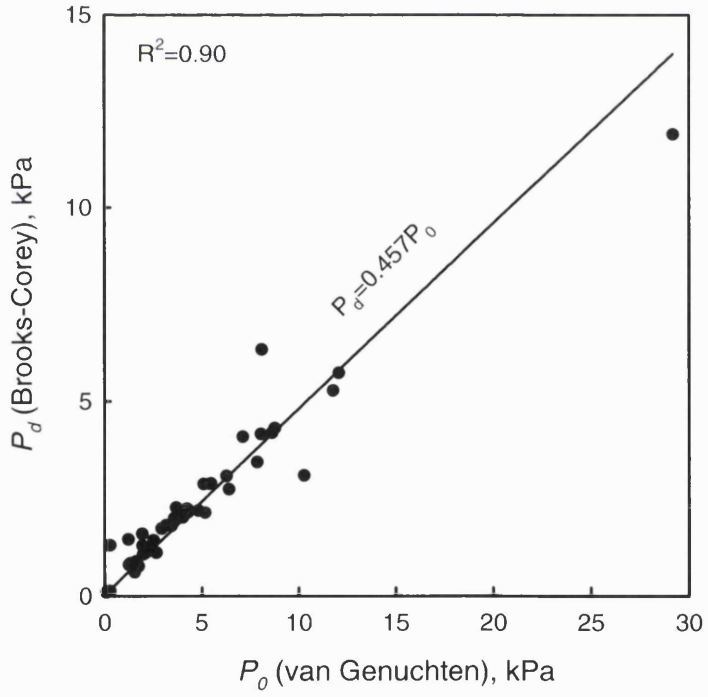

Figure 5-7 The relationship between entry pressure calculated using the van Genuchten function and by using the Brooks-Corey function.

Figure 5.8 shows how both models compare with the data obtained during the actual centrifuge experiment. The 1:1 ratio line is again included to aid interpretation as

it represents the points where measured and fitted data have the same value. The 'S_r measured' is the final point determined on the $P_c(S_w)$ curve.

The residual saturation as determined by the van Genuchten function is mostly very close to the value obtained during the experiment, with a slight tendency for the fitted S_r values to be a little higher. When fitted S_r values are lower they tend to be considerably lower and this mostly occurs for samples with high values for P_0 (e.g samples 1527/1v/1, 1530/1v/1, 1536/4v/1, 1536/10v/1, 1536/10v/2 and 1542/3v/1).

Values calculated using the Brooks-Corey function are, with few exceptions, considerably lower than the measured values. It predicts no residual saturation for four samples, most of which have high P_d values (e.g. 1534/12v/1, 1536/4v/1 and 1538/7v/1) and so these are likely to be erroneous as a high entry pressure is more likely to be consistent with a high residual saturation.

This adds weight to the claim of Stankovich and Lockington (1995) that "the van Genuchten model matches experimental data more satisfactorily than the model of Brooks and Corey".

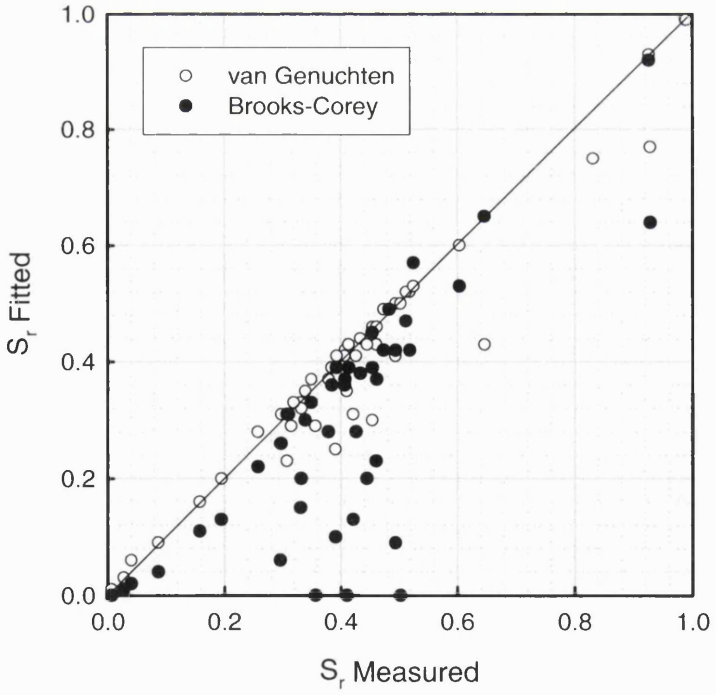

Figure 5-8 A comparison of residual saturation, S_r, as measured from the $P_c(S_w)$ curve and the values obtained by curve fitting using the van Genuchten and Brooks-Corey functions.

5.5.3 Percolation of DNAPL

As previously noted (section 5.4), the value P_0 from the van Genuchten function is close to the inflection point on the curve and so approximates to the non-wetting phase percolation threshold of the system. The inflection point, P_{ci}, in fact occurs at

$$P_{ci} = P_0 m^{1-m} \tag{5.6}$$

The associated wetting phase saturation can therefore be calculated from

$$S_w = \frac{(S_m - S_r)}{(1+m)^m} + S_r \tag{5.7}$$

and the non-wetting phase saturation can be expressed as:

$$S_{nw} = 1 - S_w \tag{5.8}$$

The non-wetting phase saturation (S_{nw}) at percolation (amount of DNAPL) has been plotted in Figure 5.9 with the corresponding value of m, the van Genuchten pore size distribution variable. The graph exhibits a linear trend with increasing DNAPL saturation as m increases. The mean S_{nw} is 0.121 (median 0.123) which suggests that on average, a percolating network will occur when approximately 12% of the pore-space is occupied. Larson *et al.* (1981) have examined percolation thresholds for a range of lattices. They obtained a percolation threshold of 0.12 for a face-centred cubic lattice which has a coordination number of 12. This might suggest that these sandstones have a similar coordination number although this issue will be further addressed in Chapter 7.

Values of m typically range from about 0.38 for materials with a large range of pore sizes to 0.88 for very uniform materials. The mean value of m for this data set is 0.51. The non-wetting fluid is more likely to occupy the large pores rather than the small pores. This suggests that for the samples with a large range of poresizes, a percolating network might occur through occupation of a continuum of relatively large pores.

Figure 5.10 shows the relationship between the residual saturation calculated by the van Genuchten function and the non-wetting phase saturation at percolation. The data show a clear linear trend indicating that at higher percolation non-wetting phase saturations the final water saturation in the core is lower. This is consistent with displacement of the water in the larger pores before a percolating network is completed.

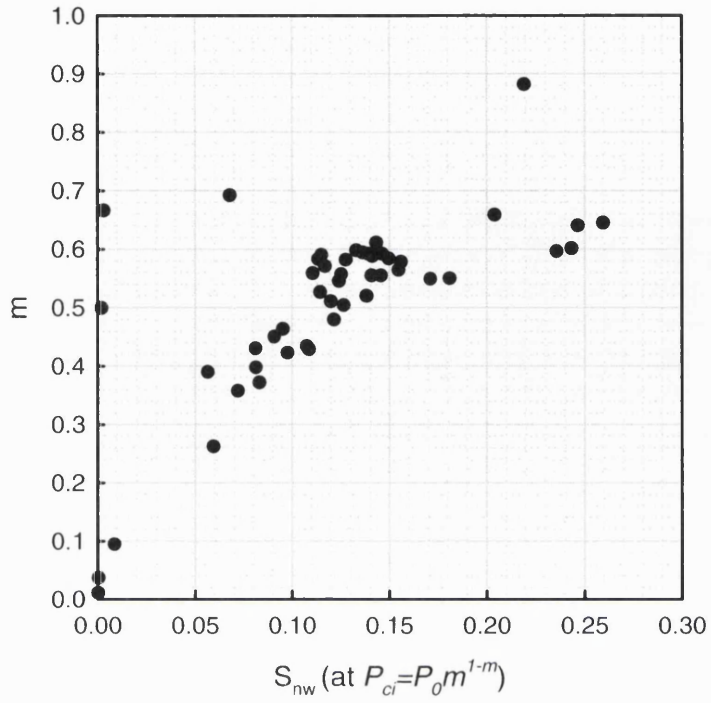

Figure 5-9 Cross plot of non-wetting phase saturation at percolation point (equation 5.8) against the van Genuchten pore size distribution variable, m.

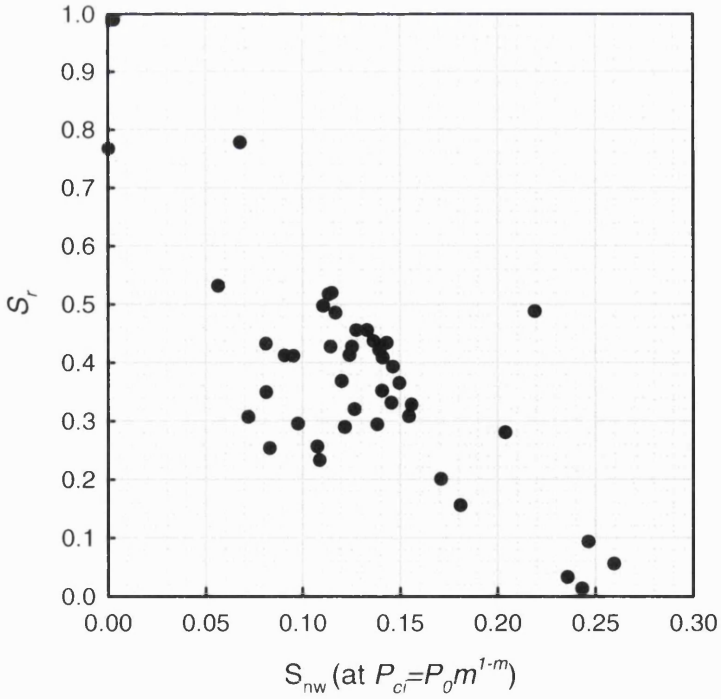

Figure 5-10 Cross plot of non-wetting phase saturation at percolation point against the van Genuchten residual saturation, S_r.

5.6 CHAPTER FIVE SUMMARY

This chapter has presented the development, validation and use of a centrifuge based method to produce pressure-saturation curves for a sub-set of Permo-Triassic sandstones, which are representative of the full data set. Most of the curves have been successfully fitted and parameterised using the van Genuchten and Brooks-Corey functions. A linear relationship between the van Genuchten 'breakthrough pressure' and the Brooks-Corey 'entry pressure' is observed, with the 'breakthrough pressure' found to be roughly double the 'entry pressure'. Based on the residual wetting phase saturation, the van Genuchten model provides a better match to experimental data than the Brooks-Corey model. The data suggest that the majority of the non-wetting phase saturation resides in the larger pore spaces. On average, a percolating network of DNAPL will occur when roughly 12% of the pore space is occupied.

6 Development of a Laboratory Method for Determining DNAPL Relative Permeability

The following section describes the development, verification, and implementation of a laboratory based method for determining relative permeability in the presence of a DNAPL for consolidated sandstone samples and producing a DNAPL residual saturation. The impact of residual saturation on the relative permeability is considered and an experiment monitoring the dissolution of a DNAPL residual saturation is presented.

6.1 DEVELOPMENT OF TECHNIQUE

6.1.1 Determining Liquid Permeability

The experimental set-up for determining liquid permeability is shown in Figures 6.1 and 6.2. Two ISCO model 500D syringe pumps were joined to form a continuous feed system which was able to be controlled from a central unit and able to deliver liquid at either a continuous pressure or constant flow rate. The pumps were both fed from a central 10 litre reservoir which filled one of the syringe pumps whilst the other was pumping water. The water used in the reservoir was of an ultra pure grade (MilliQ) with a small amount of calcium carbonate (roughly 0.005 molar) to minimise any dissolution of the rock matrix under investigation. The water was degassed under vacuum to prevent bubbles entering the system.

The outflow from the two pumps was then attached to the fluid outlet point of a Hassler-type core holder, usually used in gas permeability measurements. The core holder was then partially filled with water from the syringe pumps, before the saturated pre-weighed sandstone core for analysis was placed inside. The sample plugs used were from the same core as those used in porosity, gas permeability and pressure saturation experiments described in previous chapters and were of the same approximate 25 mm x 25 mm size. The top section of the core holder was then fitted and water allowed to flow up through the core holder and out through what would normally be the fluid inlet point at a rate of about 5 mL/min. A solvent resistant jacket, which is an integral part of the core holder assembly, was then inflated by gradually injecting water under pressure from a hand pump. As the pressure increased, the jacket conformed to the outer annulus of the core and prevented any by-pass flow around the edges of the core. A final

pressure of 3000 kPa was used to confine the sample which was measured by a Druck 3500 kPa pressure transducer connected on a 'T' to the jacket injection port of the core-holder (Figure 6.1). Higher pressures will tend to compress the sample, altering the pore structure and potentially the transport properties. The back-flushing is necessary to remove any trapped air-bubbles in the system and was continued for at least a further 2 minutes after the final confining pressure had been applied.

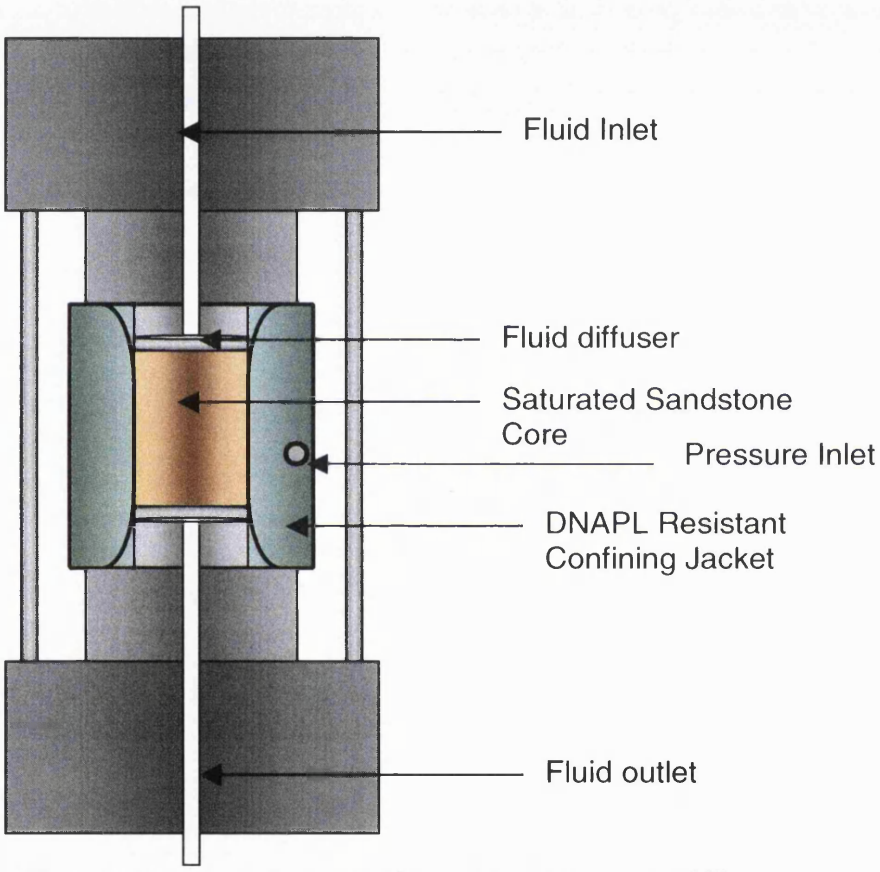

Figure 6-1 Schematic diagram of the core holder used in relative permeability measurements.

When satisfied that no further air was trapped around the core or in the core holder, the back-flushing was stopped, and the outflow from the syringe pumps was connected to the inflow of the core holder (Figure 6.2). A Druck 700 kPa differential pressure transducer was placed across the core holder to measure the pressure drop as the fluid moved through the sample. The pressure transducer was connected to a PicoLog 16 bit analogue to digital converter (ADC) and the output monitored by a PC. The monitoring frequency could be predetermined from the software provided with the analogue to digital converter. A rate of 1 recording per 10 seconds was used as a compromise between creating excessively large digital files and capturing adequate

data. The laboratory temperature was also logged on a minute basis by using the same ADC device.

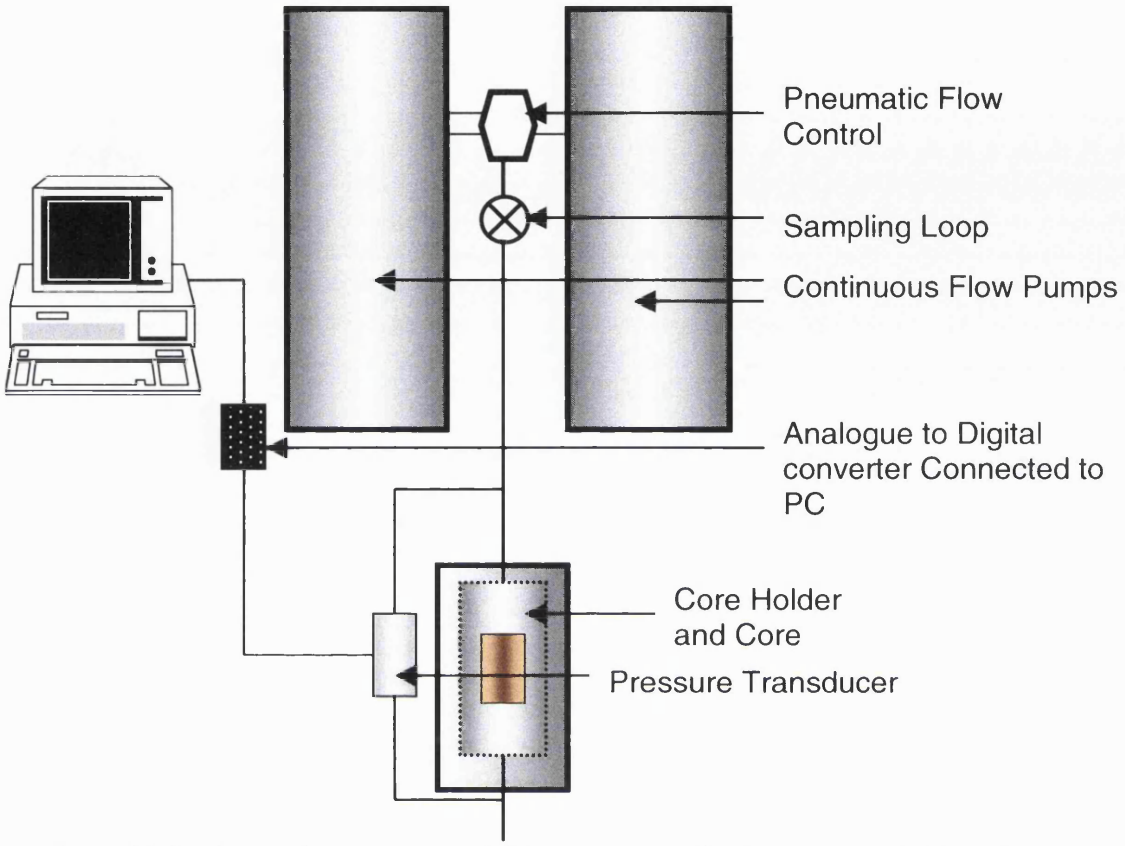

Figure 6-2 Continuous flow pumps coupled through a sampling loop to a core-holder. The pressure drop across the sample is measured by a pressure transducer and the output monitored and logged by a PC.

Water was passed, by-passing the sampling loop, into the core holder and through a diffuser which encouraged equal distribution of the fluid across the top of the core. A fixed rate of flow was used until a steady state (i.e. constant pressure) was reached on the output from the pressure transducer. Commonly a slight decrease in pressure was observed as fine material within the core was transported and redistributed. It typically took 24 hours for a steady pressure to be established with flow rates of 1 mL/min. Where sample gas permeabilities were less than 500 mD, a flow rate of 0.5 mL/min was used so that the measured pressure remained within the range of the pressure transducer. The pressure measured was used to calculate the liquid permeability (k_f). This was derived from re-arranging Darcy's equation:

$$Q = \left(\frac{k_f A}{\mu}\right)\left(\frac{\delta P}{L}\right) \tag{6.1}$$

to the form

$$k_f = 16.89 \times \frac{\mu QL}{A\delta P} \tag{6.2}$$

where μ is the fluid density (g/mL), Q is the flow rate (mL/min), L is the sample length (cm), A is the cross-sectional area of the sample (cm^2) and δP is the pressure difference across the sample (kPa). The factor 16.89 is used to convert to mD. It can be seen from the equation that a change in flow rate will lead to an inverse change in pressure difference measured across the sample i.e. if flow doubles then the pressure difference should half.

6.1.2 Introduction of a DNAPL

In a previous study attempting to measure DNAPL relative permeabilities in aquifers, Butcher (1995) used a similar core-holder arrangement. A primary problem with this work was that relative permeability was measured in a horizontal plane which caused the DNAPL to run along the bottom of the core and not evenly throughout. To avoid this problem these experiments were carried out in the vertical plane. Correspondingly equation 6.2 needs to be amended to incorporate the gravity (g) and density (ρ) terms which gives:

$$k_f = 16.89 \times \frac{\mu QL}{A(\delta P + \rho g)} \tag{6.3}$$

When a steady state was reached, a 10 mL sampling loop (see Figure 6.2) was filled from a water-capped (to prevent volatilisation) tetrachloroethene reservoir with an Ismatec Reglo 100 peristaltic pump at a flow rate of roughly 20 mL/min. The DNAPL was pumped through the sampling loop and back into the reservoir for 60 seconds, so removing any remaining water from the loop and ensuring the loop was full of DNAPL. When the loop was full of DNAPL the flow of water from the syringe pumps was diverted so as to move through the sampling loop and hence displace the DNAPL prior to distribution to the core in the core-holder. An excess of DNAPL (10 mL) relative to the pore volume (approximately 3:1) was used to flood the interconnected pore-throat network. During core flooding, the sample data monitoring interval was changed so that a value was recorded every 2 seconds.

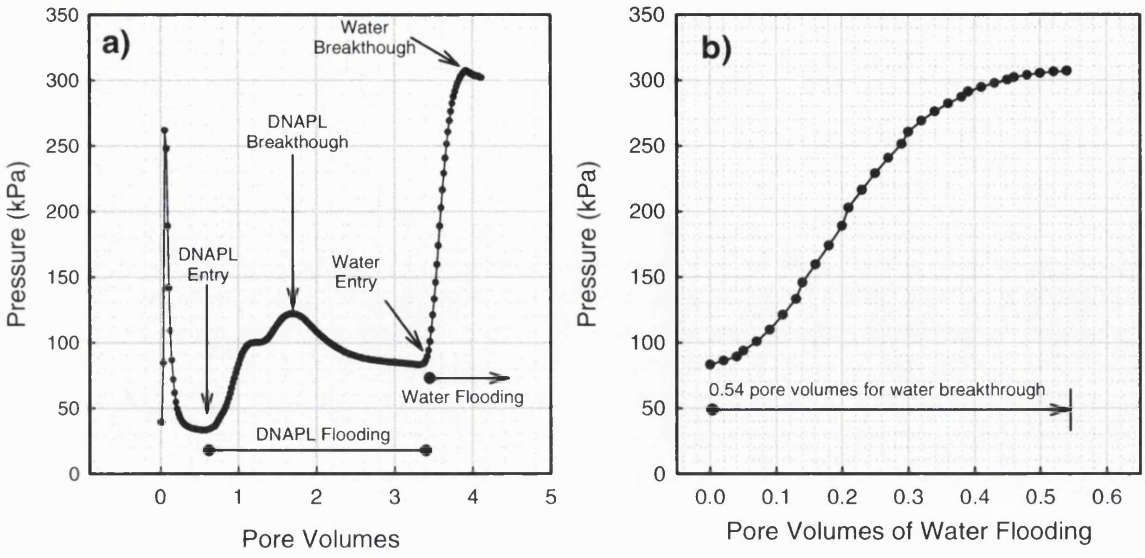

Figure 6-3 a) Example of typical changes in pressure as a function of pore volume pumped as a DNAPL then water moves though a water saturated sandstone core. b) Change in pressure during the water breakthrough componet of the experiment. A flow rate of 1 mL per minute was used.

A sampling loop system was used, rather than dedicating one of the syringe pumps to water and one to a DNAPL for 2 reasons:

1. The capacity of a syringe pump is 500 mL. At a flow rate of 1 mL/min the capacity of a single syringe pump will provide water for just over 8 hours. This is considerably less than the usual equilibration time for a liquid permeability measurement, therefore the pump would be required to stop and fill during the experiment which would disrupt the water flow.
2. A DNAPL is likely to corrode some of the plastic and rubber based linings present in the syringe pump so rendering it, at best, less accurate and at worse inoperable.

The DNAPL then moved though the system and into the core. When 10 mL of water had moved through the sampling loop, the loop was empty of DNAPL and water flows through the system again. The core is thus water saturated, then DNAPL flooded, then water flooded, leaving a DNAPL residual. Figure 6.3a shows how the measured pressure across the core changes as first DNAPL floods the core displacing water and then water floods the core displacing DNAPL and leaving a residual DNAPL concentration. Figure 6.3b shows in detail the number of pore volumes required to achieve breakthrough of water after the sample has been flooded with DNAPL.

An initial peak was often observed as the syringe pumps displaced DNAPL from the sample loop possibly due to density difference and a slight lag in the syringe pumps adjusting. This pressure then settled back to its water saturation equilibrium value. The pressure then increased until breakthrough when (a few seconds later depending on the flow rate) it was observed at the fluid outflow. As the full 10 mL passed through the core the pressure gradually decreased. Lastly, water started to enter the top of the core and the pressure again began to rise as the DNAPL was expelled from the pores by the displacing water. A maximum value was reached when water breaks-through from the bottom of the core. For most experiments the fluid flow was then stopped at this point and the final pressure reading was used in the calculation of the reduction in permeability (or the relative permeability at residual saturation) due to DNAPL occupying the (larger) pore-throats. The apparatus was then dissembled and the sample core weighed to determine its DNAPL content by using the increase in weight due to the density difference i.e.:

$$DNAPL_{content} = \frac{C_{final} - C_{dry} - PV}{0.6 \times PV} \tag{6.4}$$

where C_{final} is the mass (g) of the core at the end of the experiment, C_{dry} (g) is the dry mass of the core, PV is the total pore volume of the sample (mL), and the 0.6 is the density difference between PCE and water (g/mL).

6.1.3 Measurement of DNAPL Dissolution

Initially it was intended to continue the experiment after the water flood to observe the dissolution of DNAPL and the concomitant increase in relative permeability. Figure 6.4 demonstrates the expected output from such an experiment. In the figure, k_{p1} is the initial pressure measured for calculation of the relative permeability to water, k_{p2} is the measured pressure when water has first passed through the core after the DNAPL, and k_{p3} is the pressure after dissolution of the DNAPL.

This was attempted on three occasions on Clashac sandstones but proved difficult as the experiment needed to be continued for several days to observe any significant changes, and problems with air entrapment in the system often developed (see 6.1.4). Consequently only one successful run was made. Water samples were collected at the fluid outlet point in clean 10 mL glass vials from the time of water

breakthrough after the DNAPL flood at intervals of between 500 and 1000 pore volumes.

The water samples were then extracted into pentane using a liquid:liquid extraction with a ratio of 5 mL water to 5 mL pentane (1:1). The samples were analysed for tetrachloroethene on a Varian 3400 gas chromatograph (GC) fitted with an electron capture detector (ECD). Separation was performed on a $1/8^{th}$ inch 3 m packed column with a stationary phase of OV101 held isothermally at 80°C. The ECD was maintained at a temperature of 250°C. Tetrachloroethene was successfully separated from the pentane under these conditions and eluted after 5 minutes. Calibration of the instrument was carried out by serial dilution of a stock solution of tetrachloroethene. Calibration was over a range of three orders of magnitude from 1-1000 µg/L PCE. Liquid:liquid extractions are usually used to pre-concentrate environmental samples but in this case the sensitivity of the analytical equipment and its linear range in fact means the samples need diluting prior to analysis. Samples were diluted by a factor of 500.

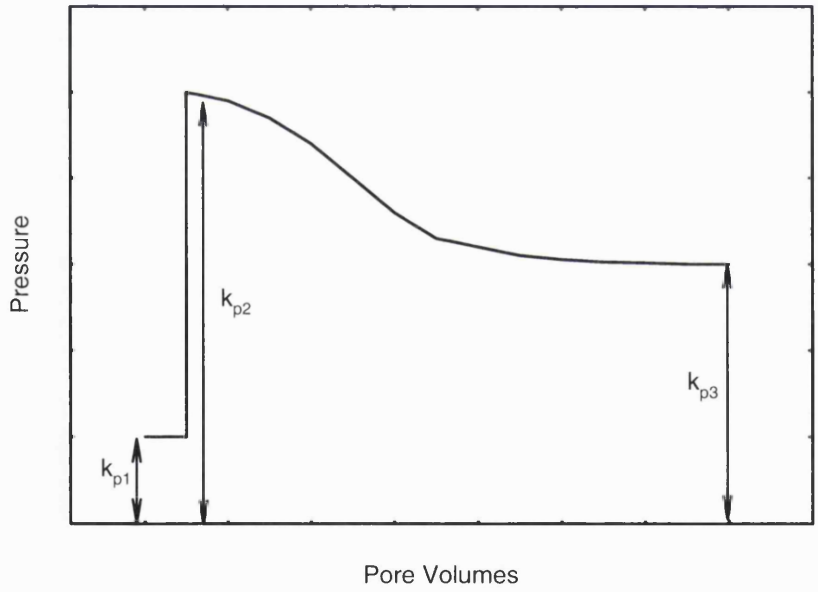

Figure 6-4 Schematic plot of pressure against pore volumes illustrating the expected change in pressure observed as DNAPL displaces water then water displaces DNAPL to create a residual saturation which is slowly dissolved.

6.1.4 Problems Encountered in Method Development

A number of experimental problems were encountered during the development of this method. These are summarised below.

1. The most common problem was air entering the system and becoming entrapped in the core. The presence of air in the pore space increases the pressure needed

for the liquid to pass through the core (and consequently can lead to a reduction in relative permeability). The impact of this on the data output was to produce a relative permeability curve that did not reach equilibrium with the pressure across the core continuing to rise. The experiment would need to be stopped, the core plug dried, evacuated and resaturated with water. Using degassed water reduced the incidence of this problem although with long experiments, especially where a lower flow rate was necessary, atmospheric air was able to dissolve back into the water reservoir.

2. A related problem was air entering the sample loop housing. The tube diameter of the switching gear was $1/16^{th}$ inch so tiny trapped air bubbles would prevent passage of water through the loop, causing a sharp rise in pressure from the syringe pumps as they tried to maintain a constant flow. In one extreme case the pressure increased so high that the $1/8^{th}$ inch nylon tubing connecting the syringe pumps to the sample loop housing, burst. Subsequently the default over-pressure setting on the syringe pumps was considerably reduced (from 20,000 kPa to 10,000 kPa) to prevent this recurring. If excessive pressure developed then the pumps would automatically shut down. If air entered the sample loop housing the loop needed to be dismantled and reassembled underwater.

3. Continuous monitoring of the laboratory temperature quickly identified that the laboratory temperature fluctuated significantly over the passage of a day and night. Figure 6.5 shows that laboratory temperatures reached a maximum of about 21°C at about 2pm. As the laboratory temperature decreased the pressure also started to fall and similarly as the temperature started to rise so do did the pressure. The temperature curve has an amplitude of about 2.5°C and the pressure curve an amplitude of roughly 1 kPa; a 1°C rise in temperature leads to a 0.4 kPa increase in pressure. It is likely that the changes in pressure across the core result from the influence of temperature on the confining pressure – as the temperature increases, the water in the confining jacket expands slightly so increasing the pressure on the core hence a slightly higher pressure is required for fluid to pass through. The variation was clearly unacceptable and was eventually rectified by improving the laboratory air-conditioning system.

4. On occasion the confining pressure would fail completely. Eventually the hand pumps for applying the pressure in the jacket were replaced with new ones and this problem disappeared.

5. It was not possible to find tubing that could be used in the peristaltic pump that was resistant to DNAPLs. This meant that periodically the tubing would fail and cause tetrachloroethene to leak and enable air to get into the sampling loop. The pump tubes were regularly changed to counter this problem.

6. During displacement of tetrachloroethene from the metal sampling loop, water would occasionally flow over the top of the DNAPL as it flowed through the nylon tubing connecting the sample loop housing to the top of the core holder. When this happened water and DNAPL would enter the core simultaneously and the experiment had to be re-run. This was a periodic fault and was eventually avoided by changing the nylon tubing after each experiment. It is possible that the DNAPL altered the wetting properties of the nylon and so changing the tubing each time gave a fresh, non-DNAPL wetted surface.

7. After some of the experiments, small amounts of core material were left in the core holder. This added to the error in measurement of DNAPL remaining in the core at the end of the experiment. To try and compensate for this the core was re-dried and then reweighed, although the whole drying process could on occasion lead to further degradation of the core sample. Volatilisation of DNAPL during the time that the core was being weighed also added to the error in measurement.

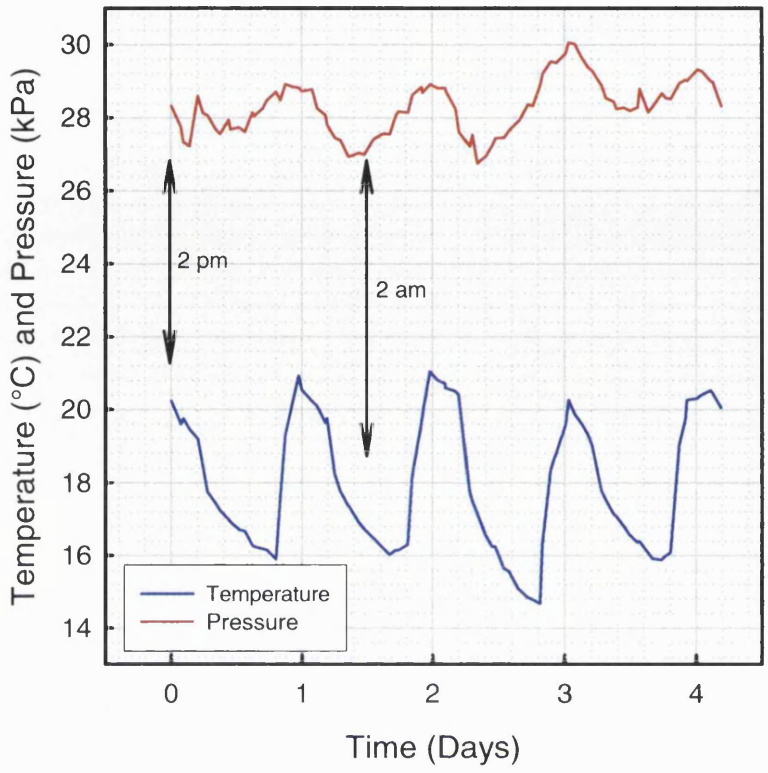

Figure 6-5 The relationship observed during method development between laboratory temperature and the pressure measured across the core sample.

6.2 METHOD VERIFICATION

The method was verified by using Clashac sandstone cores which had been specially cut to 25 mm lengths. Clashac was chosen because it is well sorted and relatively free from clay deposits, thus it is relatively homogeneous and can be expected to behave in a predictable way. However, the data from the Clashac sandstones is not included as part of the data-sets presented other than in this verification step. Five experiments were undertaken, 2 at a flow rate of 1 mL per minute, 2 at a flow rate of 3 mL per minute and 1 at a flow rate of 1 mL per minute. The permeability was allowed to equilibrate over roughly 1000 pore volumes before the DNAPL was injected. The results of these experiments are shown in Figure 6.6.

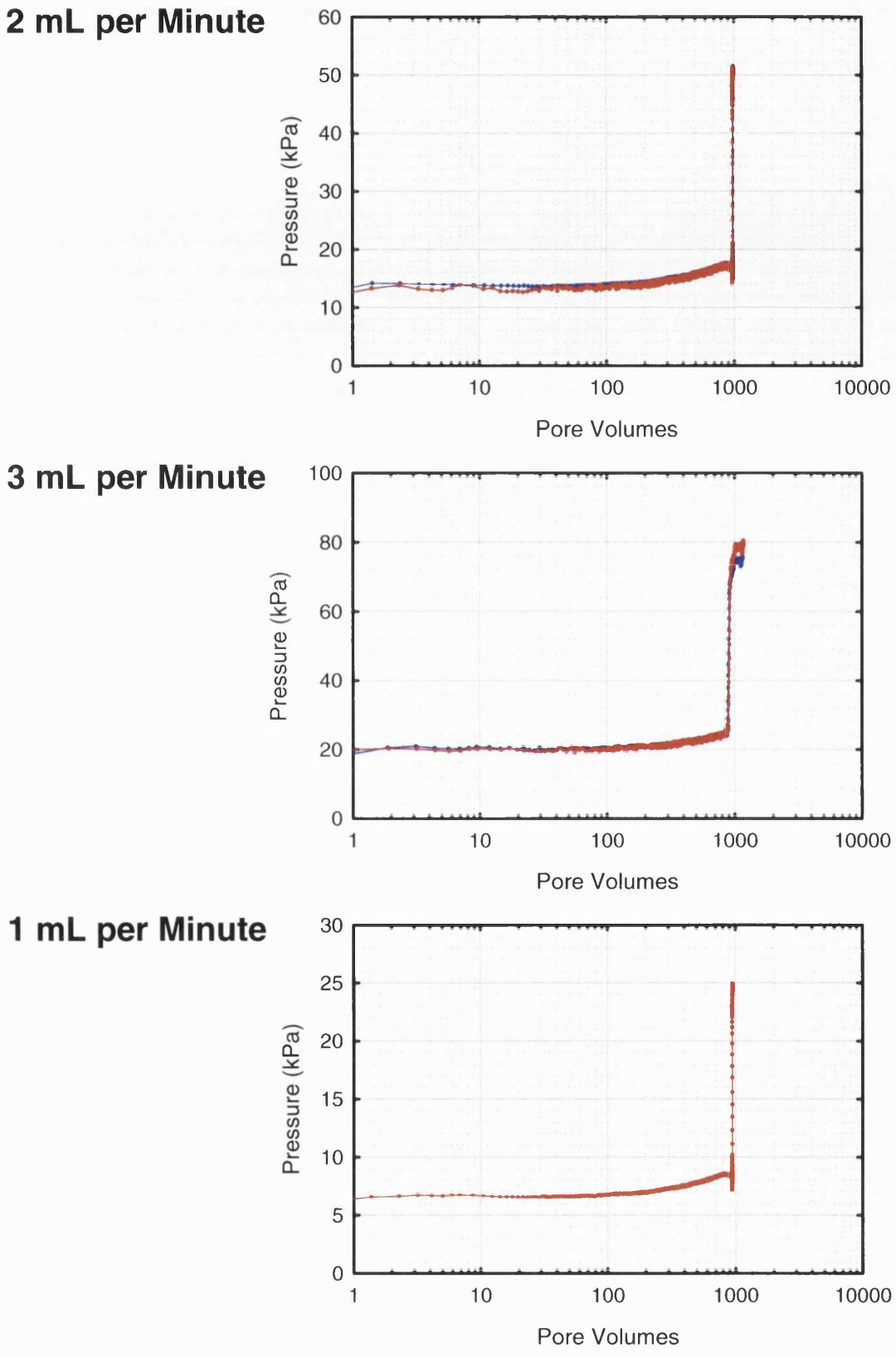

Figure 6-6 Method verification for relative permeability measurement in the absence and presence of a DNAPL. Different colours have been used to show duplicates at 2 mL and 3 mL per minute.

A good relationship between flow rate and pressure is observed, both before and after the core has been flooded with DNAPL. Converting the pressure changes to permeability gives a mean value of 0.500 μm^2 (coefficient of variation of 3.0%) before the DNAPL flood and a value of relative permeability to water of 0.166 μm^2 (coefficient of variation 2.8%) after the DNAPL flood. These values are considered very satisfactory but probably represent the best reproducibility possible, due to the homogeneous nature of the Clashac sandstone when compared with other less homogeneous sandstones.

6.3 VALIDITY OF DATA SUBSETS USED IN RELATIVE PERMEABILITY EXPERIMENTS

Due to time constraints and the period of time spent developing the method, a sub-set of 15 samples were investigated to examine their relative permeability and residual saturation properties. The physical properties of the 15 sample subset are summarised in Table 6.1. The mean gas permeability is close to that of the 151 sample data-set described in Chapter 4 (Table 4.1) although the median value is more than double that of the larger data set. The range of gas permeabilities of this data set is also smaller with the maximum roughly half the maximum of the larger data set and the minimum some four orders of magnitude higher than the minimum of the larger data set. Both the mean and median porosities are higher in this data set although the median value is relatively close to that determined for the 151 sandstones. The range of porosities covered is also substantially smaller with a range of 0.114 compared with 0.316. Mean and median pore sizes are larger than in the 151 sample data set but are relatively close. The range of pore sizes is also not as good as that covered by the larger sampler set.

Clearly the samples used favour higher gas permeabilities, higher porosities and larger pore size when compared with the larger sample set. However, it is likely that the apparatus developed would be less suitable for very small pore sizes and might not be able to generate a residual saturation under reasonable pressures. It is however acknowledged that based on the physical properties data a more representative data-set would have been desirable.

Table 6-1 Statistical summary of physical properties for sub-samples used in relative permeability and residual saturation experiments.

	k (mD)	k (μm^2)	ϕ	Median Pore size (μm)	$\sqrt{k/\phi}$ (μm)
Mean	728	0.719	0.241	18.4	1.41
s.d.	989	0.976	0.034	11.5	1.06
Median	367	0.362	0.234	16.6	1.11
Max	3560	3.51	0.293	47.5	3.90
Min	18.0	0.018	0.179	2.86	0.29
n	15	15	15	15	15

The weak acid extraction data for the 15 sample subset is given in Table 6.2. Mean and median concentrations are lower for Ca, Mg and Mn than the 151 sample data set. Similarly the ranges of these elements is less than the larger dataset although both Ca and Mg have the same minimum. Median concentrations of Fe, Si and Al are all slightly higher than the 151 sample data set. The minimum concentrations of these three elements are all similar close to the larger data set but the maximums for Fe and Al are half that of the larger data set. As with the physical properties data a more representative sub-set of data would have been desirable.

Table 6-2 Statistical summary of 0.43 M HNO_3 extraction data for sub-samples used in relative permeability and residual saturation experiments.

	Ca	Mg	Fe	Mn	Si	Al	P
				mmol/kg			
Mean	221	74.0	3.46	1.54	2.76	3.84	5.96
s.d.	274	176	7.63	2.74	1.80	2.54	6.26
Median	88.0	5.62	1.24	0.73	2.46	2.83	3.43
Max	842	688	30.3	9.34	7.48	9.89	18.5
Min	1.34	0.21	0.11	0.02	0.52	0.60	<0.01
n	15	15	15	15	15	15	15

6.4 RESULTS

6.4.1 Relative Permeability and Residual Saturation

Permeabilities to water (k_f) and the reduced permeabilities when there is a residual DNAPL present ($k_{f\ residual}$) are shown in Table 6.3 and summarised in Table 6.4. The value for k_f has been determined at the end of the equilibration period and $k_{f\ residual}$ is determined from the pressure reading when water breaks through after the DNAPL flood. Both k_f and $k_{f\ residual}$ can be seen to range over three orders of magnitude. Figure 6.7 shows a good correlation between the two sets of data ($R^2 = 0.91$).

Table 6-3 Permeability and residual saturations for sandstone samples analysed. '$k_{f\ residual}$' is the permeability in the presence of a DNAPL; 'Δk_f' is the percentage reduction in permeability that the residual DNAPL causes; '$R_{Sat.}$' is the residual saturation expressed in terms of percentage of pore space occupied by DNAPL; 'H_2O PVs' is the fractional number of pore volumes it takes water to move through the length of the core after the DNAPL flood.

Sample	k_f (mD)	k_f (μm^2)	$k_{f\ residual}$ (mD)	$k_{f\ residual}$ (μm^2)	Δk_f (%)	$R_{Sat.}$ (%)	H_2O PVs
1525/5v/1	3110	3.07	180	0.178	94	29	0.69
1526/6v/1	319	0.315	82.8	0.082	74	13	0.20
1527/3v/1	883	0.872	269	0.265	70	19	0.31
1527/4v/1	45.4	0.045	13.1	0.013	71	19	0.22
1529/6v/1	353	0.348	43.8	0.043	88	25	0.48
1530/1v/1	33.8	0.033	6.49	0.006	82	16	0.31
1530/3v/1	2060	2.03	382	0.377	81	28	0.23
1538/4v/1	114	0.113	14.7	0.015	87	22	0.38
1538/5v/1	33.9	0.033	15.5	0.015	55	11	0.31
1539/8v/1	409	0.404	71.3	0.070	83	19	0.48
1542/2v/1	5370	5.30	2790	2.76	48	32	0.54
1542/8v/1	1090	1.07	755	0.745	30	20	0.42
1542/9v/1	89.0	0.088	20.7	0.020	77	12	0.39
1542/12v/1	3.07	0.003	1.07	0.001	67	11	0.47
1542/14v/1	932	0.921	352	0.347	62	20	0.23

The relationship between k_f and $k_{f\ residual}$ in fact follows a power law of the form:

$$k_{f\cdot residual} = 0.234 k_f^{0.97} \tag{6.9}$$

Or more simply, $k_{f\,residual}$ is roughly 20% of k_f

The reduction in permeability ($\Delta k_f = 100[k_f - k_{f\,residual}]/k_f$) can be seen to vary between 30 and 94 %.

Table 6-4 Statistical summary of permeability and residual saturation for 15 samples analysed (see Table 6.3 for explanation of headings).

Sample	k_f (mD)	k_f (μm^2)	$k_{f\,residual}$ (mD)	$k_{f\,residual}$ (μm^2)	Δk_f (%)	R_{sat} (%)	H_2O PVs
Mean	990	0.977	333	0.329	71.0	19.7	0.38
s.d.	1500	1.48	712	0.703	16.9	6.6	0.14
Median	352	0.348	71.3	0.070	74.1	19	0.38
Max	5370	5.30	2800	2.76	94.2	32	0.69
Min	3.07	0.003	1.07	0.001	30.5	11	0.20
n	15	15	15	15	15	15	15

Residual saturations vary between 11% and 32%. Kueper *et al.* (1993) found residual saturations ranging from 1% to 38% for tetrachloroethene in the unconfined Bordan sand aquifer, and Chatzis and Morrow (1984) reported values to range from 27% to as high as 43% for Berea sandstones but few measurements of residual saturation have been made for DNAPLs in saturated consolidated media. Bloomfield *et al.* (1997) made some measurements on unsaturated consolidated cores and found values to range between 9% and 36%. The data set presented here falls within the ranges given by other researchers.

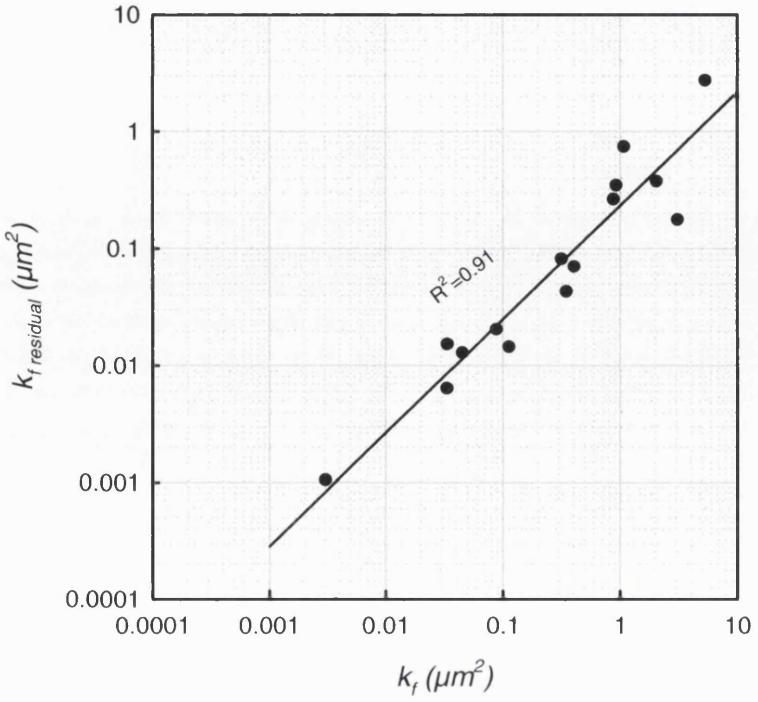

Figure 6-7 Cross plot showing the relationship between permeability (k_f) and the permeability in the presence of a DNAPL residual saturation ($k_{f\,residual}$). The equation of the regression line is given in Equation 6.9.

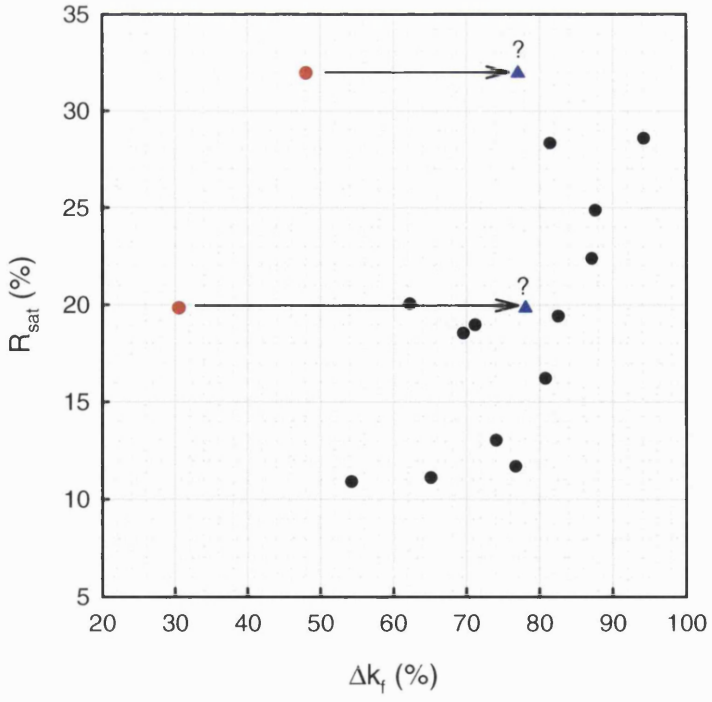

Figure 6-8 Cross plot showing the relationship between residual saturation of DNAPL and the % reduction in relative permeability. Blue triangles show where two outliers (red circles) would fall if corrected for $k_{f\,residual}$ by using k_f in Equation 6.9.

Figure 6.8 shows how for most samples larger residual saturations are associated with largest reductions in permeability. For the majority of the data a trend of greater reduction in permeability is caused by a higher residual saturation of DNAPL. This is consistent with a concept of DNAPL occupying the larger pores which impede the flow of water and so forcing it to move through the smaller pores hence reducing the permeability.

The two data points (shown in red) that lie off the trend have the largest $k_{f\ residual}$ values of all the samples and fall off the trend identified by Equation 6.9. From the measured k_f, Equation 6.9 gives a $k_{f\ residual}$ of 1.18 μm^2 for sample 1542/2v/1 (compared with 2.76 μm^2) and a $k_{f\ residual}$ of 0.249 μm^2 (compared with 0.745 μm^2) for sample 1542/8v/1. This would give a Δk_f of 77% and 78% respectively which would put the samples more in line with the other data (see blue triangles). Both of these samples also have large pore sizes (based on median pore size data from MICP measurements the pore-throats are 47 μm and 23 μm, respectively) so it is possible that these samples have a different arrangement of large pores and hence different drainage characteristics. Alternatively it could be that there is a sufficient network of large pores that the permeability is not much affected by the presence of DNAPL, and it is the residual saturation that is apparently too high.

Figure 6.9 shows how the fractional number of pore volumes of water required to percolate across the DNAPL flooded core increases as the residual saturation increases. This suggests that as relatively more of the pores are full with DNAPL a more tortuous route must be undertaken by the invading water. Where the residual saturation is low, the number of pore volumes of water is also low. It is suggested a few dominant routes exist across the core, although the distribution of water and DNAPL must relate both to pore geometry as well as pore size. It should also be noted that the flow rates used are relatively rapid compared with those expected in aquifer systems which may have implications for the distribution of residual DNAPL.

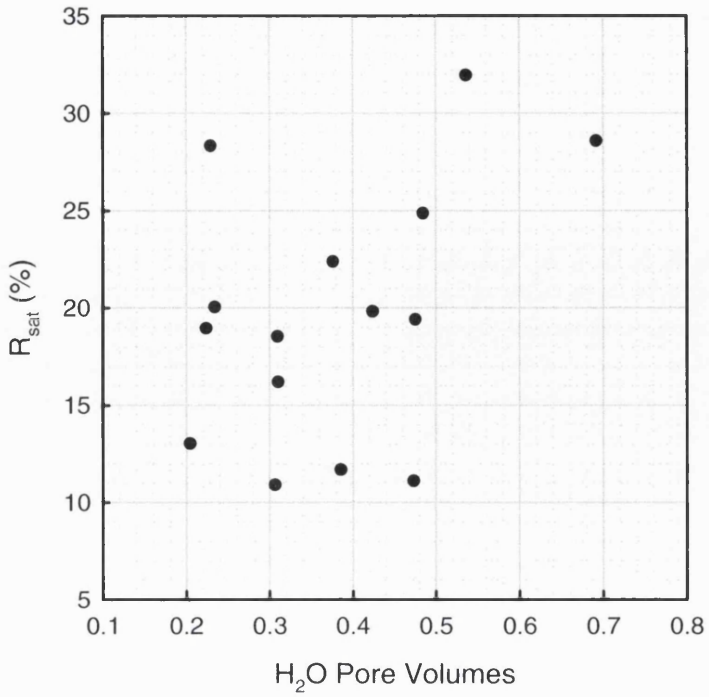

Figure 6-9 Cross plot showing the relationship between the residual DNAPL saturation and the number of pore volumes required for water to percolate across the core following the DNAPL flood.

6.4.2 DNAPL Dissolution Measurements

The most successful permeability and dissolution experiment is shown in Figure 6.10. It is judged successful in comparison to the other attempts because in this experiment relative permeability was found to increase with time (pressure decrease) although in a more step-wise fashion than anticipated (Figure 6.4) possibly due to some displacement rather than purely dissolution. The other attempts at measuring dissolution and relative permeability simultaneously resulted in relative permeability increases as most likely air became entrapped in the core. The duration of the experiments almost certainly were the cause of this problem, with the experiment in Figure 6.10 taking 13 days from start to finish.

The regression line shows very good agreement between the number of pore volumes passed through the core and the decrease in PCE concentration. Concentration and pore volumes are related by Equation 6.10:

$$Conc_{pce} = 88.66 - 0.0086 PVs \qquad (6.10)$$

where $Conc_{pce}$ is the concentration of tetrachloroethene in mg/L in the effluent and PVs is the number of pore volumes passed through the core.

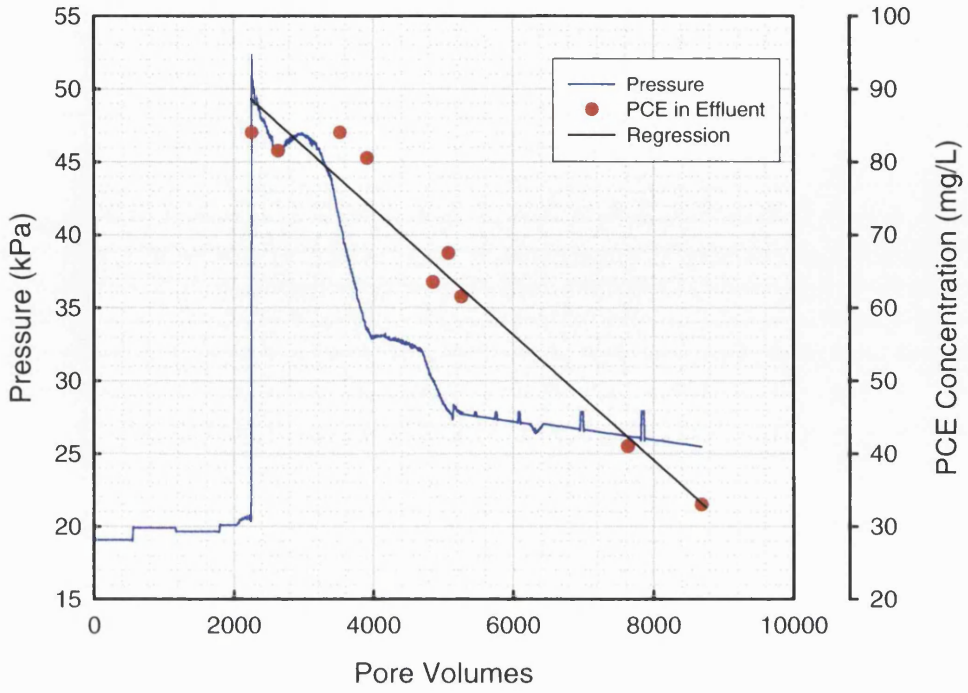

Figure 6-10 Pressure changes as DNAPL introduced into Clashac sandstone and then dissolves with water as it flows through the core.

Table 6.5 shows the concentration of PCE present in the effluent and the total volume of water that has moved through the core. Since, over this range of concentrations, the dissolution of tetrachloroethene seems to be a linear relationship with the total volume of water passing through the core, it is possible to calculate the total mass of PCE extracted from the area under the regression curve. Therefore the total mass of PCE extracted is $0.5 \times (84\text{-}33) \times (19.30\text{-}5.00) = 365$ mg, or a volume of 0.228 mL. If the core had a residual saturation of 19.7% (which would occupy a volume of 0.435 mL), taken from the mean in Table 6.4, this suggests that roughly 50% of the residual saturation has been removed in about 10 days.

As noted previously, the flow rates used during these experiments may impact on the distribution of PCE. The dissolution of a DNAPL is determined by the contact time with the aqueous phase and its relative solubility. Contact times in this experiment are short and maximum solubility (160 mg/L from Table 2.3) is not reached (Miller *et al.*, 1990). As such this experiment is poorly analogous to an environmental spill scenario (Rivett *et al.*, 2001).

Table 6-5 Effluent concentrations during relative permeability-dissolution experiment.

Pore Volumes	Absolute Volume (L)	Concentration PCE (mg/L)
2250	5.00	84
2630	5.84	82
3520	7.82	84
3900	8.87	80
4850	10.77	64
5070	11.27	67
5250	11.67	61
7630	16.95	41
8680	19.30	33

6.5 CHAPTER SIX SUMMARY

This chapter has presented the development, validation and implementation of a method to determine relative permeability in DNAPL-water-sandstone systems for a representative sub-set of Permo-Triassic sandstones. Measurements of residual saturation have also been made. Several problems were encountered in developing the method particularly with regard to excluding air from the system and fluctuations in laboratory temperature. Permeability with a DNAPL in the core is found to be roughly 20% of the permeability with no DNAPL. For the majority of the data, a trend of greater reduction in permeability is caused by a higher residual saturation of DNAPL. Higher DNAPL residual saturations also correspond with greater pore volumes of wetting phase required for percolation across the core. In a DNAPL dissolution of residual saturation experiment, the concentration of PCE in the effluent decreased linearly with the volume of water passed through the core and the relative permeability was also seen to increase. It was estimated that about 50% of the residual DNAPL was removed by dissolution in 10 days following water breakthrough.

7 A Simple 'Percolation' Model for Interpreting Mercury Intrusion Capillary Pressure Data

This chapter describes the implementation of a simple percolation based model as an alternative to the normal bundle of capillary tubes model for interpreting the mercury intrusion capillary pressure (MICP) data experiments described in Chapter 4. The details of the percolation model are given in Appendix 4. Four distribution functions are fitted to the MICP data using the percolation model and the parameters these functions produce are compared with empirical values and with those generated previously by Bloomfield *et al.* (2001) based on the capillary tubes model.

7.1 MEASURING PORE SIZE AND PORE SIZE DISTRIBUTIONS

'Pore size' has been used, by convention, in conjunction with the experimentally derived 'pore size distribution', which is the distribution density of pore volume by some length scale assigned to it. Every method of 'pore size distribution' determination defines 'pore size' in terms of a model best suited to the quantity measured. In mercury porosimetry the volume of mercury which has entered the sample is measured as a function of the pressure imposed on the mercury then the 'pore size' (more precisely, the pore-throat size) is calculated from this pressure imposed on the mercury. The 'pore size' is calculated from this pressure by Laplace's equation of capillarity (relating the pressure difference to surface tension and the mean radius of curvature) and, using the 'bundle of capillary tubes' model of pore structure, the volume of mercury is assigned to this 'pore size'.

The most representative approach to pore size distribution determination involves measurement of the sizes of all the pores on a macroscopic sample. All other methods are indirect and the results obtained by them depend on *a priori* assumptions made on the pore structure. The same model (e.g. the bundle of capillary tubes) may lead to widely different pore size distributions, depending on the type of experiment used (e.g. Klinkenberg, 1957), and similarly Dullien and Dhawan (1974) showed that different models (e.g. the shape function model or the sphere model) may also lead to widely different pore size distributions.

7.2 MODEL FORMULATION

The aim is to show how a simple percolation model can be applied to determine the distribution of throat sizes from the cumulative volume measurements of an MICP experiment (described in Chapter 4) rather than a bundle of capillary tubes model. The model developed is based on probability theory but exhibits critical probabilities and can therefore be regarded as a 'percolation theory' approach (Shante and Kirkpatrick, 1971). The percolation model provides a relationship, at a given capillary pressure, between the probability of a pore being filled, p, a throat being accessible, τ, and the coordination number, z.

In terms of an MICP experiment both p and τ can be regarded as functions of pressure or pore size, where pressure and pore size are related through the Washburn equation (see equation 4.4). Only conditions above the breakthrough point (or percolation threshold) are considered which corresponds to pressures giving $\tau=1/z$, since

$$p(\tau, z) = 0 \text{ if } \tau \leq 1/z \tag{7.1}$$

In the model all saturated pores are assumed to be connected. The model also assumes pores are either full or empty. The volume of mercury injected equals the number of pores times the probability that a pore is full times the average pore volume. Since the porosity is the total pore volume divided by the sample volume, the injected volume is given by:

$$V_i =< p > \phi V_{sample} \tag{7.2}$$

where $<p>$ is the mean probability averaged over the sample. Ignoring near surface effects, this probability can be identified with p in the model. Therefore

$$p =< p >= \frac{V_i}{\phi V_{sample}} \tag{7.3}$$

which is the required interpretation of the probability p for MICP, since V_i is the cumulative volume measured during an MICP experiment. The product ϕV_{sample} can be regarded as the cumulative volume injected at infinite pressure, assuming that all space is accessible.

The probability τ can be regarded as the probability that a throat is accessible at a given capillary pressure. That equals the probability that the throat is larger in effective radius

than that corresponding (through the Washburn equation) to the applied pressure. So τ is the cumulative pore-throat size distribution, where the integration is from large to small effective radii. Conventionally, cumulative distributions are taken as integrals from small to large, so, strictly, the throat sizes are distributed as 1-τ.

7.3 FITTING MICP DATA WITH THE PERCOLATION MODEL

The approach used is described also in Appendix 4 as 'Method 2'. MICP data occur in the form of pairs of values of pressure (simply converted to pore-throat size through the Washburn equation) and cumulative volume imbibed. The intention is to find the throat size distribution τ (strictly, $1-\tau$) and the coordination number, z, that best fit the MICP data.

It is shown in Appendix 4, equation A4.1, that p, τ and z are related through

$$p = 1 - (1 - p\tau)^z \tag{7.4}$$

which can be rearranged to give

$$\tau(p, z) = \frac{1}{p}\left[1 - (1 - p)^{1/z}\right] \tag{7.5}$$

In general, equation 7.4 can not be rearranged to provide a simple expression for $p(\tau,z)$. It is however straightforward to compute p for given values of τ and z and so it can be assumed that the function $p(\tau,z)$ exists.

To fit the MICP data using equation 7.4, an initial step is to decide on a functional form of the cumulative throat-throat size distribution, τ, and for each pressure step at which an experimental measurement is made to determine $\tau(P_c)$ or more strictly $\tau(R)$ since the pressure data has already been converted to an equivalent pore size by the Washburn equation. A natural choice of function is a cumulative probability function which gives positive values. Therefore the lognormal and gamma distributions have been evaluated as ways of describing the data. Given the field of study, relative saturation curves are also worth evaluating and so the van Genuchten function has been used. In addition, and based on the observation in Chapter 4 that many of the MICP curves obtained exhibit a power-law distribution over much of the pressure range, a power law is also evaluated in terms of how well it can describe the data.

Assuming a co-ordination number, z, the function $p(\tau(R), z)$ is found for each pressure step and compared with the MICP data. The value of p is converted to a volume by multiplying by S_r^{pore} which represents the maximum volume of mercury that could be intruded during the MICP experiment (i.e. the total connected pore volume). The difference between the function $p(\tau(R), z)S_r^{pore}$ and the MICP data is then reduced to a minimum on a least squares basis by varying the parameters of the distribution and z: Microsoft Excel Solver, was used.

7.4 DISTRIBUTION FUNCTIONS

As explained in Appendix 4 (Method 2) a functional form of $\tau(R)$ must be decided on. Suitable functions must take the form of a cumulative probability but it must be noted that these decrease from unity when R=0 to zero when R=∞. Four functional forms were employed.

7.4.1 Lognormal Distribution

The lognormal distribution is a probability distribution in which the log of the random variable is normally distributed. The lognormal distribution has the advantage over the normal distribution that it gives only positive values.

The lognormal distribution is a two-parameter distribution with parameters μ and σ_x. The probability distribution function is given by:

$$f(x) = \frac{1}{\sigma_x\sqrt{2\pi}} e^{-\frac{1}{2}\left(\frac{x-\mu_x}{\sigma_x}\right)^2} \qquad (7.6)$$

Microsoft Excel has a cumulative lognormal distribution function called LOGNORMDIST. The syntax is

$$\text{LOGNORMDIST}(x, \mu, \sigma)$$

Where x is poresize at which the distribution is to be evaluated and μ and σ are the mean and standard deviation of $\ln(x)$. The cumulative lognormal distribution for a given MICP curve is therefore calculated by:

$$\tau(x) = 1 - LOGNORMDIST(x, \mu, \sigma) \qquad (7.7)$$

The curves are therefore fitted to the MICP data by optimising with least squares on z, μ, σ and S_r^{pore}.

7.4.2 Gamma Distribution

The gamma distribution is a probability distribution that arises naturally, for example, in the study of the length of life of equipment. Its name came from the relationship of the distribution to the gamma function of advanced calculus. This distribution is related to the exponential distribution as well as the chi-squared distribution. It involves two parameters, α (the shape parameter) and β (the scale parameter), and is defined as follows:

$$f(x) = \frac{x^{\alpha-1}e^{-(x/\beta)}}{\beta^{\alpha}\Gamma(\alpha)} \tag{7.8}$$

The quantity $\Gamma(\alpha)$ is a symbol representing the value of the gamma function at the point α. This function is defined by the integral

$$\Gamma(\alpha) = \int_0^{\infty} x^{\alpha-1}e^{-x}dx \tag{7.9}$$

The mean of the distribution is the product $\alpha\beta$. Microsoft Excel has a Gamma distribution function called Gammadist. The syntax is

GAMMADIST(x, α, β, cumulative)

where x is the value at which the distribution is to be evaluated and α and β are parameters. If $\beta=1$, GAMMADIST returns the standard gamma distribution as expressed in equation 7.8. The final parameter, 'cumulative' is a logical value that determines the form of the function. If cumulative is TRUE, GAMMADIST returns the cumulative distribution function; if FALSE, it returns the probability distribution function. However, use of this function within the Excel framework often generated errors and so the function was rewritten as a visual basic module and given in Appendix 5.

7.4.3 Power Law

To fit MICP data using a power law the following equation was used

$$\tau(x) = 1 - \left(\frac{x}{PS_{\max}} \right)^{Power} \tag{7.10}$$

where x is the poresize for a given intruded volume of mercury, PS_{max} is the size of the largest pore intruded, and *Power* is the exponent to which value are raised. The curve was fitted to the MICP data by optimising on z, PS_{max}, *Power* and S_r^{pore}. The variable PS_{max} was constrained to be less than 2000 μm. As noted in Appendix 4, this function corresponds to the Brooks and Corey function.

7.4.4 van Genuchten Equation

The van Genuchten equation has previously been given in Equation 2.11 and rearranged in Equation 5.3.

$$\tau(PS) = 1 - \left(1 + \left(\frac{PS_0}{PS} \right)^n \right)^{-m} \tag{7.11}$$

7.5 RESULTS

In general, when the probability data could be fitted, a very good fit was obtained with an $R^2 > 0.99$. Figure 7.1 is an example of the MICP data and how well the four distributions can be fitted to this data. However, the figure also demonstrates how the different distributions produce very different coordination numbers for a given sample, ranging from 3 to 18. (Coordination number, z, was constrained to be ≥ 1.)

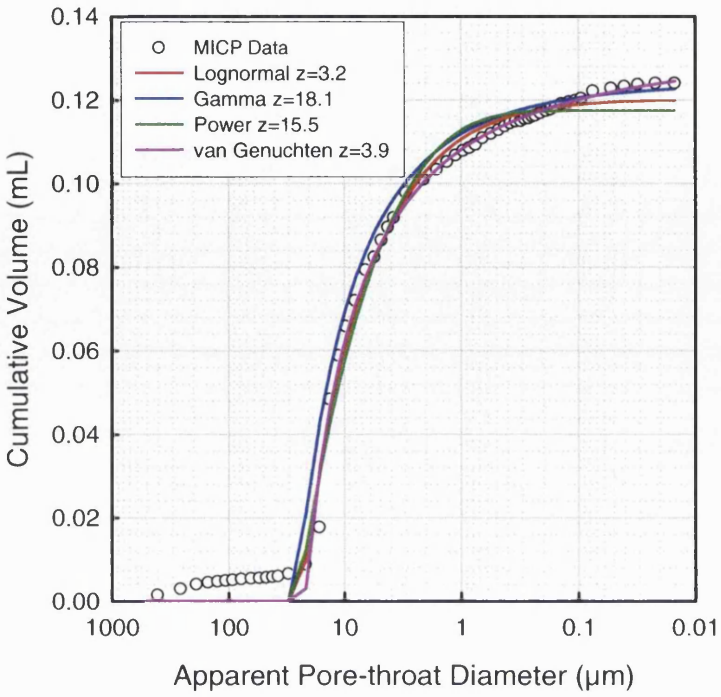

Figure 7-1 MICP data expressed for sample 1527/4v in terms of cumulative mercury imbibed and apparent pore-throat diameter based on the Washburn equation showing the best fits for lognormal, gamma, 'power' and van Genuchten distributions.

Where a function reached a constraint point for one of the fitting parameters those data have been removed (i.e. the curve parameters are not included in the statistical analysis).

A summary of the fitting parameters obtained using the lognormal distribution is presented in Table 7.1. The range of values for the coordination number z, is considerably smaller than that obtained by using any of the other distributions. The mean and median values are also closer to each other than for the other distributions suggesting fewer outliers and comparatively low standard deviation reinforces this smaller range. This distribution was the most successful at fitting the MICP data as it fitted all but one of the datasets (98%) within the allowable constraints. The geometric mean pore-throat size (e^{μ}) has been quoted rather than the arithmetic mean pore-throat size ($e^{(\mu+0.5\sigma^2)}$) since the later appeared to give exceptionally high values (up to 1.2E+239) due to high values of σ which may reflect the long tail at the beginning of the MICP data.

Table 7-1 Statistical summary of parameters fitted to the percolation model using the lognormal distribution as the probability distribution. The geometric mean pore-throat size is calculated from e^{μ} and is measured in μm.

	Geometric Mean Pore-Throat	S_r^{pore}	z
Mean	26.5	0.12	2.89
s.d.	98.2	0.18	0.90
Median	8.29	0.09	2.63
Max	793	1.45	5.28
Min	1.00	0.01	1.35
n	65	65	65

The gamma parameters are given in Table 7.2. This function achieved successful fits to the data on nearly two thirds of the samples. The gamma function predicted large mean pore-throat sizes and much larger mean and median values to the lognormal distribution for the coordination number, z. The range of values is also much larger than for the lognormal distribution.

Table 7-2 Statistical summary of parameters fitted to the percolation model using the gamma distribution as the probability distribution. The mean pore-throat size is the product αβ and measured in μm.

	Mean Pore-Throat	S_r^{pore}	z
Mean	131	0.09	8.06
s.d.	173	0.03	7.01
Median	55.8	0.10	5.00
Max	697	0.18	30.7
Min	3.08	0.01	1.04
n	46	46	46

Table 7.3 shows the range of fitted parameters determined for the MICP samples using the 'power law' as a distribution function. The function was only able to fit 40% of the samples before reaching a constraining point for at least one of the fitting parameters. This was largely because the function was found to be very insensitive to the value of z. The coordination number was eventually constrained at 32 to allow the model a considerable degree of freedom although for *regular* structures the theoretical maximum for the coordination number is thought to be 12 (Ridgway and Tarbuck, 1967). The fitting routine reached this maximum on 27 occasions. The constraining

value of PS_{max} was also achieved on 21 occasions (13 of these when the constraining value for z was also reached). On three occasion the 'power law' distribution could achieve no fit to the MICP data.

Table 7-3 Statistical summary of parameters fitted to the percolation model using a power law as the probability distribution. PS_{max} is measured in µm.

	PS_{max}	Power	S_r^{pore}	z
Mean	301	0.26	0.09	9.76
s.d.	350	0.38	0.03	8.06
Media n	204	0.11	0.09	5.97
Max	1700	1.69	0.15	28.5
Min	1.12	0.01	0.01	1.02
n	27	27	27	27

Table 7.4 shows the range of fitted parameters determined for the MICP samples using the van Genuchten function to describe the distribution of pore-throats. The function was only able to fit 66% of the samples before reaching a constraining point for at least one of the fitting parameters. The range of values for the coordination number is again relatively large with mean and median values suggesting coordination numbers of roughly 11, higher than the lognormal and gamma distributions but similar to the values obtained using the power law.

Table 7-4 Statistical summary of parameters fitted to the percolation model using the van Genuchten function as the probability distribution. PS_0 is measured in µm.

	PS_0	m	n	S_r^{pore}	z
Mean	218	0.09	1.11	0.09	10.2
s.d.	175	0.09	0.14	0.04	5.61
Median	193	0.05	1.05	0.09	11.5
Max	696	0.47	1.89	0.18	19.4
Min	0.29	0.02	1.02	0.01	2.00
n	44	44	44	44	44

For samples fitted by the lognormal distribution, the coordination number shows some correspondence with the shape of the MICP curve. Larger values of z (>4) commonly correspond with L-shaped curves with a relatively large pore-throat size and

high volumes of mercury intruded. Lower values of z (<2) often correspond with small pore-throat sizes and low volumes of mercury intruded. An example is shown in Figure 7.2. A large number of samples fall between these two ends but have coordination numbers between 2 and 4. It is interesting to note that the coordination numbers produced by the lognormal distribution are considerably lower than the z=12 suggested in Chapter 5 based on a percolation threshold. However, this value is close to those suggested by the power law and the van Genuchten function and may reflect the different fluids used in the measurement (mercury and DNAPL) as Klinkenberg (1957) showed different fluids can lead to different apparent pore size distributions.

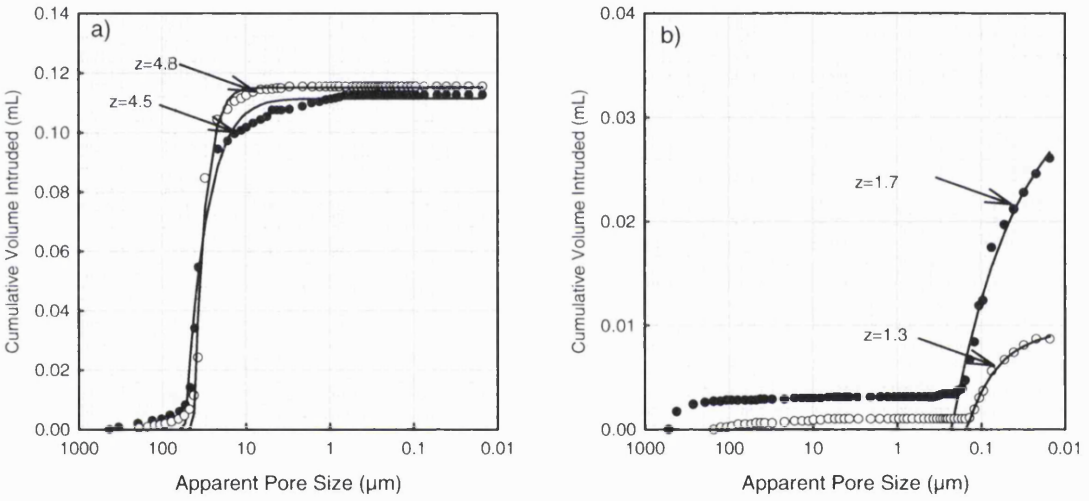

Figure 7-2 Relationship between MICP curve shape and coordination number, z for the case of a MICP data with z large (a) and z small (b) using the lognormal distribution in the percolation model.

The van Genuchten function has a pore size distribution index as one of its parameters (m). From Figure 7.3 it can be seen that this parameter is correlated with the coordination number, z. Based on all the distributions applied it appears that the model is generally very insensitive to the coordination number.

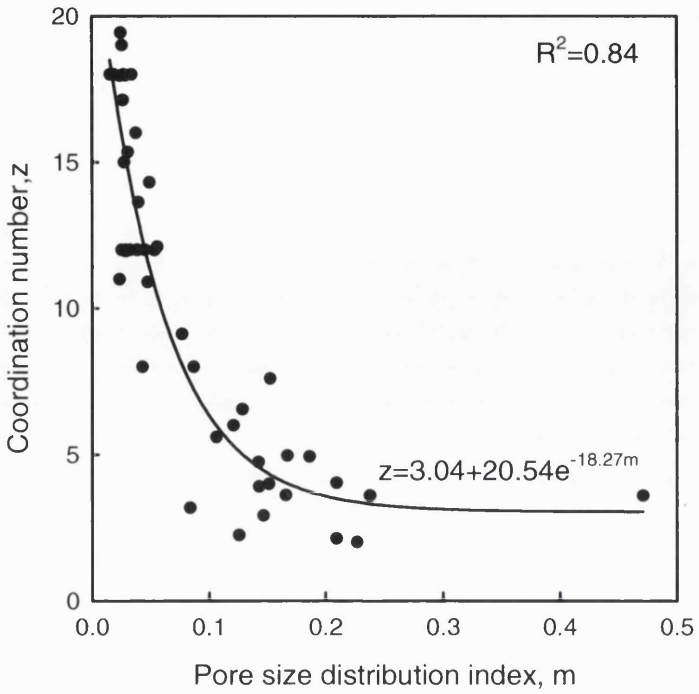

Figure 7-3 Comparison of coordination number, z, and pore size distribution index, m, when the percolation model is used with the van Genuchten equation.

7.6 DATA COMPARISON

The trend of the relation between coordination number and porosity found in the literature with respect to regular packs of spheres (e.g. Kruyer, 1958) indicates an increase of the coordination number of the *solid particles* with decreasing porosity or increasing solids fraction (the two are complimentary, i.e. $\Phi = 1-\phi$, where Φ is the solids fraction and ϕ is the porosity (pore fraction)). In common with the procedure followed by Yanuka *et al.* (1986), it is appropriate to compare the data to those found in the literature for random packs and expressed by the empirical relationship of Ridgway and Tarbuck (1967)

$$\Phi = 1 - \phi = 1.072 - 0.1193z + 0.004312z^2 \qquad (7.12)$$

where ϕ (used by Ridgway and Tarbuck) was replaced by $1-\Phi$.

This equation was solved for z for the porosity values described in Chapter 4. The coordination number obtained in this way is compared with that from using the lognormal distribution in Figure 7.4. The relationship is poor but does show a general increasing trend with coordination numbers occurring over similar ranges. The polynomial equation established by Ridgway and Tarbuck was based on samples with much higher porosities and so using it with this data set could be over-extrapolating.

Literature values for the coordination number of sandstones have been found as 2.9 for Berea sandstone (Yanuka *et al.*, 1986) and 3.4–3.8 for Fontainebleau sandstone (Linquist *et al.* 2000), which is similar to the range found by using the lognormal distribution with the percolation model.

The MICP curves have been previously fitted by just using the van Genuchten equation by Bloomfield *et al.* (2001) based on a bundle of capillary tubes model. A summary of the parameters determined is given in Table 7.5. In that work they defined the variable D_{P0} as the equivalent pore-throat diameter for the characteristic van Genuchten pressure P_0. The variable S_r was defined as the 'residual' saturation of mercury at the end of the experiment to make it analogous to S_r in the van Genuchten equation although in fact the true residual saturation should be $1\text{-}S_r$ since MICP is a drainage process.

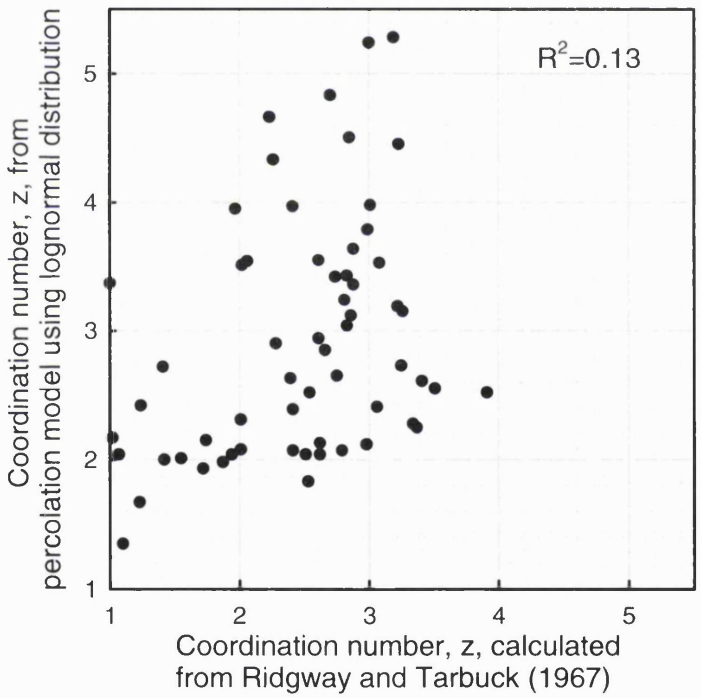

Figure 7-4 Cross plot of coordination number, z, obtained using the lognormal distribution in the percolation model with the empirical polynomial of Ridgway and Tarbuck (1967), Equation 7.12.

As all of the distributions needed to be scaled using S_r^{pore} it is possible to compare this value with S_r from the van Genuchten equation as used by Bloomfield *et al.* (2001). This is shown in Figure 7.5. The majority of the data fall on the 1:1 line suggesting good agreement between the recalculated data and S_r. Four values obtained for S_r^{pore} using the lognormal distribution fall to the left of the parity line which indicates an over-estimate of the final saturation of mercury. The gamma (with the

exception of 1 data point) consistently overestimates the final saturation. Considerably fewer data points exist for the power law distribution, those there are fall close to the 1:1 ratio. When the van Genuchten function is used with the percolation model good agreement is achieved for S_r^{pore} with the data obtained by the bundle of capillary tubes model used by Bloomfield *et al.* (2001).

Table 7-5 Statistical summary of van Genuchten parameters determined for Permo-Triassic Sandstone samples by Bloomfield *et al.* (2001) based on bundle of capillary tubes model, compared with pore sizes determined using the percolation model. D_{p0}, Mean Pore-Throat, PS_{max} and PS_0 are in μm.

	Capillary Tubes Model			Percolation Model			
	D_{P0}	S_r	m	Lognormal Geometric Mean Pore-Throat	Gamma Mean Pore-Throat	Power PS_{max}	van Genuchten PS_0
Mean	31.5	0.13	0.492	26.5	131	301	218
s.d.	23.3	0.25	0.211	98.2	173	350	175
Median	28.0	0.09	0.516	8.29	55.8	204	193
Max	120	2.06	0.904	793	697	1700	696
Min	0.011	0.010	0.004	1.00	3.08	1.12	0.29
n	66	66	66	65	46	27	44

The relationship between the coordination number determined using the lognormal distribution with the percolation model and the pore size distribution index, *m*, from the van Genuchten function determined by Bloomfield *et al.* (2001) is shown in Figure 7.6. The graph shows a relatively horizontal linear relationship for $z \approx 2$ where m is between 0 and 0.4. However, where $m > 0.4$, there is a clear linear increase in z as m increases. Large values of m are consistent with more uniform materials (low values tend to have a range of pore sizes). This data therefore suggests that where the sandstone has a more ordered structure it also has greater interconnection between pores.

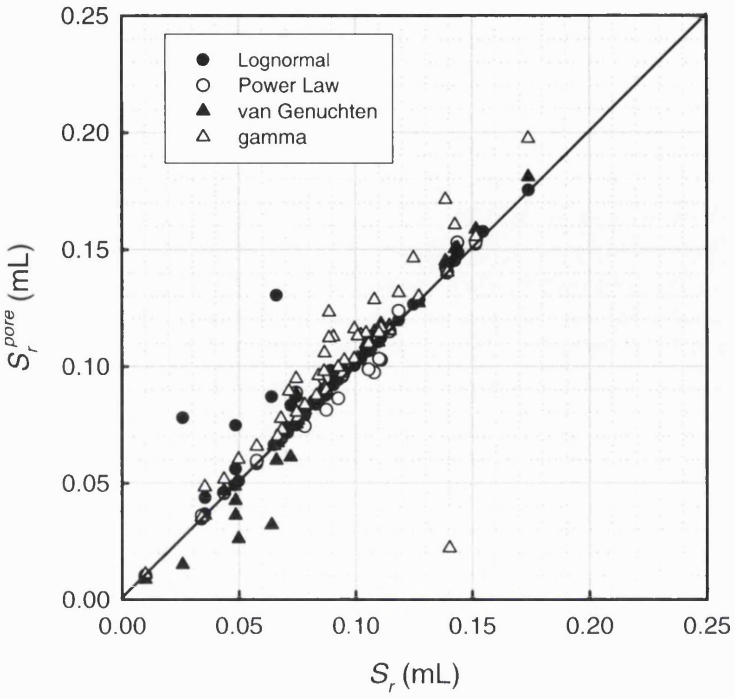

Figure 7-5 Comparison of S_r^{pore} obtained during the fitting routine for all distributions considered with S_r from Bloomfield *et al.* (2001).

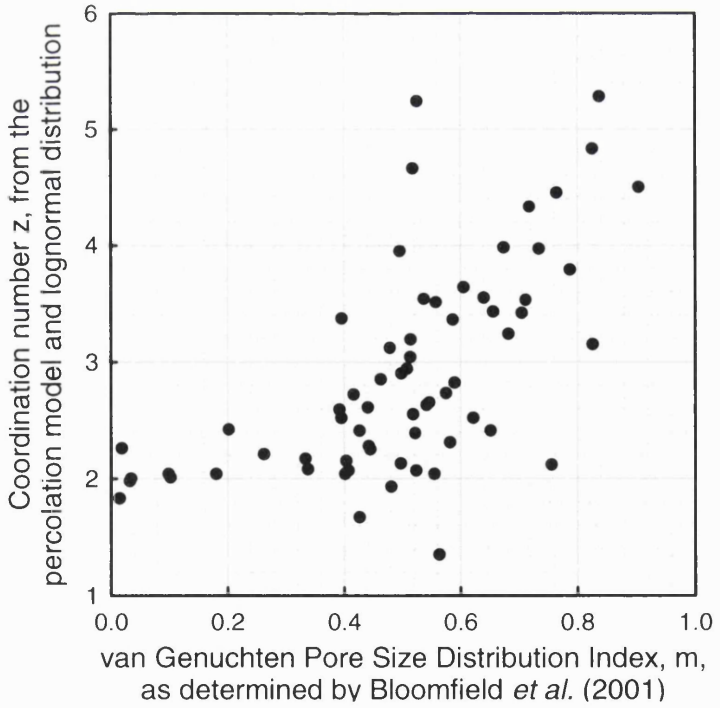

Figure 7-6 Cross plot of coordination number, z, obtained using the lognormal distribution in the percolation model with the van Genuchten pore size distribution index m as determined by Bloomfield *et al.* (2001).

It is also possible to compare the values of PS_0, PS_{max} and Mean and Median pore-throat size using the percolation model with D_{P0} obtained by the bundle of capillary tubes model used by Bloomfield *et al.* (2001) (Table 7.5). An example cross-plotting the full data sets is given in Figure 7.7. A clear positive trend can be observed between PS_0 and D_{P0} although the correlation coefficient is not strong (R^2=0.35). Figure 7.7 shows that PS_0 is roughly five times greater than D_{P0}. Therefore, when using the van Genuchten function with the percolation model to interpret the MICP data, it suggests that breakthrough occurs at a pore-throat size five times greater than when using the van Genuchten function with the bundle of capillary tubes model.

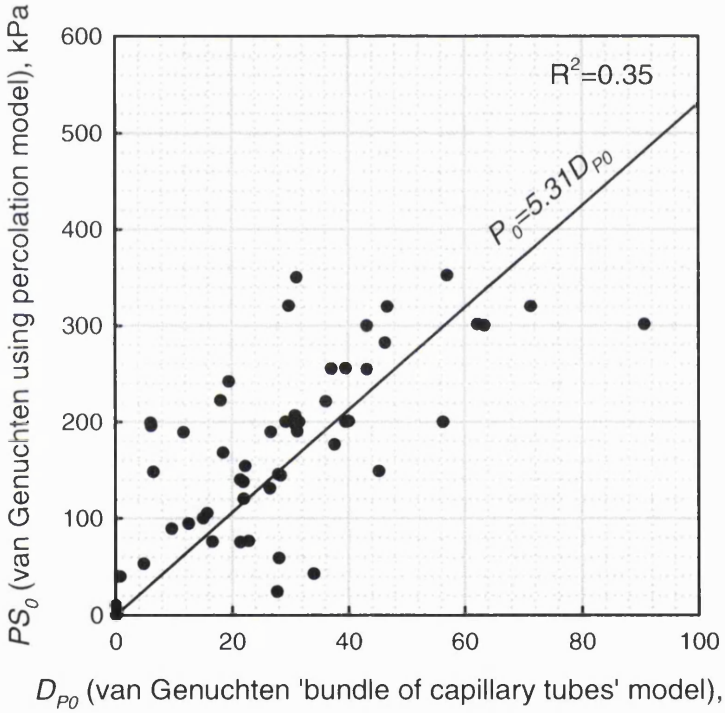

Figure 7-7 Cross plot of P_0 as determined from the van Genuchten function using the percolation model and D_{P0} from Bloomfield *et al.* (2001).

Figure 7.8 shows an example of the τ functions for the four probability density functions as determined by fitting them to the MICP data by using the percolation model. As with Figure 7.7, the functions all suggest the likelihood of larger pores being present than is revealed by conventional analysis of the MICP data by the bundle of capillary tubes model. The bundle of capillary tubes model shows intrusion first occurs at pressures corresponding to pore-throat sizes around 270 μm for this sample whereas the percolation model, using the gamma distribution suggest pores of up to 1000 μm (1 mm) and the other distributions suggest even larger pores. It must be emphasised that

the percolation model only provides large pore sizes by extrapolating via the chosen function $\tau(R)$, which can only be fitted to the actual corresponding data points. The presence of considerably larger pores than suggested by convention analysis of the MICP data could have implications for contaminant transport in sandstones and will be discussed further in Chapter 8.

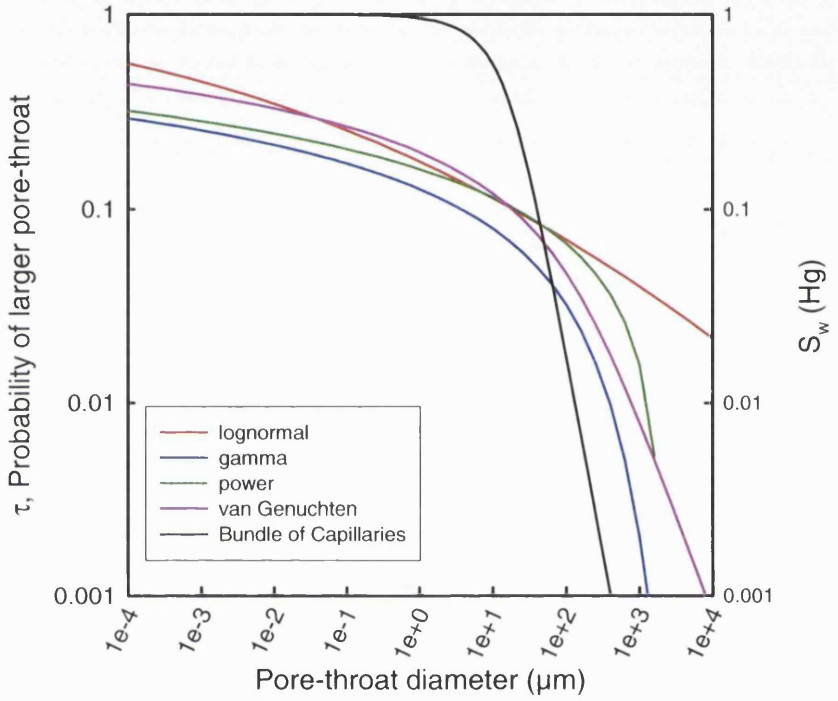

Figure 7-8 Plot of τ, the probability of a pore-throat being larger (left-hand axis), against pore size for the four probability density functions using the percolation model. Black curve shows the MICP data as represented by the bundle of capillaries model (right-hand axis). Example is for sample 1529/6v where conventional analysis of the MICP data shows initial penetration of the core at approximately 270 μm.

7.7 CHAPTER SEVEN SUMMARY

This chapter has described the use of a percolation based model to obtain coordination numbers and insight into MICP data. The model requires the pore-throat size data to be represented by an analytical function: cumulative probability functions and the van Genuchten function were chosen for this purpose. Of the four distributions evaluated, the lognormal distribution successfully fitted the data most often and generated the narrowest range of coordination numbers which were are also similar in range to those produced by the empirical relationship of Ridgway and Tarbuck (1967) based on sample porosity. The magnitude of coordination numbers generated by the power law and by the van Genuchten function is similar to that suggested in Chapter 4. The

percolation model appears to be very insensitive to the coordination number. However, the model does suggest the presence of much larger pore-throats which have implications for contaminant transport.

8 Discussion

A number of general observations regarding the permeability of the sandstones and their pore size distributions are made. Following this, data presented in Chapters 4 to 7 is integrated to provide a coherent interpretation of the physical and chemical controls on DNAPL behaviour in the matrix of Permo-Triassic sandstones. The implications of the data interpretation for aquifer remediation are discussed and the essential parameters that need to be measured for an understanding of a DNAPL spill in Permo-Triassic sandstone are assessed.

8.1 GENERAL OBSERVATIONS

8.1.1 Gas and Liquid Permeability

It is known that intrinsic permeabilities obtained by standard core analysis techniques using gas are different from those obtained using water. This is because gas measurements may be affected by a molecular phenomena referred to as gas slippage. The gas permeability data from Chapter 4 has been compared with the liquid permeability data from Chapter 6 in Figure 8.1. The figure demonstrates that there is a reasonable linear relationship between the data. Bloomfield and Williams (1995) developed an empirical liquid permeability-gas permeability correlation which was of the form:

$$\log_{10} k_l = 1.17 \log_{10} k_g + 1.51 \qquad (8.1)$$

where k_l is the liquid permeability and k_g is the gas permeability. The new data falls reasonably close to this line which gives confidence in the technique used.

8.1.2 Geological controls on pore-throat size distributions

No petrographic analysis has been undertaken as part of the present study, however a number of observations can still be made concerning the lithological controls on the physical properties of the Permo-Triassic sandstones investigated. The most significant factors controlling porosity and pore-throat size distribution in the sandstones are cement and grain dissolution and the presence or absence of clays, although primary grain size distribution (sorting) and grain packing are also important. Previous studies have shown that sandstones that exhibit development of cement dissolution porosity and/or grain dissolution porosity are generally well sorted with relatively open packing

(Strong and Milodowski 1987, and Strong 1993). Cement dissolution and grain dissolution are generally absent from samples with smaller dominant pore-throat sizes, which generally exhibit poor sorting, closer packing and relatively high interstitial clay contents. The samples in this study are consistent with these observations. The samples with permeabilities greater than about 0.001 μm^2 (1 mD) generally appear to be well sorted. The coarser grained sandstones are relatively friable indicating only limited cementation. Samples with permeabilities less than 0.001 μm^2 generally exhibit one or more of the following lithological characteristics: poor sorting, well cemented, fine grained, and relatively high clay content.

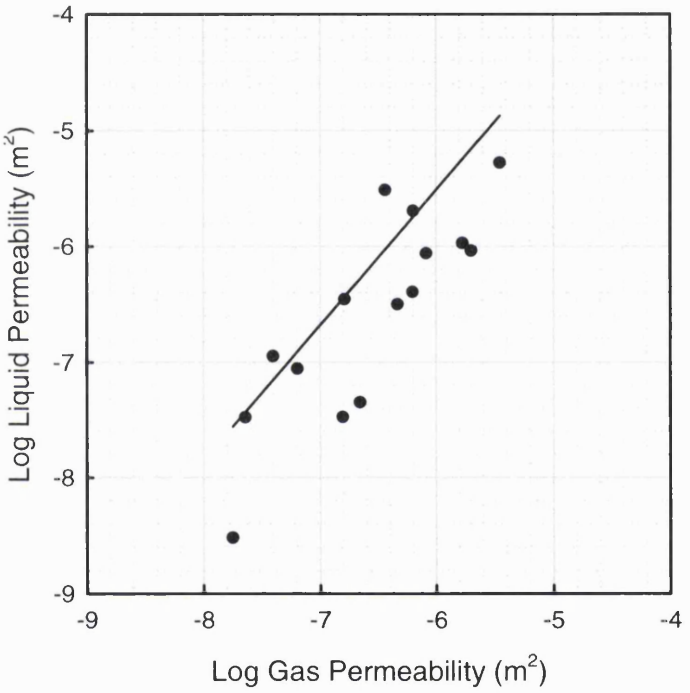

Figure 8-1 Comparing liquid permeability and gas permeability for samples analysed. The black line shows the correlation determined by Bloomfield and Williams (1995).

8.1.3 General implications of pore-throat sizes for contaminant transport

Only a fraction of the samples described in this study have relatively small pore-throat sizes and associated low permeabilities. Assuming that the samples described in this study are representative of the Permo-Triassic sandstone aquifer as a whole, although these low permeability sandstones are volumetrically inferior to the high permeabililty sandstones they may exert a disproportionately significant effect on the movement and distribution of contaminants and pathogens within the anisotropic aquifer.

Knowledge of pore structure can be of key importance in microbiological studies. Micro-organisms generally encountered in groundwater range in size from 1 to

10 μm and Harvey *et al.* (1995) suggest they can be classed as colloids. Transport of microbes is therefore subject to the mechanisms described by colloid filtration theory (Matthess and Pekdeger 1981, Harvey and Garabedian 1991). The basic tenets of this are that unretained particles move faster than the average pore water velocity and that particles are filtered by the medium. Figure 8.2 shows the distribution of median pore-throat sizes for all 66 MICP intrusion curves. The average value of these median pore-throat sizes is about 17 μm but a second peak in the population can also be observed around 0.1 μm. Superimposed on this pore-throat size frequency distribution are the sizes of some common micro-organisms. Figure 8.2 shows that many of the Permo-Triassic sandstones in the UK offers little resistance to pathogen movement through the aquifer system. For micro-organisms such as *Cryptosporidia* that can cause severe diarrhoea and even fatality at low concentrations in infected individuals (Bukhari *et al.*, 1997), roughly 70% of the sandstones tested would not filter this parasite. For the smallest faecal enteroccoci this figure rises to 96.5%. In addition, as colloids, transport of the active oocysts could take place more rapidly and hence over longer distances than transmissivity data might suggest. Clearly, the spatial and depth distribution of the sandstones with small pore-throat sizes and the connectivity and correlation of big pore-throats would be an important consideration in assessing the risk of pathogen transport in the matrix of the sandstones.

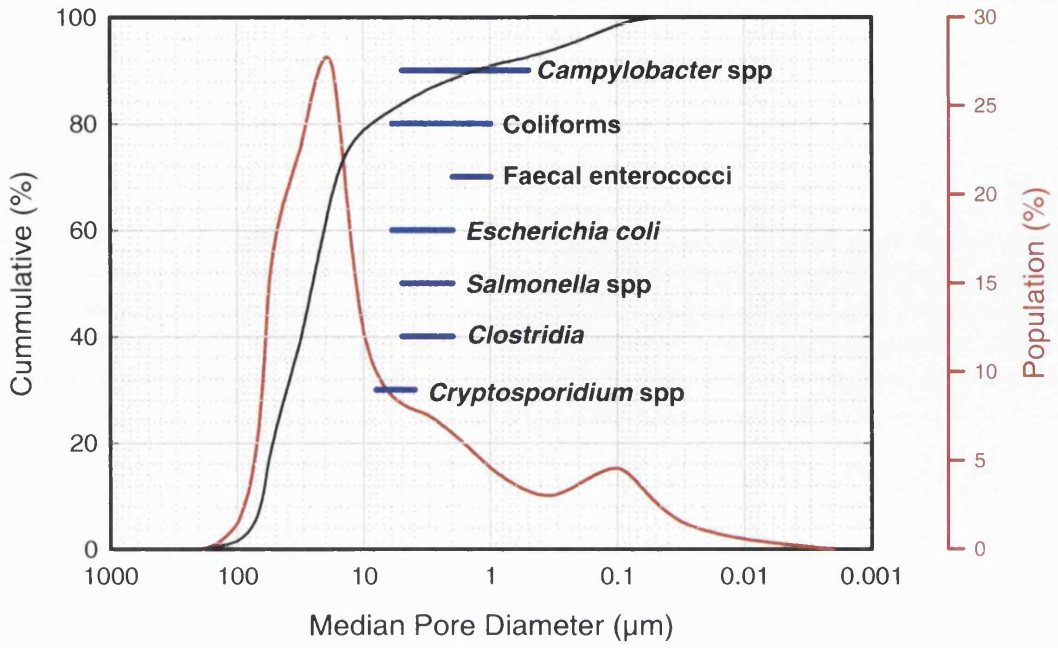

Figure 8-2 Distribution of median pore-throat sizes with ranges in size of several commonly encountered pathogens superimposed for comparison.

8.2 DNAPL ENTRY PRESSURES FOR PERMO-TRIASSIC SANDSTONES AND THE EFFECT OF CARBONATES

Data from the centrifuge method described in Chapter 5 has been combined with the MICP data for pore size from Chapter 4. Figure 8.3 shows effective entry pressure, P_0, obtained from the van Genuchten function to the centrifuge pressure-saturation curves, plotted against median pore size from the MICP tests (the figure also shows the equivalent height of PCE column on the right-hand y-axis). Super-imposed on the same graph are a series of reference contours for IFTs calculated from Equations 2.1 and 2.3 for a contact angle of 40°. It can be seen that most of the observations cluster between the 0.005 N/m and 0.015 N/m IFT contours. The interfacial tension, however, for PCE is 0.044 N/m, consequently, the observed entry pressures are systematically and significantly lower (on average seven times lower) than those predicted by Equation 2.3. One way to explain this could be a lower than predicted value of IFT and/or a larger than predicted contact angle.

By taking a contact angle of 40° and fitting Equation 2.3 to the observed data (using Excel Solver and optimising on a least squares basis) an apparent IFT of 0.007 N/m is obtained. In supplementary and supporting research Harrold *et al.* (2003) undertook a series of batch tests using PCE and dry Permo-Triassic sandstone. IFT

values close to the 0.045 N/m value determined by Mercer & Cohen (1990) were measured. A small decrease in IFT from 0.044 N/m to 0.040 N/m over a period of 20 minutes and then a further decrease to 0.038 N/m over the next 8 hours was observed. Given this observation it seems unlikely that an apparent IFT of 0.007 N/m could account for the unexpectedly low entry pressures. Therefore, a larger than predicted contact angle is probably a more likely explanation for the low observed entry pressures. The best fit line through the observed values (R^2=0.79) shown on Figure 8.3 based on an IFT of 0.038 N/m requires an effective contact angle of 81.8°.

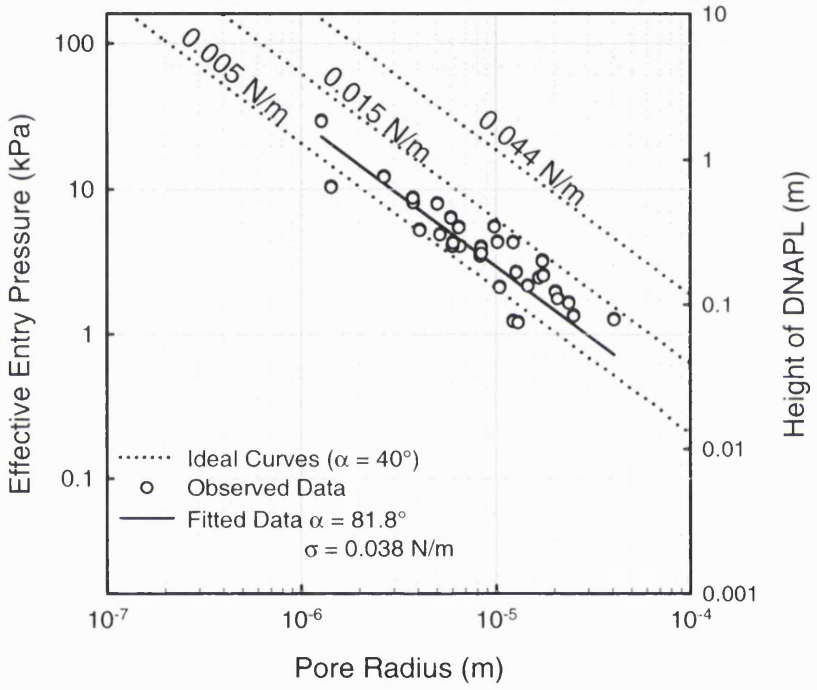

Figure 8-3 The relationship between pore size and the height of DNAPL required to overcome the entry pressure. Observed data falls considerably below that predicted from capillary theory and suggests that the contact angle is much larger than previously expected.

It has been shown that the observed PCE entry pressures are significantly lower than would be expected on the basis of standard capillary theory and that it is unlikely that this is due to changes in the IFT of the solvent. From this it has been inferred that the difference between observed and predicted entry pressures is due to unexpectedly large contact angles in the PCE-water-sandstone system. Barranco *et al.* (1997) found contact angles increase near the pH of the zero surface charge of quartz (around pH 2), however, the system investigated in this study is pH neutral. Anderson (1987a) noted that surface roughness effects will generally diminish the apparent contact angle, so even if surface roughness affects are active in the samples that have been tested they

will tend to reduce rather than increase the contact angle. Other workers have noticed significant changes in wettability and contact angles with time. Powers and Tamblin (1995) observed increases in contact angle for sands exposed to petroleum mixtures for between 14-60 days. Harrold *et al.* (2001) noted an increase in contact angle from 20° to 40° over 24 hours for a trichloroethene-sand system. In the present study, however, the sandstones were only exposed to solvent for relatively short times, typically of the order of 2 hours. On the basis of the observations of Harrold *et al.* (2001) and Powers and Tamblin (1995), it is unlikely that the length of exposure of the sandstones to PCE in the present study was sufficient to significantly modify the contact angle and hence to explain the observed entry pressures. Significant increases in wettability have also been observed with 'field', 'real-world' or 'dirty' solvents containing a cocktail of different solvents and impurities (Jackson and Dwarakanath, 1999; Dwarakanath and Pope, 2000; Harrold *et al.*, 2001). The solvent used in the present system was an analytical reagent grade PCE and so there are no significant quantities of impurities or surfactants in the PCE-water-sandstone system to affect the wettability.

In water-oil-rock systems it has been observed that sandstones tend to be water-intermediate wetting, whereas carbonate rocks tend to be intermediate or oil wetting (Lake 1989; Taylor *et al.*, 2000). It is known that carbonate cements are present in the sandstones as shown in Figure 4.9a, and this raises the following question, can the differences in observed and predicted entry pressures be explained by changes in the surface chemistry of the sandstones? A plot of calcium and magnesium per unit porosity (Figure 8.4) has been constructed to test the observation that limestones (calcium and magnesium carbonates) tend to have more neutrally wetting properties than sandstone. Calcium and magnesium have been plotted against the percentage difference between observed and predicted entry pressures, as given by the following expression

$$Diff_{Pc} = \frac{P_0 - P_c}{P_0} \times 100 \qquad (8.2)$$

where P_0 is the effective entry pressure obtained by fitting the centrifuge data with the van Genuchten function (Equation 2.11), and P_c is the predicted entry pressure based on ideal capillary behaviour, i.e. solution of Equation 2.1 given a contact angle, α, of 40°, and an interfacial tension, σ, of 0.044 N/m. The plot shows a log-linear increase in the difference between the observed and predicted values of entry pressure with increasing calcium and magnesium per unit porosity. Higher calcium and magnesium contents are

associated with lower than expected entry pressures. From this observation it is inferred that the surface chemistry of the sandstones, in particular the presence of calcite and dolomite cements, has a significant effect on the wetting properties of the rock, although through extrapolation to the origin in Figure 8.4 it can be seen that this can not solely explain the reduction in entry pressures observed. A similar plot of silicon and aluminium per unit porosity showed no strong relationship with the difference between observed and predicted entry pressures. Hence, it is inferred that the clay content of the samples does not significantly contribute to a reduction in solvent entry pressure.

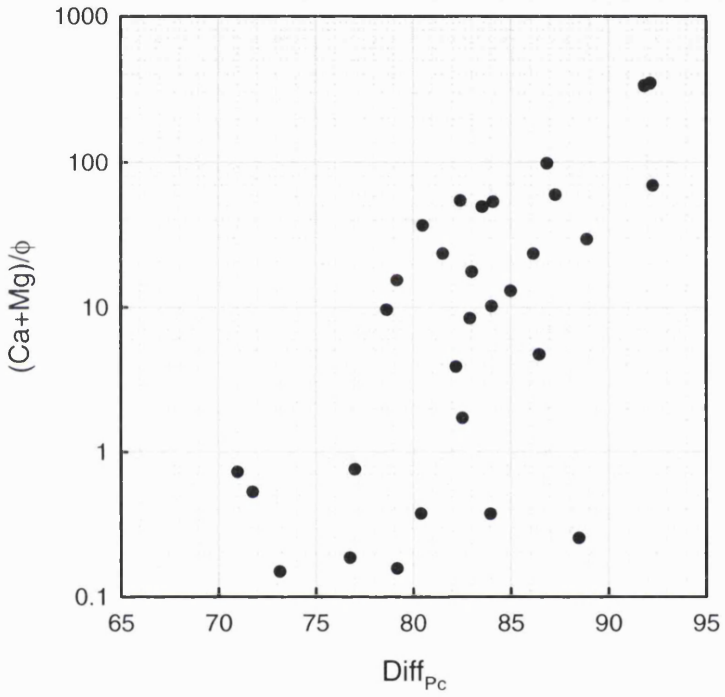

Figure 8-4 Calcium and magnesium per unit porosity plotted against the % difference between calculated and observed entry pressures. Samples with higher calcium and magnesium contents per unit porosity reduce measured entry pressures by more than those with low concentrations.

The observations that effective PCE entry pressure is a function of the surface chemistry of the Permo-Triassic sandstones, and that within a single sample there is a wide range of pore-throat sizes (Bloomfield *et al.* 2001), and that the sandstones exhibit variable cement mineralogy and morphology (Burley 1984, Strong 1993), all suggest that the standard conceptual model of the microscopic pore structure, i.e. that of a bundle of capillary tubes may not be appropriate (Dullien, 1992). A more sophisticated pore-scale conceptual model of the sandstone porosity is needed to describe DNAPL entry pressure behaviour in the sandstones.

Figure 8.5 shows a conceptual model of the pore scale structure of sandstones and the effect of surface chemistry on PCE contact angle (Gooddy *et al.*, 2002). Where DNAPL is in contact with silica, a water-wetting (solvent non-wetting) type contact angle of less than c.70° is assumed. However, where DNAPL is in contact with carbonates, e.g. calcitic or dolomitic material, the contact angle is between 70-110°. Under these circumstances the DNAPL will behave as a neutral or even wetting phase and hence the entry pressure required will be reduced relative to theoretical values based on a static measure of contact angle on a silicon slide. The variable nature of carbonate cements at the pore scale may mean that some pores may be more water wet and some may be more neutral or even DNAPL wet, depending on the amount and nature of carbonate cementation. However, the cumulative effect of the carbonate cement is to increase the effective, average (macroscopic), contact angle and so reduce the effective entry pressure.

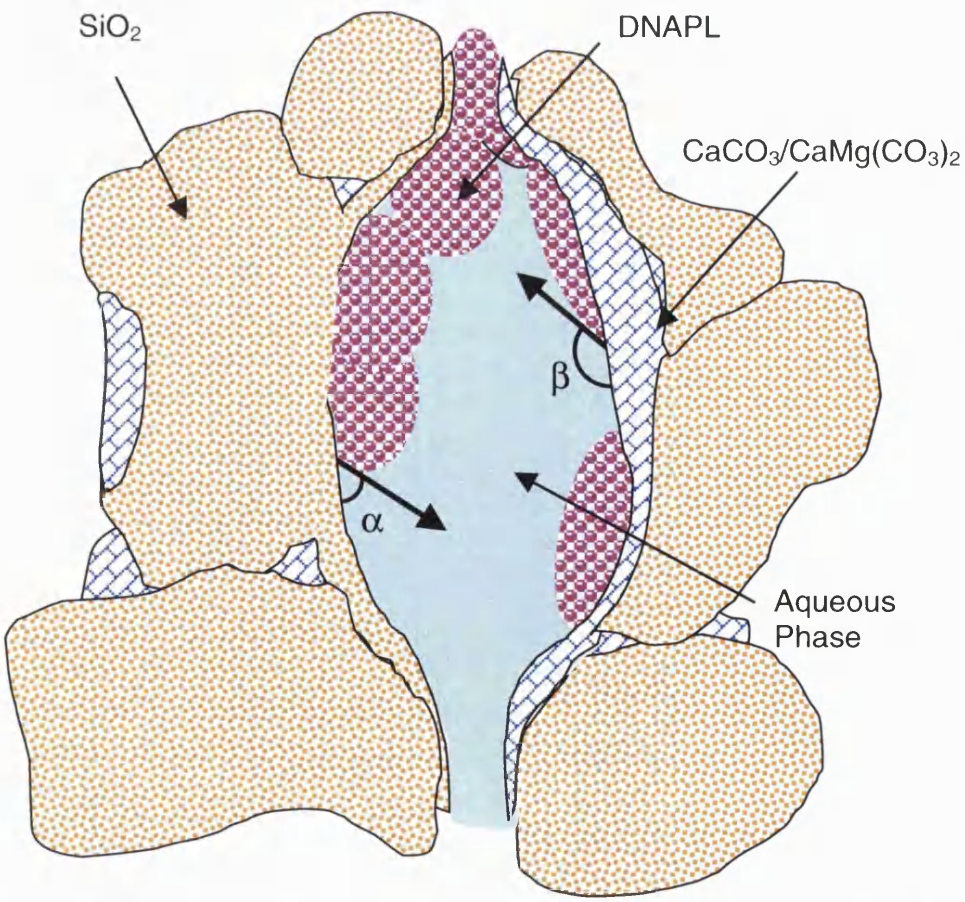

Figure 8-5 Conceptual pore scale model to describe the suppression of entry pressure of PCE into Permo-Triassic sandstone due to an overall reduction in contact angle due to the presence of calcium and magnesium carbonates.

Therefore, the bundle of capillary tubes model does explain the data to some extent if the wettability of the system is modified to take into account the mineralogy and if an effective new wettability is assigned to the model to give a contact angle of roughly 80° but does not explain the bulk of the difference. It is important to note that Figure 8.5 is still a bundle of capillaries model.

The bundle of capillaries model does not provide an adequate representation of the pore-size distribution within sandstones. Evidence from the percolation model discussed in Chapter 7 showed that the true pore-size distribution may be quite different from those inferred from standard analysis of MICP data. The percolation model suggested the presence of much larger pores although the different probability distribution functions produced widely varying pore distributions and some functions were better at fitting the MICP data than others (from best to worst: lognormal, gamma, van Genuchten, Power) which leads to a degree of uncertainty. From the, admittedly relatively weak, correlation between pore-throat size using the van Genuchten function and the bundle of capillary tubes model and pore-throat size using the van Genuchten function and the percolation model (Figure 7.7), it was shown that there was a large discrepancy in the percolation pore size. If it is assumed that wettability has been little altered by the presence of the carbonates and the contact angle is 40° then comparing this with the contact angle derived in Figure 8.3:

$$\frac{\cos 40°}{\cos 81.8°} = 5.37 \qquad (8.3)$$

which is exceptionally close to the 5.31 factor difference between the bundle of capillary tubes model and the percolation model using the van Genuchten equation (Figure 7.7). Therefore the observed entry pressures may either be interpreted in terms of an increase in contact angle (bundle of capillary tubes model) or the presence of more large and connected pores (percolation model) or indeed both.

Powell *et al.* (2003) have recently demonstrated the vulnerability of sandstones in UK urban areas to microbial contamination through transport along fractures. If there is a larger and more connected pore network than described by the bundle of capillary tubes model then the potential for pathogen and colloidal transport is considerably enhanced and the matrix of the Permo-Triassic sandstones is in fact more vulnerable than suggested by Figure 8.2.

8.3 THE IMPACT OF COORDINATION NUMBER ON DNAPL PERCOLATION

It was noted in Chapter 5 that from the van Genuchten parameterisation of the $P_c(S_w)$ curves that the final residual water content could be related to the non-wetting phase saturation at the percolation threshold. Chapter 7 noted that the coordination number could be in part related to the van Genuchten pore size distribution index, *m*, as determined by Bloomfield *et al.* (2001).

Having noted that entry pressures are suppressed, at least in part relating to the presence of mineral phases in the pores, it would be useful to elucidate as to the influence of sandstone structure on DNAPLs once they have entered the core. A continuous network of pores and pore-throats needs to be completed for percolation to occur and it is reasonable to consider this process will relate to the way in which the pores are interconnected. By combining data on the coordination number with the percolation non-wetting phase saturation it should be possible to determine the degree to which structure would effect DNAPL moving through the matrix.

Figure 8.6 shows two cross plots comparing coordination number with the DNAPL content of the matrix at percolation. Neither of the graphs show very strong correlations between *z* and percolation saturation. Figure 8.6a shows a general trend of increasing coordination number with greater DNAPL saturation whereas Figure 8.6b shows no correlation between the two parameters. Higher coordination numbers with higher residual DNAPL would imply a more tortuous route followed. The DNAPL would have to move through the matrix filling many inter-connected pore-throats before breaking through.

It is disappointing that a better trend is not observed with the coordination number data, especially that obtained by using the probability based model and the lognormal distribution. Figure 5.8 shows that a better correlation between non-wetting phase saturation and structure is obtained by considering the van Genuchten pore size distribution index, *m*.

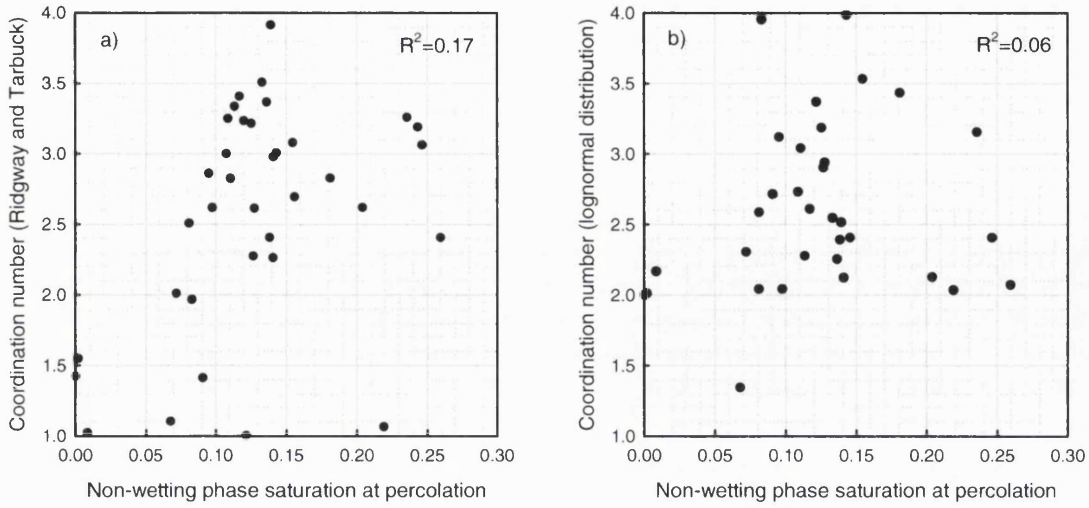

Figure 8-6 The influence of coordination number determined by a) Ridgway and Tarbuck (Equation 7.12) and b) from the percolation model using the lognormal distribution on the non-wetting phase saturation at the percolation pressure (Equation 5.8) as determined from the van Genuchten equation.

In Chapter 7 the value of m suggested that the higher coordination numbers corresponded with a more uniform arrangement of pore-throats (Figure 7.6). A more uniform arrangement will have many pore-throats with similar entry pressures. Therefore no 'preferential' route will be followed, which is more likely to happen if there are a range of pore-throat sizes, and the DNAPL must permeate through a larger proportion of the matrix before breakthrough.

As the non-wetting fluid (DNAPL) should favour the large pores, this data suggests that within the Permo-Triassic sandstone the large pores show greater structural connectivity. Figure 8.7 shows a cross plot of the mean pore diameter $2\sqrt{k/\phi}$ against the pore size distribution index, m. It can be clearly seen that the larger mean pore sizes correspond with the highest m values. This considerably improved relationship with using the value of m rather than z suggests that it is more important for immiscible displacement processes to consider the pore-throat size distribution than the average number of pore connections.

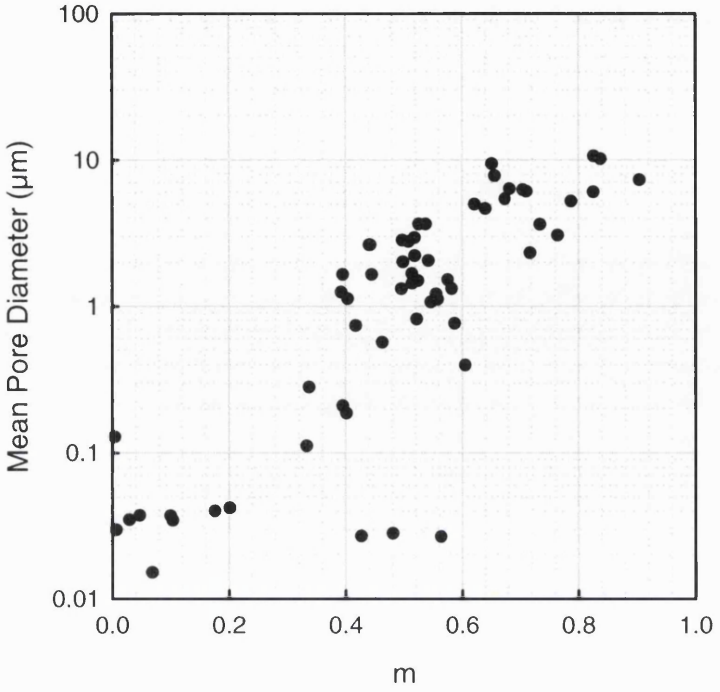

Figure 8-7 The relationship between mean pore diameter $2\sqrt{k/\phi}$ and pore size distribution index m. Note mean pore diameter is plotted on a log scale.

8.4 RELATIVE PERMEABILITY

8.4.1 Reduction in Permeability and Pore Size

Chapter 4 established a relationship between the mean pore diameter $2\sqrt{k/\phi}$ and the median pore size from MICP measurement (Equation 4.8). In Chapter 6 it was shown that the permeability, k_f, and the reduced permeability caused by a DNAPL, $k_{f\,residual}$, could be related by a simple power law function (Equation 6.9). As pore size is likely to have a significant effect on permeability, by combining data from Chapter 4 on pore size with data from Chapter 6 on relative permeabilities it is possible to see whether or not these properties can be related.

Figure 8.8 shows cross plots for permeability before and after the DNAPL flood as a function of median pore size as determined by the MICP measurements. Both sets of data could be best fitted by using a power law:

$$k_f = 0.0021 \times PS_{Med}^{1.78} \tag{8.4}$$

$$k_{fresidual} = 0.0002 \times PS_{Med}^{2.14} \tag{8.5}$$

Neither of the curves provide very convincing correlations: for Equation 8.4, $R^2 = 0.38$; and, for Equation 8.5, $R^2 = 0.54$.

However, if the same exercise is repeated for the mean pore diameter (Figure 8.9), a considerably better set of correlations are obtained. The data can be described by Equations 8.6 and 8.7.

$$k_f = 0.0515 \times PS_{Mean}^{2.14} \tag{8.6}$$

$$k_{fresidual} = 0.0102 \times PS_{Mean}^{2.41} \tag{8.7}$$

Equation 8.6 gives $R^2 = 0.70$ and Equation 8.7 gives $R^2 = 0.87$.

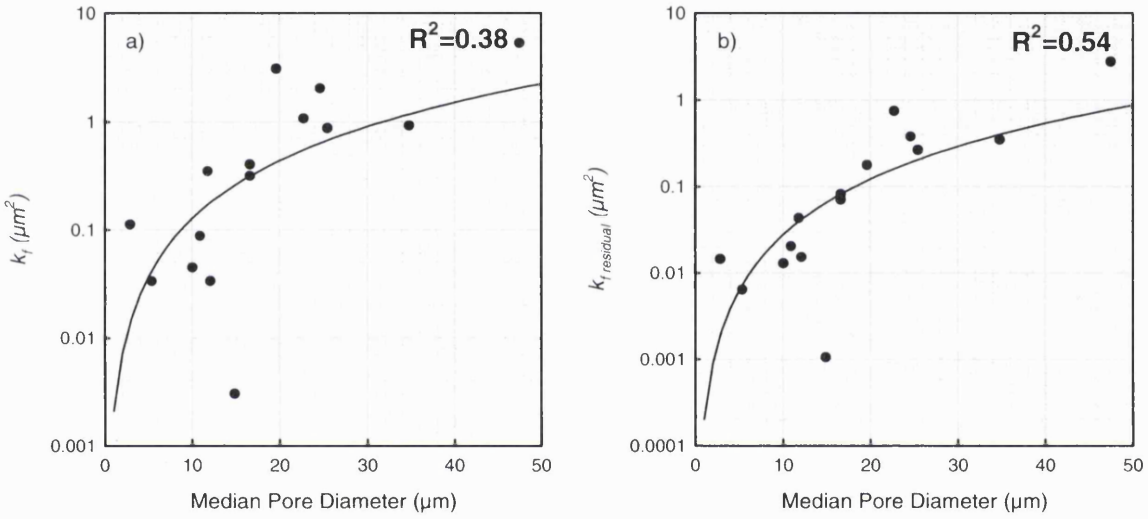

Figure 8-8 The relationship between a) permeability and median pore diameter and b) permeability with residual DNAPL and median pore diameter.

Taking the ratio of k_f to $k_{fresidual}$ shows the reduction in permeability. If this is then compared with the mean pore diameter, it is possible to determine the reduction in permeability that will be caused due to a DNAPL spill for a given pore size. Figure 8.10 is a model of this relationship from taking the ratio of the best fit Equations 8.6 and 8.7.

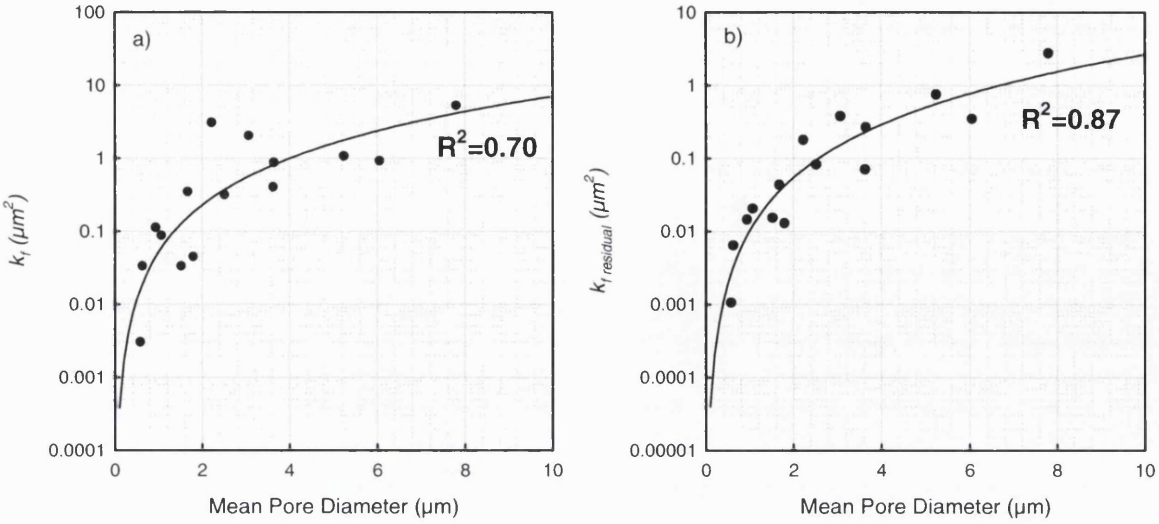

Figure 8-9 The relationship between a) permeability and mean pore diameter $2\sqrt{k/\phi}$ and b) permeability with residual DNAPL and mean pore diameter.

Figure 8.10 demonstrates that the reduction in permeability is less as the mean pore size increases. This means that the reduction in permeability will be comparatively small for sandstones with large pore sizes compared to sandstones with small pore sizes. Larger pores drain more easily than small pores so residual saturation should be lower. Figure 8.2 shows that the majority of the sandstones tested have a median pore size of roughly 20 μm which from Equation 4.7 corresponds to a mean pore size of approximately 3 μm. In Figure 8.10, a pore size of 3 μm suggests a three to four-fold decrease in permeability. At this point on the curve the change in residual saturation becomes less sensitive to the pore size.

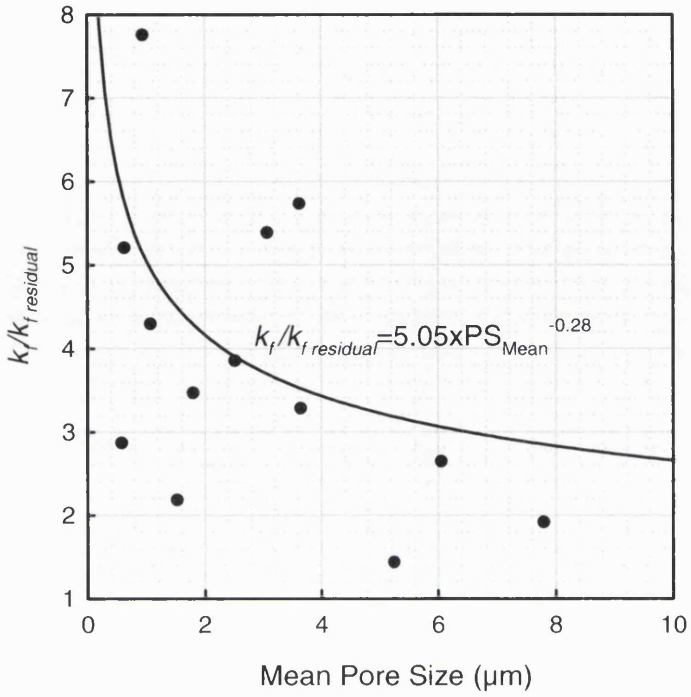

Figure 8-10 Ratio of reduction in relative permeability based on best fit data against mean pore diameter. Measured data is shown as black circles.

8.4.2 Comparing Relative Permeability Methods

As described in Chapter 2 (section 2.4.5), $P_c(S_w)$ data can be used to determine relative permeability. The λ from the Brooks-Corey function and m from the van Genuchten function determined in Chapter 5 can be used in Equations 2.17-2.20 to determine the wetting phase and non-wetting phase relative permeability, respectively. This data has been combined with the relative permeability data described in Chapter 5. The relative permeability experiment in Chapter 5 produces a single data point at the end of the sample run, the water content of the sample core at this point is taken as the wetting phase saturation and the change in relative permeability is expressed as a fraction of the original liquid permeability. The data has been compared with relative permeability curves produced from the van Genuchten (Figure 8.11) and Brooks-Corey function (Figure 8.12).

Generally the agreement between permeability determined experimentally and that determined indirectly from the $P_c(S_w)$ curves is good, with best agreement observed by the curves generated by using the λ value from the Brooks-Corey equation. The reasons for this are unclear although it may reflect the insensitivity of the Brooks-Corey function to the initial imbibition of DNAPL but possible better characterisation of parts

of the $P_c(S_w)$ curve which are more dominant for relative permeability. The Brooks-Corey based data tends to suggest higher non-wetting phase saturations. Worst agreement between the methods is observed for the samples with the larger pore sizes. This could be a result of DNAPL draining from the larger pores during the relative permeability experiment.

From the 12 samples, 11 show no permeability to the wetting phase (water) occurs ($k_f = 0$) at water saturations less than approximately 60% (a DNAPL saturation of 40%). The exception to this is sample 1542/2v which has the largest pore size and $k_f = 0$ at around 40% saturation. Therefore, where DNAPL occupies roughly 40% of the available pore space then no flow will occur. The largest residual saturation measured was 32% (Table 6.4) so clearly this threshold was not reached.

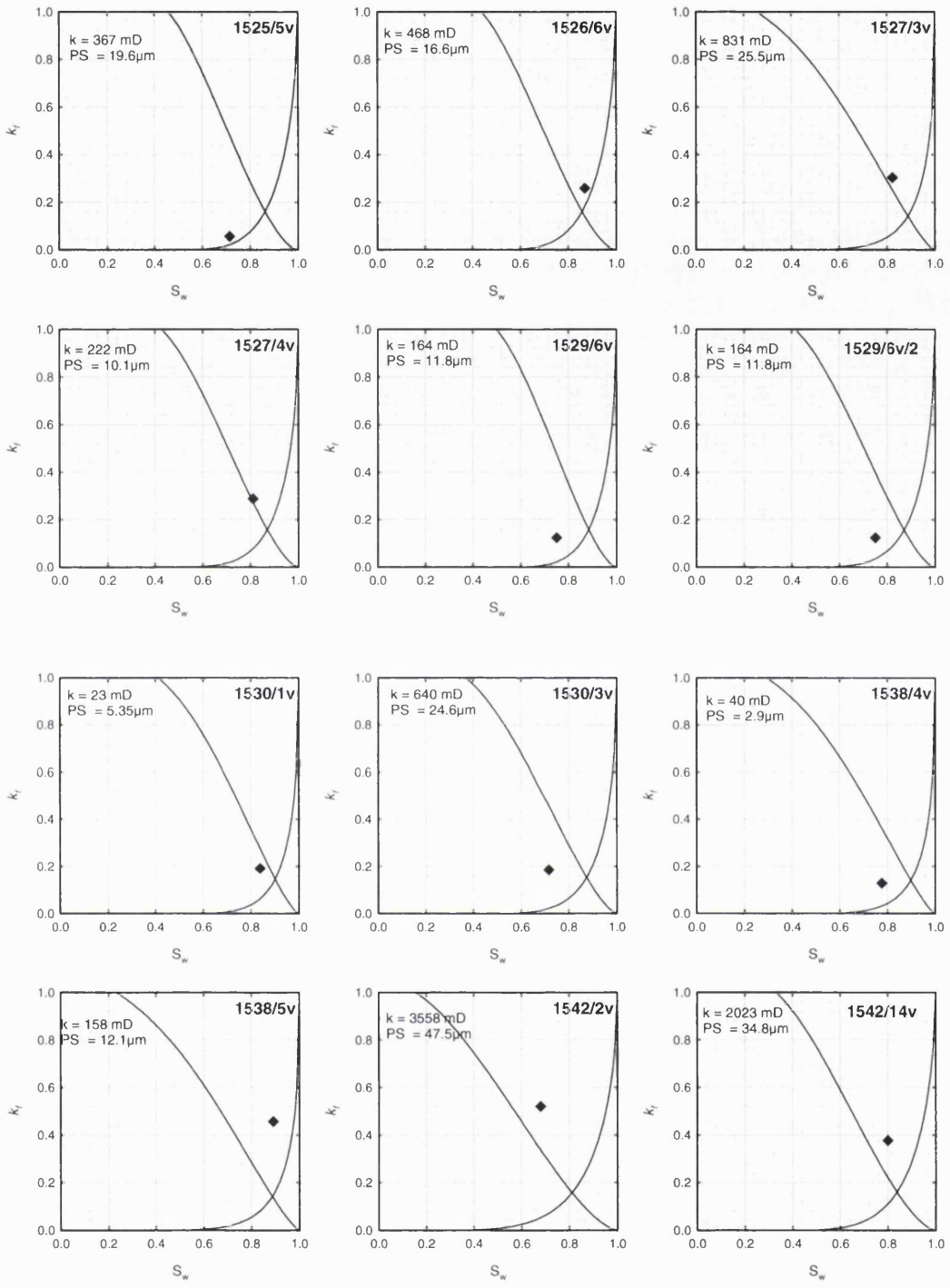

Figure 8-11 Relative permeability curves generated using the van Genuchten function. Wetting phase saturation tracks from where $S_w = 1$ and $k_f = 1$ (right hand, k_{rw} curve, in all samples). The non-wetting phase saturation is $1-S_w$. Relative permeability data determined by direct experiment is shown by the black diamond and relates to the k_{rw} curve. See Equations 2.19 and 2.20 and Figure 2.6).

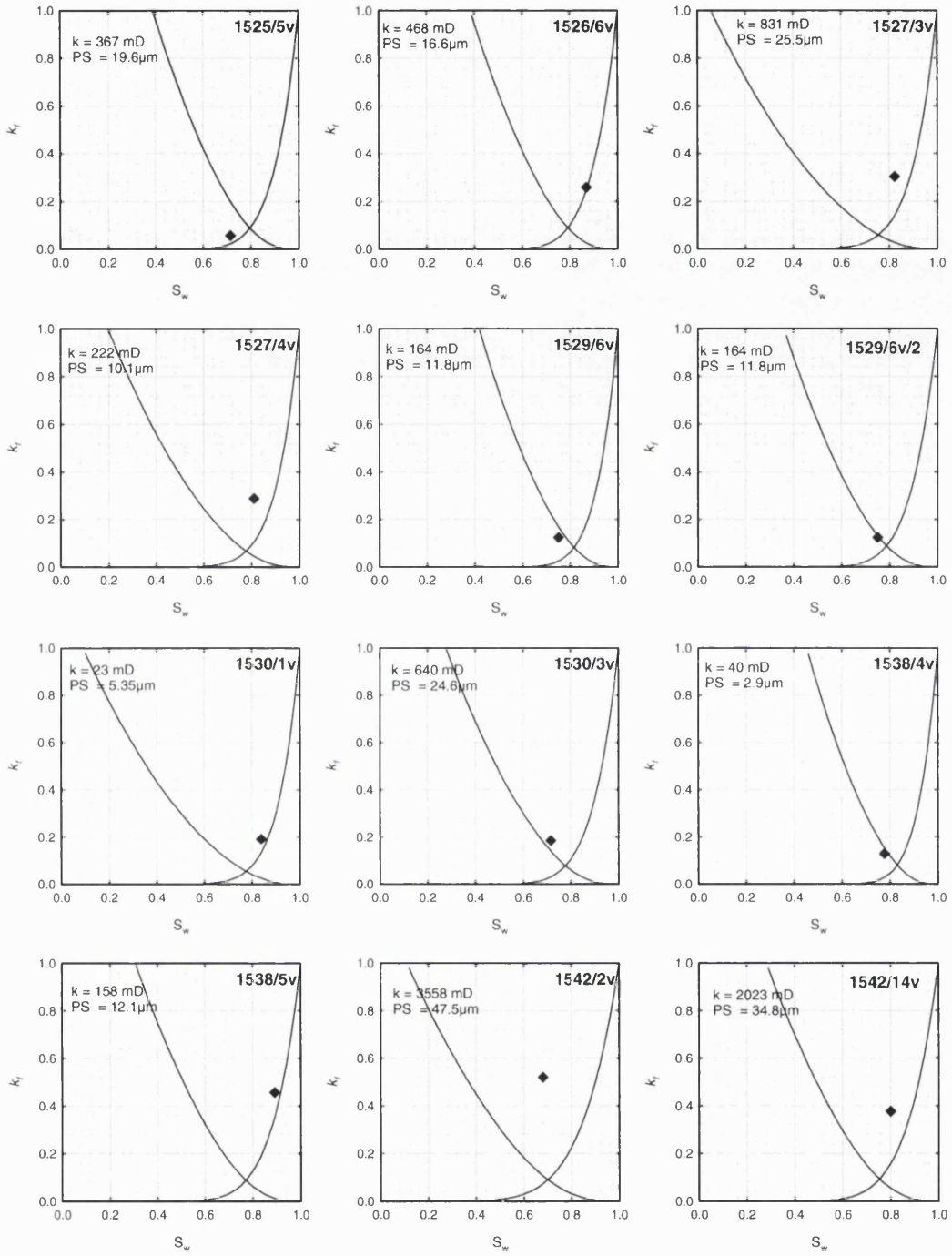

Figure 8-12 Relative permeability curves generated using the Brooks-Corey function. Wetting phase saturation tracks from where $S_w = 1$ and $k_f = 1$ (right hand, k_{rw} curve, in all samples). Relative permeability data determined by direct experiment is shown by the black diamond and relates to the k_{rw} curve. See Equations 2.17 and 2.18 and Figure 2.6.

8.5 DNAPL SATURATION AND PORE SIZE

8.5.1 DNAPL saturation in sample cores as related to pore size and pressure

Using the Brooks-Corey and van Genuchten fits to the $P_c(S_w)$ curves, it is possible to determine the degree of DNAPL saturation at any given pressure, not just those pressure steps measured during the experiment.

Figure 8.13 shows the relationship between the degree of DNAPL saturation at 4 kPa pressure plotted against mean pore size and median pore size. Both graphs show an excellent correlation between pore size and the degree of DNAPL saturation, with the best correlation for mean pore size, with the largest pores having the highest DNAPL saturation. It is possible to obtain good linear regression fits to the data for any pressure in the range determined as shown in Figure 8.14. The data show that the correlation decreases with increasing pressures, which probably reflects the fact that there are fewer samples with very large pore sizes to constrain the curves.

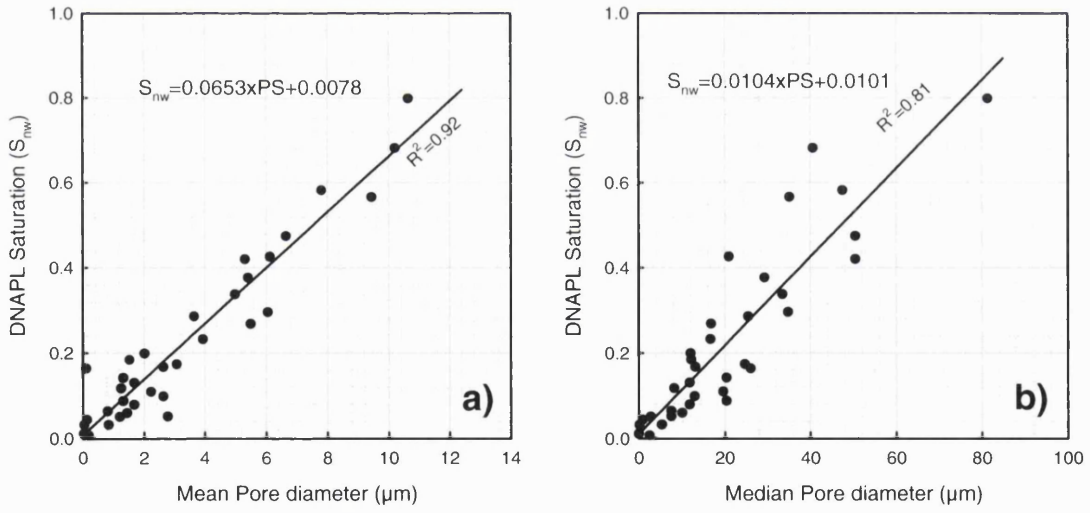

Figure 8-13 The relationship between DNAPL saturation of the core and pore size expressed as a) mean pore diameter and b) median pore diameter. Data is extrapolated from van Genuchten fitting of $P_c(S_w)$ curves at a pressure of 4 kPa.

The curves are of considerable interest as they show the vulnerability of Permo-Triassic sandstones to DNAPL contamination. Section 8.4.2 showed that relative permeability falls to zero at around 40% DNAPL saturation. For a pressure of 4 kPa (or an equivalent head of 25 cm of PCE), 40% DNAPL saturation (0.4 S_{nw} on the graph in Figure 8.14) will occur in sandstones of a mean throat diameter of 6 µm. Similarly, for a pressure of 20 kPa (1.25 m of PCE) sandstones with a mean diameter of 2.2 µm will be

at 40% DNAPL saturation (although this is not a residual saturation). From Table 4.1 the mean of the mean pore radius for all samples is 1.15 µm or a diameter of 2.3 µm. Therefore on this basis, roughly half the samples would be susceptible to having sufficient pore space filled with DNAPL that would prevent continuous flow of water, the wetting phase.

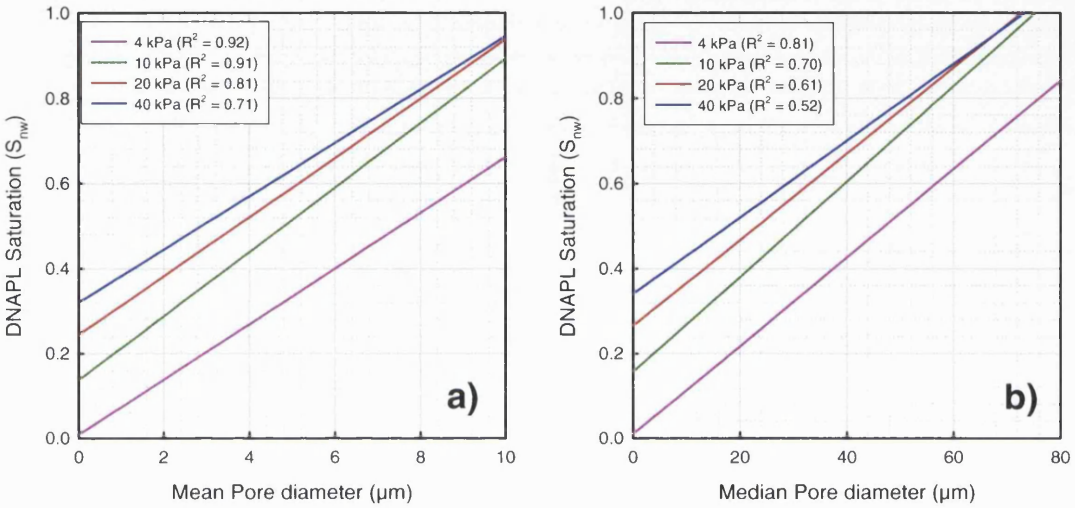

Figure 8-14 Best fit curves showing the relationship between a) mean pore diameter and b) median pore diameter and the degree of DNAPL saturation at a range of pressures. (Example data are shown in Figure 8.13 for 4 kPa)

8.5.2 Generic Pressure Saturation Curves for Permo-Triassic Sandstone

Capillary pressure saturation curves are of considerable value for assessing the likely implications for the contamination of groundwater by a DNAPL. For example the shape of the curve indicates the likely rate of DNAPL intrusion, so a steeper curve will allow more DNAPL to penetrate at a lower pressure. Obtaining capillary pressure curves can be time consuming and for consolidated media requires specialised equipment developed in Chapter 5.

By using the same approach as in 8.5.1 and solving the $P_c(S_w)$ for S_w, using the van Genuchten equation, it is possible to determine the amount of DNAPL saturation for each sample at any given pressure and plot this pressure against the pore diameter of that sample (since obviously DNAPL saturation and pressure are related by the $P_c(S_w)$ curve). Table 8.1 shows the linear regression parameters determined for DNAPL saturation cross plotted against the mean pore diameter. Mean pore diameter rather than median pore diameter provided the best fit to the data as demonstrated by the correlation coefficients in Figure 8.14a and Figure 8.14b. By using these constants it is possible to

generate a $P_c(S_w)$ curve, based on mean pore size (i.e. a knowledge of the sample porosity and permeability), for a PCE-water-sandstone system. The procedure for

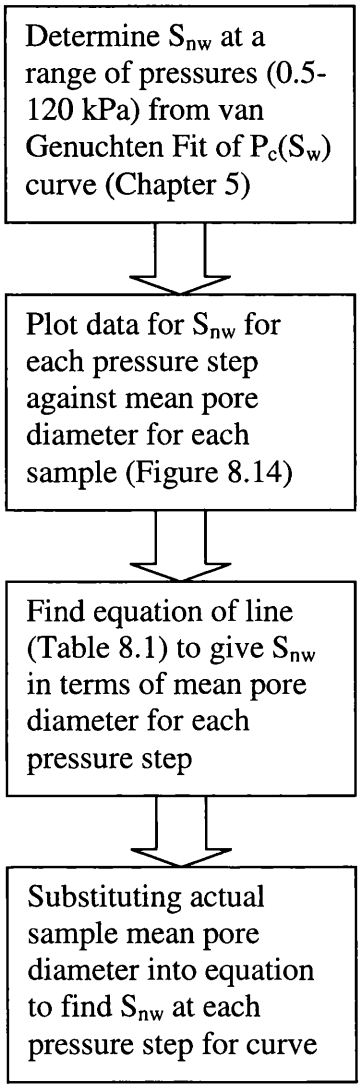

generating the generic curves is summarised in Figure 8.15.

Figure 8-15 Procedure for generating generic pressure saturation curves for PCE in Permo-Triassic sandstones based on a knowledge of sample porosity and permeability.

Four examples showing how the derived variables fit the data from Chapter 5 are shown in Figure 8.16. A range of mean pore sizes have been used to demonstrate the applicability of this approach, an approach that can be used to predict entry pressure and wetting fluid saturation based only on a knowledge of sample porosity and permeability.

Table 8-1 Regression constants determined ($S_{nw}=x<PS>+ C$). 1 kPa is equivalent to roughly 6.4 cm of PCE.

Capillary Pressure (kPa)	*x*	C	R^2
0.5	0.0023	0.0018	0.329
1	0.0012	-0.0046	0.556
2	0.0367	-0.0165	0.763
4	0.0937	0.0078	0.916
6	0.0739	0.0554	0.939
8	0.0761	0.1000	0.930
10	0.0756	0.1371	0.912
15	0.0728	0.2024	0.861
20	0.0694	0.2435	0.816
30	0.0654	0.2919	0.751
40	0.0626	0.3198	0.706
50	0.0604	0.3381	0.674
60	0.0592	0.3512	0.649
70	0.0581	0.3610	0.629
80	0.0570	0.3686	0.614
90	0.0564	0.3748	0.600
100	0.0559	0.3799	0.589
120	0.0547	0.3879	0.571

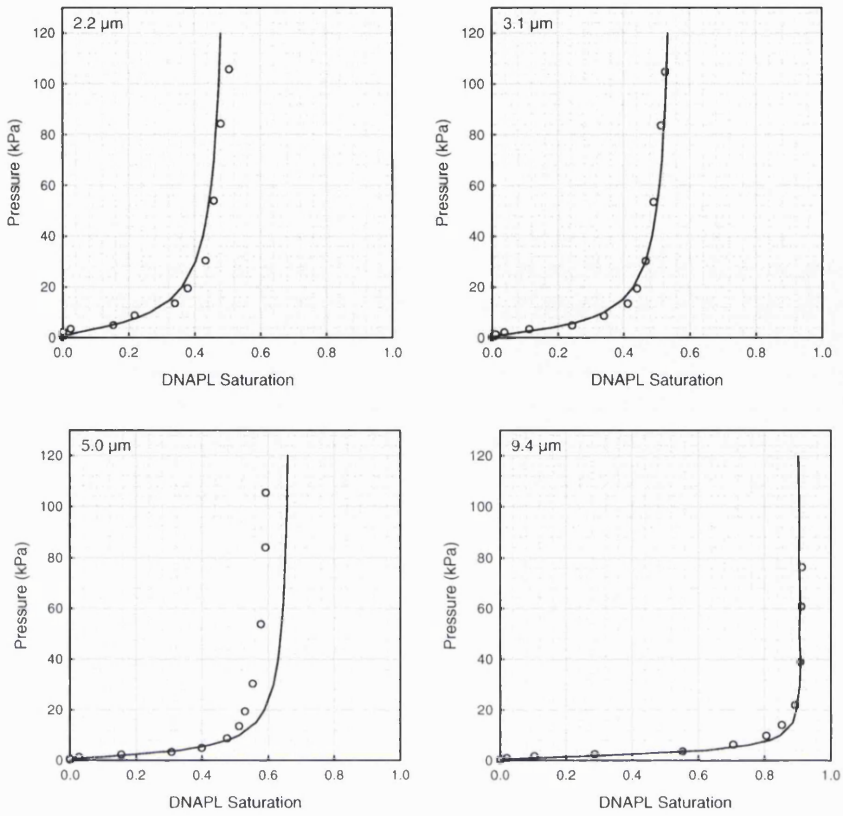

Figure 8-16 Examples of generic constants applied to four samples with mean pore sizes of 2.2 µm, 3.1 µm, 5.0 µm and 9.4 µm. The centrifuge data is represented by the open cycles and the fitted data, derived from the relationship between entry pressure and mean pore diameter $2\sqrt{k/\phi}$, is shown by the solid black line.

8.6 IMPLICATIONS FOR AQUIFER CONTAMINATION AND REMEDIATION

8.6.1 Entry and movement in the aquifer

Based on the apparent greater affinity of PCE to sandstones with carbonate cement, combined with the previously observed long term changes in the wetting properties of the rock (Harrold *et al.*, 2001), it would appear that remediation of sites contaminated with PCE may be more problematic than previously thought. This is due to the greater affinity that the DNAPL has for the matrix of the sandstones leading to pockets of residual saturation occurring in the more solvent wetting compartments of the rock i.e. where there is a greater amount of carbonates.

It has been established that the PCE tends to reside in the larger pores of the Permo-Triassic sandstones. It has also been suggested that the presence of carbonate minerals in the pores will tend to lower the entry pressure for PCE. Therefore it is important to see if carbonate content of the pores is related to the size of the pores.

Figure 8.17 examines this relationship by once more taking the sum of the extracted calcium and magnesium per unit porosity as a proxy for the carbonate content of the pores and comparing this with mean pore size. The data show a trend of decreasing amounts of carbonate in the pores as the pore size gets larger. This is perhaps not surprising as the pore size will commonly be related to the dissolution of carbonates; where more carbonate has been dissolved then the pore will be larger. Significantly, this suggests the large pores will be less wetting towards PCE and therefore the DNAPL will be harder to remove once it is entrapped.

An additional consideration is the distribution of carbonate minerals as a function of depth. Figure 8.18 shows how the amount of carbonate in the pores varies with depth. Although quite a broad range is displayed, especially for the deeper samples, a sizeable group of the shallow samples show low concentrations of carbonate in the pore space. This dissolution of carbonates in the shallow samples is likely to be due to acid rain. Therefore for these samples, entry pressures are less likely to be suppressed due to the presence of neutrally wetting minerals. This is significant as it is the shallow part of the aquifer which is likely to be at greatest risk from a DNAPL spill. However, by their very nature DNAPLs are able to penetrate deep into the aquifer and for the majority (60%) of samples below 10 m considerably more than 10 mmol per unit porosity of carbonate is present, so these sandstones will be more DNAPL wetting.

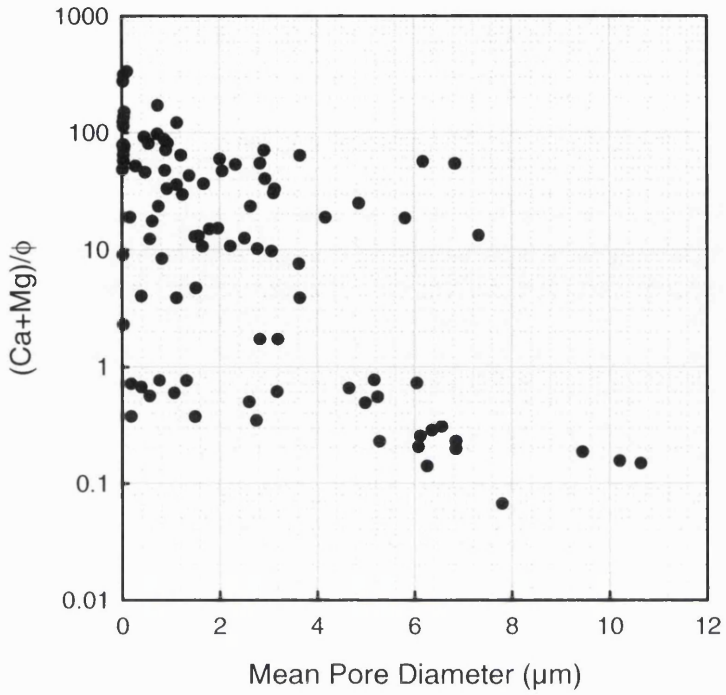

Figure 8-17 Carbonate content per unit porosity as related to the mean pore size for the entire data set.

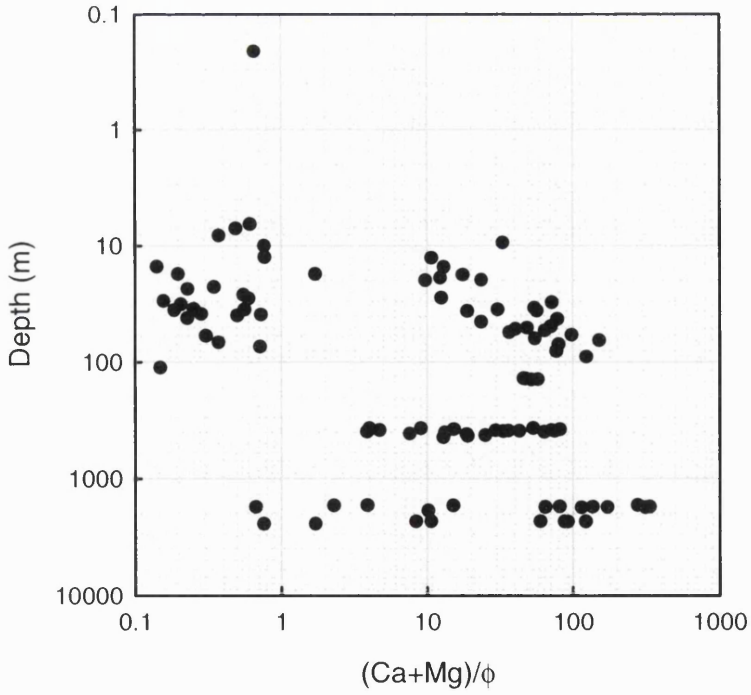

Figure 8-18 The distribution of carbonate in pore space as a function of depth (note log scales).

The observation that PCE entry pressures for Permo-Triassic sandstones are significantly lower than predicted on the basis of capillary theory has implications for

the modelling of PCE migration in the sandstones, and for monitoring and site remediation. A recent study has shown that some fractures in the Permo-Triassic sandstones are sediment filled (Wealthall *et al.* 2001). This coupled with comparatively low fracture frequency in some formations within the sandstone sequence suggests that solvent migration through the matrix of the sandstones may be more important than suggested by previous studies (Steele and Lerner, 2001). The relatively low entry pressures mean that solvents will be able to invade the matrix of the sandstone more readily and that they will be able to penetrate deeper and spread laterally more easily than previously expected. This also means the ratio of solvent saturation relative to porous rock mass will be lower than predicted. When considering the transport and fate of PCE in sandstones, hydrogeologists and modellers should be aware that not only are theoretical values of entry pressure into the matrix of consolidated sandstones probably overestimates, but that 'real world' DNAPLS including 'dirty' PCE is likely to be more wetting than purer PCE, and that in both cases invasion of the matrix of the sandstones is more likely. For example, the lower entry pressures suggested could be important in relation to the industrial usage of PCE as a dry cleaning agent. In this context spill volumes are usually small, however, this study suggests that even relatively small spills (leading to PCE columns of less than 10 cm) may cause invasion into the sandstones, especially if the matrix contains high concentrations of carbonate minerals. Indeed, Slough *et al.* (1999) have shown that the volume of DNAPL entering the rock matrix increases dramatically as the entry pressure of the rock matrix decreases.

8.6.2 Residual Saturation

It is observed that residual saturation of DNAPL results in a significant reduction of the water saturation which in turn significantly reduces the relative permeability (Figures 8.12 and 8.13). Lawrence *et al.* (1991) considered a residual saturation of greater than 20% as the point where groundwater flow through the contaminated part of the aquifer would be considerably reduced, as in effect groundwater would need to 'by-pass' the body of residual. In Chapter 6 the mean residual saturation was 19.7%. As the rate of dissolution of DNAPL is dependant upon the surface area:volume ratio of the DNAPL in contact with flowing groundwater, it is clear that any re-routing of groundwater flow will extend the persistence of the residual saturation in the aquifer.

In a layered sandstone aquifer, residual saturation would be lower in the more uniform sandstone layers (see Figures 8.7 and 8.10) than those with a greater range of

pore sizes primarily due to 'snap-off' in the more complicated pore geometries that occur. During a 'pump and treat' type of remediation, flow would be dominated by the uniform sandstone layer where both the relative permeability and the intrinsic permeability are likely to be greatest. Consequently, the dissolution of DNAPL would be more rapid in the more uniform layer but slower in the less uniform layers. In these less uniform layers dissolution is likely to be principally controlled by diffusion and so would be a very long process.

8.6.3 DNAPL dissolution

Once a DNAPL has penetrated the aquifer it will act as a secondary source of contamination. The rate of dissolution of the DNAPL depends on the shape of the DNAPL pool and the on groundwater velocity at the surface of the pool, both of which are very difficult to predict in Permo-Triassic sandstones.

Although the DNAPL dissolution rate calculated in Chapter 6 was linear with respect to time (assuming a constant flow), this is unlikely to be the case, it is interesting to determine the time scale that this dissolution rate represents if the contaminant was removed by recharge alone. If it is assumed that the dissolution continues at a constant rate (which is very unlikely, as the rate will decrease with time) assuming the dissolution rate given in Equation 6.10 (relating the concentration of PCE to the number of pore volumes of fresh water passed through the core), it would take 10310 minutes to reach 0 mg/L at a flow rate of 2 mL/min (2×10^{-6} m^3/min). In that time the total volume of water passed through the core would be: $2 \times 10^{-6} \times 10310 = 2.1 \times 10^{-2}$ m^3. With an assumed recharge rate in the UK of 500 mm/a (equivalent to 9.5×10^{-7} m/min) applied over the area of the 0.025 m diameter core plug gives

$$9.5\times10^{-7} \times \left(\frac{\pi D^2}{4} \right) = 4.6\times10^{-10} \text{ m}^3/\text{min}$$

To remove 100% of the solvent at this rate would take:

$$\frac{2.1\times10^{-2}}{4.6\times10^{-10}} = 5\times10^{7} \text{ min or 95 years.}$$

8.6.4 Source identification from isotopic composition

As DNAPL contamination of potable groundwater supplies can be extremely expensive to remediate, there is increasing interest in finding the source of the contamination and

enforcing the principal of 'the polluter pays'. Extensive site characterisation can involve costly core drilling and pore water sampling in an attempt to understand the hydrogeology and DNAPL distribution within the aquifer.

Recently Jendrzejewski *et al.* (2001) have proposed using isotope ratios of chlorinated hydrocarbons as a tool for investigating environmental pollution problems. By determining the isotopic $\delta^{13}C$ values of a range of DNAPLs from different manufactures they were able to find distinctive values which characterised the products of the different manufacturers. Therefore, it is considered that a water sample containing dissolved phase PCE could be characterised in terms of its point of manufacture and the likely source thus established.

Harrold *et al.* (2003) and several other authors (e.g. Powers and Tamblin, 1995; Jackson and Dwarakanath 1999) have remarked that there is a considerable degree of interaction between DNAPLs and the porous media they are in contact with. The isotopic measurements made in Chapter 4 revealed a very wide range of values for the $\delta^{13}C$ in the carbonate cements. It is therefore suggested that there could be considerable alteration of the isotopic ratio of the DNAPL due to interaction with the sandstone matrix and that the measured $\delta^{13}C$ ratio in the DNAPL would reflect a mixture of its manufacturing signature and that found in the carbonate cement of the sandstone. The contamination source might thus be wrongly identified.

9 Conclusions

During this laboratory based investigation a large number of parameters have been physically determined or derived so as to understand the controlling factors on DNAPL distribution in the matrix of Permo-Triassic sandstones. Table 9.1 lists these parameters.

Table 9-1 Summary of major parameters used to determine DNAPL penetration of Permo-Triassic Sandstones. vG is an abbreviation for van Genuchten and BC an abbreviation for Brooks-Corey.

Parameter/Symbol	Description	Defined in Section:
P_0	Entry pressure (vG fit for DNAPL)	2.4.3
S_r	Wetting fluid residual (vG fit for DNAPL)	2.4.3
m	Pore size distribution index (vG fit for DNAPL)	2.4.3
P_d	Breakthrough pressure (BC fit for DNAPL)	2.4.3
S_r	Wetting fluid residual (BC fit for DNAPL)	2.4.3
λ	Pore size distribution index (BC fit for DNAPL)	2.4.3
k_{rnw}	Relative permeability to non-wetting phase	2.4.5
k_{rw}	Relative permeability to wetting phase	2.4.5
z	Coordination number	2.5
Sample Location	Geographical location in UK	3.3
Sample Depth	Depth of subsample	3.3
Munsel Colour	Colour classification	3.3
k_g	Gas permeability	4.1
ϕ	Effective porosity	4.2
$2\sqrt{k/\phi}$	Mean pore-throat diameter	4.3
PSD	Pore Size Distribution, also gives Median Pore Diameter	4.4
Ca, Mg, Al ,Si...	Inorganic chemistry parameters determined by 0.43M HNO_3 extraction	4.5
TOC	Total organic carbon	4.5
$\delta^{13}C$, $\delta^{18}O$	Carbon and oxygen isotope content	4.6
S_w	Wetting phase saturation	5.4.1
k_f	Liquid permeability	6.1.1
Δk_f	Change in liquid permeability	6.4.1
R_{sat}	Residual saturation	6.4.1
H_2O PVs	Number of pore volumes for water breakthrough after DNAPL flood	6.4.1
m	Pore size distribution index (vG Fit for MICP)	7.6

When the data is examined it appears that several of these parameters are redundant or serve to corroborate each other whilst some are crucial to understanding

DNAPL behaviour. The following six measurements are considered to be most important although are not structured in any rank order.

1. Gas permeability. From this routine physical properties measurement it is also possible to derive the liquid permeability (see Equation 8.1) and also a reasonable estimate of porosity (Equation 4.6).

2. Porosity. Another routine physical properties laboratory measurement that provides the most basic of characterisation information and needed for calculating the mean pore size.

3. Mean Pore Radius, $\sqrt{k/\phi}$ and mean pore diameter $2\sqrt{k/\phi}$. This parameter, which correlates well with the median pore size from the MICP data (Figure 4.9), has been found to provide most of the best correlations with the DNAPL data produced (e.g. Figure 8.13a and 8.14a). A knowledge of mean pore size means a reasonable estimate of permeability (Equation 8.6) and relative permeability (Equation 8.7), hence also the reduction in permeability (Equation 6.9). Using the regression constants in Table 8.1 will also produce generic $P_c(S_w)$ curves for PCE in a consolidated sandstone system. If parameterisation of these curves is required then the van Genuchten function can be fitted.

4. Surface chemistry, 0.43 M HNO_3 extraction. The carbonates content can have a large effect on DNAPL wetting properties. If the sandstone is water or neutral wetting it will influence the entry of the DNAPL, the degree of spreading and depth of penetration.

5. Pressure saturation curve using centrifuge method along with curve fitted using van Genuchten formula. Although generic parameters have been established for producing $P_c(S_w)$ curves based on the mean pore size, these are only valid for PCE as another DNAPL will behave differently. The function also generates wetting phase (Equation 2.19) and non-wetting phase (Equation 2.20) saturations.

6. Sample depth and geographical location. A knowledge of sample depth and location can be used to find existing data on physical and chemical properties of the strata.

Porosity, permeability and pore-size-distribution measurements have been made on representative samples of Permo-Triassic sandstones. A rapid, centrifuge-based method has been developed to characterise effective PCE entry pressures in the matrix of the Permo-Triassic sandstones of the UK. Another method has been developed and used to measure relative permeability and residual saturation for PCE in a range of Permo-Triassic sandstones. Weak acid extraction and chemical analysis have been used to characterise the surface chemistry of the sandstones and isotopic measurements made on a few selected samples. A pore-scale probabilistic 'percolation' model has been used to try and determine coordination numbers from the pore size distribution measurements and to attempt to find greater insight into sandstone structure.

PCE entry pressure and median pore diameter show a log-linear relationship, however, the observed entry pressures are systematically and significantly lower than those predicted by capillary pressure theory. The difference between observed and predicted PCE entry pressures may be explained either by a lower than predicted value of interfacial tension and/or a larger than predicted contact angle. Based on independent measurements of IFT in similar PCE-sandstone systems, it is unlikely that the disparity between observed and predicted entry pressures is due to low values of IFT. Therefore, a larger than predicted contact angle is probably a more likely explanation for the low observed entry pressures. The best-fit line through the data suggests an effective contact angle of 82°, compared with a literature value of about 40°.

The differences in observed and predicted entry pressures, and the inferred higher contact angles, can be explained to some extent in terms of the surface chemistry of the sandstones although not completely. A plot of calcium and magnesium per unit porosity against the difference between observed and predicted entry pressures, shows a linear relationship. Higher calcium and magnesium contents are associated with lower than expected entry pressures. From this observation it is inferred that the presence of calcite and dolomite cements has a significant effect on the wetting properties of the rock.

Standard conceptual models of microscopic pore structure, e.g. that of a bundle of capillary tubes, are not appropriate for the system studied, and a conceptual model has been developed to describe the pore scale structure of sandstones and the effect of surface chemistry on PCE contact angle. Where a DNAPL is in contact with silica a water-wetting (solvent non-wetting) type contact angle of less than c.70° is assumed.

Where DNAPL is in contact with carbonates, e.g. calcitic or dolomitic material, the contact angle is between 70-110°. Under these circumstances the DNAPL will behave as a neutral or even wetting phase. The cumulative effect of the carbonate cement is to increase the effective, macroscopic, contact angle and so reduce the effective entry pressure.

Using the probabilistic percolation model it has been suggested that considerably larger pores exist than suggested by the bundle of capillary tubes model and that the order of magnitude of these pores may explain the experimentally observed DNAPL entry pressure data. Percolation phenomenon must be active in this system. There is however some degree of uncertainty in the percolation model with widely differing results produced by each of the probability distribution functions used although all suggested the presence of much larger pores.

The thesis has not resolved whether or not the observed entry pressures are as a result of an increase in contact angle caused by surface chemistry or that larger pores are present as suggested by the probabilistic percolation model. As there is good evidence to support both theories it is reasonable to surmise that the observed phenomena occurs as a combination of increased contact angles caused by calcite and dolomite in the pore-linings and the presence of larger pores-throats suggested by the probabilistic percolation model than by the conventional bundle of capillaries model.

By examining the relationships between coordination number produced using the percolation model and the non-wetting phase saturation it was anticipated that in general, larger coordination numbers related to higher non-wetting saturations at the point of percolation. A relationship between the 'type' of MICP curve could be determined with the larger values of z associated with a few dominant pore sizes and lower values associated with low porosity samples with a greater range of pore sizes. The spread of the data suggest, that by either method of computing coordination number, the coordination number is rather insensitive to the percolation point. A far better relationship was observed (Figure 5.9) between the percolation point and the pore size distribution index, m, calculated from the van Genuchten equation for the MICP curves based on the bundle of capillaries model, and it is therefore suggested that it is more important to consider the distribution of pores rather than the average number of connections between them for immiscible displacement processes.

Measurements of residual saturation of DNAPL showed most values are close to 20% (Table 6.4) and a relationship between residual saturation and relative permeability with highest reductions in permeability occurring with the largest residual saturations (Figure 6.8). Measurements identify that relative permeability and the change in permeability caused by a residual saturation of DNAPL can be related to the mean pore size. Calculated curves using the van Genuchten m (Figure 8.11) and Brooks-Corey λ values (Figure 8.12) identified a cut off value close to 40% residual saturation where flow of the wetting phase is no longer continuous.

By finding a good linear relationship between the DNAPL saturation and the mean pore size over a range of pressures, it has been possible to produce generic pressure saturation curves (Figure 8.15) for a PCE-water-sandstone system. These 'synthetic' curves show very good agreement with the data for a range of pore-sizes and if fitted by an algebraic function (such as van Genuchten) can be used to predict entry pressure and wetting fluid saturation based only on a knowledge of sample porosity and permeability.

The observation that PCE entry pressures for Permo-Triassic sandstones are lower than would be predicted on the basis of capillary theory (Figure 8.3) has implications for the modelling of PCE transport in the sandstones, and for monitoring and site remediation. Not only are theoretical values of entry pressure into the matrix of consolidated sandstones probably overestimates, but that 'real world' DNAPLS including 'dirty' PCE is likely to be more wetting than purer PCE, and that in both cases invasion of the matrix of the sandstones is more likely than previously conceptualised. However, many sandstones with larger pores were found to have less calcium and magnesium per unit porosity (Figure 8.16) these samples should have a lower entry pressure than those with smaller pores, the reduction in the amount of carbonates suggests these pores will be less DNAPL wetting. In addition, a number of shallow samples which are more vulnerable to DNAPL contamination, also have lower carbonate content (Figure 8.17) so their DNAPL wettability will be proportionately less. Given the apparent greater affinity of PCE to sandstones with carbonate cement, and possible long-term changes in the wetting properties of PCE-sandstone systems, remediation of sites contaminated with PCE may be more problematic than previously thought due to the distribution of carbonates and increased DNAPL wettability.

9.1 FURTHER WORK

This thesis has focused on one DNAPL, tetrachloroethene. An obvious extension of this work is to investigate the pressure saturation relationships that exist for other DNAPLs, mixtures of DNAPLs and 'field' or 'dirty' DNAPLs based on the method developed in Chapter 5. Recent studies (Dwarakanath and Pope, 2000; Harrold *et al.*, 2001; Harrold *et al.*, 2003) have suggested that additives contained within solvents can both reduce their IFTs and alter the wetting behaviour of the rock material. A systematic study of other DNAPLs would therefore be an important linkage in understanding their fate under environmental conditions.

Investigation into relative permeabilites was not able to progress as rapidly with as broad a range of samples due to the length of time taken in developing the method in Chapter 6. Future work might consider refining the method further so that larger samples could be used which would facilitate the use of more 'field representative' flow values and should reduce the influence of sample heterogeneity. With a more reliable method it would be possible to obtain better dissolution data. Additionally, hysteresis effects could be better investigated by repeated solvent-flood/water flood cycles.

The thesis was unable to provide a single explanation for the observed changes in entry pressure. An SEM study of a range of sandstones would provide valuable data as to the amount and distribution of calcite and dolomite in the matrix of Permo-Triassic sandstones. In addition, the injection of a resin or Wood's metal to provide a visual imprint of the pore structure of the Permo-Triassic sandstone cores may assist in detertmining the presence or absence of the very large pores suggested by the perolation based model described in Chapter 7.

Work on the $\delta^{13}C$ of calcite and dolomite in Chapter 4 showed a range of values were obtained for the different samples. Firstly it would be a worthy extension of this work to characterise the $\delta^{13}C$ of all the samples analysed in this thesis for use in studies to date groundwater using the $\delta^{13}C$ of HCO_3 in the water. Secondly, it would be useful to see what degree of interaction there is between the $\delta^{13}C$ of a DNAPL and the $\delta^{13}C$ contained in the cement material since this may influence the use of the isotopic signature of DNAPLs in source identification.

10 References

Akselrod S M and Putkaradze L A 1994. Determination of current and residual oil saturation in old oilfields. Nuclear Geophysics 8, 3, 281-290.

Al-Aasm I S, Taylor B E and South B 1990. Stable isotope analysis of multiple carbonate samples using selective acid extraction. Chemical Geology 80, 119-125.

Al-Fossail K A, Ali M T H A and Almajed A A 1995. Experimental factors affecting mercury capillary pressure curves. Journal of Colloid and Interface Science 175, 2, 515-517.

Anderson W G 1987a. Wettability Literature Survey-Part 4: Effects of wettability on capillary pressure. Journal of Petroleum Technology 39, 10, 1283-1300.

Anderson W G 1987b. Wettability Literature Survey-Part 5: The effects of wettability on relative permeability. Journal of Petroleum Technology 39, 11, 1453-1468.

Anderson W G 1987c. Wettability Literature Survey-Part 6: The effects of wettability on waterflooding. Journal of Petroleum Technology 39, 12, 1605-1622.

Allen D J, Bloomfield J P, Gibbs B R and Wagstaff S J 1998. Fracturing and the hydrogeology of the Permo-Triassic sandstones in England and Wales. British Geological Survey Technical Report WD/98/1.

Allen D J, Brewerton L J, Coleby L M, Gibbs B R, Lewis M A, Wagstaff S J and Williams A T 1997. The Physical Properties of Major Aquifers in England and Wales. British Geological Survey Technical Report WD/97/34.

Ataie-Ashtiani B, Hassanizadeh S M and Celia M A 2002. Effects of heterogeneities on capillary pressure-saturation-relative permeability relationships. Journal of Contaminant Hydrology 56, 175-192.

Aurand K, Friesel P, Milde G and Neumayr V 1981. Behaviour of organic solvents in the environment. Studies in Environmental Science 12, 481-487.

Aziz CE , Fitch M W, Linquist L K, Pressman J G, Georgiou G and Speitel G E 1995. Methanogenic degradation of trichloroethylene in a hollow-fibre membrane bioreactor. Environmental Science and Technology 29, 10, 2574-2583.

Barbee G C 1994. Fate of chlorinated aliphatic hydrocarbons in the vadose zone and ground water. Ground Water Monitoring and Remediation 14, 1, 129-140.

Barranco F T, Dawson H E, Christener J M and Honeyman B D 1997. Influence of aqueous pH and ionic strength on the wettability of quartz in the presence of dense non-aqueous phase liquids. Environmental Science and Technology 31, 3, 676-681.

Bath A H, Edmunds W M and Andrews J N 1979. In Isotope Hydrology 1978. Volume II, IAEA Vienna.

Berger L M, Pajak A P and Robb Jr A E 1987. Contaminated groundwater: above-ground treatment alternatives. Journal of Hazardous Materials 14, 51-70.

Berkowitz B and Balberg I 1993. Percolation theory and its application to groundwater hydrology. Water Resources Research 29, 4, 775-794.

Bloomfield J P, Gooddy D C, Bright M I, Williams P J 2001. Pore-throat size distributions in sandstones and some implications for contaminant hydrogeology. Hydrogeology Journal 9, 3, 219-230.

Bloomfield J P, Gooddy D C and Williams A T 1997. Laboratory measurements of chlorinated solvent residual saturation in the Helsby and Wilmslow Sandstones. British Geological Survey Technical Report Series WD/97/30C.

Bloomfield J P and Williams A T 1995. An empirical liquid permeability-gas permeability correlation for use in aquifer properties studies. Quarterly Journal of Engineering Geology 28, S143-S150.

Boekhold A E, Temminghoff E J M and Van Der Zee S E A T M 1993. Influence of electrolyte composition and soil pH on Cd sorption by an acid sandy soil. Journal of Soil Science 44, 85-96.

Boukadi FB H, Watson R W and Owolabi O O 1994. The influence of reservoir properties on ultimate oil-recovery in radial-core waterfloods. Journal of Canadian Petroleum Technology 33, 6, 23-34.

Bouwer E J, Riffman B E and McCarty P L 1981. Anaerobic degradation of halogenated 1- and 2-carbon organic compounds. Environmental Science and Technology 15, 5, 596-599.

Bradford S A, Abriola L M and Rathfelder K M 1998. Flow and entrapment of dense nonaqueous phase liquids in physically and chemically heterogeneous aquifer formations. Advances in Water Resources 22, 2, 117-132.

Bradford S A and Leij F J 1995. Fractional wettability effects on two-and three-fluid capillary pressure-saturation relations. Journal of Contaminant Hydrology 20, 89-109.

Bradford S A, Phelan T J and Abriola L M 2000. Dissolution of residual tetrachloroethylene in fractional wettability porous media: correlation development and application. Journal of Contaminant Hydrology 45, 35-61.

Broadbent S K and Hammersley J M 1957. Percolation processes I. Crystals and mazes, Proceedings of the Cambridge Philosophical Society 53, 629-641.

Brooks R H and Corey A T 1966. Properties of porous media affecting fluid flow. Journal of the Drainage and Irrigation Division, American Society of Engineering 92, IR2, 61-88.

Brown R A, Norris R D and Brubaker G R 1985. Aquifer restoration with enhanced bioreclamation. Pollution Engineering, November 17, 25-28.

Brownless M A, Talbot J C, Darling W G and Neal M 1994. Operation of the VG-Optima mass spectrometer, Wallingford Stable Isotope Laboratory. British Geological Survey Technical Report WD/94/52.

Bukhari Z, Smith H V, Sykes N, Humphreys S W, Paton C A, Girdwood R W A and Fricker C R 1997. Occurrence of Cryptosporidium oocysts and Giardia SPP

cysts in sewage effluents from treatment plants in England. Water Science and Technology 35, 385-390.

Burdine N T 1953. Relative permeability calculations from pore-size distribution data. Petroleum Transactions American Institute of Mining and Metallurgy Engineers 198, 71-77.

Burley S D 1984. Patterns of diagenesis in the Sherwood Sandstone Group (Triassic), United Kingdom. Clay Minerals 19, 403-440.

Burston M W, Nazari M M, Bishop P K and Lerner D N 1993. Pollution of groundwater in the Coventry region (UK) by chlorinated hydrocarbon solvents. Journal of Hydrology 149, 137-161.

Busby R D, Lenhard R J and Rolston D E 1995. An investigation of saturation-capillary pressure relations in two- and three-fluid systems for several NAPLS in different porous media. Ground Water 33, 4, 570-578.

Butcher A S 1995. Laboratory characterisation of physical controls involved in Dense Non Aqueous Phase Liquid (DNAPL) transport in the saturated zone of aquifers. MSc Dissertation, University of Reading.

Carmen P C 1941. Capillary rise and capillary movement of moisture in fine sands. Soil Science 52, 1.

Chatzis I and Morrow N R 1984. Correlation of capillary number relationships for sandstone. Society of Petroleum Engineers Journal 24, 5, 555-562

Chatzis I, Morrow N R and Lim H T 1983. Magnitude and detailed structure of residual oil saturation. Society of Petroleum Engineers Journal, 23, 2, 311-326.

Chatzis I and Dullien F A L 1977. Modelling pore structure by 2-d and 3-d networks with applications to sandstones. The Journal of Canadian Petroleum Technology, January-March, 97-108.

Childs E C and Collis-George N 1950. The permeability of porous materials, Proceedings of the Royal Society of London A 201, 392-405.

Darling W G 1999. The analysis of carbon stable isotopes in waters, gases and solids. British Geological Survey Technical Report WD/99/47R.

Dawson H E and Roberts P V 1997. Influence of viscous, gravitational, and capillary forces on DNAPL saturation. Ground Water 35, 2, 261-269.

Day J B W 1986. The occurrence of groundwater in the United Kingdom. In Groundwater: Occurrence, development and protection. Brandon T E (ed). Institution of Water Engineers and Scientists, London, England.

Dean J A 1979. Lange's Handbook Chemistry. New York, McGraw-Hill.

Dekker L W and Ritsema C J 1994. How water moves in a water repellent sandy soil, 1, potential and actual water repellency. Water Resources Research 30, 2507-2519.

Demond A H, Desai F N and Hayes K F 1994. Effect of cationic surfactants on organic liquid-water capillary pressure-saturation relationships. Water Resources Research 30, 2, 333-342.

Donaldson E C, Thomas R D and Lorenz P B 1969. Wettability determination and its effect on recovery efficiency. Society of Petroleum Engineering Journal, March, 13-20.

Driscoll F G 1986. Groundwater and wells, 2nd Edition. Johnson Filtration Systems, St. Paul, Minnesota.

Dullien F A L 1992. Porous Media. Fluid Transport and Pore Structure. Academic, New York.

Dullien F A L 1975. Effects of pore structure on capillary and flow phenomena in sandstones. The Journal of Canadian Petroleum Technology, July-September, 48-55.

Dullien F A L and Dhawan G K 1974. Characterisation of pore structure by a combination of quantitative photomicrography and mercury porosimetry. Journal of Colloid and Interface Science 47, 2, 337-349.

Dwarakanath V and Pope G A 2000. Surfactant phase behaviour with field degreasing solvent. Environmental Science and Technology 34, 22, 4842-4848.

Eastwood P R, Lerner D N, Bishop P K and Burston M W 1991. Identifying land contaminated by chlorinated hydrocarbon solvents. Journal of the Institution of Water and Environmental Management 5, April, 163-171.

Elgaghah S A, Tiab D and Osisanya S O 2001. A new approach for obtaining J-function in clean and shaly reservoir using in situ measurements. Journal of Canadian Petroleum Technology 40, 7, 30-37.

Epstein S, Graf D L and Degens E T 1964. Oxygen isotope studies on the origin of dolomites. In H Craig, S L Miller and G J Wasserburg (Editors), Isotopic and Cosmic Chemistry. North-Holland Publishing Co., Amsterdam, 169-180.

Fatt I 1956a. The network model of porous media I. Capillary characteristics, Petroleum Transactions American Institute of Mining and Metallurgy Engineers 207, 144-159.

Fatt I 1956b. The network model of porous media II. Dynamic properties of a single size tube network, Petroleum Transactions American Institute of Mining and Metallurgy Engineers 207, 160-163.

Fatt I 1956c. The network model of porous media III. Dynamic properties of networks with tube radius distribution. Petroleum Transactions American Institute of Mining and Metallurgy Engineers 207, 164-181.

Ferrand L A and Celia M A 1992. The effect of heterogeneity on the drainage capillary pressure-saturation relation. Water Resources Research 28, 3, 859-870.

Field J A, Sawyer T E, Schroth M H, Humphrey M D and Istok J D 2000. Effect of cation exchange on surfactant-enhanced solubilization of trichloroethene. Journal of Contaminant Hydrology 46, 131-149.

Flathman P E, Jerger D E and Bottomley, L S 1989. Remediation of contaminated groundwater using biological techniques. Ground Water Monitoring Review 9, 1,105-119.

Fountain J C, Waddell-Sheets C, Lagowski A, Taylor C, Frazier D and Byrne M 1995. Enhanced removal of dense nonaqueous phase liquids using surfactants: capabilities and limitations from field trials. American Chemical Society Symposium Series 594, pp 177-190.

Geller J T and Hunt J R 1993. Mass transfer from nonaqueous phase organic liquids in water-saturated porous media. Water Resources Research 29, 4, 833-845.

Gooddy D C and Lawrence A R 1994. Groundwater contamination of the Chalk aquifer by the chlorinated solvents: A review of remediation techniques. British Geological Survey Report SD/94/1.

Gooddy D C, Shand P, Kinniburgh D G and van Riemsdijk W H 1995. Field-based partition coefficients for trace elements in soil solutions. European Journal of Soil Science 46, 265-285.

Gooddy D C, Bloomfield J P and Bright M 1999. Development of a centrifuge method for the rapid determination of solvent pore-entry pressures. British Geological Survey Technical Report WD/99/6.

Gooddy D C, Bloomfield J P, Harrold G and Leharne S A. 2002. Towards a better understanding of tetrachloroethene entry pressure in the matrix of Permo-Triassic sandstones. Journal of Contaminant Hydrology 59, 3-4, 247-265.

Grey D R C, Kinniburgh D G, Barker J A and Bloomfield J P 1995. Groundwater in the UK. A strategic study. Issues and research needs. Groundwater Forum Report FR/GF1. Pub. Foundation for Water Research, Marlow, UK.

Hagoort J 1980. Oil recovery by gravity drainage. Society of Petroleum Engineering Journal 20, 139-150.

Haines W B 1930. Studies in the physical properties of soil 5. The hysteresis effect in capillary properties and the modes of moisture distribution, Journal of Agricultural Science 20, 97-116.

Halden K and Chase H A 1991. Methanotrophs for renovation of polluted aquifers. Chemical Engineering Research and Design 69, A3, 181-183.

Hammecker C and Jeannette D 1994. Modeling the capillary imbibition kinetics in sedimentary-rocks - role of petrographic features. Transport in Porous Media 17, 3, 285-303

Harrold G, Gooddy D C, Lerner D N and Leharne S A 2001. Wettability changes in trichloroethylene contaminated sandstone. Environmental Science and Technology 35, 7, 1504-1510.

Harrold G, Gooddy D C, Reid S, Lerner D N and Leharne S A 2003. Changes in the interfacial tension values for chlorinated solvents following their transport through various UK soil systems. Environmental Science and Technology 37, 9, 1919-1925.

Harvey R W and Garabedian S P 1991. Use of colloid filtration modeling movement of bacteria through a contaminated sandy aquifer. Environmental Science and Technology 25,1, 178-185.

Hassler G L and Brunner E 1945. Measurement of capillary pressures in small core samples. Petroleum Transactions American Institute of Mining and Metallurgy Engineers 160, 114-123.

Hayden N J, Voice T C and Wallace R B 1997. Residual gasoline in unsaturated soil with and without organic matter. Journal of Contaminant Hydrology 25, 271-281.

Hirsch L M and Thompson A H 1994. Size-dependent scaling of capillary invasion including buoyancy and pore size distribution effects. Physical Review E 50, 3, 2069-2086.

Hoffman R N 1963. A technique for the determination of capillary pressure curves using a constantly accelerated centrifuge. Society of Petroleum Engineers Journal 3, 227-235.

Huling S G and Weaver J W 1991. Dense non-aqueous phase liquids. US EPA/540/4-91/002. Robert S Kerr Environmental Research Laboratory, Ada, Oklahoma.

Hunt J, Sitar N and Udel K S 1988. Non aqueous phase liquid transport and clean up. I. Analysis of mechanisms. Water Resources Research 24, 8, 1247-1258.

Hutchins S R, Downs W C, Wilson J T, Smith G B, Kovacs D A, Fine D D, Douglass R H and Hendrix D J 1991. Effect of nitrate addition on biorestoration of fuel-contaminated aquifer: field demonstration. Ground Water 29, 4, 571-580.

Illangasekare T H, Ramsey Jr J L, Jensen K H and Butts M B 1995. Experimental study of movement and distribution of dense organic contaminants in heterogeneous aquifers. Journal of Contaminant Hydrology 20, 1-25.

Ioannidis M A and Chatzis I 1993. A mixed-percolation model of capillary hysteresis and entrapment in mercury porosimetry. Journal of Colloid and Interface Science 161, 278-291.

Jackson R E 1998. The migration, dissolution and fate of chlorinated solvents in the urbanized alluvial valleys of the southwestern USA. Hydrogeology Journal 6, 144-155.

Jackson R E and Dwarakanath V 1999. Chlorinated degreasing solvents: Physical-chemical properties affecting aquifer contamination and remediation. Ground Water Monitoring and Remediation 19, 4, 102-110.

James R A 1995. Application of petrographic image-analysis to the characterisation of fluid-flow pathways in a highly-cemented reservoir - Kane-field, Pennsylvania, USA. Journal of Petroleum Science and Engineering 13, 3-4, 141-154.

Jendrzejewski N, Eggenkamp H G M and Coleman M L 2001. Characterisation of chlorinated hydrocarbons from chlorine and carbon isotopic compositions: scope of application to environmental problems. Applied Geochemistry 16, 9-10, 1021-1031.

Jerauld G R and Salter S J 1990. The effect of pore-structure on hysteresis in relative permeability and capillary pressure: pore-level modelling. Transport in Porous Media 5, 103-151.

Kantzas A, Nikakhtar B, Ruth D and Pow M 1995. Two phase relative permeabilites using the ultracentrifuge. The Journal of Canadian Petroleum Technology 34, 7, 58-63.

Katz A J and Thompson A H 1986. quantitative prediction of permeability in porous rock. Physical Review B-Condensed Matter 34, 8179-8181.

Katz A J and Thompson A H 1987. Prediction of rock electrical-conductivity from mercury. Journal of Geophysical Research-Solid Earth & Planets 92, 599-607.

Keuper B H, Abbot W and Farquhar G 1989. Experimental observations of multiphase flow in heterogeneous porous media. Journal of Contaminant Hydrology 5, 83-95.

Keuper B H, Redman D, Starr R C, Reitsma S and Mah M 1993. A field experiment to study the behaviour of tetrachloroethylene below the water table: spatial distribution of residual and pooled DNAPL. Ground Water 31, 5, 756-766.

Kia S F 1988. Modeling of the retention of organic contaminants in porous media of spherical particles. Water Research 22, 10, 1301-1309.

Kinniburgh D G, Gale I N, Gooddy D C, Darling W G, Marks R J, Gibbs B R, Coleby L M, Bird M J and West J M 1999. Denitrification in the unsaturated zones of the British Chalk and Sherwood Sandstone aquifers. British Geological Survey Technical Report WD/99/2

Kinniburgh D G and Miles D L 1983. Extraction and chemical analysis of interstitial water from soils and rocks. Environmental Science and Technology 17, 6, 362-368.

Klinkenberg L J 1957. Pore size distribution of porous media and displacement experiments with miscible liquids. Petroleum Transactions, AIME 210, 366-369.

Knox R W O B, Burgess W G, Wilson K S and Bath A H 1984. Diagenetic influences on reservoir properties of the Sherwood Sandstone (Triassic) in the Marchwood geothermal borehole, Southampton, UK. Clay Mineralogy 19, 3, 441-456.

Kool J B and Parker J C 1987. Development and evaluation of closed-form expressions for hysteretic soil hydraulic properties. Water Resources Research 23, 1, 105-114.

Kosugi K 1996. Lognormal distribution model for unsaturated soil hydraulic properties. Water Resources Research 32, 9, 2697-2703.

Kruyer S 1958. Transactions of the Faraday Society 54, 1758.

Lake L W 1989. Enhanced Oil Recovery. Englewood Cliffs, New Jersey: Prentice Hall.

Lanzarone N A and McCarty P L 1990. Column studies on methanotrophic degradation of trichloroethene and 1,2-dichloroethane. Ground Water 28, 6, 910-919.

Larson R G and Davis H T 1982 Conducting backbone in percolating Bethe lattices. Journal of Physics C: Solid State Physics 15, 2327-2331

Larson R G, Scriven L E and Davis H T 1981a. Percolation theory of two phase flow in porous media. Chemical Engineering Science 36, 57-73.

Larson R G, Davis H T and Scriven L E 1981b. Displacement of residual nonwetting fluid from porous media. Chemical Engineering Science 36, 75-85.

Larson R G and Morrow N R 1981. Effects of sample size on capillary pressures in porous media. Powder Technology 30, 123-138.

Lawrence A R, Barker J A, Bird M J, Gooddy D C, Marks R J and Stuart M 1992. Review of groundwater pollution of the Triassic Sandstone aquifer by the halogenated solvents. NRA R&D Note 47, Bristol, UK, 71pp.

Lawrence A R and Foster S S D 1991. The legacy of aquifer pollution by industrial chemicals: technical appraisal and policy implications. Quarterly Journal of Engineering Geology 24, 231-239.

Lenhard R J 1992. Measurement and modelling of three-phase saturation-pressure hysteresis. Journal of Contaminant Hydrology 9, 243-269.

Lenhard R J and Oostrom M 1998. A parametric model for predicting relative permeability-saturation-capillary pressure relationships of oil-water systems in porous media with mixed wettability. Transport in Porous Media 31, 1, 109-131.

Lenhard R J, Parker J C and Mishra S 1989. On the correspondence between Brooks-Corey and van Genuchten models. Journal of Irrigation and Drainage Engineering 115, 4, 744-751.

Lerner D N, Gosk E, Bourg A C M, Bishop P K, Burston M W, Mouvet C, Degranges P and Jakobsen R 1993. Postscript: summary of the Coventry groundwater investigation and implications for the future. Journal of Hydrology 149, 257-272.

Leverett M C 1938. Flow of oil-water mixtures through unconsolidated sands. Petroleum Transactions American Institute of Mining and Metallurgy Engineers 132, 149-171.

Lindquist W B, Venkatarangan A, Dunsmuir J and Wong TF 2000. Pore and throat size distributions measured from synchrotron X-ray tomographic images of Fontainebleau sandstones. Journal Of Geophysical Research-Solid Earth 105 (B9), 21509-21527.

Lovelock P E R 1977. Aquifer properties of the Permo-Triassic sandstones of the United Kingdom. Bulletin of the Geological Survey of Great Britain No. 56, 50pp.

Mackay D M and Cherry JA 1989. Groundwater contamination - pump-and-treat remediation. 2. Environmental Science and Technology 23, 6, 630-636.

Marx J W 1956. Determining gravity drainage characteristics on the centrifuge. Transactions of the American Institute for Mining and Metallurgical Engineers 207, 88-91.

Matthess G and Pekdeger A 1981. Concepts of a survival and transport model of pathogenic bacteria and viruses in groundwater. Science of the Total Environment 21, 149-159.

Meiri D, Ghiasi M, Patterson R J, Ramanujam N and Tyson M P 1990. Extraction of TCE-contaminated groundwater by subsurface drains and a pumping well. Ground Water 28, 1, 17-24.

Meng B. 1994. Pore structure and moisture transport in sandstones - determination of relevant microstructural properties. Studies In Surface Science and Catalysis 87, 771- 780.

Mercer J W and Cohen R M 1990. A review of immiscible fluids in the sub-surface: properties, models, characterization and remediation. Journal of Contaminant Hydrology 6, 107-163.

Milde G, Nerger M and Merger R 1988. Biological degradation of volatile chlorinated hydrocarbons in groundwater. Water Science and Technology 20, 3, 67-73.

Miller C T, Poirier-McNeill M M and Mayer A S 1990. Dissolution of trapped nonaqeous phase liquids: mass transfer characteristics. Water Resources Research 26, 2783-2796.

Monkhouse R A and Richards H J 1982. Groundwater resources of the United Kingdom. Commission of the European Communities. Th. Schafer Druckerei GmbH, Hannover.

Morel-Seytoux H J, Meyer P D, Nachabe M, Touma J, Van Genuchten, M Th, and Lenhard R J 1996. Parameter equivalence for the Brooks-Corey and Van Genuchten soil characteristics: Preserving the effective capillary drive. Water Resources Research 32, 5, 1251-1258.

Morrow N R 1976. Capillary pressure correlations for uniformly wetted porous media. The Journal of Canadian Petroleum Technology, 15, 4, 49-69.

Morrow N R, Chatzis I and Lim H 1985. Relative permeabilities at reduced residual saturations. Journal of Canadian Petroleum Technology 24, 4, 62-69.

Moss P D and Edmunds W M 1992. Trace-metals in interstitial waters from sandstones - acidic inputs to shallow groundwater. Environmental Pollution 77, 2-3, 129-141.

Mualem Y 1976. A new model for predicting the hydraulic conductivity of unsaturated porous media. Water Resources Research 12, 513-522.

Nelson M J K, Montgomery S O and Pritchard P H 1988. Trichloroethylene metabolism by microorganisms that degrade aromatic compounds. Applied and Environmental Microbiology 54, 2, 604-606.

Netto A S T 1993. Pore-size distribution in sandstones. The American Association of Petroleum Geologists Bulletin 77, 6, 1101-1104.

Nikakhtar B, Kantzas A, De Wit P, Pow M and George A 1996. On the characterising of rock/fluid and fluid/fluid interactions in carbonate rocks using the ultracentrifuge. The Journal of Canadian Petroleum Technology 35, 1, 47-56.

O'Brian R P and Stenzol M H 1984. Combining granular activated carbon and air stripping. Public Works 115, 12, 54-58.

Orth W S and Gillham R W 1996. Dechlorination of trichloroethene in aqueous solution using Fe-O. Environmental Science and Technology 30, 1, 66-71.

O'Hannesin S F and Gillham R W 1998. Long-term performance of an in situ 'iron wall' for remediation of VOCs. Ground Water 36, 1, 164-170.

Osoba J S, Richardson J G, Kerver J K, Hafford J A and Blair P M 1951. Laboratory measurements of relative permeability. Petroleum Transactions, AIME 192, 47-56.

Pankow J F and Cherry J A 1996. Dense chlorinated solvents and other DNAPLs in groundwater. Waterloo Press, Waterloo.

Pantazidou M, Abu-Hassanein Z S and Riemer M F 2000. Centrifuge study of DNAPL transport in granular media. Journal of Geotechnical and Geoenvironmental Engineering 126, 2, 105-115.

Parker J C , Lenhard R J and Kuppansamy 1987. A parametric model for constitutive properties governing multiphase flow in porous media. Water Resources Research 23, 4, 618-624.

Pennell K D, Pope G A and Abriola L M 1996. Influence of viscous and buoyancy forces on the mobilization of residual tetrachloroethylene during surfactant flushing. Environmental Science and Technology 30, 4, 1328-1335.

Pettijohn F J, Potter P E and Siever R 1972. Sand and Sandstones. Springer-Verlag, Berlin, 618pp.

Powell K L, Taylor R G, Cronin A A, Barrett M H, Pedley S, Sellwood J, Trowsdale S A and Lerner D N 2003. Microbial contamination of two urban sandstone aquifers in the UK. Water Research 37, 2, 339-352.

Powers S E and Tamblin M E 1995. Wettability of porous media after exposure to synthetic gasolines. Journal of Contaminant Hydrology 19, 105-125.

Price M 1990. Hydrogeology: Session chairman's summary. In Chalk: Proceedings of the International Chalk Symposium, Brighton 1989, 552-552, London, Thomas Telford.

Price M, Morris B L and Robertson A S 1992. A study of intergranular and fissure permeability in Chalk and Permian aquifers, using double-packer injection testing. Journal of Hydrology 54, 401-423.

Reitsma S and Kueper B H 1994. Laboratory measurement of capillary pressure-saturation relationships in a rock fracture. Water Resources Research 30, 4, 865-878.

Renault P. 1991. The effect of spatially correlated blocking-up of some bonds or nodes of a network on the percolation threshold. Transport in Porous Media 6, 451-468.

Ridgway k and Tarbuck K J 1967. The random packing of speres. British Journal of Chemical Engineering 12, 3, 384-388.

Rivett M O, Feenstra S and Cherry J A 2001. A controlled field experiment on groundwater contamination by a multicomponent DNAPL: creastion of the emplaced-source and overview of dissolved plume development. Journal of Contaminant Hydrology 49, 111-149.

Rivett M O, Lerner, D N, Lloyd J W 1990. Chlorinated solvents in UK Aquifers. Journal of the Institution of Water and Environmental Management 4, 242-250.

Roberts P V, Hopkins G D, Mackay D M and Semprini L 1990. A field evaluation of in-situ biodegradation of chlorinated ethenes: Part 1, methodology and field site characterization. Ground Water 28, 4, 591-604.

Ruth D and Wong S 1990. Centrifuge capillary pressure curves. The Journal of Canadian Petroleum Technology 29, 3, 67-72.

Sahimi M 1995. Flow and transport in porous media and fractured rock. VCH Verlagsgesellschaft mbH, Weinheim, Germany.

Samaroo B H and Guerrero E T 1981. The effect of temperature on drainage capillary pressure in rocks using a modified centrifuge. SPE Paper 10153, Annual Fall Technical Conference of the Society of Petroleum Engineers AIME, 56th.

Schwille F 1988. Dense chlorinated solvents in porous and fractured media. Lewis Publishers, Boca Raton, Florida.

Semprini L, Roberts P V, Hopkins G D and McCarty P L 1990. A field evaluation of in-situ biodegradation of chlorinated ethenes: Part 2, results of biostimulation and biotransformation experiments. Ground Water 28, 5, 715-727.

Shante V K S and Kirkpatrick S 1971. An introduction to percolation theory. Advances in Physics 42, 325-357.

Sigmund P M and McCaffery F G 1979. An improved unsteady-state procedure for determining the relative permeability characteristics of heterogeneous porous media. Society of Petroleum Engineers Journal, February, 15-28.

SITE 1989. The Superfund innovative technology evaluation program: technology profiles. EPA/540/5-89/013.

Slobod RL and Chambers A 1951. Use of centrifuge for determining connate water, residual water, and capillary pressure curves of small core samples. Transactions American Institute of Mining Engineering 192, 127-134.

Slough K J, Sudicky E A and Forsyth P A 1999. Importance of rock matrix entry pressure on DNAPL migration in fractured geologic materials. Ground Water 37, 2, 237-244.

Spearing M and Matthews G P 1991. Modelling characteristic properties of sandstones. Transport in Porous Media 6, 71-90.

Speital G E and Closmann F B 1991. Chlorinated solvent biodegradation by methanotrophs in unsaturated soils. Journal of Environmental Engineering 117, 5, 541-548.

Standberg G W, Donaldson T L and Farr L L 1989. Degradation of trichloroethylene and trans-1.2-dichloroethylene by a methanotropic consortium in a fixed-film, packed bed bioreactor. Environmental Science and Technology 23, 11, 1422-1425.

Stankovich J M and Lockington D A 1995. Brooks-Corey and van Genuchten soil-water-retention models. Journal of Irrigation and Drainage Engineering 121, 1, 1-7.

Steele A and Lerner D N 2001. Predictive modelling of NAPL injection tests in variable aperture spatially correlated fractures. Journal of Contaminant Hydrology 49, 287-310.

Strong G E 1993. Diagenesis of the Triassic Sherwood Sandstone group of rocks, Preston, Lancashire, UK: a possible evaporitic cement precursor to secondary porosity? In: North, C.P., Prosser, D.J. (eds) Characterisation of fluvial and aeolian reservoirs. Geological Society of London, Special Publication 73, 279-289.

Strong G E and Milodowski A E 1987. Aspects of diagenesis of the Sherwood Sandstones of the Wessex Basin and their influence on reservoir characteristics. In: Marshall, D.J. (ed) Diagenesis of sedimentary sequences. Geological Society of London, Special Publication 36, 325-337.

Szabo M T 1970. New methods for measuring the imbibition capillary pressure and electrical resistivity curves by centrifuge. SPE Paper 3038, Annual Fall Technical Conference of the Society of Petroleum Engineers AIME, 45th.

Taylor S C, Hall C, Hoff W D and Wilson M A 2000. Partial wetting in capillary liquid absorption by limestones. Journal of Colloid and Interface Science 224, 351-357.

TeKrony M C and Ahlert R C. Residual saturation of packed columns with chlorinated solvents. Journal of Hazardous Materials 60, 127-142.

Thakur S, Schenewerk P, Wolcott J and Groves Jr. F 1995. Flow characteristics of DNAPLs in sand packs: water-influx displacement. Journal of Environmental Science and Health Part A 30, 5, 1105-1118.

Thomas J M and Ward C H 1989. In situ biorestoration of organic contaminants in the subsurface. Environmental Science and Technology 23, 7, 760-766.

Travis C C and Doty C B 1990. Can contaminated aquifers at Superfund sites be remediated? Environmental Science and Technology 21, 8, 727-736.

Tsakiroglou C D and Payatakes A C 1991. Effects of pore-size correlations on mercury porosimetry curves. Journal of Colloid and Interface Science 146, 2, 479-494.

Van Geel P J and Sykes J F 1997. The importance of fluid entrapment, saturation hysteresis and residual saturations on the distribution of a lighter-than-water non-aqueous phase liquid in a variably saturated sand medium. Journal of Contaminant Hydrology 25, 249-270.

van Genuchten M Th. 1980. A closed form equation for predicting the hydraulic conductivity of unsaturated soils. Soil Science Society of America Journal 44, 892-898.

van Spronsen E 1982. Three phase relative permeability measurements using the centrifuge method. SPE/DOE Paper 10688, Joint Symposium on Enhanced Oil Recovery, 3rd.

Vavra C L, Kaldi J G and Sneider R M 1992. Geological applications of capillary pressure: a review. American Association of Petroleum Geologists Bulletin, 76, 840-850.

Vogel T M, Criddle C S and McCarty P L 1987. Transformations of halogenated aliphatic compounds. Environmental Science and Technology 21, 8, 722-736.

Vogel T M and McCarty P L 1985. Biotransformation of tetrachloroethylene to trichloroethylene, dichloroethylene, vinyl chloride, and carbon dioxide under methanogenic conditions. Applied and Environmental Microbiology 49, 5, 1080-1083.

Washburn E W 1921. The dynamics of capillary flow. Physics Review, 17, 273-283.

Walters Jr L J, Claypool G A and Choquette P W 1972. Reaction rates and δO^{18} variation for the carbonate-phosphoric acid preparation method. Geochimica et Cosmochimica Acta 36, 129-140.

Wealthall G P, Steele A, Bloomfield J P, Moss R H and Lerner D N 2001. Sediment filled fractures in the Permo-Triassic sandstones of the Cheshire Basin: observations and implications for pollutant transport. Journal of Contaminant Hydrology 50, 41-51.

Welge H J and Bruce W A 1947. Drilling and Production Practices. American Petroleum Institute, p166.

West C C and Harwell J H 1992. Surfactants and subsurface remediation. Environmental Science and Technology 26, 12, 2324-2330.

White M D and Oostrom M 1998. Modeling surfactant-enhanced nonaqueous-phase liquid remediation of porous media. Soil Science 163, 931-940.

Whitehead R L 1996. Ground water atlas of the United States, Montana, North Dakota, South Dakota, Wyoming. US Geological Survey Report HA 730-I.

Wilkinson D 1984. Percolation model of immiscible displacement in the presence of buoyancy forces. Physical Review A 30, 1, 520-531.

Wilkinson D and Willemsen J F 1983. Invasion percolation: a new form of percolation theory. Journal of Physics A: Mathematical and General 16, 3365-3376.

Wilson J L, Conrad S H, Mason W R, Peplinski W and Hagen E 1990. Laboratory investigation of residual liquid organics. USEPA/600/6-90/004, Robert S. Kerr Environmental Research Laboratory, Ada, Oklahoma, 267 pp.

Wilson J T, Leach L E, Henson M and Jones J N 1986. In-situ biorestoration as a ground water remediation technique. Ground Water Monitoring and Remediation 6, 4, 56-65.

Winslow D N, Cohen M D, Bentz D P, Snyder K A and Garboczi E J 1994. Percolation and pore structure in mortars and concrete. Cement And Concrete Research 24, 1, 25-37.

Wong P 1988. The statistical physics of sedimentary rock. Physics Today, December, 24-32.

Woodwell J C 1989. In-situ removal of VOCs from soil using vapour extraction. Water and Wastewater International. October, 16-19.

Yanuka M, Dullien F A L and Elrick D E 1986. Percolation processes and porous media 1. Geometrical controls and topological model of porous media using a three-dimensional joint pore size distribution. Journal of Colloid and Interface Science 112, 1, 24-41.

APPENDIX 1. Physical Properties Data

Sample number	Porosity	Grain Density (g/cm^3)	Bulk Density (g/cm^3)	Gas Permeability (mD)	Gas Permeability (μm^2)	Median Pore Size (μm)
1524/3v	0.343	2.634	2.074	2320	2.294310	
1524/4v	0.286	2.648	2.177	178	0.175841	
1524/4v2	0.284	2.639	2.174	163	0.160819	
1525/1v	0.317	2.615	2.102			
1525/5v	0.293	2.632	2.153	367	0.362443	19.62
1525/6v	0.329	2.640	2.101	2070	2.039756	33.44
1526/1v	0.325	2.613	2.089	830	0.819269	
1526/4v	0.284	2.651	2.181	500	0.493414	13.12
1526/4v2						12.97
1526/4v2	0.278	2.642	2.186	380	0.374537	
1526/6v	0.281	2.646	2.184	193	0.190765	16.60
1526/6v2	0.292	2.637	2.159	468	0.461570	
1526/8v	0.298	2.645	2.155	1320	1.297844	
1526/10v	0.257	2.658	2.232	36.6	0.036142	
1526/10v2	0.262	2.659	2.225			
1527/1v	0.055	2.705	2.612	0.01	0.000010	0.08
1527/1v2	0.062	2.662	2.558	0.01	0.000008	
1527/2V	0.043	2.658	2.586	0.48	0.000478	24.59
15272v2	0.062	2.663	2.560			
1527/3v	0.247	2.608	2.210	831	0.819926	25.46
1527/3v2	0.237	2.615	2.233	703	0.693455	
1527/4v	0.267	2.622	2.189	140	0.138445	10.06
1527/4v2	0.272	2.622	2.181	222	0.219250	
1527/5v	0.068	2.710	2.593	0.01	0.000012	0.08
1527/5v2	0.071	2.710	2.589	0.01	0.000010	
1527/6v	0.153	2.685	2.428	2.80	0.002762	
1527/6v2	0.160	2.687	2.417	1.35	0.001330	
1527/7v	0.070	2.698	2.580	0.03	0.000031	5.70
1527/7v2	0.076	2.703	2.574	0.03	0.000027	
1527/8v	0.040	2.703	2.635	0.01	0.000009	0.04
1527/8v2	0.041	2.702	2.632	0.01	0.000013	
1528/1v	0.057	2.713	2.615	0.02	0.000018	
1528/1v2	0.049	2.701	2.618	0.005	0.000005	
1528/2v	0.210	2.630	2.287	411	0.405733	7.55
1528/2v2	0.210	2.630	2.287	448	0.442091	
1528/3v	0.037	2.712	2.649	0.15	0.000152	0.92
1528/3v2	0.040	2.702	2.633	0.68	0.000674	
1529/1v	0.248	2.679	2.263	1830	1.808626	29.26
1529/1v2	0.173	2.685	2.393	372	0.367443	
1529/3v	0.228	2.679	2.296	499	0.492572	27.50
1529/3h	0.228	2.678	2.295	1880	1.854246	
1529/3h2	0.234	2.684	2.291	2280	2.250154	
1529/5h	0.211	2.676	2.321	78.9	0.077903	
1529/6v	0.231	2.681	2.293	163.8	0.161660	11.80

Sample number	Porosity	Grain Density (g/cm^3)	Bulk Density (g/cm^3)	Gas Permeability (mD)	Gas Permeability (μm^2)	Median Pore Size (μm)
1529/6v2	0.234	2.683	2.290	163.8	0.161660	
1529/8v				21.4	0.021143	10.37
1529/10v				452	0.446356	
1529/10v2	0.222	2.675	2.303			
1529/12v	0.082	2.695	2.556			
1530/1v				26.0	0.025651	5.35
1530/1v2	0.234	2.681	2.288	23.3	0.023010	
1530/2v				23.7	0.023426	2.87
1530/2v2	0.227	2.683	2.300	18.9	0.018687	
1530/3v	0.269	2.659	2.213	641	0.632735	24.6
1530/8v				2680	2.641881	50.4
1530/8v2	0.245	2.660	2.252	2900	2.858962	
1530/9v	0.266	2.657	2.216			
1530/10v				3100	3.058532	
1530/10v2	0.231	2.648	2.267	2230	2.202921	
1534/2v						5.69
1534/3v	0.181	2.494	2.223			
1534/4v	0.171	2.466	2.215	443	0.436907	
1534/5v	0.265	2.483	2.091	6980	6.888617	40.6
1534/5v2						
1534/6v	0.253	2.473	2.100	5710	5.640339	35.1
1534/7v	0.258	2.527	2.133	1820	1.796843	
1534/10v	0.263	2.549	2.141	2870	2.834223	
1534/10v2				3010	2.975202	
1534/11v	0.190	2.576	2.276	108	0.107064	16.6
1534/11v2				0.02	0.000018	
1534/12v	0.108	2.603	2.429	0.93	0.000920	
1534/13v	0.271	2.599	2.166	7770	7.669436	81.3
1535/1v	0.220	2.571	2.225			
1535/4v	0.204	2.722	2.371	0.03	0.000029	
1535/5v	0.202	2.681	2.341	0.01	0.000012	0.03
1535/9v	0.214	2.736	2.365	0.06	0.000056	
1535/10v	0.211	2.684	2.329	0.14	0.000133	
1535/11v	0.120	2.589	2.399	0.02	0.000024	0.12
1536/1v	0.203	2.605	2.280	140	0.138601	13.0
1536/3v	0.177	2.576	2.297	181	0.179051	12.0
1536/3v2	0.166	2.571	2.310	124	0.122450	
1536/4v	0.190	2.617	2.309	32.4	0.031980	7.54
1536/4h	0.222	3.273	2.768	55.7	0.054949	
1536/5v	0.154	2.586	2.342	29.5	0.029069	
1536/7v	0.122	2.579	2.386	39.6	0.039041	9.58
1536/7h	0.119	2.685	2.484	26.5	0.026194	
1536/8v	0.164	2.624	2.358	8.70	0.008582	
1536/9v	0.211	2.607	2.268	428	0.422070	16.8
1536/9h	0.178	2.591	2.308	371	0.366304	
1536/10v	0.151	2.607	2.365	66.5	0.065671	20.4
1536/10v	0.151	2.607	2.365	66.5	0.065671	22.4
1536/10v2	0.146	2.560	2.333	50.3	0.049626	

Sample number	Porosity	Grain Density (g/cm^3)	Bulk Density (g/cm^3)	Gas Permeability (mD)	Gas Permeability (μm^2)	Median Pore Size (μm)
1536/11v	0.162	2.562	2.310	165	0.162963	
1536/12v	0.164	2.577	2.318	377	0.372029	
1536/12h	0.141	2.644	2.412			
1537/1v	0.145	2.680	2.435	11.2	0.011026	
1537/1h	0.148	2.619	2.380	43.5	0.042967	
1537/2v	0.046	2.590	2.517	0.14	0.000142	26.0
1537/2v2	0.041	2.604	2.538			
1537/3v	0.089	2.655	2.507	0.03	0.000031	0.17
1537/4v	0.211	2.622	2.280	8.20	0.008096	
1537/5v	0.102	2.625	2.458	0.03	0.000031	2.67
1537/5v2	0.031	2.625	2.574	0.03	0.000032	
1537/6v	0.088	2.614	2.472	12.2	0.012015	41.6
1537/7v	0.050	2.664	2.580	0.02	0.000017	1.31
1537/7v2				0.11	0.000113	
1537/9v	0.077	2.666	2.537	0.03	0.000025	
1538/1v	0.143	2.705	2.462	0.02	0.000018	
1538/2v	0.176	2.635	2.347	242	0.238716	16.9
1538/2v2	0.211	2.642	2.295	245	0.241589	
1538/4v	0.211	2.654	2.305	78.9	0.077877	2.86
1538/4v2	0.179	2.679	2.379	40.0	0.039523	
1538/5v	0.270	2.602	2.170	158	0.156076	12.1
1538/6v	0.194	2.652	2.331	40.3	0.039723	
1538/7v	0.235	2.649	2.261	93.0	0.091823	8.16
1538/7h	0.347	4.524	3.302	327	0.323101	
1538/8v	0.222	2.645	2.279	71.5	0.070578	
1538/8h	0.231	2.643	2.264	381	0.376398	
1538/9v	0.241	2.680	2.275	117	0.115300	
1538/10v	0.212	2.687	2.330	7.67	0.007572	
1538/10v2	0.229	2.655	2.276	50.0	0.049311	
1539/1v	0.143	2.628	2.252	5.74	0.005669	22.0
1539/2v	0.226	2.638	2.042	221	0.218387	
1539/3v	0.115	2.667	2.359	0.05	0.000046	0.69
1539/4v	0.151	2.637	2.238	48.0	0.047328	17.0
1539/4v2	0.154	2.634	2.382	118	0.116294	
1539/5v	0.156	2.646	2.234	525	0.517936	27.0
1539/6v	0.233	2.643	2.027	3160	3.116819	29.2
1539/8v	0.190	2.640	2.138	634	0.625278	16.6
1539/8v2	0.189	2.637	2.328	573	0.565397	
1539/9v	0.163	2.645	2.214	1390	1.371208	
1539/10v	0.161	2.646	2.219	965	0.952095	
1539/11v	0.130	2.645	2.302	0.93	0.000918	
1539/13v	0.203	2.640	2.105	116	0.114271	
1539/13h	0.196	2.640	2.122	927	0.914719	
1540/1v	0.176	2.655	2.188	10.2	0.010067	
1540/2v	0.165	2.655	2.216	32.8	0.032404	
1540/3v	0.189	2.644	2.145	203	0.200370	13.7
1540/3h	0.179	2.651	2.176	335	0.331077	
1540/5v	0.136	2.682	2.317	0.04	0.000041	0.64

Sample number	Porosity	Grain Density (g/cm^3)	Bulk Density (g/cm^3)	Gas Permeability (mD)	Gas Permeability (μm^2)	Median Pore Size (μm)
1540/5h	0.247	2.626	1.976	1.60	0.001583	
1540/6v	0.150	2.626	2.232	3.00	0.002962	4.21
1541/1v	0.236	2.597	1.984	35.1	0.034679	12.2
1541/1v2	0.237	2.593	2.216	76.4	0.075430	
1541/2v						16.5
1542/1v	0.210	2.583	2.041	1150	1.138762	34.4
1542/2v	0.231	2.591	1.993	3560	3.512082	47.5
1542/3v	0.200	2.607	2.085	1.77	0.001748	2.55
1542/4v	0.223	2.607	2.027	2210	2.180666	32.1
1542/4v2	0.227	2.609	2.243	2310	2.284606	
1542/5v	0.247	2.598	1.956	2930	2.895829	
1542/5v2	0.251	2.598	2.197	3170	3.124062	
1542/6v	0.226	2.600	2.012	433	0.427851	
1542/6v2	0.331	2.600	2.071	447	0.440731	
1542/7v	0.233	2.603	1.997	2760	2.725335	
1542/8v	0.246	2.596	1.957	1710	1.688725	22.7
1542/8v2	0.243	2.599	2.210	1240	1.226314	
1542/9v	0.224	2.593	2.014	64.8	0.063983	10.9
1542/10v	0.248	2.595	1.952	2320	2.285624	
1542/11v	0.255	2.593	1.933	2410	2.383042	20.9
1542/12v	0.215	2.600	2.042	17.5	0.017315	14.9
1542/13v	0.229	2.606	2.008	2350	2.318528	52.1
1542/14v	0.218	2.604	2.035	2020	1.996401	34.8
1542/15v	0.212	2.601	2.051	364	0.359255	
1542/15v2	0.205	2.585	2.260	192	0.189316	

APPENDIX 2. 0.43 M HNO_3 Extraction Data

	Ca	Mg	Na	P	K	Si	Al	Fe	Mn
	mmol/kg	mmol/kg	mmol/kg	mmol/kg	mmol/kg	mmol/kg	mmol/kg	mmol/kg	mmol/kg
1524/1	14.8	10.0	0.440	3.04	1.25	1.27	3.91	0.68	0.103
1524/2	18.6	8.52	0.832	5.62	1.94	2.36	5.02	2.38	0.949
1524/3	20.0	6.39	0.473	5.72	1.61	1.62	3.74	0.706	0.160
1524/4	200	173	1.22	7.90	3.22	3.93	3.88	0.841	0.571
1525/1	12.0	3.49	0.277	3.25	0.767	0.750	3.19	0.438	0.197
1525/2	312	232	1.68	5.58	1.61	2.31	2.32	0.956	1.04
1525/4	145	108	0.799	4.58	1.52	2.55	2.30	0.626	0.557
1525/5	138	112	0.897	5.75	1.98	3.47	2.82	0.708	0.500
1525/6	183	132	1.48	6.84	2.15	3.10	2.70	0.577	0.636
1526/1	12.3	7.53	0.473	3.27	1.23	1.44	4.05	0.774	0.110
1526/2	13.5	5.03	0.179	2.26	1.06	2.13	3.13	0.739	0.130
1526/4	383	285	1.48	7.53	2.70	3.02	3.49	1.36	1.58
1526/6	208	158	1.32	6.31	2.70	2.94	3.60	0.623	0.901
1526/8	343	219	1.29	5.00	1.94	1.98	2.55	0.772	1.16
1526/10	350	252	1.22	9.92	3.53	4.14	4.05	1.44	1.36
1527/1	1500	8.30	66.6	7.23	8.69	1.51	2.17	0.863	3.80
1527/3	87.9	8.08	26.2	3.34	2.86	2.78	2.00	2.63	0.240
1527/4	405	4.81	51.0	18.5	6.43	2.94	2.30	1.24	1.21
1527/6	13.7	2.00	61.7	4.22	6.10	2.67	2.73	0.596	0.022
1528/2	145	69.7	113	5.80	22.3	2.41	1.85	20.0	0.833
1528/4	228	178	152	4.12	20.5	1.18	1.13	20.5	1.19
1529/1	1220	3.89	1.61	5.37	1.44	1.01	1.70	0.722	3.27
1529/3	920	3.33	1.39	6.86	2.05	1.79	2.74	1.05	3.85
1529/5	1350	4.44	1.52	9.70	2.34	1.47	2.54	0.947	3.97
1529/6	842	3.76	1.55	8.81	2.93	2.21	3.44	1.28	6.91
1529/8	1550	4.63	1.84	0.15	1.53	0.44	0.040	0.017	3.73
1529/10	1210	5.55	1.88	5.59	2.30	1.23	1.41	1.81	7.61
1529/12	1230	8.36	5.04	7.40	8.34	2.86	3.44	1.84	7.00
1530/1	408	2.87	1.42	15.4	5.05	5.34	8.22	2.01	1.02
1530/2	277	2.93	2.95	17.3	4.70	5.69	8.16	2.05	0.938
1530/3	259	2.12	1.09	14.9	3.32	4.03	5.77	1.54	0.730
1530/6	467	2.60	1.91	13.7	3.11	3.23	4.80	1.34	1.07
1530/8	1330	3.73	2.04	4.46	1.65	1.04	1.92	1.02	3.22
1530/9	810	3.12	1.65	7.50	2.95	2.20	3.19	1.03	3.00
1530/10	1300	4.41	1.65	7.90	2.38	1.87	3.10	1.14	2.95
1534/3	565	33.9	1.48	4.07	3.22	6.92	10.4	2.66	4.26
1534/4	28.1	1.24	0.865	0.169	0.767	0.67	1.20	0.109	0.194
1534/5	3.70	0.438	1.26	0.048	0.441	0.81	0.957	0.120	0.152
1534/6	4.15	0.546	1.13	0.051	0.518	0.92	1.11	0.134	0.292
1534/7	5.31	0.583	0.310	0.061	0.786	1.14	1.39	0.073	0.239
1534/10	7.18	0.886	0.212	0.061	0.940	1.31	1.65	0.099	0.199
1534/11	6.21	0.886	0.245	0.073	0.844	1.22	1.58	0.150	0.457
1534/12	6.81	0.938	0.343	0.075	1.09	1.30	1.72	0.066	0.292
1534/13	3.57	0.457	0.473	0.041	0.480	0.71	0.876	0.106	0.160
1535/1	920	661	13.5	6.41	7.81	6.25	0.017	0.017	6.63

	Ca	Mg	Na	P	K	Si	Al	Fe	Mn
	mmol/kg	mmol/kg	mmol/kg	mmol/kg	mmol/kg	mmol/kg	mmol/kg	mmol/kg	mmol/kg
1535/4	857	739	18.4	15.3	7.71	5.80	7.47	0.282	5.47
1535/5	531	451	146	15.9	5.83	7.67	8.46	0.509	4.18
1535/9	953	749	296	12.1	11.8	6.73	6.38	0.786	5.45
1535/10	919	710	240	14.1	10.7	5.21	6.22	0.587	6.03
1535/11	835	642	139	7.68	6.48	5.74	5.35	1.02	3.07
1536/1	165	51.2	76.4	20.9	2.74	2.46	1.55	2.35	1.86
1536/3	882	175	46.1	6.22	2.44	1.26	1.60	8.41	6.95
1536/4	114	45.4	77.4	15.8	3.36	2.30	2.23	3.85	1.69
1536/5	1241	105	30.8	6.78	2.86	1.10	1.49	5.22	6.64
1536/7	992	498	37.3	6.24	2.26	1.05	1.28	21.4	16.7
1536/8	825	678	85.6	0.57	5.47	1.27	0.317	2.83	18.5
1536/9	34.2	1.98	29.0	6.35	1.06	1.43	0.712	0.33	0.042
1536/10	9.17	2.27	40.9	3.43	2.32	1.28	1.35	0.38	0.044
1537/1	1170	8.05	23.4	5.69	27.8	1.15	1.40	1.37	5.50
1537/2	1510	12.5	12.7	0.17	11.8	0.18	0.054	0.020	3.77
1537/3	1200	8.15	72.5	6.58	11.3	2.02	2.41	0.681	1.24
1537/4	13.1	1.02	27.9	4.23	26.5	1.60	1.78	0.434	0.027
1537/5	658	5.68	15.2	10.3	17.5	1.42	1.28	1.02	2.53
1537/6	1490	13.4	5.59	0.010	9.69	0.18	0.064	0.036	8.12
1537/7	1560	7.07	21.7	0.007	11.1	0.21	0.049	0.024	4.73
1537/9	866	13.0	34.0	4.38	6.58	1.79	2.15	2.07	5.18
1538/1	84.8	44.1	18.0	12.4	8.92	9.32	7.80	4.65	0.511
1538/2	667	273	16.8	8.71	3.07	3.02	2.85	6.77	5.50
1538/4	767	688	11.2	<0.005	2.74	1.27	0.598	30.3	9.34
1538/5	83.1	44.1	21.4	10.4	7.65	7.48	6.08	5.95	0.803
1538/6	742	639	17.6	7.30	5.49	3.15	3.69	21.2	11.3
1538/7	404	290	34.3	8.40	5.62	6.06	6.02	15.7	6.03
1538/8	438	362	22.5	9.67	6.06	5.61	5.72	16.1	6.96
1538/9	571	466	26.4	11.4	7.25	7.67	7.97	20.1	4.88
1538/10	456	306	20.8	10.9	6.68	7.13	7.02	15.3	4.16
1539/1	34.1	23.5	26.2	3.69	2.03	1.59	1.30	2.69	0.341
1539/2	185	160	77.4	5.00	3.63	2.67	1.82	9.74	1.97
1539/3	453	409	69.2	4.97	4.55	3.63	3.02	22.8	2.00
1539/4	37.4	21.0	36.9	7.04	5.58	2.65	2.29	2.48	0.448
1539/5	530	462	8.92	3.82	2.97	1.06	1.47	22.3	6.28
1539/6	167	141	35.0	3.66	2.42	1.68	1.32	8.92	2.69
1539/8	80.8	63.3	47.1	2.86	4.01	2.46	2.01	4.43	0.921
1539/9	160	144	12.0	2.00	1.50	0.796	0.631	9.45	2.08
1539/10	218	185	19.2	2.27	2.74	0.977	0.893	10.9	3.02
1539/11	131	114	32.7	2.93	2.80	1.43	1.38	5.94	1.33
1539/13	141	121	37.3	4.74	8.65	2.38	1.83	9.27	1.54
1540/1	452	356	7.98	4.15	3.59	1.97	2.01	28.1	7.44
1540/2	532	255	7.52	3.58	3.66	1.99	2.01	19.7	6.35
1540/3	554	334	6.61	2.95	2.51	1.53	1.52	33.6	7.86
1540/5	599	186	9.38	4.26	5.14	2.81	2.43	16.0	5.93
1540/6	772	8.08	10.0	3.63	4.14	2.53	1.95	3.80	5.47
1541/1	13.2	4.78	27.2	6.24	2.05	3.69	6.38	2.81	0.239
1541/2	97.7	2.99	7.23	12.1	2.69	6.01	5.99	2.31	0.819
1542/1	13.2	0.537	<0.082	6.07	1.07	0.636	33.1	6.71	0.059

	Ca	Mg	Na	P	K	Si	Al	Fe	Mn
	mmol/kg	mmol/kg	mmol/kg	mmol/kg	mmol/kg	mmol/kg	mmol/kg	mmol/kg	mmol/kg
1542/2	1.34	0.210	0.147	1.79	0.518	0.523	9.89	0.471	0.029
1542/3	2.81	4.69	0.832	0.402	3.09	1.36	12.1	0.419	0.229
1542/4	1.95	1.19	0.179	0.073	0.575	0.529	0.776	0.048	0.012
1542/5	2.75	2.13	0.375	0.114	0.652	0.740	0.946	0.270	0.027
1542/6	5.46	2.39	0.408	0.131	1.88	0.729	1.59	0.075	0.164
1542/7	3.72	1.61	0.962	0.092	1.32	0.598	1.05	0.136	0.098
1542/8	7.93	5.62	1.13	0.354	3.22	1.40	2.63	0.113	0.186
1542/9	7.71	5.62	1.19	0.346	3.11	1.40	2.63	0.113	0.179
1542/10	3.07	2.02	0.147	0.119	0.978	0.756	1.23	0.077	0.039
1542/11	4.00	2.45	0.310	0.191	1.04	0.956	1.72	0.200	0.120
1542/12	6.77	5.28	0.538	0.366	2.03	1.51	2.57	0.177	0.154
1542/13	4.36	2.17	0.408	0.179	0.729	0.796	1.28	0.251	0.089
1542/14	10.1	5.74	1.13	0.312	2.42	1.67	3.02	0.232	0.016
1542/15	6.70	3.92	0.506	0.247	1.38	1.15	2.04	0.240	0.036
Max	1560	749	296	20.9	27.8	9.32	33.1	33.6	18.5
Min	1.34	0.210	0.000	0.000	0.441	0.179	0.017	0.017	0.012
Mean	423	128	24.8	5.51	4.50	2.46	3.26	4.59	2.73
Median	213	8.33	6.61	4.97	2.83	1.73	2.26	1.03	1.20

	Li	Be	B	Sc	V	Ti	Cr	Co	Ni
	µmol/kg	µmol/kg	µmol/kg	µmol/kg	µmol/kg	µmol/kg	µmol/kg	µmol/kg	µmol/kg
1524/1	5.99	21.2	71.7	3.10	1.47	1.25	0.301	0.974	2.68
1524/2	9.58	20.2	76.9	6.11	2.36	1.88	2.12	5.96	7.41
1524/3	6.29	23.8	73.9	5.77	1.62	0.939	0.278	1.53	3.96
1524/4	9.35	20.6	111	8.96	3.09	<0.313	0.743	4.25	3.07
1525/1	2.64	15.5	67.1	7.86	0.59	0.939	0.246	1.20	2.94
1525/2	8.03	9.79	93.9	10.0	1.47	<0.313	1.60	5.43	3.07
1525/4	6.03	10.3	78.2	6.54	1.47	<0.313	0.767	3.44	1.28
1525/5	6.79	14.5	83.3	6.01	1.62	<0.313	0.554	3.60	1.53
1525/6	7.65	11.5	96.7	8.89	1.77	<0.313	0.861	4.33	1.53
1526/1	8.28	24.4	75.3	3.14	1.62	1.25	0.350	1.11	3.07
1526/2	8.15	26.2	67.2	4.70	1.91	1.10	0.648	1.79	2.43
1526/4	8.26	16.1	80.3	11.5	3.09	<0.313	2.23	8.30	6.52
1526/6	8.20	13.1	67.8	7.41	3.09	<0.313	1.94	5.56	3.07
1526/8	6.32	14.4	55.5	12.7	2.94	<0.313	2.09	7.83	3.19
1526/10	9.67	21.0	59.0	11.4	4.27	<0.313	2.04	8.33	2.94
1527/1	191	13.3	377	1.60	9.57	<0.313	3.88	14.9	1.41
1527/3	77.9	0.965	115	1.52	3.09	9.39	208	19.3	4.98
1527/4	63.1	2.59	133	15.2	10.9	12.2	46.9	4.67	1.79
1527/6	175	8.10	284	1.27	5.59	4.70	7.62	3.35	2.04
1528/2	114	4.24	687	13.6	18.0	<0.313	2.85	21.6	1.53
1528/4	178	3.61	727	16.6	11.6	<0.313	1.48	4.73	1.53
1529/1	95.0	5.85	44.8	18.9	5.89	<0.313	1.11	23.6	4.60
1529/3	9.66	4.65	22.7	21.0	8.10	<0.313	0.776	10.7	4.85
1529/5	3.77	4.64	11.4	30.9	6.48	<0.313	1.53	33.2	10.3
1529/6	1.92	6.60	23.3	25.0	10.5	<0.313	0.648	8.10	5.62
1529/8	2.26	<0.027	408	0.500	0.589	<0.313	0.242	45.2	5.88
1529/10	4.15	3.26	392	20.4	11.9	<0.313	1.02	7.64	10.6
1529/12	16.7	10.5	423	19.0	19.6	<0.313	1.92	9.32	10.5
1530/1	44.9	27.5	448	15.2	13.3	3.91	1.05	20.1	6.90
1530/2	59.8	34.0	492	11.3	14.7	5.79	1.24	19.1	6.77
1530/3	42.6	17.7	476	11.2	11.6	2.97	0.970	10.9	5.88
1530/6	27.4	16.6	458	10.3	11.9	<0.313	0.979	18.9	5.49
1530/8	16.7	5.70	424	11.9	4.42	<0.313	1.53	39.9	8.69
1530/9	15.4	10.3	425	21.0	7.66	<0.313	0.953	14.0	12.4
1530/10	15.8	7.40	398	15.1	7.51	<0.313	1.28	24.9	10.1
1534/3	26.3	11.2	450	9.01	26.6	5.64	3.66	27.7	6.39
1534/4	0.890	11.5	32.8	0.784	1.03	1.10	0.929	0.877	<1.02
1534/5	0.681	5.56	37.3	4.42	1.03	3.13	0.561	59.4	4.85
1534/6	0.973	8.26	31.0	5.05	1.03	3.29	0.175	4.49	2.94
1534/7	0.764	11.7	27.8	1.17	0.883	2.19	0.163	26.1	3.96
1534/10	0.949	10.8	461	9.81	1.47	2.97	0.340	278	2.81
1534/11	1.97	9.39	32.0	10.1	1.03	2.82	0.161	44.6	3.58
1534/12	1.73	8.87	26.8	11.2	0.589	1.10	0.197	1.11	2.17
1534/13	0.404	5.23	27.5	6.14	1.03	4.23	0.221	41.9	2.17
1535/1	36.8	<0.027	460	0.367	0.442	<0.313	0.222	7.23	1.53
1535/4	32.2	2.39	479	0.968	17.5	<0.313	1.32	4.73	1.79
1535/5	51.5	3.52	1100	8.07	23.3	<0.313	1.31	4.39	1.28
1535/9	76.5	3.24	678	2.32	30.9	<0.313	1.76	3.58	1.53

	Li	Be	B	Sc	V	Ti	Cr	Co	Ni
	µmol/kg	µmol/kg	µmol/kg	µmol/kg	µmol/kg	µmol/kg	µmol/kg	µmol/kg	µmol/kg
1535/10	91.8	3.68	833	7.21	47.3	<0.313	3.35	4.37	1.53
1535/11	67.2	2.04	582	9.79	34.0	5.79	1.79	3.10	1.53
1536/1	8.26	7.68	482	13.3	11.6	31.5	15.4	5.96	2.30
1536/3	28.3	2.78	407	15.1	39.5	<0.313	14.0	15.3	4.60
1536/4	13.8	8.32	67.4	17.0	11.5	15.2	14.2	8.94	3.07
1536/5	31.8	5.43	394	29.4	14.9	<0.313	9.10	11.4	3.07
1536/7	22.5	5.23	855	54.1	76.4	<0.313	5.37	34.5	13.8
1536/8	20.5	2.34	899	0.417	<0.294	<0.313	1.16	43.3	20.7
1536/9	8.22	3.68	68.5	0.951	5.59	7.05	26.9	11.3	<1.02
1536/10	11.1	8.86	276	1.00	10.7	8.46	8.72	3.04	1.79
1537/1	24.4	3.37	403	11.2	3.24	<0.313	4.05	1.96	1.15
1537/2	22.1	<0.027	384	0.58	0.589	<0.313	0.147	2.15	<1.02
1537/3	95.7	7.83	498	9.61	13.5	<0.313	0.959	2.15	1.15
1537/4	46.2	4.94	563	1.22	6.04	8.14	0.567	5.72	3.19
1537/5	17.4	2.16	410	5.42	1.62	<0.313	0.956	4.05	<1.02
1537/6	8.96	<0.027	383	0.584	<0.294	<0.313	0.153	6.42	<1.02
1537/7	32.1	<0.027	390	0.567	<0.294	<0.313	0.147	1.91	<1.02
1537/9	62.3	7.43	474	6.91	3.98	<0.313	0.825	1.82	1.41
1538/1	27.0	14.0	218	6.81	8.24	5.48	0.578	2.68	6.13
1538/2	15.9	2.59	523	13.2	11.0	<0.313	14.3	10.1	9.84
1538/4	13.1	0.491	404	0.167	<0.294	<0.313	0.324	18.8	7.66
1538/5	20.2	16.9	175	10.0	14.7	5.32	2.00	11.2	8.81
1538/6	16.6	5.14	448	16.8	16.0	<0.313	2.67	22.1	7.66
1538/7	27.2	5.58	509	18.0	18.4	6.58	9.92	16.9	7.92
1538/8	27.0	4.69	519	20.0	17.5	<0.313	7.15	12.3	5.75
1538/9	37.8	6.69	519	50.7	76.7	2.82	9.56	14.4	7.41
1538/10	32.6	6.47	507	37.0	70.4	5.17	17.3	11.8	6.26
1539/1	2.19	4.16	55.2	2.87	3.68	0.626	2.17	63.8	3.07
1539/2	9.30	8.40	474	9.31	10.6	2.82	7.78	61.2	2.68
1539/3	18.2	19.7	440	21.9	15.3	<0.313	5.00	13.4	6.00
1539/4	5.53	4.05	69.1	4.77	4.71	5.95	2.21	18.7	1.66
1539/5	14.1	5.12	426	8.66	25.2	<0.313	8.23	21.6	8.05
1539/6	5.61	4.84	481	9.16	8.83	6.58	3.41	148	4.47
1539/8	7.69	8.12	80.8	6.69	5.59	4.07	2.56	18.2	1.92
1539/9	2.73	2.54	450	4.69	7.66	1.72	1.29	65.3	2.68
1539/10	6.23	3.27	453	11.9	12.7	1.41	4.26	30.8	4.85
1539/11	10.6	5.84	74.0	8.32	6.92	3.44	8.41	6.44	1.79
1539/13	13.9	12.7	98.9	12.9	8.54	5.64	17.1	48.0	3.32
1540/1	19.7	15.1	1460	12.2	24.0	<0.313	8.25	13.2	9.84
1540/2	13.1	14.8	1270	10.9	20.6	<0.313	5.60	14.2	11.0
1540/3	19.1	12.6	1200	11.9	27.5	<0.313	8.75	27.1	14.7
1540/5	19.9	33.9	1610	19.5	17.5	<0.313	8.01	10.8	18.0
1540/6	7.47	19.0	877	13.1	19.7	<0.313	2.10	8.51	23.0
1541/1	2.60	22.6	76.2	5.27	11.0	5.95	0.572	3.80	3.19
1541/2	12.3	23.8	48.3	6.24	11.8	3.29	0.737	4.88	8.30
1542/1	0.788	<0.027	468	0.367	5.01	153	4.49	0.829	<1.02
1542/2	0.281	0.740	492	0.534	25.8	129	7.77	0.363	1.66
1542/3	4.82	15.2	469	7.64	3.24	6.26	1.96	2.42	6.77
1542/4	<0.038	2.15	49.5	2.90	1.33	0.470	0.174	61.6	30.4

	Li	Be	B	Sc	V	Ti	Cr	Co	Ni
	µmol/kg	µmol/kg	µmol/kg	µmol/kg	µmol/kg	µmol/kg	µmol/kg	µmol/kg	µmol/kg
1542/5	0.488	4.16	43.9	3.60	2.21	0.626	0.212	1.77	<1.02
1542/6	0.802	6.80	39.5	4.34	1.47	0.939	0.085	4.52	4.09
1542/7	0.369	5.11	38.4	3.49	1.33	0.626	0.157	0.912	1.79
1542/8	0.435	9.03	34.8	8.32	2.80	0.626	0.208	1.41	5.11
1542/9	0.577	17.5	45.8	8.29	2.65	0.626	0.246	0.843	4.85
1542/10	<0.038	6.57	32.1	3.94	1.47	1.10	0.154	2.24	2.43
1542/11	<0.038	11.0	34.6	4.85	2.06	0.783	0.075	5.67	1.28
1542/12	0.222	24.8	39.0	8.31	1.62	0.626	0.203	3.48	4.47
1542/13	0.368	7.65	32.9	5.02	1.91	0.783	0.169	3.07	1.28
1542/14	3.63	16.7	35.2	9.39	5.59	3.13	0.421	0.810	2.30
1542/15	1.98	8.22	34.5	6.07	2.06	2.35	0.235	1.75	1.66
Max	191	34.0	1610	54.1	76.7	153	208	278	30.4
Min	0.000	0.00	11.4	0.17	0.000	0.000	0.075	0.363	0.000
Mean	23.5	9.59	329	9.99	10.6	4.79	5.54	17.4	4.90
Median	10.6	8.11	380	8.32	6.26	3.13	1.30	7.96	3.45

	Cu	Zn	Ga	Ge	As	Rb	Sr	Y	Zr
	µmol/kg	µmol/kg	µmol/kg	µmol/kg	µmol/kg	µmol/kg	µmol/kg	µmol/kg	µmol/kg
1524/1	2.99	10.3	0.977	0.318	<5.00	1.12	22.3	21.2	5.18
1524/2	6.61	17.9	1.39	0.334	<5.00	1.77	31.6	24.2	5.10
1524/3	2.92	31.2	1.31	0.402	<5.00	0.859	26.2	23.8	6.37
1524/4	14.6	17.3	1.04	0.230	<5.00	1.09	40.5	33.4	12.5
1525/1	5.63	8.60	1.80	0.640	<5.00	0.981	25.9	35.2	6.07
1525/2	6.16	14.5	1.19	0.180	<5.00	0.767	53.2	30.8	26.5
1525/4	4.69	14.7	1.03	0.186	<5.00	0.882	30.6	21.4	28.6
1525/5	15.3	27.2	1.11	0.223	<5.00	0.978	30.1	22.9	28.5
1525/6	7.36	27.0	1.17	0.279	<5.00	0.854	38.6	27.9	38.9
1526/1	3.24	11.0	1.47	0.521	<5.00	1.31	23.0	25.3	3.84
1526/2	7.18	46.2	1.24	0.323	<5.00	0.875	8.56	14.7	3.00
1526/4	17.1	48.6	1.75	0.259	<5.00	1.61	44.3	39.6	13.6
1526/6	50.1	27.3	1.71	0.323	<5.00	2.02	38.8	28.1	19.2
1526/8	19.3	25.6	1.86	0.384	<5.00	1.41	43.8	29.1	24.2
1526/10	171	31.1	2.84	0.671	<5.00	2.08	54.4	41.9	8.56
1527/1	8.49	13.1	5.68	0.728	<5.00	3.31	358	51.7	0.888
1527/3	107	43.4	3.92	1.61	<5.00	2.10	214	10.3	17.2
1527/4	5.41	13.4	13.1	6.04	<5.00	2.57	215	48.1	13.4
1527/6	32.4	15.1	1.46	0.783	<5.00	2.71	92.4	6.21	2.40
1528/2	3.46	12.6	3.87	2.71	<5.00	4.65	337	19.2	6.70
1528/4	4.11	17.8	3.73	2.33	<5.00	4.56	512	16.2	3.71
1529/1	62.6	24.5	12.8	5.65	<5.00	0.954	132	47.7	7.26
1529/3	63.3	26.4	34.4	17.9	<5.00	1.57	119	43.8	13.3
1529/5	67.5	12.6	73.2	42.0	<5.00	2.24	181	61.6	5.88
1529/6	158	12.0	167	71.6	<5.00	3.73	108	36.7	8.31
1529/8	4.35	7.46	0.731	0.130	<5.00	1.18	150	2.12	3.64
1529/10	43.0	7.46	2.72	0.395	<5.00	1.87	175	65.1	8.30
1529/12	81.3	10.2	3.82	0.887	19.0	6.25	353	76.9	5.26
1530/1	2.89	11.8	3.52	0.530	13.0	2.15	70.6	56.1	15.2
1530/2	4.74	13.8	3.81	0.480	11.0	2.26	61.1	59.3	16.8
1530/3	7.74	13.8	3.19	0.537	7.01	1.99	51.8	50.0	20.0
1530/6	14.0	17.7	3.16	0.686	8.01	1.50	81.7	57.7	20.4
1530/8	21.8	15.3	2.90	0.632	<5.00	0.874	140	76.4	4.59
1530/9	53.7	34.1	2.68	0.881	<5.00	1.48	103	62.7	13.3
1530/10	22.2	18.6	3.36	0.864	<5.00	1.10	137	78.1	6.55
1534/3	30.0	24.8	3.82	0.328	<5.00	1.95	671	42.5	3.61
1534/4	4.63	10.6	0.223	0.025	<5.00	1.28	15.6	3.14	1.57
1534/5	9.55	10.3	0.153	<0.003	<5.00	1.08	5.39	1.74	0.540
1534/6	19.0	21.9	0.283	<0.003	<5.00	1.32	6.59	2.87	0.430
1534/7	8.39	11.9	0.158	0.014	<5.00	1.77	8.13	2.03	0.330
1534/10	10.5	12.8	0.158	0.081	<5.00	2.23	9.76	3.67	0.354
1534/11	26.7	29.7	0.105	0.031	<5.00	1.97	10.7	4.62	0.355
1534/12	11.8	15.6	0.146	<0.003	<5.00	2.70	10.6	1.94	0.549
1534/13	2.02	3.56	0.050	<0.003	<5.00	1.11	7.45	2.33	0.348
1535/1	1.27	9.75	1.59	0.040	<5.00	1.12	449	9.51	5.80
1535/4	0.923	9.87	2.49	0.778	10.0	1.06	637	80.1	5.81
1535/5	43.2	13.2	2.24	0.447	6.01	1.83	562	63.0	2.59
1535/9	1.67	20.3	2.17	0.535	<5.00	1.42	496	61.8	4.44

	Cu	Zn	Ga	Ge	As	Rb	Sr	Y	Zr
	µmol/kg	µmol/kg	µmol/kg	µmol/kg	µmol/kg	µmol/kg	µmol/kg	µmol/kg	µmol/kg
1535/10	16.1	22.3	2.94	0.705	6.01	1.91	591	71.2	3.47
1535/11	29.6	34.9	1.98	0.092	<5.00	2.47	1230	35.4	3.63
1536/1	24.9	45.2	2.96	0.551	9.01	1.71	218	73.8	12.9
1536/3	15.7	40.3	3.14	0.530	<5.00	1.40	713	55.6	2.90
1536/4	71.5	38.4	2.07	0.551	7.01	2.51	128	53.0	4.97
1536/5	25.0	28.0	4.60	0.354	<5.00	1.65	754	64.9	2.97
1536/7	23.1	54.5	6.05	0.412	<5.00	0.975	627	98.0	2.13
1536/8	3.12	41.0	4.10	0.045	<5.00	1.30	273	0.16	2.06
1536/9	18.2	28.8	1.43	0.231	6.01	1.52	120	23.0	3.68
1536/10	15.9	14.2	0.659	0.175	5.01	2.05	18.7	11.7	1.31
1537/1	6.74	26.7	2.27	0.185	<5.00	5.12	203	39.4	2.23
1537/2	3.59	13.1	1.13	0.039	<5.00	1.15	360	0.028	0.919
1537/3	7.02	31.2	1.90	0.437	6.01	3.77	301	43.0	1.93
1537/4	313	49.1	0.716	0.087	<5.00	4.64	143	13.3	1.03
1537/5	17.1	17.1	3.00	0.533	<5.00	2.54	198	44.0	3.37
1537/6	4.33	23.4	1.90	0.026	<5.00	0.650	269	0.54	0.244
1537/7	1.37	5.51	1.35	<0.003	<5.00	1.57	211	0.19	0.218
1537/9	17.6	16.5	2.67	0.413	<5.00	3.14	202	45.2	0.843
1538/1	25.2	33.3	2.94	0.659	10.0	4.20	163	43.8	1.91
1538/2	22.2	46.8	3.09	0.624	12.0	1.30	152	58.1	8.94
1538/4	5.98	30.6	2.73	0.279	<5.00	0.753	113	5.01	1.98
1538/5	38.5	7.23	1.98	0.541	20.0	3.51	157	36.9	1.22
1538/6	24.5	24.4	4.28	0.597	<5.00	1.64	169	64.7	1.86
1538/7	38.9	20.2	3.12	0.560	<5.00	1.98	152	48.1	5.23
1538/8	19.5	29.3	3.54	0.457	<5.00	1.97	145	53.4	6.58
1538/9	36.2	34.3	3.56	0.951	<5.00	1.97	183	69.1	2.70
1538/10	157	43.9	3.77	0.737	<5.00	2.10	150	58.7	4.02
1539/1	15.0	14.2	0.619	0.107	<5.00	0.944	12.2	11.6	6.56
1539/2	270	34.6	1.71	0.427	<5.00	1.46	33.4	30.9	13.8
1539/3	2.88	18.0	3.29	0.580	<5.00	1.72	79.4	48.7	10.0
1539/4	9.69	14.1	0.986	0.391	<5.00	3.02	20.6	15.9	10.2
1539/5	27.0	34.1	3.15	0.589	<5.00	1.79	57.9	31.7	10.0
1539/6	11.1	15.7	1.25	0.195	<5.00	1.16	23.0	20.7	13.5
1539/8	8.51	12.8	0.901	0.323	<5.00	1.76	21.6	19.3	13.0
1539/9	14.1	14.6	1.02	0.147	<5.00	1.41	17.2	18.3	5.68
1539/10	7.79	13.7	1.55	0.433	<5.00	2.10	24.3	19.7	7.12
1539/11	13.6	16.3	1.20	0.078	<5.00	1.88	30.9	15.9	7.41
1539/13	28.0	24.9	1.55	0.348	<5.00	4.53	31.9	20.7	19.7
1540/1	1.20	24.1	3.20	0.479	<5.00	1.97	72.7	32.2	23.8
1540/2	0.774	15.4	2.83	0.317	<5.00	1.67	71.1	31.0	19.5
1540/3	4.90	27.0	3.34	0.519	<5.00	1.53	83.2	32.6	18.6
1540/5	1.81	21.9	3.57	0.714	21.0	3.33	93.3	37.9	13.3
1540/6	2.90	8.14	3.73	0.498	36.0	2.32	76.3	33.6	9.49
1541/1	4.61	8.72	1.48	0.280	6.01	1.68	16.6	40.8	8.65
1541/2	6.13	6.19	3.30	1.15	<5.00	1.36	30.5	47.8	9.47
1542/1	34.9	31.3	3.60	0.020	<5.00	0.842	10.0	0.536	5.22
1542/2	64.0	52.8	0.287	0.038	<5.00	2.02	2.57	0.305	3.80
1542/3	3.84	18.4	0.156	<0.003	<5.00	7.28	17.0	6.47	1.46
1542/4	65.5	5.62	0.084	<0.003	<5.00	1.14	5.14	0.797	0.297

	Cu	Zn	Ga	Ge	As	Rb	Sr	Y	Zr
	µmol/kg	µmol/kg	µmol/kg	µmol/kg	µmol/kg	µmol/kg	µmol/kg	µmol/kg	µmol/kg
1542/5	23.2	25.7	<0.007	0.007	<5.00	1.61	7.96	1.72	0.180
1542/6	5.03	15.1	0.073	0.056	<5.00	2.66	10.7	3.78	0.434
1542/7	30.1	39.8	0.287	0.093	<5.00	2.15	7.10	2.18	0.773
1542/8	8.01	13.9	0.263	0.039	<5.00	2.50	22.9	3.06	1.79
1542/9	2.88	13.4	0.346	0.058	<5.00	3.18	22.9	7.78	1.18
1542/10	2.93	42.7	0.113	<0.003	<5.00	1.31	7.70	2.69	0.757
1542/11	4.29	16.5	0.250	0.021	<5.00	1.82	11.7	1.96	0.235
1542/12	5.90	22.4	0.298	0.091	<5.00	2.52	18.7	4.13	0.712
1542/13	56.5	69.3	0.115	<0.003	<5.00	2.06	11.4	1.41	0.184
1542/14	12.3	18.2	0.182	0.036	<5.00	5.20	31.2	2.62	0.401
1542/15	18.2	20.5	0.188	0.021	<5.00	3.88	20.0	1.58	0.207
Max	313	69.3	167	71.6	36.0	7.28	1230	98	38.9
Min	0.774	3.56	0.000	0.000	0.000	0.650	2.57	0.028	0.18
Mean	28.0	22.4	4.66	1.702	2.07	2.07	148	30.4	7.16
Median	13.8	18.1	1.90	0.402	8.51	1.78	70.87	28.6	4.78

	Mo	La	Ce	Pr	Nd	Sm	Eu	Gd	Tb
	µmol/kg	µmol/kg	µmol/kg	µmol/kg	µmol/kg	µmol/kg	µmol/kg	µmol/kg	µmol/kg
1524/1	<0.011	6.27	5.63	3.20	15.0	3.92	1.10	4.23	0.541
1524/2	0.175	5.75	11.2	3.17	15.3	4.44	1.24	5.24	0.681
1524/3	0.027	6.98	9.46	3.71	17.8	4.87	1.36	5.47	0.688
1524/4	0.051	12.0	19.6	5.84	27.3	7.79	2.21	8.76	1.16
1525/1	0.015	6.99	9.61	4.82	25.0	6.95	2.04	8.11	1.06
1525/2	0.126	10.7	14.7	4.89	22.7	6.16	1.74	7.31	0.967
1525/4	0.101	7.35	10.9	3.51	16.5	4.61	1.33	5.37	0.694
1525/5	0.033	8.52	12.9	4.01	18.5	5.02	1.40	6.04	0.749
1525/6	0.071	9.44	15.1	4.45	21.0	5.92	1.58	6.94	0.930
1526/1	<0.011	7.84	7.12	3.79	17.8	4.50	1.26	5.05	0.634
1526/2	0.130	3.41	6.35	2.18	10.7	3.08	0.922	3.61	0.442
1526/4	0.153	13.5	22.1	6.23	29.1	8.51	2.37	9.79	1.33
1526/6	0.040	10.4	17.9	4.87	23.1	6.52	1.78	7.35	0.935
1526/8	0.117	9.92	16.4	4.60	22.8	6.34	1.75	7.14	0.927
1526/10	0.121	16.9	30.9	7.47	34.8	9.78	2.55	11.0	1.42
1527/1	0.092	38.9	79.9	12.1	50.6	12.4	3.53	13.6	1.61
1527/3	0.583	9.56	21.4	2.68	10.5	2.46	0.621	2.63	0.311
1527/4	0.533	41.9	60.0	13.5	54.4	12.2	3.10	13.2	1.63
1527/6	0.135	2.07	5.35	0.94	4.65	1.68	0.484	1.84	0.238
1528/2	0.145	3.99	9.62	2.18	11.8	5.62	1.61	7.31	0.859
1528/4	0.132	3.94	9.59	1.93	10.1	4.93	1.54	6.51	0.778
1529/1	0.175	17.8	69.2	8.35	40.8	11.65	3.03	13.9	1.69
1529/3	0.080	18.7	69.9	8.82	39.1	10.11	2.81	15.3	1.70
1529/5	0.099	24.7	76.9	10.4	47.5	11.39	2.85	18.6	2.14
1529/6	0.053	8.76	48.3	3.92	18.0	3.88	0.747	7.33	0.768
1529/8	0.169	0.328	0.725	0.188	1.20	0.216	0.051	0.225	0.034
1529/10	0.073	12.7	25.3	5.58	41.5	9.48	2.28	10.3	1.23
1529/12	0.061	22.1	47.2	9.11	58.4	12.0	2.83	13.1	1.55
1530/1	0.031	21.7	38.0	8.60	51.5	9.15	2.03	9.25	1.09
1530/2	<0.007	20.6	39.9	9.43	50.7	8.52	1.89	9.10	1.05
1530/3	0.067	16.9	28.0	6.50	40.0	7.36	1.53	7.39	0.908
1530/6	0.054	18.9	29.0	7.73	44.2	8.39	1.74	8.33	1.09
1530/8	0.039	20.0	39.0	8.89	47.4	9.67	2.01	9.72	1.17
1530/9	0.058	21.3	42.3	8.82	50.7	9.32	2.16	9.08	1.11
1530/10	<0.007	25.1	56.4	9.72	60.3	10.4	2.47	11.0	1.30
1534/3	0.030	17.3	45.0	5.63	32.8	5.83	1.32	6.44	0.771
1534/4	<0.007	0.379	1.13	0.238	1.05	0.296	0.076	0.46	0.041
1534/5	<0.007	0.072	1.57	0.048	0.251	0.096	0.039	0.179	0.026
1534/6	0.020	0.084	1.43	0.032	0.257	0.114	0.027	0.218	0.022
1534/7	<0.007	0.059	0.304	0.019	0.130	0.077	0.028	0.109	0.018
1534/10	<0.007	0.039	1.78	0.020	0.144	0.143	0.050	0.322	0.048
1534/11	<0.007	0.062	2.85	0.047	0.323	0.161	0.071	0.427	0.063
1534/12	<0.007	0.055	0.400	0.017	0.158	0.060	0.032	0.153	0.013
1534/13	<0.007	0.061	1.51	0.037	0.217	0.169	0.038	0.321	0.040
1535/1	0.053	3.36	8.88	1.15	7.17	1.16	0.281	1.45	0.157
1535/4	<0.007	24.8	65.7	8.91	58.4	12.4	2.70	13.8	1.51
1535/5	0.068	18.9	34.3	7.25	52.0	12.6	2.65	12.5	1.40
1535/9	0.012	19.9	52.1	7.06	45.4	9.65	2.13	11.0	1.31

	Mo	La	Ce	Pr	Nd	Sm	Eu	Gd	Tb
	µmol/kg	µmol/kg	µmol/kg	µmol/kg	µmol/kg	µmol/kg	µmol/kg	µmol/kg	µmol/kg
1535/10	0.011	22.6	63.1	8.68	56.0	11.9	2.64	13.5	1.57
1535/11	0.128	10.4	29.2	3.48	21.6	4.52	1.03	5.23	0.668
1536/1	0.497	23.3	53.9	7.20	42.7	7.86	1.78	9.46	1.22
1536/3	0.140	24.2	50.3	7.36	39.2	7.12	2.05	7.75	0.931
1536/4	0.469	15.7	39.3	5.42	30.4	6.08	1.53	7.35	0.985
1536/5	0.173	37.7	67.2	9.64	49.2	8.66	2.35	9.43	1.06
1536/7	0.236	26.7	71.7	10.8	56.9	11.9	3.32	12.9	1.72
1536/8	0.012	0.136	0.120	<0.002	0.094	0.004	<0.003	0.009	<0.003
1536/9	0.198	11.9	24.9	3.19	17.7	3.24	0.664	3.72	0.434
1536/10	0.227	2.85	6.95	1.06	6.02	1.55	0.311	1.74	0.228
1537/1	0.076	14.7	29.7	4.80	28.2	5.16	1.16	5.65	0.643
1537/2	0.015	0.03	<0.006	<0.002	<0.007	0.006	<0.003	<0.003	<0.003
1537/3	0.030	34.2	27.2	7.86	38.4	6.30	1.60	6.53	0.777
1537/4	0.052	6.87	9.01	2.18	11.3	2.42	0.594	2.80	0.296
1537/5	0.033	35.1	43.9	8.71	41.4	7.07	1.61	7.55	0.840
1537/6	0.011	0.398	0.203	0.018	0.114	0.051	0.032	0.03	<0.003
1537/7	<0.007	0.091	0.023	<0.002	<0.007	0.023	<0.003	<0.003	<0.003
1537/9	0.014	9.47	29.7	5.87	34.9	7.53	1.65	7.74	0.884
1538/1	<0.007	13.2	24.3	5.57	37.0	9.40	2.38	10.4	1.19
1538/2	0.138	13.8	27.5	5.75	37.3	9.64	2.37	11.2	1.20
1538/4	<0.007	3.17	2.87	0.406	2.99	0.35	0.034	0.481	0.023
1538/5	0.019	12.5	21.3	5.68	32.1	7.42	1.73	7.98	0.895
1538/6	<0.007	12.9	21.4	5.73	33.6	7.20	1.90	8.61	1.05
1538/7	0.018	13.4	24.1	5.42	30.8	7.00	1.73	7.77	0.944
1538/8	0.015	13.2	22.5	5.25	30.9	6.96	1.80	7.88	1.02
1538/9	<0.007	21.7	37.5	7.65	43.6	9.39	2.40	10.7	1.29
1538/10	0.052	19.4	35.2	6.67	41.1	9.16	2.55	10.3	1.25
1539/1	0.087	2.87	5.42	1.13	7.55	2.46	0.608	2.60	0.258
1539/2	0.089	10.1	16.7	2.90	17.1	4.13	1.19	4.62	0.553
1539/3	0.039	16.9	28.7	5.18	28.5	6.66	1.51	7.49	0.867
1539/4	0.135	4.72	7.99	1.66	10.4	2.92	0.769	3.28	0.397
1539/5	0.021	10.5	23.1	2.53	13.9	3.86	1.01	4.97	0.569
1539/6	0.111	4.20	8.11	1.33	8.2	2.18	0.623	2.94	0.313
1539/8	0.101	5.39	9.41	1.85	10.2	2.92	0.728	3.44	0.373
1539/9	0.107	3.46	8.42	1.20	7.06	2.43	0.596	2.77	0.265
1539/10	0.184	5.65	11.2	1.53	7.85	2.37	0.604	2.55	0.310
1539/11	0.055	5.68	10.5	1.55	7.82	2.25	0.548	2.52	0.318
1539/13	0.210	6.84	12.8	2.03	11.4	2.93	0.698	3.77	0.391
1540/1	0.088	8.82	18.0	2.60	15.0	3.56	0.890	4.25	0.491
1540/2	0.091	7.04	15.7	2.45	14.0	3.63	1.02	4.33	0.517
1540/3	0.150	11.1	21.3	3.11	17.4	4.31	1.00	4.70	0.484
1540/5	0.679	9.80	23.9	3.14	16.3	3.83	0.974	5.06	0.561
1540/6	0.999	8.40	18.9	2.72	17.1	4.74	1.26	5.86	0.601
1541/1	0.009	4.24	11.3	2.12	13.6	3.48	0.822	5.19	0.643
1541/2	<0.007	17.2	22.0	5.78	31.8	6.59	1.55	7.74	0.859
1542/1	16.9	0.792	1.17	0.091	0.634	0.137	0.037	0.109	0.005
1542/2	0.438	0.164	0.777	0.037	0.210	0.102	0.028	0.082	<0.003
1542/3	0.032	0.847	1.47	0.183	1.01	0.354	0.100	0.596	0.068
1542/4	0.047	0.047	0.120	0.027	0.177	0.093	0.026	0.145	0.007

	Mo	La	Ce	Pr	Nd	Sm	Eu	Gd	Tb
	µmol/kg	µmol/kg	µmol/kg	µmol/kg	µmol/kg	µmol/kg	µmol/kg	µmol/kg	µmol/kg
1542/5	<0.007	0.036	0.188	0.011	0.217	0.144	0.036	0.247	0.016
1542/6	<0.007	0.070	0.181	0.057	0.993	0.421	0.087	0.523	0.048
1542/7	<0.007	0.061	0.128	0.087	1.12	0.358	0.078	0.464	0.034
1542/8	<0.007	0.047	0.301	0.037	0.484	0.186	0.062	0.438	0.036
1542/9	<0.007	0.088	0.373	0.089	1.25	0.516	0.180	0.923	0.096
1542/10	0.033	0.027	0.124	0.034	0.506	0.241	0.047	0.504	0.032
1542/11	<0.007	0.058	2.08	0.060	0.812	0.377	0.092	0.397	0.042
1542/12	<0.007	0.055	1.70	0.073	0.946	0.402	0.126	0.679	0.073
1542/13	<0.007	0.029	0.463	0.018	0.259	0.164	0.049	0.240	0.017
1542/14	<0.007	0.071	0.232	0.020	0.304	0.169	0.086	0.329	0.023
1542/15	<0.007	0.039	0.232	0.029	0.262	0.181	0.056	0.211	0.014
Max	16.9	41.9	79.9	13.5	60.3	12.6	3.53	18.6	2.14
Min	<0.007	0.03	<0.006	<0.002	<0.007	0.004	<0.003	<0.003	<0.003
Mean	0.251	10.33	21.0	3.86	21.1	4.81	1.20	5.53	0.659
Median	0.084	8.64	15.7	3.20	17.3	4.47	1.24	5.30	0.681

	Dy	Ho	Er	Tm	Yb	Lu	Ag	Cd	Sn
	µmol/kg	µmol/kg	µmol/kg	µmol/kg	µmol/kg	µmol/kg	µmol/kg	µmol/kg	µmol/kg
1524/1	2.40	0.440	1.21	0.134	0.956	0.128	<0.139	0.129	<0.506
1524/2	2.95	0.549	1.45	0.167	1.12	0.139	<0.139	0.213	<0.506
1524/3	3.05	0.544	1.42	0.170	1.05	0.131	<0.139	0.162	<0.506
1524/4	5.31	0.938	2.42	0.276	1.73	0.226	0.626	0.164	33.9
1525/1	4.71	0.879	2.37	0.262	1.50	0.172	<0.139	0.125	<0.506
1525/2	4.63	0.856	2.29	0.278	1.79	0.227	1.04	0.379	52.2
1525/4	3.17	0.538	1.41	0.145	1.00	0.118	0.556	0.113	22.7
1525/5	3.29	0.589	1.53	0.175	1.02	0.125	0.487	0.177	21.9
1525/6	4.11	0.702	1.86	0.210	1.27	0.165	0.765	0.705	31.0
1526/1	2.87	0.507	1.37	0.155	1.06	0.154	<0.139	0.145	<0.506
1526/2	1.93	0.337	0.863	0.100	0.609	0.078	<0.139	0.342	<0.506
1526/4	6.02	1.093	2.80	0.312	1.97	0.253	1.32	0.432	64.5
1526/6	4.29	0.722	1.90	0.214	1.22	0.164	0.765	0.186	36.6
1526/8	4.26	0.751	1.94	0.222	1.41	0.196	1.11	1.03	58.4
1526/10	6.52	1.105	2.76	0.327	1.87	0.229	1.04	0.197	57.6
1527/1	6.79	1.167	2.97	0.345	1.96	0.237	2.99	1.08	236
1527/3	1.45	0.254	0.746	0.076	0.474	0.066	0.278	1.00	<27.2
1527/4	7.76	1.367	3.51	0.429	2.48	0.294	1.18	1.18	1.64
1527/6	0.987	0.152	0.380	0.046	0.24	0.030	<0.139	0.086	<0.506
1528/2	3.28	0.536	1.21	0.137	0.683	0.076	<0.139	0.121	21.3
1528/4	2.96	0.532	1.03	0.126	0.680	0.084	0.973	0.490	39.7
1529/1	7.03	1.354	3.33	0.366	2.16	0.326	3.06	1.17	160
1529/3	6.77	1.362	3.28	0.361	2.03	0.281	6.67	3.09	106
1529/5	8.63	1.783	4.66	0.450	2.77	0.391	3.13	0.948	185
1529/6	3.11	0.728	1.95	0.177	1.17	0.204	2.43	0.564	87.1
1529/8	0.182	0.032	0.056	0.004	0.048	0.005	3.13	0.924	227
1529/10	6.04	1.119	2.45	0.277	1.52	0.197	2.99	0.704	160
1529/12	7.10	1.393	2.93	0.366	1.57	0.230	3.06	1.23	174
1530/1	5.29	1.024	2.21	0.278	1.28	0.198	1.11	0.145	1.07
1530/2	5.74	1.052	2.31	0.234	1.34	0.175	0.765	0.219	<13.8
1530/3	4.69	0.973	2.16	0.288	1.30	0.164	0.765	0.261	<13.5
1530/6	5.79	1.059	2.33	0.293	1.43	0.185	1.25	0.488	14.2
1530/8	5.52	1.153	2.51	0.299	1.78	0.259	3.13	1.17	183
1530/9	5.81	1.100	2.57	0.292	1.62	0.238	2.09	0.600	78.4
1530/10	6.84	1.324	2.96	0.411	2.01	0.270	2.64	0.940	171
1534/3	4.08	0.727	1.70	0.233	1.03	0.147	1.67	0.241	34.1
1534/4	0.318	0.064	0.104	0.016	0.061	0.007	<0.139	0.053	<0.506
1534/5	0.265	0.040	0.094	0.008	0.061	0.009	0.209	0.262	<0.506
1534/6	0.211	0.056	0.126	0.020	0.083	0.015	0.626	1.53	<0.506
1534/7	0.101	0.027	0.074	0.010	0.048	0.008	<0.139	1.31	<0.506
1534/10	0.320	0.072	0.184	0.016	0.104	0.026	<0.139	0.084	<0.506
1534/11	0.412	0.096	0.285	0.026	0.126	0.018	0.348	0.413	<0.506
1534/12	0.101	0.033	0.083	0.006	0.028	0.003	0.278	0.238	<0.506
1534/13	0.285	0.057	0.147	0.013	0.074	0.011	<0.139	0.251	<0.506
1535/1	0.746	0.142	0.325	0.030	0.158	0.021	2.57	0.013	98.4
1535/4	7.87	1.476	3.38	0.363	2.10	0.247	2.22	0.018	81.1
1535/5	6.42	1.243	2.66	0.339	1.58	0.221	1.67	<0.005	20.7
1535/9	6.18	1.182	2.76	0.342	1.57	0.208	3.13	<0.005	104

	Dy	Ho	Er	Tm	Yb	Lu	Ag	Cd	Sn
	µmol/kg	µmol/kg	µmol/kg	µmol/kg	µmol/kg	µmol/kg	µmol/kg	µmol/kg	µmol/kg
1535/10	7.48	1.361	3.08	0.371	1.74	0.260	2.22	<0.005	92.2
1535/11	3.46	0.696	1.59	0.176	0.962	0.142	4.17	5.12	77.2
1536/1	6.74	1.347	3.20	0.391	2.06	0.259	0.487	0.120	<23.6
1536/3	4.88	0.988	2.22	0.282	1.66	0.217	2.85	0.664	85.9
1536/4	5.04	1.060	2.28	0.302	1.50	0.191	0.348	0.082	17.5
1536/5	5.67	1.122	2.68	0.343	1.84	0.265	3.27	1.05	160
1536/7	9.11	1.802	4.32	0.494	3.01	0.393	4.31	<0.005	30.2
1536/8	0.035	<0.002	<0.003	<0.003	<0.003	<0.002	5.08	0.031	16.6
1536/9	2.08	0.416	0.965	0.117	0.555	0.069	<0.139	<0.005	<0.506
1536/10	1.17	0.250	0.501	0.067	0.303	0.034	<0.139	0.244	<0.506
1537/1	3.24	0.660	1.47	0.163	1.00	0.125	3.27	1.51	156
1537/2	0.006	<0.002	<0.003	<0.003	<0.003	<0.002	3.75	0.476	225
1537/3	3.77	0.754	1.70	0.218	1.04	0.138	3.13	0.270	167
1537/4	1.47	0.251	0.580	0.066	0.340	0.040	<0.139	<0.005	<8.03
1537/5	4.29	0.832	1.64	0.213	1.12	0.130	2.02	0.586	49.0
1537/6	0.008	<0.002	<0.003	<0.003	<0.003	<0.002	4.31	2.00	224
1537/7	0.007	<0.002	0.003	<0.003	<0.003	<0.002	3.89	1.07	233
1537/9	4.35	0.764	1.57	0.168	0.938	0.123	2.78	0.191	94.5
1538/1	4.94	0.855	1.65	0.187	0.743	0.113	<0.139	<0.005	7.20
1538/2	5.63	1.01	2.14	0.266	1.16	0.166	2.29	<0.005	52.3
1538/4	0.093	0.033	0.032	0.007	<0.003	<0.002	1.95	0.217	80.9
1538/5	3.89	0.696	1.45	0.167	0.642	0.088	<0.139	<0.005	5.75
1538/6	5.65	1.17	2.47	0.342	1.60	0.242	2.71	0.270	71.1
1538/7	4.81	0.943	1.98	0.250	1.21	0.139	1.32	<0.005	6.19
1538/8	5.01	0.974	2.10	0.283	1.24	0.152	1.46	0.736	12.8
1538/9	6.30	1.27	2.86	0.369	1.78	0.213	1.39	0.049	33.8
1538/10	5.94	1.11	2.37	0.332	1.29	0.218	1.18	0.082	14.5
1539/1	1.34	0.211	0.445	0.054	0.211	0.027	1.81	1.24	<0.506
1539/2	2.73	0.581	1.29	0.167	0.823	0.121	0.695	0.040	<13.3
1539/3	4.55	0.939	2.08	0.294	1.41	0.165	1.25	0.028	<19.6
1539/4	1.71	0.331	0.663	0.087	0.312	0.038	1.81	0.623	<0.506
1539/5	3.11	0.585	1.25	0.154	0.739	0.118	3.89	3.00	32.5
1539/6	1.74	0.344	0.797	0.118	0.442	0.056	1.46	0.369	<25.9
1539/8	1.89	0.347	0.673	0.093	0.419	0.045	0.695	0.225	6.38
1539/9	1.58	0.321	0.688	0.107	0.412	0.073	3.55	2.65	<24.8
1539/10	1.82	0.361	0.873	0.116	0.588	0.067	0.695	<0.005	<24.0
1539/11	1.50	0.291	0.683	0.081	0.412	0.057	1.67	0.902	18.4
1539/13	2.15	0.409	0.910	0.115	0.545	0.075	2.22	4.76	21.0
1540/1	3.09	0.600	1.32	0.192	0.922	0.111	0.973	<0.005	16.1
1540/2	2.76	0.521	1.29	0.181	0.883	0.104	1.67	<0.005	28.4
1540/3	2.87	0.573	1.44	0.196	0.913	0.137	0.973	0.036	41.6
1540/5	3.20	0.709	1.47	0.214	1.02	0.140	1.67	0.052	39.7
1540/6	3.14	0.631	1.44	0.194	0.923	0.116	2.50	0.147	71.2
1541/1	3.89	0.755	1.81	0.294	1.47	0.200	<0.139	<0.005	<0.506
1541/2	5.01	0.928	2.00	0.276	1.35	0.182	0.348	0.028	13.1
1542/1	0.092	0.009	0.022	<0.003	0.015	<0.002	16.1	3.66	<0.506
1542/2	0.033	0.006	0.017	0.003	<0.003	<0.002	11.3	6.84	<0.506
1542/3	0.473	0.089	0.211	0.037	0.136	0.018	0.278	0.085	<0.506
1542/4	0.107	0.009	0.027	<0.003	0.010	0.008	1.25	<0.005	<0.506

	Dy	Ho	Er	Tm	Yb	Lu	Ag	Cd	Sn
	µmol/kg	µmol/kg	µmol/kg	µmol/kg	µmol/kg	µmol/kg	µmol/kg	µmol/kg	µmol/kg
1542/5	0.143	0.024	0.072	0.007	0.026	<0.002	1.11	0.506	<0.506
1542/6	0.327	0.060	0.166	0.023	0.083	0.021	0.278	0.112	<0.506
1542/7	0.227	0.046	0.092	0.012	0.026	0.006	3.13	4.86	<0.506
1542/8	0.254	0.059	0.115	0.016	0.061	0.011	0.209	0.591	<0.506
1542/9	0.589	0.131	0.273	0.033	0.187	0.022	0.278	0.929	<0.506
1542/10	0.216	0.060	0.111	0.017	0.064	0.008	<0.139	<0.005	<0.506
1542/11	0.289	0.052	0.100	0.013	0.072	0.008	0.348	0.177	<0.506
1542/12	0.442	0.087	0.156	0.033	0.124	0.015	0.278	0.669	<0.506
1542/13	0.149	0.026	0.076	0.005	0.024	<0.002	0.626	1.26	<0.506
1542/14	0.237	0.051	0.114	0.009	0.066	0.013	0.209	1.98	<0.506
1542/15	0.099	0.022	0.074	0.008	0.018	<0.002	4.03	3.06	<0.506
Max	9.11	1.80	4.66	0.494	3.01	0.393	16.1	6.84	236
Min	0.006	<0.002	<0.003	<0.003	<0.003	<0.002	<0.139	<0.005	<0.506
Mean	3.20	0.609	1.41	0.172	0.903	0.121	1.74	0.731	44.1
Median	3.11	0.594	1.44	0.175	0.981	0.130	1.67	0.396	52.2

	Sb	Cs	Ba	Tl	Pb	Bi	Th	U
	µmol/kg	µmol/kg	µmol/kg	µmol/kg	µmol/kg	µmol/kg	µmol/kg	µmol/kg
1524/1	0.016	0.052	47.0	0.003	1.01	0.005	1.30	0.288
1524/2	0.054	0.074	47.4	0.007	1.96	0.009	1.98	0.190
1524/3	0.008	0.043	16.9	0.002	1.16	0.005	2.50	0.180
1524/4	0.031	0.047	29.2	0.002	2.28	0.010	8.17	0.458
1525/1	0.014	0.054	38.4	0.004	13.8	0.017	1.39	0.105
1525/2	0.041	0.056	40.2	0.006	18.9	0.031	7.56	0.334
1525/4	0.031	0.069	21.2	0.004	24.8	0.038	5.60	0.211
1525/5	0.034	0.065	8.38	0.003	21.3	0.034	5.29	0.240
1525/6	0.030	0.074	11.7	0.005	11.4	0.024	7.58	0.344
1526/1	0.012	0.053	46.9	0.004	1.22	0.005	1.53	0.357
1526/2	0.015	0.043	20.6	0.002	2.26	0.012	1.88	0.071
1526/4	0.059	0.076	26.6	0.008	2.25	0.008	9.84	0.584
1526/6	0.028	0.087	32.3	0.004	3.98	0.012	8.08	0.358
1526/8	0.034	0.065	24.2	0.002	4.74	0.011	6.52	0.431
1526/10	0.091	0.061	42.8	0.005	4.36	0.014	13.1	0.529
1527/1	0.128	0.374	236	0.008	0.701	<0.0004	0.023	0.414
1527/3	0.163	0.316	213	0.011	6.88	0.053	3.32	0.205
1527/4	0.179	0.566	201	0.063	8.68	0.018	21.0	0.656
1527/6	0.071	0.662	162	0.004	4.02	0.020	4.11	0.088
1528/2	0.009	0.102	53.3	0.016	0.662	0.009	11.1	0.106
1528/4	0.040	0.105	177	0.032	1.98	0.010	5.95	0.095
1529/1	0.082	0.040	88.4	0.001	0.457	0.002	6.35	0.494
1529/3	0.071	0.100	114	0.007	0.827	<0.0004	10.4	0.465
1529/5	0.018	0.036	98.8	0.007	0.520	0.006	9.50	0.711
1529/6	0.145	0.083	195	<0.0003	0.408	<0.0004	6.38	0.272
1529/8	0.093	0.045	24.9	0.001	<0.003	0.001	0.048	0.053
1529/10	0.077	0.085	43.6	0.006	0.516	0.002	2.97	0.398
1529/12	0.038	0.299	59.4	<0.0005	1.55	0.006	2.76	0.659
1530/1	0.043	0.087	193	0.006	2.51	0.009	4.52	0.392
1530/2	0.060	0.066	203	0.002	0.602	0.004	4.50	0.380
1530/3	0.070	0.040	122	0.004	0.706	0.008	3.29	0.399
1530/6	0.083	0.048	101	0.003	1.03	0.004	3.53	0.425
1530/8	0.156	0.039	247	<0.0005	0.944	0.006	1.73	0.204
1530/9	0.082	0.046	419	0.006	0.603	0.001	3.16	0.308
1530/10	0.045	0.040	135	0.003	0.771	0.004	3.55	0.296
1534/3	0.049	0.039	227	0.006	7.50	0.039	1.22	0.620
1534/4	0.053	0.038	13.3	0.001	1.18	0.005	0.128	0.011
1534/5	0.019	0.025	20.8	0.002	0.302	0.001	0.112	0.016
1534/6	0.113	0.014	33.3	0.002	0.178	0.002	0.113	0.037
1534/7	0.062	0.018	28.5	<0.0005	0.248	0.007	0.109	0.018
1534/10	0.026	0.068	28.9	0.007	0.349	0.001	0.147	0.078
1534/11	0.022	0.033	52.4	0.001	0.081	0.002	0.160	0.070
1534/12	0.019	0.048	32.1	<0.0005	0.042	0.001	0.141	0.050
1534/13	<0.006	0.028	22.1	<0.0005	0.316	0.004	0.141	0.046
1535/1	0.018	0.059	16.7	0.004	<0.003	<0.0004	0.026	<0.001
1535/4	<0.006	0.009	210	<0.0005	<0.003	0.003	0.025	0.493
1535/5	0.026	0.040	204	0.003	0.496	0.005	2.21	1.000
1535/9	0.029	0.013	24.3	0.001	<0.003	0.001	0.177	0.429

	Sb	Cs	Ba	Tl	Pb	Bi	Th	U
	µmol/kg	µmol/kg	µmol/kg	µmol/kg	µmol/kg	µmol/kg	µmol/kg	µmol/kg
1535/10	0.027	0.041	39.7	0.002	0.771	0.002	0.905	0.884
1535/11	0.062	0.073	37.9	0.001	1.17	0.004	1.92	0.874
1536/1	0.231	0.098	19.4	0.010	14.3	0.062	5.01	1.031
1536/3	0.059	0.057	15.2	0.005	2.96	0.013	1.93	1.387
1536/4	0.107	0.243	18.5	0.005	6.70	0.037	2.46	0.507
1536/5	0.018	0.081	23.8	0.003	8.31	0.041	2.16	2.980
1536/7	0.148	0.052	10.0	<0.0005	1.87	0.014	1.99	0.206
1536/8	0.136	0.072	7.51	0.006	<0.003	0.001	0.080	<0.001
1536/9	0.195	0.089	10.9	0.007	7.59	0.056	2.45	0.943
1536/10	0.350	0.240	6.69	0.007	13.0	0.065	0.857	0.415
1537/1	0.051	0.769	69.8	0.019	6.22	0.033	3.28	0.128
1537/2	<0.006	0.104	6.47	0.023	<0.003	<0.0004	0.014	0.314
1537/3	0.068	0.580	11.6	0.017	2.61	0.020	3.74	0.353
1537/4	0.082	0.971	465	0.016	1.86	0.028	2.32	0.079
1537/5	0.008	0.392	205	0.015	0.968	0.011	7.21	0.264
1537/6	0.039	0.081	95.5	0.191	<0.003	<0.0004	0.060	0.031
1537/7	0.021	0.107	7.40	0.016	<0.003	0.002	<0.013	0.029
1537/9	0.008	0.781	27.4	0.018	1.28	0.009	2.80	0.067
1538/1	0.052	0.156	5.82	0.003	0.254	0.004	5.28	0.396
1538/2	0.008	0.029	105	0.002	0.232	0.013	4.09	0.197
1538/4	0.018	0.031	2.38	0.001	<0.003	<0.0004	0.072	<0.001
1538/5	0.076	0.210	62.2	0.001	0.318	0.006	4.04	0.399
1538/6	0.026	0.041	55.6	0.005	0.086	0.001	2.00	0.406
1538/7	0.063	0.076	129	0.006	0.314	0.005	3.01	0.365
1538/8	0.010	0.081	110	0.003	0.309	0.004	3.54	0.324
1538/9	0.084	0.052	25.4	0.010	0.842	0.008	2.42	0.870
1538/10	0.106	0.065	25.1	0.007	0.706	0.007	3.61	0.616
1539/1	0.079	0.053	2.76	0.011	0.274	0.067	1.39	0.250
1539/2	0.105	0.082	3.25	<0.0005	0.474	0.007	1.80	0.277
1539/3	0.105	0.067	6.03	0.002	0.460	0.009	3.28	0.413
1539/4	0.119	0.139	10.5	0.004	0.317	0.012	1.87	0.212
1539/5	0.074	0.052	7.73	0.001	0.659	0.002	1.42	0.315
1539/6	0.109	0.042	3.14	<0.0005	0.683	0.005	0.788	0.216
1539/8	0.053	0.074	6.80	0.004	0.939	0.010	1.18	0.207
1539/9	0.032	0.070	2.87	<0.0005	0.214	0.002	0.525	0.106
1539/10	0.034	0.104	3.69	0.005	0.937	0.005	0.707	0.183
1539/11	0.053	0.052	4.94	0.001	0.300	0.006	0.976	0.268
1539/13	0.090	0.176	5.38	0.004	0.303	0.006	1.32	0.258
1540/1	0.115	0.093	7.34	0.002	0.235	0.006	2.74	0.232
1540/2	0.045	0.102	20.0	0.001	0.214	0.004	2.68	0.196
1540/3	0.076	0.084	13.0	0.004	0.323	0.008	2.50	0.257
1540/5	0.214	0.220	48.2	0.006	0.378	0.021	2.84	0.266
1540/6	0.157	0.164	53.1	0.007	0.210	0.022	3.17	0.297
1541/1	0.102	0.041	35.7	<0.0005	0.454	0.004	1.57	1.204
1541/2	0.051	0.028	56.7	0.009	0.407	0.007	2.87	0.636
1542/1	0.192	0.187	7.84	0.001	1.66	0.015	0.250	0.050
1542/2	0.369	0.045	30.2	0.006	1.22	0.033	0.157	0.186
1542/3	0.037	0.056	50.7	0.011	0.340	0.008	0.216	0.634
1542/4	<0.006	0.029	10.2	0.003	0.063	<0.0004	0.068	0.051

	Sb	Cs	Ba	Tl	Pb	Bi	Th	U
	µmol/kg	µmol/kg	µmol/kg	µmol/kg	µmol/kg	µmol/kg	µmol/kg	µmol/kg
1542/5	<0.006	0.012	11.7	0.003	0.156	0.003	0.053	0.094
1542/6	<0.006	0.028	25.7	0.005	0.079	0.003	0.093	0.151
1542/7	0.026	0.016	17.2	0.003	0.080	0.005	0.104	0.078
1542/8	0.011	0.006	47.0	0.002	0.258	<0.0004	0.078	0.111
1542/9	0.018	<0.001	46.8	0.004	0.139	<0.0004	0.086	0.291
1542/10	<0.006	0.029	15.3	0.004	0.063	0.004	0.089	0.080
1542/11	0.017	0.007	28.9	0.004	0.008	<0.0004	0.056	0.268
1542/12	0.037	0.015	32.7	0.004	0.065	<0.0004	0.057	0.342
1542/13	0.028	0.023	31.0	<0.0005	0.064	0.005	0.096	0.231
1542/14	<0.006	0.040	86.2	0.006	0.134	0.002	0.103	0.928
1542/15	<0.006	0.036	40.9	<0.0005	0.231	<0.0004	0.111	0.181
Max	0.369	0.971	465	0.191	24.8	0.067	21.0	2.98
Min	0.000	0.000	2.38	0.000	0.000	0.000	0.000	0.000
Mean	0.065	0.114	63.2	0.007	2.27	0.011	2.76	0.353
Median	0.053	0.061	30.6	0.004	0.683	0.007	1.98	0.277

APPENDIX 3. Pressure Saturation Data for PCE

24/3v/1	4.73	24/4v/1	4.48	24/4v/2	3.77	25/5v/1	3.28	25/6v/1	5.02	26/4v/1	4.32
ml	Pc(KPa)	ml	Pc(KPa)	ml	Pc(KPa)	ml	Pc(KPa)	ml	Pc(KPa)	ml	Pc(KPa)
0	0.14	0	0.13	0	0.11	0	0.10	0.001	0.13	0	0.13
0	0.54	0.002	0.53	0	0.46	0.002	0.41	0.002	0.54	0.025	0.53
0.002	1.22	0.007	1.20	0	1.02	0.007	0.92	0.137	1.21	0.042	1.20
0.552	2.18	0.008	2.13	0	1.82	0.009	1.64	0.782	2.15	0.157	2.14
1.282	3.40	0.018	3.33	0.07	2.84	0.039	2.56	1.542	3.36	0.492	3.34
1.782	4.90	0.168	4.80	0.38	4.10	0.319	3.68	2.002	4.84	1.052	4.81
2.212	8.71	0.798	8.54	0.87	7.28	0.844	6.54	2.392	8.60	1.467	8.55
2.487	13.61	1.178	13.34	1.15	11.38	1.144	10.22	2.572	13.44	1.782	13.36
2.672	19.60	1.468	19.21	1.36	16.38	1.344	14.72	2.662	19.36	1.902	19.24
2.782	30.62	1.783	30.01	1.72	25.60	1.569	23.00	2.782	30.25	2.017	30.06
2.837	54.43	1.933	53.36	1.945	45.51	1.679	40.90	2.902	53.77	2.122	53.44
2.892	85.05	2.078	83.37	2.025	71.11	1.749	63.90	2.972	84.02	2.217	83.50
2.914	106.69	2.158	104.58	2.035	89.20	1.791	80.16	2.977	105.39	2.277	104.75

26/4v/2	3.68	26/6v/2	3.83	26/10v	4.10	27/1v/1	0.96	27/2v/1	0.69	27/3v/1	4.55
ml	Pc(KPa)	ml	Pc(KPa)	ml	Pc(KPa)	ml	Pc(KPa)	ml	Pc(KPa)	ml	Pc(KPa)
0	0.12	0	0.11	0	0.57	0	0.13	0.01	0.12	0.07	0.14
0.015	0.50	0.057	0.46	0.1	2.28	0	0.54	0.04	0.47	0.135	0.57
0.021	1.12	0.062	1.03	0.4	9.12	0	1.21	0.135	1.06	0.355	1.29
0.037	1.98	0.093	1.84	0.55	11.54	0	2.16	0.2	1.88	0.725	2.29
0.094	3.10	0.553	2.87	0.775	14.25	0	3.37	0.285	2.93	1.165	3.58
0.529	4.47	1.023	4.13	0.9	17.24	0	4.85	0.305	4.23	1.575	5.16
0.949	7.94	1.488	7.34	1	20.52	0	8.63	0.435	7.51	2.16	9.18
1.274	12.41	1.748	11.47	1.025	24.08	0	13.48	0.445	11.74	2.465	14.34
1.405	17.86	1.913	16.52	1.105	27.93	0	19.41	0.45	16.90	2.675	20.65
1.54	27.91	2.023	25.81	1.19	32.06	0	30.33	0.455	26.41	2.9	32.26
1.671	49.62	2.113	45.89	1.23	36.48	0	53.91	0.465	46.95	3.055	57.35
1.763	77.54	2.153	71.70	1.27	41.18	0	84.24	0.47	73.36	3.135	89.61
1.795	97.26	2.168	89.95	1.325	46.17	0	105.67	0.471	92.02	3.205	112.41
				1.35	51.44	0	63.10				
				1.35	57.00	0	112.18				
				1.42	62.84	0	175.29				
				1.42	68.97	0	252.42				
				1.44	75.38	0.002	343.57				
				1.485	82.08	0.007	448.74				
				1.505	89.06	0.007	567.93				
				1.535	96.32	0.017	701.15				
				1.555	103.88	0.032	1009.66				
				1.56	111.71	0.047	1577.59				
				1.58	119.84	0.077	2026.33				
				1.58	128.24	0.107	2271.74				
				1.59	227.99	0.137	2531.16				
				1.65	356.23	0.162	2804.61				
				1.695	512.97						
				1.75	698.21						

27/4v/1	4.51	27/5v/1	1.29	27/5v/2	1.11	27/8v/2	0.72	28/2v/1	2.99	28/3v/1	0.53
ml	Pc(KPa)	ml	Pc(KPa)	ml	Pc(KPa)	ml	Pc(KPa)	ml	Pc(KPa)	ml	Pc(KPa)
0.005	0.14	0	0.14	0	0.11	0	0.13	0.001	0.13	0.005	0.11
0.025	0.55	0	0.55	0	0.46	0	0.54	0.011	0.53	0.015	0.46
0.025	1.24	0	1.24	0	1.03	0	1.21	0.016	1.19	0.016	1.03
0.045	2.20	0	2.21	0	1.82	0	2.16	0.018	2.12	0.016	1.83
0.05	3.44	0	3.45	0	2.85	0	3.37	0.028	3.31	0.016	2.85
0.42	4.96	0	4.97	0	4.10	0	4.85	0.148	4.77	0.018	4.11
1.05	8.82	0	8.84	0	7.30	0	8.63	0.688	8.48	0.023	7.30
1.46	13.77	0	13.81	0	11.40	0	13.48	0.938	13.25	0.028	11.41
1.79	19.83	0	19.89	0	16.42	0	19.41	1.123	19.08	0.03	16.43
2.095	30.99	0	31.08	0	25.65	0	30.33	1.343	29.81	0.032	25.67
2.355	55.10	0	55.26	0	45.60	0	53.91	1.493	52.99	0.037	45.63
2.505	86.09	0	86.34	0	71.25	0	84.24	1.593	82.79	0.039	71.30
		0	108.30	0	89.37	0	105.67	1.613	103.86		
						0	121.31				
						0	114.28				
						0	178.56				
						0	257.12				
						0	349.97				
						0	457.11				
						0.002	578.53				
						0.004	714.23				
						0.006	1028.49				
						0.008	1607.02				
						0.012	2064.13				
						0.016	2314.11				
						0.017	2578.37				
						0.018	2856.92				

29/1v/2	2.48	29/6v	3.86	29/6v/2	3.18	29/8v/1	2.19	30/1v/1	3.71	30/3v/1	4.23
ml	Pc(KPa)	ml	Pc(KPa)	ml	Pc(KPa)	ml	Pc(KPa)	ml	Pc(KPa)	ml	Pc(KPa)
0	0.12	0	0.13	0	0.13	0	0.09	0	0.13	0	0.14
0	0.50	0	0.54	0.025	0.52	0.065	0.36	0.08	0.52	0.02	0.57
0.025	1.12	0	1.21	0.035	1.16	0.07	0.80	0.085	1.18	0.025	1.27
0.48	1.99	0.001	2.16	0.05	2.06	0.072	1.43	0.087	2.10	0.11	2.26
0.78	3.11	0.091	3.37	0.09	3.22	0.077	2.23	0.092	3.27	0.625	3.53
1.01	4.48	0.591	4.85	0.66	4.64	0.192	3.21	0.094	4.72	1.145	5.09
1.2	7.96	0.841	8.63	1.065	8.25	0.632	5.71	0.334	8.38	1.615	9.04
1.27	12.43	1.311	13.48	1.29	12.89	0.892	8.91	0.724	13.10	1.855	14.13
1.305	17.90	1.461	19.41	1.387	18.57	1.037	12.84	0.909	18.86	2.08	20.34
1.36	27.97	1.671	30.33	1.567	29.01	1.187	20.06	1.269	29.47	2.32	31.79
1.402	49.72	1.771	53.91	1.709	51.57	1.307	35.66	1.549	52.39	2.49	56.51
1.433	77.69	1.851	84.24	1.851	80.58	1.397	55.72	1.749	81.86	2.61	88.30
1.453	97.46	1.951	105.67	1.886	101.08	1.467	70.52	1.879	102.69	2.63	110.76

30/8v	4.27	30/8v/2	3.76	30/10v	3.22	34/5v/1	2.47	34/6v/1	2.23	34/11v/1	2.15
ml	Pc(KPa)	ml	Pc(KPa)	ml	Pc(KPa)	ml	Pc(KPa)	ml	Pc(KPa)	ml	Pc(KPa)
0	0.13	0	0.13	0.01	0.60	0	0.10	0	0.10	0	0.10
0.005	0.52	0.005	0.54	1.38	2.40	0.06	0.41	0.001	0.39	0.09	0.41
0.685	1.17	0.265	1.21	2.255	9.60	0.185	0.91	0.046	0.88	0.11	0.92
1.49	2.07	0.915	2.15	2.335	12.15	0.555	1.62	0.236	1.56	0.12	1.64
1.83	3.24	1.435	3.35	2.385	15.00	1.205	2.53	0.641	2.43	0.275	2.56
2.125	4.66	1.79	4.83	2.435	18.15	1.63	3.65	1.236	3.50	0.775	3.68
2.275	8.29	2.03	8.59	2.455	21.60	2.01	6.49	1.576	6.22	1.465	6.54
2.375	12.95	2.16	13.42	2.465	25.35	2.2	10.13	1.801	9.72	1.665	10.22
2.425	18.65	2.24	19.32	2.475	29.41	2.29	14.59	1.906	14.00	1.835	14.72
2.505	29.14	2.32	30.19	2.495	33.76	2.36	22.80	1.996	21.88	1.935	23.00
2.525	51.80	2.375	53.68	2.52	38.41	2.42	40.53	2.031	38.89	2.01	40.90
2.56	80.93	2.42	83.87	2.53	43.36	2.45	63.33	2.036	60.77	2.04	63.90
2.595	101.52	2.45	105.21	2.535	48.61	2.452	79.45	2.041	76.22	2.065	80.16
				2.545	54.16						
				2.545	60.01						
				2.555	66.16						
				2.555	72.61						
				2.57	79.36						
				2.58	86.42						
				2.585	93.77						
				2.59	101.42						
				2.59	109.37						
				2.59	117.62						
				2.59	126.17						
				2.59	135.02						
				2.59	240.04						
				2.6	375.07						
				2.64	540.09						
				2.655	735.13						
				2.675	960.17						
				2.685	1215.21						
				2.69	1500.26						

34/12v/1	1.07	34/13v/1	2.87	35/5v	2.88	36/3v	2.92	36/4v	2.58	36/9v	2.37
ml	Pc(KPa)	ml	Pc(KPa)	ml	Pc(KPa)	ml	Pc(KPa)	ml	Pc(KPa)	ml	Pc(KPa)
0	0.10	0	0.12	0	0.12	0	0.10	0	0.09	0	0.09
0.03	0.41	0.1	0.47	0.02	0.47	0.025	0.39	0.04	0.35	0.04	0.37
0.04	0.92	0.72	1.06	0.025	1.06	0.035	0.89	0.045	0.78	0.05	0.84
0.042	1.64	1.53	1.88	0.027	1.89	0.04	1.58	0.07	1.38	0.075	1.49
0.044	2.56	2	2.94	0.028	2.95	0.21	2.46	0.075	2.16	0.155	2.33
0.046	3.68	2.4	4.23	0.029	4.25	0.54	3.55	0.077	3.11	0.435	3.35
0.081	6.54	2.535	7.52	0.031	7.56	1.035	6.31	0.297	5.53	1.13	5.95
0.156	10.22	2.635	11.75	0.032	11.82	1.235	9.86	0.527	8.64	1.395	9.30
0.191	14.72	2.71	16.92	0.033	17.02	1.42	14.19	0.817	12.44	1.47	13.40
0.291	23.00	2.755	26.43	0.033	26.59	1.555	22.18	1.177	19.44	1.58	20.93
0.381	40.90	2.78	46.99			1.75	39.43	1.392	34.55	1.665	37.21
0.496	63.90	2.785	73.43			1.895	61.60	1.547	53.99	1.74	58.15
0.531	80.16	2.795	92.11			1.95	77.27	1.662	67.73	1.76	72.94

36/10v	2.61	36/10v/2	2.72	37/2v	0.75	37/3v	1.44	37/5v	1.65	37/6v	1.10
ml	Pc(KPa)	ml	Pc(KPa)	ml	Pc(KPa)	ml	Pc(KPa)	ml	Pc(KPa)	ml	Pc(KPa)
0.045	0.13	0.08	0.14	0.055	0.12	0	0.13	0	0.13	0	0.10
0.075	0.51	0.08	0.56	0.056	0.49	0.035	0.51	0.016	0.51	0.02	0.40
0.115	1.15	0.11	1.26	0.066	1.11	0.035	1.16	0.016	1.14	0.08	0.90
0.175	2.05	0.135	2.24	0.066	1.97	0.045	2.06	0.016	2.03	0.13	1.60
0.225	3.20	0.17	3.51	0.066	3.07	0.046	3.22	0.016	3.17	0.245	2.50
0.44	4.60	0.29	5.05	0.136	4.43	0.046	4.63	0.016	4.57	0.35	3.60
0.705	8.18	0.58	8.98	0.171	7.87	0.046	8.23	0.017	8.12	0.435	6.39
0.875	12.79	0.795	14.03	0.201	12.30	0.051	12.86	0.017	12.70	0.495	9.99
1.03	18.42	1.015	20.20	0.216	17.70	0.052	18.52	0.017	18.28	0.52	14.39
1.21	28.77	1.3	31.56	0.221	27.66	0.053	28.94	0.017	28.56	0.545	22.48
1.34	51.15	1.35	56.11	0.251	49.18	0.063	51.45	0.017	50.78	0.59	39.96
1.445	79.93	1.58	87.67	0.281	76.84	0.083	80.39	0.017	79.34	0.62	62.44
1.51	100.26	1.66	109.97	0.296	96.39	0.103	100.84	0.017	99.53	0.63	78.32

37/7v	0.79	38/2v	2.86	38/4v	2.75	1538/5v	3.81	1538/7v	4.57	1542/2v	3.85
ml	Pc(KPa)	ml	Pc(KPa)	ml	Pc(KPa)	ml	Pc(KPa)	ml	Pc(KPa)	ml	Pc(KPa)
0	0.12	0	0.13	0	0.11	0.09	0.11	0.1	0.15	0.01	0.13
0.4	0.49	0.02	0.52	0.03	0.43	0.11	0.42	0.11	0.61	0.07	0.53
0.4	1.11	0.025	1.18	0.045	0.97	0.12	0.95	0.16	1.37	0.77	1.19
0.405	1.97	0.065	2.09	0.046	1.72	0.155	1.69	0.225	2.44	1.29	2.12
0.406	3.07	0.535	3.27	0.076	2.68	0.445	2.64	0.415	3.82	1.97	3.31
0.406	4.43	0.985	4.71	0.151	3.86	0.735	3.79	0.815	5.50	2.55	4.76
0.406	7.87	1.23	8.37	0.306	6.87	1.015	6.75	1.295	9.77	2.81	8.46
0.406	12.29	1.435	13.08	0.506	10.74	1.575	10.54	1.595	15.27	2.97	13.22
0.406	17.70	1.56	18.83	0.706	15.46	1.96	15.18	1.885	21.99	3.08	19.04
0.406	27.66	1.665	29.43	0.976	24.15	2.12	23.72	2.105	34.35	3.14	29.75
0.411	49.17	1.785	52.31	1.326	42.94	2.345	42.17	2.325	61.07	3.19	52.89
0.411	76.84	1.86	81.74	1.451	67.10	2.535	65.88	2.5	95.43	3.24	82.64
0.411	96.38	1.89	102.53	1.501	84.17	2.64	82.64	2.695	119.71	3.241	103.67

1542/3v	3.38	1542/11v	4.21	1542/14v	3.65
ml	Pc(KPa)	ml	Pc(KPa)	ml	Pc(KPa)
0.01	0.13	0	0.14	0	0.13
0.03	0.51	0.08	0.54	0.1	0.53
0.031	1.14	0.28	1.22	0.17	1.20
0.032	2.02	0.99	2.18	0.4	2.13
0.032	3.16	1.7	3.40	0.68	3.33
0.032	4.55	2.02	4.89	1.54	4.79
0.032	8.08	2.42	8.70	1.825	8.52
0.152	12.63	2.585	13.60	2.035	13.31
0.292	18.19	2.715	19.58	2.225	19.16
0.512	28.42	2.8	30.59	2.32	29.95
0.782	50.52	2.875	54.39	2.38	53.24
1.082	78.94	2.95	84.98	2.47	83.18
1.197	99.02	2.96	106.60	2.49	104.34

APPENDIX 4. Simple Percolation Model for the Interpretation of MICP Data

(Prepared by J.A. Barker)

PURPOSE OF THE MODEL

It is well understood that MICP data give a rather poor distribution of pore throats when compared with more reliable methods. However, MICP data are generally very easy to obtain in relation to other approaches, so it is worth attempting to derive as much information as possible from those data.

The model described in outline here, was developed to provide an alternative interpretation of MICP data to that simply based on the inverse correspondence between applied pressure and throat diameter: ie the application of the 'bundle of capillary tubes' model. More precisely, the aim was to provide an interpretation that would take into account the percolation nature of the mercury invasion to indicate that larger throats could exist and to suggest a method for approximately quantifying the distribution of those large pores.

This note only aims to provide a basic description of the model. A paper currently in preparation will provide fuller details including numerical experiments to explore MICP behaviour and justify use of the model.

DESCRIPTION OF THE MODEL

Let us start by considering a very specific case (Fig. A4.1). Consider a lattice of equal-sized cubic pores which are connected by circular throats of varying radii. If every face, which is shared by two pores, has a throat then the system would have a coordination of 6 and unit porosity. (By having some faces without throats and some pores with no throats at all, we can vary the coordination number and the porosity.)

The model, in its general form, keeps constant: the pore size and the coordination number of each pore. The pore throats are however assumed to have random sizes drawn from a continuous probability distribution. The aim is to determine that distribution from MICP data.

Once a pore is invaded with mercury, if the pressure exceeds that required to pass through a throat to an empty neighbouring pore, that pore will also be invaded at that pressure. It will be assumed that the MICP experiment is carried out sufficiently slowly that this process proceeds without need to consider the delay in movement from pore to pore.

To be precise, the model assumptions are:-

1. All volume is in the pores and all the pores have the same volume.

2. Pores are connected by the same number of throats, which are uncorrelated. (The coordination number, z, is the same for all pores but will not be assumed integer.)
3. The (harmonic mean) throat radius is characterised by a known distribution function.
4. All pores are either empty (vacuum) or full.
5. All full pores are connected.
6. If a pore is invaded at a given pressure then neighbouring pores connected by throats large enough to be entered at that pressure.

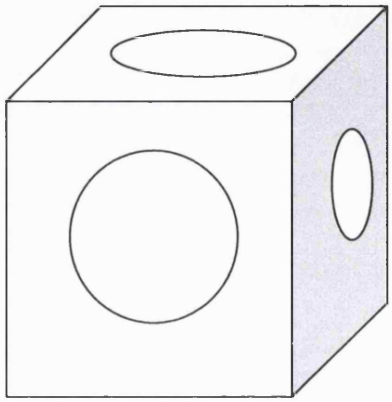

Fig. A4.1. A possible realisation of a single cell in the percolation model.

MODEL PARAMETERS

The model is characterised by the coordination number, z, and two probability functions:

- p*(Pc)* be the probability that pore *n* is full when the applied pressure is *Pc*.

- τ*(Pc)* be the probability that a pore throat is accessible at pressure *Pc*.

Numerical simulation experiments were performed to understand how the probability p would vary with distance from the rock surface. It was found that once a critical value of τ (ie a critical pressure PC) had been reached, within about five pore depths from the injection surface the probability p had tended to an asymptotic value. Since five pore depths represents little porosity, it was decided to work with the 'asymptotic form of the model.

This asymptotic model effectively assumes that every pore has the same chance of being full of mercury at a given pressure (value of τ). It is then readily shown that the following relation must exist between p, τ, and z:

$$p = \begin{cases} 0 & \tau < 1/z \\ 1-[1-p\tau]^z & \tau \geq 1/z \end{cases} \qquad \text{(A4.1)}$$

This relationship is the key result of the model.

When the pressure just exceeds a value which gives a probability of throat entry of 1/z, mercury can penetrate beyond the surface right through the test sample, so $\tau = 1/z$ can be described as the percolation condition: percolation occurs when the probability of passing entry to any given throat equals the reciprocal of the coordination number.

Before attempting to apply equation (A4.1), we need to relate it back to an MICP experiment: we must understand the probability functions in terms of such an experiment.

Interpretation of p

Since (in the model) all saturated pores are connected, the volume of mercury injected equals the number of pores times the probability that a pore is full (in the model pores are full or empty) times the average pore volume. Since the porosity is the total pore volume divided by the sample volume, the injected volume is given by:

$$V_i = \langle p \rangle \phi V_{sample} \qquad \text{(A4.2)}$$

where <p> is the mean probability averaged over the sample. Ignoring near surface effects, this probability can be identified with p in the model. We therefore have:

$$p = \langle p \rangle = V_i / (\phi V_{sample}) \qquad \text{(A4.3)}$$

which is the required interpretation of the probability p for MICP, since V_i is the cumulative volume measured during an MICP experiment.

We can regard the product ϕV_{sample} as the cumulative volume injected at infinite pressure, assuming that all space is accessible.

Interpretation of τ

Turn now to the probability τ which can be regarded as the probability that a throat is accessible at a given capillary pressure. That equals the probability that the throat is larger in effective radius than that corresponding (through the Washburn equation) to the applied pressure. So τ is the cumulative throat-size distribution, where the integration is from large to small effective radii. (Conventionally, cumulative distributions are taken as integrals from small to large, so, strictly, the throat sizes are distributed as $1-\tau$.)

FITTING REAL MICP DATA WITH THE MODEL

The data are in the form of pairs of values of pressure (normally converted to 'Pore Size') and cumulative volume imbibed. (Strictly speaking MICP is a 'drainage' process.)

The problem is to find the throat size distribution τ (or $1-\tau$) and the co-ordination number, z, that best fit the data. (Another parameter to be fitted is the volume that would be injected at infinite pressure, ϕV_{sample}, although this could in principle be determined by other means.)

Essentially two approaches are possible, based on the use of the two functional dependencies: $\tau(p,z)$ and $p(\tau,z)$, respectively.

Method 1: Interpretation based on $\tau(p,z)$

We can rearrange

$$p = 1 - [1 - p\tau]^z \qquad \text{(A4.4)}$$

to give

$$\tau(p,z) = \frac{1}{p}\left[1 - (1-p)^{1/z}\right] \qquad \text{(A4.5)}$$

Note that when p=1, τ=1, but when p=0, τ=1/z (obtained by taking the limit).

Given MICP data comprising pairs of values of V_i and P_c (or pore size, PS), we can envisage two approaches.

Method 1a

(1) Estimate ϕV_{sample} either from direct measurement or by extrapolating V_i to infinite pressures.
(2) For each pressure, obtain $p = V_i / (\phi V_{sample})$
(3) Choose a coordination number, z.
(4) Calculate $\tau(p,z)$ from the above formula.

As an alternative to (1) and (2) both upper and lower bounds on the cumulative volume could be chosenV_{min} and V_{max} say, to give:

$$p = (V_i - V_{min}) / (V_{max} - V_{min}) \qquad \text{(A4.6)}$$

Method 1b

(1) Decide on a functional form for $V_i(P_c)$ or $V_i(PS)$ noting the need to extract p in Step 3.
(2) Use a fitting procedure to obtain V_i as a function of the parameters chosen.
(3) For each pressure, obtain p , e.g. from $= V_i / (\phi V_{sample})$
(4) Choose a coordination number, z.
(5) Calculate $\tau(p,z)$ from the above formula.

Note that Step 3 must give values of p in the range zero to unity.

There are two shortcomings with Methods 1a and 1b. Firstly, it is necessary to choose the coordination number, *a priori*. Secondly, the resulting distribution for $\tau(p,z)$ will only occupy the range from 1/z to 1.

The choice of functional form in Method 1b is somewhat arbitrary although it is best that this form reveals $\phi\, V_{sample}$ as the asymptotic value of V_i for infinite pressures. For example, we might choose a power-law distribution:

$$V_i(P_c) = V_\infty + (V_0 - V_\infty)\theta(P_c)$$
$$\theta(P_c) = \begin{cases} (P_b / P_c)^\lambda & P_c \geq P_b \quad \lambda > 0 \\ 1 & P_c \leq P_b \end{cases} \qquad \text{(A4.7)}$$

This is essentially the Brooks and Corey function for effective saturation, θ, where P_b is the 'bubbling' pressure.

The corresponding probability $p(P_c)$ would be identified with $\theta(P_c)$. (The Washburn equation is required to change the functional dependencies from pressure to radius, i.e. to change $p(P_c)$ and $\tau(P_c)$ to $p(R)$ and $\tau(R)$.)

Method 2: Interpretation based on $p(\tau,z)$

We cannot, in general, rearrange

$$p = 1 - [1 - p\tau]^z \qquad \text{(A4.8)}$$

to provide a simple functional form $p(\tau,z)$. Solving that equation for $p(\tau,z)$ is equivalent to finding the root(s) of

$$f(p) = p - 1 + [1 - p\tau]^z = 0 \qquad \text{(A4.9)}$$

Fortunately, it has been possible to show that Newton's method of root finding, starting at p=1, is guaranteed to provide the (single) non-zero root of f(p). So fast accurate determination of the function $p(\tau,z)$ poses no practical difficulties.

METHOD 2

(1) Decide on a functional form for $\tau(P_c)$ (or $\tau(R)$).
(2) For each P_c at which an observation is made, determine $\tau(P_c)$.
(3) For a given z, compute $p(\tau(P_c),z)$ for each P_c.
(4) Convert p to a volume introducing further parameters. e.g. $p=V_i / (\phi\, V_{sample})$
(5) Use a fitting procedure to obtain estimates of: (i) the parameters describing $\tau(P_c)$ in Step 1, (ii) z (Step 3), and (iii) the parameters introduced in Step (4). This essentially iterates over Steps (1) to (4).

In Step 1, the most natural choice of function is a (cumulative) probability function, $F_p(P_c)$ or $F_r(R)$ say, which gives positive values. The lognormal is such a function. But note that because τ is cumulative from large pores to small, we must have $\tau(P_c) = F_p(P_c)$ while $\tau(R)=1 - F_r(R)$.

Given the field of study, other candidate functions worth considering are the relative saturation curves. One example is the Brooks and Corey function (see Method 1b above) and another is the van Genuchten function which can be written, in terms of capillary pressure:

$$\tau(P_c) = \theta(P_c) = \left[1 + (P_C / P_0)^n\right]^{-m} \qquad P_c \geq 0 \quad n > 1 \quad m = 1 - 1/n \tag{A4.10}$$

or, in terms of pore size, PS:

$$\tau(PS) = 1 - \theta(PS) = 1 - \left[1 + (PS_0 / PS)^n\right]^{-m} \qquad PS \geq 0 \tag{A4.11}$$

These two functions are simply related through the pressure being inversely proportional to pore size.

In Step 4 we might for example put minimum and maximum values on the cumulative injection volume, V_{min} and V_{max} say, to give:

$$V_i = V_{min} + (V_{max} - V_{min})p \tag{A4.12}$$

Since during MICP the sample is initially evacuated (free of mercury) V_{min} should be zero but introducing such a value can accommodate 'compliance' at the start of mercury injection. V_{max} would represent ϕV_{sample} if all of the pores could be accessed by the mercury.

CONCLUSIONS

A simple percolation model has been introduced which can be used to interpret MICP data: two methods of data analysis are suggested:

1. Method 1 is simple to use but requires the coordination number to be given *a priori*, and only throat sizes greater than that corresponding to percolation can be derived.

2. Method 2 requires a throat-size distribution function to be chosen then the method reveals the parameters of that distribution and the coordination number. It needs to be emphasized that while this procedure can provide a throat size distribution which ranges across all pressures or radii, the distribution beyond the percolation size is only obtained as the extrapolation of the chosen distribution function. So the choice of that function is particularly important.

APPENDIX 5. Visual Basic Code for Calculating Gamma Distribution

```
Function cumg(x As Double, alpha As Double, beta As Double) As Double

   cumg = gammp(alpha, x / beta)

End Function
Function gammp(a As Double, x As Double) As Double

Dim gamser As Double, gln As Double, gammcf As Double

If x < a + 1# Then
  Call gser(gamser, a, x, gln)
  gammp = gamser
Else
  Call gcf(gammcf, a, x, gln)
  gammp = 1# - gammcf
End If

End Function

Sub gser(gamser As Double, a As Double, x As Double, gln As Double)

Dim ap As Double, del As Double, sum As Double

   itmax = 100
   eps = 0.0000003

   gln = gammln(a)
   If x <= 0 Then
     gamser = 0#
     Exit Sub
   End If

   ap = a
   sum = 1# / a
   del = sum
   For n = 1 To itmax
     ap = ap + 1#
     del = del * x / ap
     sum = sum + del
     If Abs(del) < Abs(sum) * eps Then GoTo 1
   Next n

1:    gamser = sum * Exp(-x + a * Log(x) - gln)

End Sub


Sub gcf(gammcf As Double, a As Double, x As Double, gln As Double)

Dim eps As Double, fpmin As Double, b As Double, c As Double, d As Double
Dim h As Double, del As Double

itmax = 100
eps = 0.0000003
fpmin = 1E-30

gln = gammln(a)
b = x + 1# - a
c = 1# / fpmin
d = 1# / b
h = d
For i = 1 To itmax
  an = -i * (i - a)
  b = b + 2#
  d = an * d + b
  If Abs(d) < fpmin Then d = fpmin
  c = b + an / c
  If Abs(c) < fpmin Then c = fpmin
  d = 1# / d
  del = d * c
  h = h * del
  If Abs(del - 1#) < eps Then GoTo 1
Next i

1: gammcf = Exp(-x + a * Log(x) - gln) * h

End Sub
Function gammln(x As Double) As Double
```

```
gammln = Application.WorksheetFunction.GammaLn(x)
End Function
```